SCUOLA DI ALTA FORMAZIONE DOTTORALE

MACRO-AREA SCIENZE E TECNOLOGIE

Dottorato di Ricerca in Scienze della Terra e dell'ambiente

Fabrizio Troilo

Glacial risks monitoring and management

Anno Accademico 2022-2023
Ciclo 36°

Coordinatore
Prof. Silvio Seno

Tutor
Prof. Francesco Zucca

Co-tutor(s)
Dott.Daniele Giordan, Prof. Alberto Godio.

Glacial risks monitoring and management

Fabrizio Troilo - PhD Thesis

Università di Pavia – Fondazione Montagna sicura

Foreword

Glaciers are a peculiarity of mountain and polar environments on Earth. The landscape of the Alps, in particular, finds one of its most fascinating traits in the snow and ice capped mountains. If it has been this way in the past centuries, nowadays not only scientists but both local populations and tourists alike can observe that large, unusual changes are happening in the high mountain environment of the Alps. Very little snow cover is left during the summer season, perennial snow and subsequent equilibrium line altitude is a lot higher than in the past, and glaciers experience more and more debris cover from increasingly frequent rockfalls. The darkening of the alpine landscape should really be an indicator for populations to care more about environmental changes caused by anthropogenic global climate change. If the adaptation to the bitter sensation of observing the vanishing of alpine glaciers may be subjective and have a relatively mild impact, the consequences of climate change and a strong ongoing degradation of alpine cryosphere could be severe: water scarcity during summer droughts and an increase in the frequency and intensity of extremely severe meteorological phenomena are only two of the consequences that will have to be faced in the future. In between large-scale phenomena such as those just mentioned, locally, the evolution of natural hazards linked to a rapidly changing cryosphere will also need to be faced and adaptation sought. The early detection and monitoring of a very rapidly evolving territory are challenging in the extreme. It is from this standpoint that the present PhD project was conceived.

1. Introduction

The executive PhD project supported by the Fondazione Montagna sicura (FMS) and the University of Pavia, which I carried out as the principal investigator, was conceived in order to pursue research and development activities on the topic of the monitoring and the understanding of the dynamics and processes leading to glacial instabilities and glacial risks (Faillettaz et al., 2016; Faillettaz et al., 2015). The involvement of the CNR IRPI Section of Turin, GMG 'Geohazard Monitoring Group', was fundamental in the integration of historical monitoring data and experimental activities on specific monitoring sites as well as the extensive input that derives from their expertise in the monitoring of natural hazards and the development of innovative monitoring solutions. The project's research topic stems from a distinct need: even though great improvements have been made in recent years using new technologies, many uncertainties are still present in many steps of the monitoring and the subsequent decision-making process when a road is closed or houses have to be evacuated due to potential glacial instability. Therefore, the need for a strong integration of research activity

into risk management has become a priority. In this frame, the 'monitoring' side (that is mainly represented as the private investor in the PhD project: Fondazione Montagna Sicura) represents the applied side of the scientific project, while the understanding of the processes is more purely scientific, one that is more affine to the academic side represented by the university. The joint efforts that were combined in this partnership well represent the structure of the executive PhD that should blend industry and academia in a pathway of research and development around a common subject of interest. In the field of glacial hazards, a great leap forward for both the scientific community and policy makers involved in the management and monitoring of glacial risk situations has been made in recent years by the intergovernmental study group Gaphaz, first with its establishment and, later, with the very relevant publication of: 'Assessment of Glacier and Permafrost Hazards in Mountain Regions, Technical guidance document' (Allen et al., 2022). This document synthetises a large quantity of information related to destabilisation phenomena in high mountain environments. A large part of the work analyses risks of a glacial origin; cascading processes which will be the focus of the present work. Nonetheless, the Gaphaz document carefully describes phenomena and largely deals with the early identification of hazards, and possible modelling approaches, for the definition of risk scenarios. The scientific community worldwide should refer to this document for guidelines on early hazard detection and a preliminary definition of risk scenarios, which represent the core of the Gaphaz work. Nonetheless, what is not included in this document is everything that happens when, at a specific site, a hazardous situation is detected and highly destructive impacts are estimated by means of modelling approaches (Emmer et al., 2022; Mergili et al., 2020). Therefore, what comes into play is the "monitoring" phase of the phenomenon (Faillettaz et al., 2016; Pralong & Funk, 2006), and this part of the process represents the main topic of the present work. The final steps of the Gaphaz document provide some indications and examples as to the kind of approach that could be used for the further investigation (a general indication of a possible approach is given, but is not developed further) of specific sites, but this does extend to a critical analysis of existing approaches and methodologies, their pros and cons, limits, cost and other important details. I believe that the relevance of the present study resides in the aim of analysing the current situation and increasing knowledge of it. Principally, this project was born because, in the frame of glacial monitoring activities managed by the FMS, many difficulties are due to the current degree of knowledge of the glacial processes that may, potentially, generate risk situations. Often, these processes are poorly understood and also less studied compared to other glacial processes. This focus in the field of glaciology has a motivation, and the efforts of the glaciological community having a major focus on better understanding the global consequences of future glacier melt is highly motivated by the global impacts that it will have in future climate change scenarios. Even if impacts of glacial risks have more local impacts, in present climate change scenarios, they could represent major problems to be faced by mountain communities (Pandey et al., 2022). In this context, we focused our attention on providing an in-depth review of the existing methodologies and the scientific understanding of glacial destabilisation processes. The main objective of the present PhD study is to understand whether the integration of a stronger and updated scientific approach to an existing glacial risk monitoring plan could benefit present procedures and if new knowledge applied to the management and monitoring of glacial risks could help researchers, practitioners and policy makers. This knowledge would, in turn, benefit populations living in the mountains who have to cope with glacial risks. Another aim of the project would be, ideally, to create or at least lay out a pathway for standardised procedures and methodologies that could be replicated and diffused in order to be used and applied by other mountain communities around the world.

The Fondazione Montagna Sicura is a non-profit organisation dedicated to the study of safety in high mountain environments. It has developed specific departments studying snow and

avalanche science, mountain medicine, risk communication and glaciological studies applied to the prevention of glacial risks. The Foundation began its operations in 2002.

Before exploring these issues, it is worth summarising the natural processes involved in the risk assessment and management of glacial hazards; a simple yet effective classification can better guide the reading and the understanding of the content that will follow.

A classification of glacial risk phenomena

Mountain glaciers are the main source of freshwater for human activities in the surrounding regions (Barnett et al., 2005; Hock et al., 2005). Furthermore, glaciological processes (e.g., ice break-offs, glacier outbursts, snow/ice avalanches) can threaten populations, urban areas and infrastructure (Kääb et al., 2005). In densely populated areas, such as the European Alps, the interaction between glaciers and anthropic activities is very frequent (Haeberli et al., 1989) and is of crucial importance in the study of glaciers in order to understand their evolution and as a response to climate change. Moreover, glaciers are expected to reduce their area coverage and increase their instability (Deline, Gruber, et al., 2015). The long-term monitoring of glaciological processes is often complicated and expensive, especially in remote areas and inaccessible terrains, which are common in mountain environments (Kenner et al., 2018). A practical approach is the adoption of remote sensing instrumentation that allows for the observation of glacial processes with minimal risk for scientists and technicians. In recent years, the free availability of data acquired from satellite platforms has largely improved the possibility to observe wide areas remotely with a relatively high spatiotemporal resolution. Nevertheless, satellite surveys suffer complex geometries and the revisit time might be not adequate for glaciers and the measurement of rapid processes. Therefore, the use of close-range remote sensing systems is often the most effective solution for glacier monitoring (Dematteis et al., 2018).

Before going further into the study, it is important to summarise the principal types of instability that can affect glaciers and their surrounding environment.

Glacial instabilities can be divided in two large categories of phenomena:

A) Phenomena linked to destabilisation of solid ice masses (glacier collapses)

B) Phenomena linked to destabilisations involving unstable water accumulations into, onto or near to glaciers (GLOFs)

A third class may be identified as a crossover between the two aforementioned classes and that involves solid and liquid water phases but, more generally, as other solid phases may be incorporated in mass movements like rock or snow. We define this class as instabilities linked to ‘cascading processes’ and, therefore, define it as:

C) A destabilisation involving complex cascading processes with the presence of different phases into mass movements.

A) Glacier collapses

Glacier collapses can be divided into two major groups: serac falls and temperate glacier destabilisations. These are typically gravity driven instabilities involving solid ice masses (Faillettaz et al., 2016).

Serac falls occur when glaciers are frozen to the bedrock, meaning that they have negative temperatures at the ice-bedrock interface throughout the whole year. No basal sliding happens in these conditions and the dynamics of such ice bodies are determined by internal deformation and damage only, thus providing an opportunity to interpret accelerating deformations as a precursor (Pralong et al., 2005) of a major failure in the ice body (Figure 1). The failure is driven by accretion of the ice body to a critical geometry which becomes unstable and is, essentially, driven by ice accumulation and gravity that generates periodical large failures.

Figure 1. Large serac falls of the Whymper Serac occurred in September 2014.

Temperate glacier collapses occur as a consequence of different dynamics (compared to serac falls) that such glaciers manifest due to the presence of liquid water at the ice-bedrock interface at the base of the glacier (Pralong & Funk, 2006). Along this interface, the basal friction is weakened and in a complex equilibrium between melting and refreezing along asperities, a distributed drainage network can build up; during the melting season the drainage network can build up more consistently and organise itself in a channelised network. In this subglacial drainage network, positive water pressures may build up because of sudden increases of water input from increased snow/ice melt or liquid precipitation, and a drop in basal friction of the glacier can be experienced. A decrease of basal friction causes the ice mass to accelerate. Such accelerations may destabilise certain types of glacier and cause the triggering of large ice avalanches (Alean, 1985). Such avalanches can occur on steep glaciers (Figure 2) that sit on hard bedrock (such as the Allalingletscher ice avalanche, 1965) (Faillettaz et al., 2012), but it has been recently observed (for example at Aru Lake in 2016) (Gilbert et al., 2018) that glacier tongues lying on a soft sediment base may also become destabilised, even with very low angle slopes. This last type of destabilisation has never been described for alpine case studies.

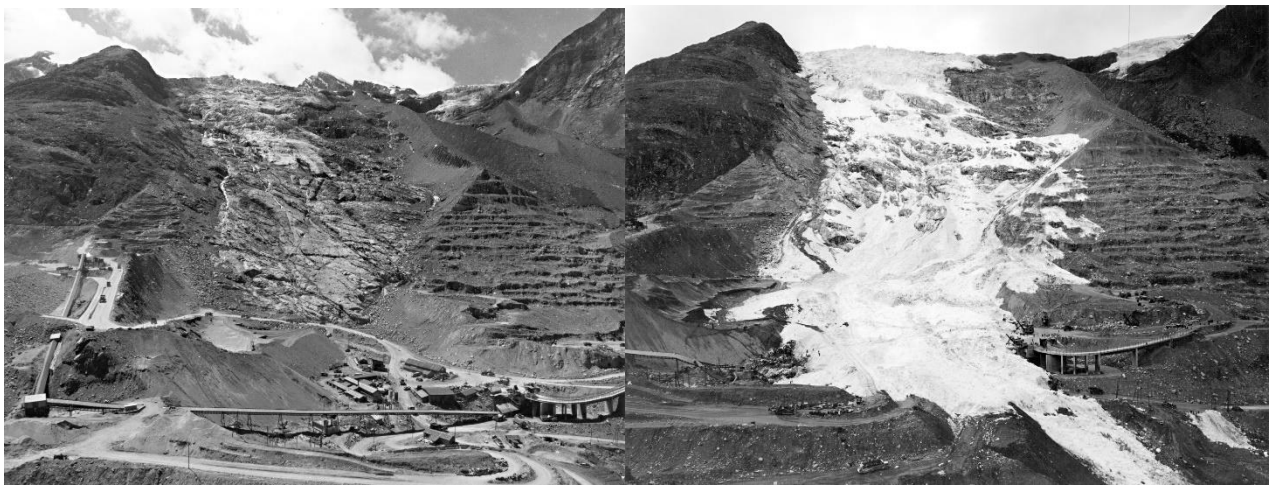

Figure 2. Destabilisation of a temperate glacier tongue. The ice avalanche of 30 August 1965 at Allalingletscher (Wallis Canton-CH)

B) Glacier lake outburst floods (GLOFs)

GLOFs are generated by the accumulation of liquid water onto, into or near to ice bodies. These can become unstable and trigger sudden collapses of the ice dams retaining the liquid water mass, thus generating floods downslope (Emmer, 2017). Generally, if the lakes have a free surface (Figure 3), they can be fairly easily observed both on-site and from satellite observations so they can be readily detected (Taylor et al., 2023). If a critical and potentially dangerous geometry is identified, more specific assessments must be made such as water volume estimation, flood runout modelling and ice subsurface imaging by geophysical investigations. If a risk for downslope communities or infrastructures exists, active measures such as drainage channel excavations, water lowering by pumping or passive measures such as monitoring systems linked to early warning systems are normally taken into account (Wang et al., 2022).

Figure 3. The Grand Croux glacial Lake (Cogne – Aosta Valley) which originated a GLOF on 14 August 2016.

C) Cascading processes

Cascading processes are phenomena that can be triggered as a single mass movement but that later evolve into a different type of mass movement due to the uptake of, or combination with, other phases or materials along their paths (Mergili et al., 2020). A classic example of cascading processes in high mountain environments involving glaciers are so called 'rock-ice avalanches'. In this case, rock failures from rock walls that fall onto glaciers can uptake ice and/or snow from the glacier surface (Shugar et al., 2021) (or eventually destabilising the whole glacier in extreme cases) so that the mixture of rock, ice and snow is 'lubricated' with a drop in friction coefficients of the moving mass, giving rise to an extension of the run outs compared to the starting, single-phase, event (Figure 4). The array of different cases is extremely wide with existing examples ranging from glacier collapses ending up in lakes that trigger floods, to ice avalanches that end up blocking streams and can trigger subsequent debris flows along streams.

Figure 4. A rock-ice avalanche powder cloud reaches the hamlet of Entrèves, Courmayeur on 16 January 1998.

1.1 Area of study

The Aosta Valley (Italian: Valle d'Aosta) is a mountainous autonomous region in northwestern Italy (Figure 5). It is bordered by Auvergne-Rhône-Alpes, France, to the west, Valais, Switzerland, to the north, and by Piedmont, Italy, to the south and east. The regional capital is Aosta. Covering an area of 3,263 km^2 and with a population of approximately 128,000, it is the smallest, least populous, and least densely populated region in Italy. Provincial administrative functions are provided by the regional government and the region is divided into 74 municipalities. The Aosta Valley is an Alpine valley which, with its tributary valleys, includes the Italian slopes of Mont Blanc, Monte Rosa, Gran Paradiso and the Matterhorn; its highest peak is Mont Blanc (4,810 m). The valleys, usually reaching above 1,600m on their lowlands, annually have a cold continental climate. The inner parts of the region, orographically protected by the main incoming weather fronts, are particularly dry, with mean annual precipitations as low as 500-600mm, while the outer parts of the region, in the bordering areas, can reach 1800-2000mm of precipitation per year, on average. With about 40% of the regional territory above 2500m, the presence of glaciers is widespread around the whole region.

Figure 5. Localisation of the Aosta Valley region on the national Italian territory.

In the New Italian Glacier Inventory (Smiraglia et al., 2015), 903 glaciers are described, covering a total area of 369.90 km² ± 2%. The largest part of the glacier coverage is, in fact located, in the Aosta Valley Autonomous Region (36.15% of the total). Only three glaciers in the national inventory exceed 10 km² of glacier surface: the Forni Glacier (11.36 km²) in Lombardy, the Adamello Glacier (16.44 km²) in both Lombardy and in the Autonomous Province of Trento, and the Miage Glacier (10.47km²), which is located in the Autonomous Region of Aosta. In this high alpine environment, 4% of the Aosta Valley territory is still covered by glaciers (2015). The Regional Glacier Inventory, with its update to 2019, counts 184 glaciers. The actual trend of glacial regression has been ongoing for several decades, and the analysis of three successive glacier inventories of the Aosta Valley region, performed by Diolaiuti et al. (2012) for the years 1975, 1999 and 2005 on 174 glacial bodies (that were common in all three inventories), provides a good description of the trends of recent decades: Aosta Valley glaciers lost 44.3 km² during 1975-2005 (about 27% of the initial area), and the real change rate accelerated over time: the 1999-2005 mean area loss was of 2.8 km²/year while the 1975-1999 mean area loss had been of 1.1 km²/year, the total glacierised surfaces 163.9 km² in 1975, 136.6 km² in 1999, and 119.6 km² in 2005. Owing to its high Alpine environment and special geomorphology, the Aosta Valley population is highly exposed to risks related to glaciers. The area of study of the present PhD project is particularly interesting for two main reasons:

- In a small (3200km²) area, there are case studies comprising all the glacial instability types numbered in the precedent section with both historical events and actually monitored sites.
- The Aosta Valley region was one of the first alpine regions to adopt an official glacial risk monitoring plan.

1.2 Case studies

One of the core functions of the Fondazione Montagna Sicura has been, since its creation (that was strongly supported by the Autonomous Regional government), to be an operative branch dealing with problems linked to high mountain environments, especially snow avalanches on one the hand and glacial hazards and risk on the other. To address the glaciological issues, the foundation's Technical and Research Area has worked, since its inception, to conceive and apply a glacial risk monitoring plan (Schindelegger, 2019). The specific methods used for its management and application are described in the following chapters of the thesis, but it is fundamental to stress that the selection of case studies was naturally guided by existing case studies, where monitoring of glacial instabilities had been carried out in the past or is still ongoing. Therefore, some of the specific monitoring sites on which glacial instabilities are being monitored have been chosen, the choice mainly being guided by the quantity and quality of existing data available from the different sites.

Single specific monitoring sites of the glacial risk monitoring plan of the Aosta Valley, chosen for further investigation, are briefly presented hereafter:

Grandes Jorasses

The Whymper Serac is located in the upper part of the Grandes Jorasses Glacier, in Val Ferret, in the municipality of Courmayeur, at approximately 4000m a.s.l. (Figure 6). Six boreholes drilled in January 1998 showed basal temperatures below 0°C. Recent observations indicate that the basal temperature has risen ((Vincent et al., 2020) and Vincent 2021, personal communication). The serac is 45°-steep and is classified as an unbalanced hanging glacier (Pralong & Funk, 2006). The Whymper Serac follows an evolution cycle characterised by its progressive volume increase until its shape and mass reach unstable conditions, and consequently, it collapses. The last break-offs occurred in August 1993 (causing the death of eight mountaineers), in June 1998, in September 2014 and during autumn 2020. Major destabilisations of the Whymper Serac have twice been successfully detected in the past thirty years, with a very good estimation of the time of failure of the ice mass in both cases. The methodologies used for the monitoring and the prediction of the time of failure have been published both for the 1998 case and for the 2014 case (Faillettaz et al., 2016). A predictive model based on the analyses of inverse surface velocities of the ice mass has proven to be effective as long as most of the ice-bed interface is frozen.

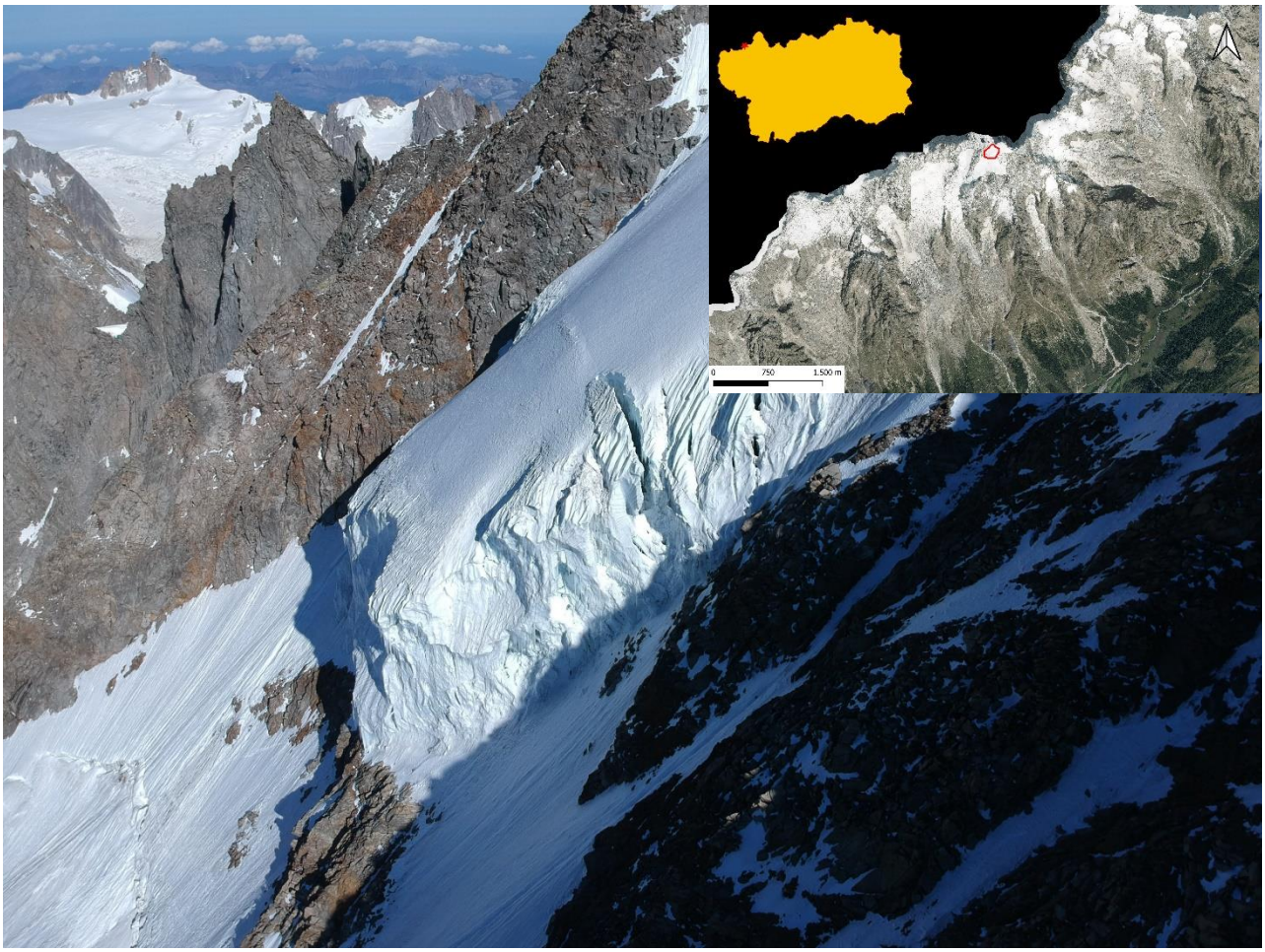

Figure 6. The Grandes Jorasses summit and the Whymper Serac

Planpincieux Glacier

The Planpincieux Glacier (RGI60-11.02991) is a medium-sized (Area: 1.013km^2) glacier located in the Italian part of the Mont Blanc massif (Figure 7). It is situated in the municipality of Courmayeur, Aosta Valley region. Its aspect is mostly south and its accumulation area is overlooked by rock faces from the Grandes Jorasses (4208m), reaching as high as 700m of vertical drop. It drains in Val Ferret, in the municipality of Courmayeur. The ablation area of the Planpincieux Glacier is composed of two lobes. One lobe, on the left part of the glacier front, does not show signs of destabilisation (Giordan, Dematteis, et al., 2020). The unstable part is represented by the right lobe, known as the 'Montitaz Lobe', which is a 32°-steep icefall whose terminus lies at 2600m a.s.l. and ends in correspondence with a bedrock cliff that induces frequent calving and subsequent ice-avalanches. The monitoring systems that are active for the monitoring of the Montitaz lobe consist in a wide array of instruments that are detailed in the following chapters. Large instabilities were detected by the monitoring systems in 2019 and 2020, leading authorities to undertake safety measures such as road closures and the evacuation of houses in Planpincieux village.

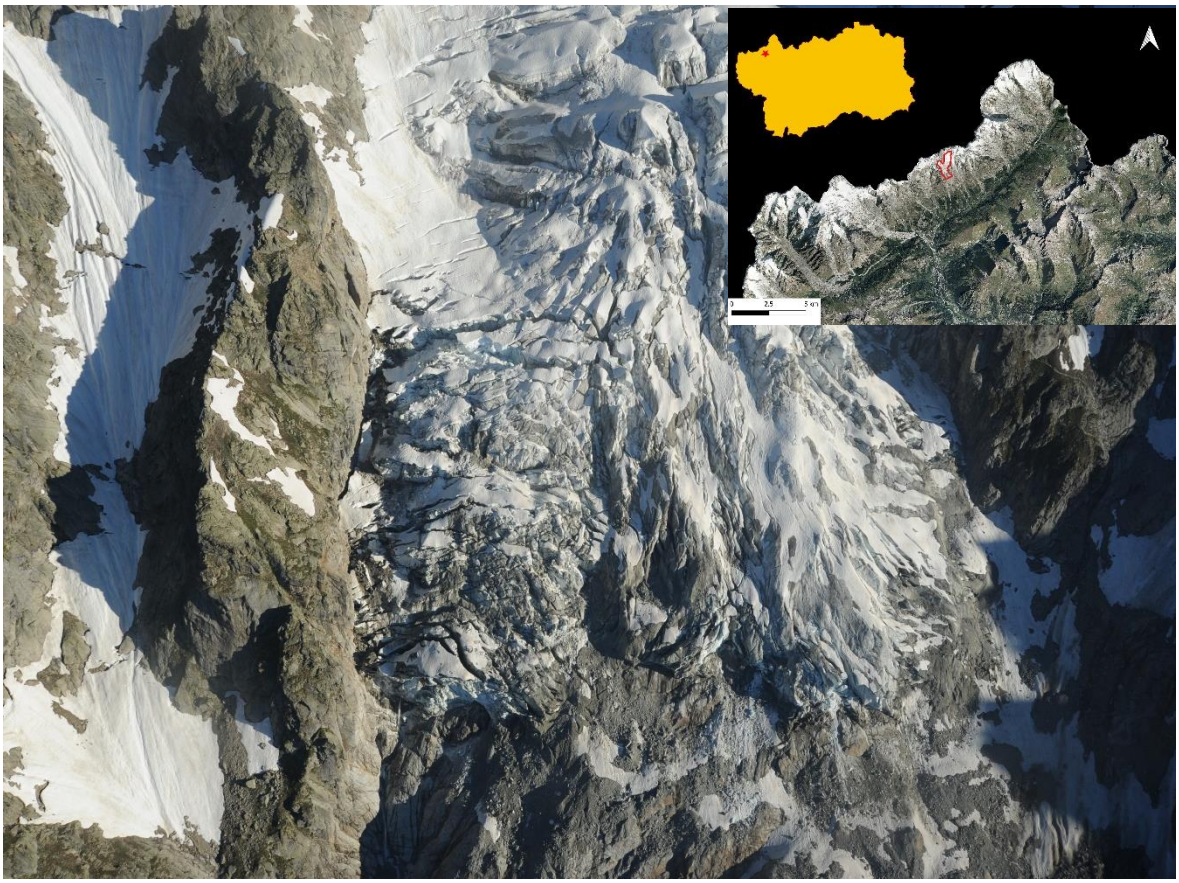

Figure 7. The lower part of the Planpincieux Glacier, with the Montitaz Lobe to its right

Brenva Rock Spur

The Brenva Rock Spur is located at the head of the Brenva Glacier, on the southeastern slopes of the Mont Blanc summit (Figure 8). The southeastern side of Mont Blanc is constituted of high granitic peaks affected by different degrees of fracturing. In the past hundred years, two major ice-rock avalanche events took place on the Brenva Glacier involving volumes of more than 2*10^6 m^3. In September 2016, a volume of 35,000m^3 detached from the previous rock avalanche

scar and was deposited on the higher part of the Brenva Glacier (Deline, Akçar, et al., 2015). This new event has pushed Aosta Valley Autonomous Region's authorities to investigate in more detail the 'Sperone della Brenva' rock mass. During autumn 2017, deformation of the rock wall was monitored with a ground-based InSAR system. No significant mass movement was detected, nevertheless three rockfall events occurred between July 2017 and October 2018, indicating that some activity remains. Some specific monitoring activity was subsequently initiated. The presence of leaking water on the rock wall has been observed, suggesting that the interaction between permafrost and melted water influences greatly the stability of the Sperone della Brenva. Repeated aerophotogrammetrical surveys have been performed yearly. Point clouds have been analysed in order to analyse potentially unstable volumes of the rock mass via a structural analysis of the rock face. Yearly rockfall volumes were also calculated by differencing the single point clouds. By combining all these observations, the scenarios have been ranked in terms of hazard level. If the collapse of mid-volumes of about $1*10^5$ m^3 is rather likely the failure probability is lower for larger volumes. However, due to global warming and annual snow cover variations, the monitoring (measuring instruments and/or monitoring activity) needs to be continued in order to permanently re-evaluate the probability of failure of each scenario. The monitoring systems adopted are, as of now, composed of a digital optical system capable of detecting movement and triggering alarms in case of rockfalls (Geosurveyor system); a temporary GBInSAR acquisition is made every summer for a couple of months depending on snow on the ground; a photogrammetric survey of the failure scar is performed every year. The very small displacements recorded by the GbSAR acquisition maintain a medium to low level of attention to this specific site. If an increase in rockfall activity is detected, a rise in monitoring procedures can be undertaken with 24/7 GbSAR installation or other early warning solutions.

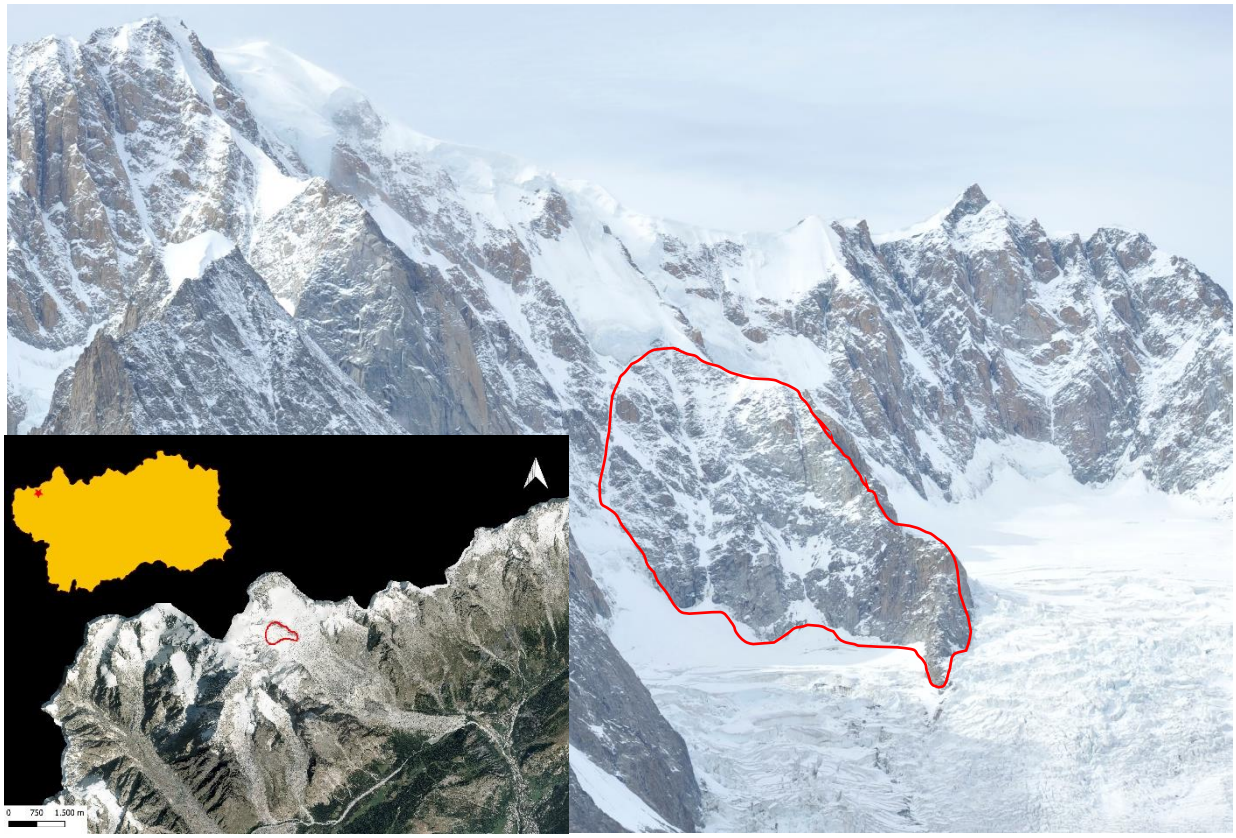

Figure 8. The south side of the Mont Blanc with the Brenva Rock Spur evidenced in red

Grand Croux glacial lake

The Grand Croux Centrale Lake is a proglacial lake that has started forming since 2000 on the left snout of the Grand Croux Centrale Glacier, located in the Valnontey Valley (in the municipality of Cogne, Aosta Valley Region) (Figure 9). The lake gave evidence of a subglacial outburst flood (GLOF) in 2016, when local authorities documented it and more than sixty people had to be evacuated from the lower valley area as bridges had been blocked by the flood wave (Giordan, Adams, et al., 2020). After this first recent event, regular observations of the lake formation began via Sentinel 2 satellite optical image monitoring. Even though the lake did not form again in 2017, observation of Planetscope satellite optical images in 2018 was useful for the identification of the lake formation in late spring. Because of the potential risk of another GLOF and the steady water volume increase due to glacial melt and the lake surface increase, a plan for a possible artificial lake drainage was made. A first water level lowering via pumping was performed during August 2018 and a permanent drainage channel that halved the lake volume was excavated at the end of summer 2018.

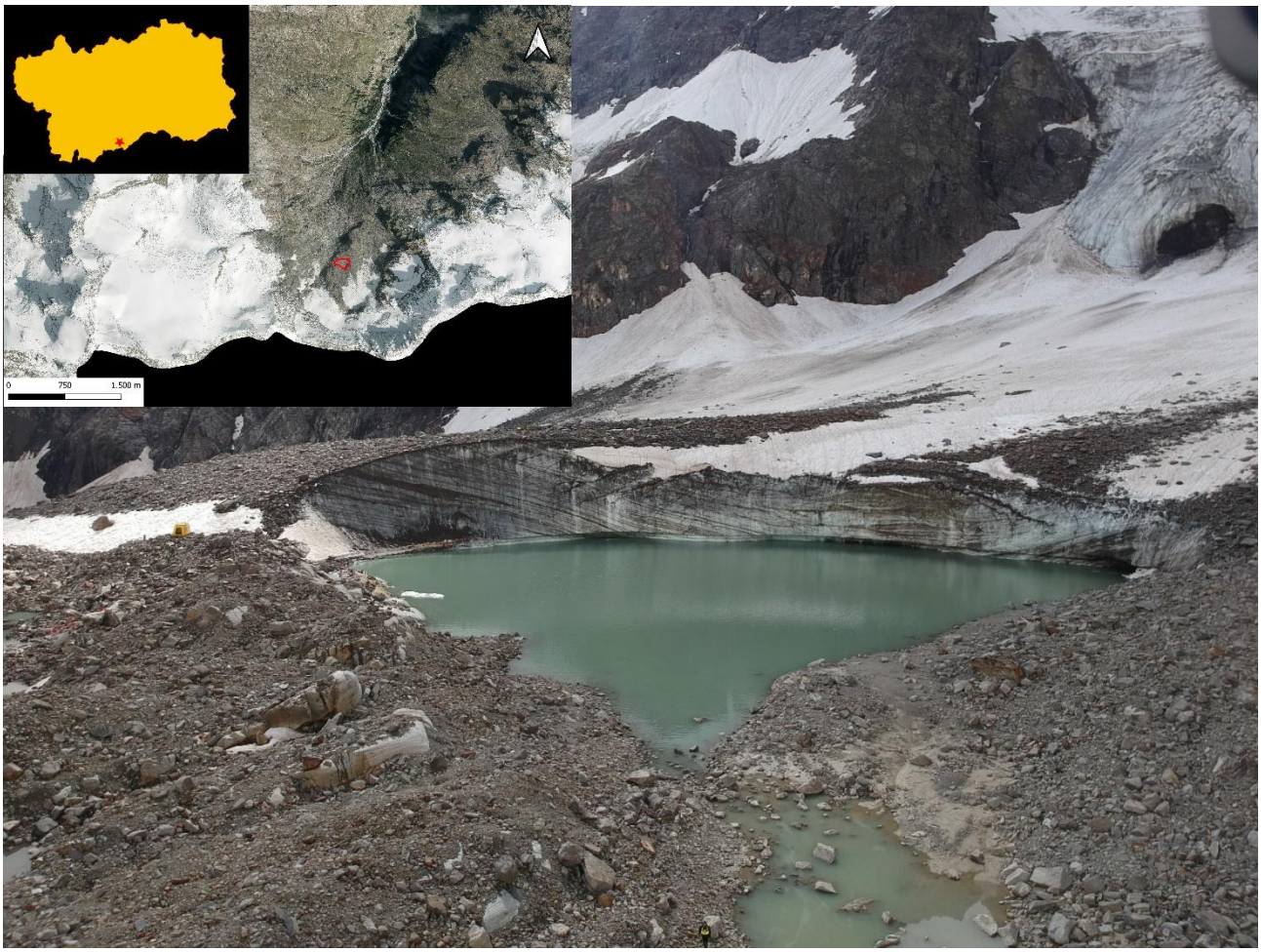

Figure 9. The central Grand Croux Glacier and its glacial lake

2. Materials

Many of the datasets used in the present work derive from archived datasets from the glaciological monitoring activity of the Fondazione Montagna Sicura; when deriving from other sources, data attribution is cited accordingly. The principal datasets used in the present study are summarised in the following paragraphs. Specific smaller datasets used in specific studies are detailed in the materials chapter of every single manuscript of the paper collection presented in the PhD thesis.

The glacial risk monitoring plan in the Aosta Valley region

The Fondazione Montagna Sicura has managed a regional glacial risk monitoring plan on behalf of the Aosta Valley region since 2012. The strong relations with the glaciology section of ETH Zurich began in 1997, before the start of the foundation's activities, with a direct link between the ETH and the Regione Autonoma Valle d'Aosta (Aosta Valley autonomous region). The first case study of glacial risk in Aosta Valley is, in fact, represented by the Whymper Serac ice avalanche monitoring of 1998 (Margreth & Funk, 1999) (Faillettaz et al., 2016). In 2009, the monitoring of the Whymper Serac on a 24/7 basis begun, becoming the first site-specific, high-frequency glacial risk monitoring plan in the Aosta Valley region and in Italy (Margreth et al., 2011). Together with the expertise of Prof. Martin Funk, a full Regional Monitoring Plan of Glacial Risk was set up in order to cover the entire regional area with low frequency monitoring and to have a framework to implement site-specific, high-frequency monitoring if needed (Schindelegger, 2019). The structure of the plan was built on experience from the Swiss territory, where a certain number of sites and events had been monitored in recent decades (Huggel et al., 2004). The very first large-scale action, started by the Fondazione in 2005, was the institution of a regular regional glacier inventory update with the aim of having a more frequent update of the inventory, compared to the national and global inventories, and that would serve as the database on which to construct the regional glacial risk monitoring plan. The second large-scale action comprised in the plan was the scheduling of a yearly screening of all the glacial bodies in the region, by means of a photographic helicopter flight over the whole regional area. It was during one of these flights that a potentially large instability was identified at Planpincieux Glacier in Val Ferret (Courmayeur). A prospective knowledge monitoring plan had been conceived and setup during 2012 and 2013, and since 2014 eventually became operational with the installation of monitoring time-lapse cameras (still ongoing) and, later, the installation in 2019 of GBInSAR instrumentation for high-frequency monitoring and a Doppler radar system for early-warning monitoring due to an exacerbation in the accelerations of the unstable glacier front. Since 2012, the regional glacial risk monitoring plan has been officially mandated from the Aosta Valley region to the Fondazione Montagna Sicura every year until the present.

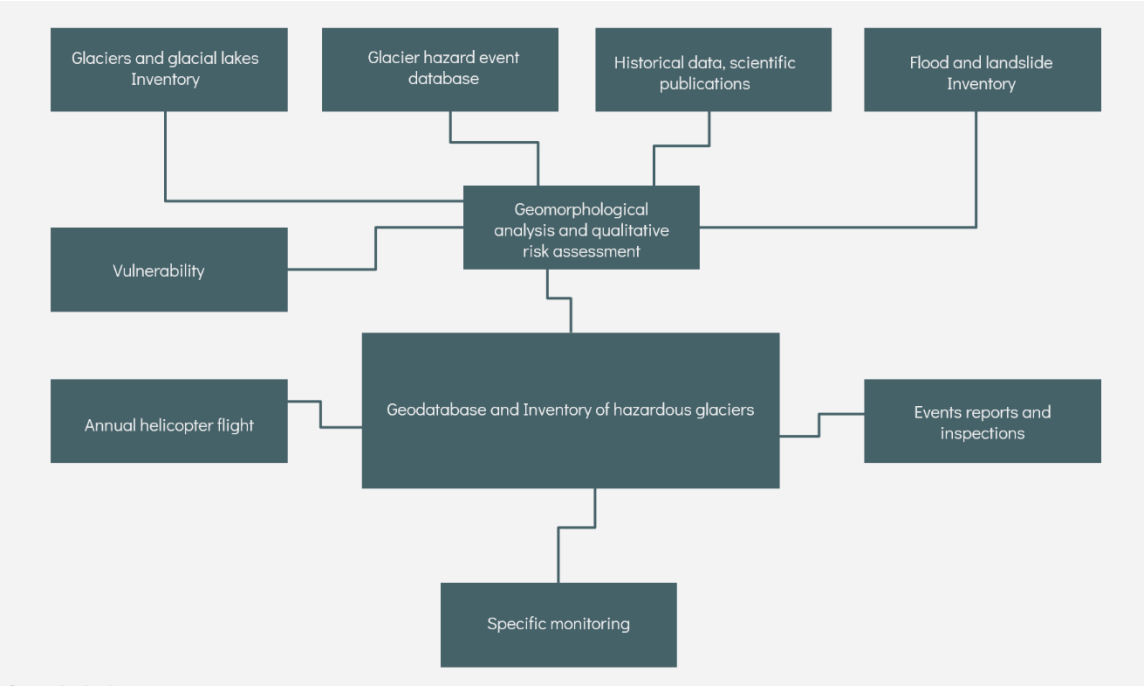

Figure 10. Workflow of the regional glacial risk monitoring plan.

The monitoring plan can be summarised by the workflow above (Figure 10)

- The regional glacier inventory is the main database on which all further analysis is performed. It is updated whenever aerial photogrammetric flights are performed over the region (4-6 years on average). Both glacier outlines and glacial lake shapefiles are produced and attributes are filled according to international guidelines.

- A secondary database from which information is integrated is the regional database of mass movements, which is constantly updated by the Autonomous Region of Aosta Valley, when phenomena occur in glacial and periglacial environments.

- In addition to these two large databases, the Fondazione Montagna Sicura maintains and updates an archive database of historical data and scientific studies performed in the region regarding glacial and periglacial hazards.

- The geo-referenced information of the above-mentioned database is included in a Geographic Information System (GIS) database.

- A preliminary qualitative assessment of the vulnerability is performed with the integration of the digitised information of the human structures and infrastructures present on the territory.

- A subset of the glaciers from the regional glacier inventory, which had had impacts in the past or, potentially, may have impacts on people and structures because of glacial hazards, form a class denominated 'Potentially hazardous glaciers' which have a single specific descriptive data sheet for each glacier.

- The database of 'Potentially hazardous glaciers' is updated every year by means of a yearly photographic helicopter flight.

- A great yearly input derives from events documented by alpine guides, mountaineers, geologists and other professionals who frequent the mountain environment, and that are communicated to the Autonomous Region of Aosta Valley. The regional offices forward them to

the Fondazione Montagna Sicura, which, in turn, evaluates whether they may need further investigation.

- At sites where a high-level of possible impact is detected, specific investigations and specific monitoring sites are activated. Specific safety concepts are developed together with a numerical simulations analysis and closure zones mapping when needed (Margreth et al., 2017).

Time-lapse cameras

Time-lapse cameras (TLCs) were installed in August 2013 and 2016 to monitor the Planpincieux Glacier (Giordan et al., 2016) and Whymper Serac, respectively. The TLCs were placed on the Mont de La Saxe crest (2300m a.s.l.) and at Pointe Helbronner (3400m a.s.l.). The TLC distances from the respective glaciers are approximately 3800m and 4800m, respectively. The monitoring station of the Planpincieux Glacier comprises of a UMTS modem, a DSLR Canon EOS 700D equipped with a 297mm lens (another TLC targets the Planpincieux Glacier with a 120mm lens), a Raspberry-Pi 3 computer, a fan heater, a power module composed of several solar panels, a backup battery and two surveying webcams. The TLCs are mounted on a cemented pillar independent from the shelter box. This means minimum misregistration, even in the presence of strong winds. Occasionally, bad weather and snow cover cause a system stand-by, but it reactivates autonomously. The monitoring station is completely autonomous and it is remotely accessible. The TLCs acquire with hourly frequency and the images are transmitted using a UMTS connection. We experimented with both auto and manual focus modalities for image acquisition. The advantage of the former is that, in general, the photographs are sharper, while using manual focus they are frequently blurred. On the other hand, autofocus may fail in the presence of slight condensation on the viewing window. To solve this issue, we equipped the monitoring station with a fan heater that eliminates the condensation. In the end, we opted for the autofocus acquisition mode because image blurring affects DIC results (Dematteis & Giordan, 2021). Since DIC suffers from surface shadow pattern change (Schwalbe & Maas, 2017) (Travelletti et al., 2012), we implemented an automatic machine learning-based procedure to autonomously select and process the images acquired in diffuse illumination conditions (Dematteis et al., 2019). Thereby, we significantly reduced the human efforts required to monitor the glacier continuously. Images are used to apply the DIC using the spatial cross-correlation calculated in the Fourier space. In 2020, we adopted the zero-mean normalised cross-correlation metrics. This latter method is computationally demanding but it is less affected by environmental noise (Dematteis & Giordan, 2021). The TLC that targets the Whymper Serac is a DSLR Canon EOS 1200D equipped with a 400mm lens. The TLC acquires photos in auto-focus mode. The monitoring system is connected to the power grid and transmits, depending on the season, one to four images per hour via a WiFi connection. The shelter box is mounted on the metallic pillars of the Skyway cable car station of Pointe Helbronner. We observed strong image misregistration. The image registration was hampered by the presence/absence of snow on the stable surfaces that were adopted as reference. To partially reduce this hindrance, we adopted the cosine similarity method (Dematteis & Giordan, 2021), which proved to be less affected by this issue. The pixel footprints of the TLCs are approximately 54mm px^{-1} and 52mm px^{-1} (Planpincieux Glacier and Whymper Serac images, respectively). The TLC that monitors the Planpincieux Glacier acquired more than 23,500 photographs between August 2013 and December 2020, while that of the Whymper Serac acquired more than 10,500 images between August 2016 and December 2020. The time-lapse time series of the Planpincieux Glacier and Whymper Serac are among the longest continuous glaciological TLC surveys worldwide.

Robotic total station

An RTS Leica TM30 was installed in the Planpincieux hamlet in 2010 to monitor the Whymper Serac, acquiring a measurement every two hours. The Whymper Serac is approximately 4800m from the RTS and the elevation difference is 2400m. This distance is beyond the declared operational range for the automatic target recognition acquisition mode, which is 3000m for standard prisms (Leica TM30 Technical Data. Available online: https://w3.leica-geosystems.com/downloads123/zz/tps/tm30/brochuresdatasheet.pdf (accessed on 1 February 2021). For this reason, often, not all targets were detected during a single measurement session. The declared accuracy by the manufacturer at a distance of 4800m, is approximately 8mm. A network of several prisms (with an optimal view angle of 40° for both the horizontal and vertical axes) was arranged on the Whymper Serac with the aid of alpine guides. To minimise the risk of losing the prism visibility for the tilting/rotation of the supporting pole, we adopted V-shaped bars that prevent rotation along the z-axis; furthermore, in October 2020, we installed a prism with 360° and 120° view angles along the z- and x-axes, respectively. Due to logistic difficulties, only two reference prisms were installed in the surrounding bedrock. The exceptionally high-mountain conditions caused a frequent loss of prisms, and in-field interventions to replace or substitute missing targets were often necessary. A total of 42 prisms have been installed on the Whymper Serac surface since 2010. Over this period, on average, 2-5 prisms were concurrently present. The RTS collected more than 26,000 measurement epochs and approximately 15,000 had at least one reference prism available. The RTS dataset of the Whymper Serac is likely one of the longest continuous time series of a glacier worldwide. The extreme weather conditions and the critical operational range introduced high noise to the RTS measurement. To analyse the RTS data before the 2014 break-off, Faillettaz and others used a robust method to filter most of the artefacts in the data (Faillettaz et al., 2008).

Terrestrial radar interferometry

In the Grandes Jorasses area, six experimental TRI campaigns have been conducted since 2013. Among the different typologies of TRI apparatuses, three models of GBSAR – IBIS-L (IDS GeoRadar), FastGBSAR (Metasensing), and GBinSAR LiSALab (LiSALab) – and one RAR – GPRI (Gamma Remote Sensing) – were adopted. All the radars operated in Ku-band and provided VV polarisation; FastGBSAR additionally had fully polarimetric capability. All radars were installed in the Planpincieux hamlet in order to have the apparatuses connected to the power grid. The distances from Planpincieux Glacier and Whymper Serac were of 2500m and 4800m, respectively. Using the RAR, we also experimented with the positioning on the Mont de La Saxe crest, near the TLC monitoring system of the Planpincieux Glacier. In this case, the sensor-to-distance increased. The exceptional mountain environment introduced a series of data-processing issues (Monserrat et al., 2014) (Luzi et al., 2018). The variable atmospheric conditions and the large elevation difference caused a strong disturbance. Liquid and solid precipitation modified the surface scattering properties and caused data degradation. Therefore, we implemented specific methods to minimise the atmospheric effects and to remove corrupted data effectively (Dematteis et al., 2017). A further critical issue concerned the sensor-to-target distance. GBSAR devices have a limited operational range, up to 4-5km. Therefore, *ad hoc* software/hardware adjustments were applied to monitor the Whymper Serac, e.g., the adoption of high-gain antennas. The long distances also affected the results' spatial resolution. The azimuth resolution linearly decreases with the range. Using the GBSARs, the resolution was approximately 10-15m for Planpincieux Glacier and 15-20m for Whymper Serac. Unlike the GBSAR systems, the RAR was affected less by the operational range due to its higher SNR, but its azimuth resolution was twice as coarse. Another issue concerned the radargrams' georeferencing, which was fundamental to evaluate the active glacier portions precisely. Therefore, we proposed a method based on the spatial correlation between amplitude maps and a digital terrain model, obtaining high georeferencing precision (Dematteis et al., 2018).

Satellite imagery

A relevant dataset largely used in the PhD project is **Esa Copernicus Sentinel-2** optical satellite imagery. The Sentinel-2 mission is composed of two twin satellites – Sentinel-2A and Sentinel-2B – orbiting on sun-synchronous orbits at an altitude of 786km. Free availability of 13 multispectral bands (443 nm-2190 nm central wavelengths) with ground resolutions ranging between 10m and 60m, a revisit time as low as three days for some areas (three days for most areas) and global coverage, make this product a very important resource for glaciological studies. In particular, Sentinel-2 near infrared band B08 processing level L1C is used for the application of feature tracking on glacial surfaces as suggested by previous studies (Paul et al., 2016). Based on different publications (Millan et al., 2019) (Paul et al., 2016) the geometric error of Sentinel-2 can show up to 1.5 pixel offsets in the horizontal plane. Therefore, an image co-registration process is normally needed for multitemporal analyses.

When high resolution imagery (0.5m-3m) was needed in the study, and mostly when stereo acquisition was needed to retrieve altitudinal information, we generally relied on commercial **AIRBUS Pléiades imagery**. The AIRBUS Pleiades satellite constellation is an optical satellite constellation providing very high-resolution products (50cm) with a 20km swath. Both the space and the ground segment have been designed to provide information in record time, offering daily revisit capacity to any point on the globe and outstanding acquisition capabilities. The Pléiades constellation is composed of two very-high-resolution optical Earth-imaging satellites – Pléiades-1A and Pléiades-1B – that were launched in December 2011 and 2012, respectively. The two satellites operate in the same phased orbit and are offset at 180° to offer a daily revisit capability over any point on the globe. The Pléiades also share the same orbital plane as the SPOT 6 and 7, forming a larger constellation with four satellites 90° apart from one another. Their orbit is sun-synchronous, phased, near-circular, and of a mean altitude of 695km. The multi-spectral detection is made with five detectors of 1500 pixels each: 13 µm wide. Each detector consists in four assembly lines, enabling four-colour imaging (blue, green, red, near infrared).

Drone photogrammetric surveys in this study were performed using two different drones: an Autel Evo 2 Enterprise quadcopter equipped with a 6K digital camera (sensor width of 1”). Images acquired during the surveys have a resolution of 5472x3648 pixels and the geocoding of the images was conducted in RTK mode using virtual base stations of the SPIN GNSS (www.spingnss.it). Also used was a Mavic 2 Pro UAV. It was equipped with a 4K Hasselblad digital camera shooting 20MP images with geotagging done on a classic GNSS system with no additional RTK or PPK corrections; surveys performed with this drone needed introductions of GCPs or co-registration with higher accuracy DEMs.

When **helicopter-borne photogrammetry** was performed, a Nikon **D850 camera** was used. The D850 is a full-frame digital single-lens reflex camera (DSLR) produced by Nikon. It features a Nikon FX format and a 45.7 megapixel back-illuminated (BSI) CM sensor. In order to Geotag (image positioning information of pictures such as latitude, longitude, altitude), a GPS Nikon GP-1 module was added to the camera. Geotagging was, therefore, written onto the Exif file of the images.

All the **GNSS** surveys performed in this study were carried out with a pair of Geomax Zenith 25 Pro receivers used in RTK survey mode and a Virtual Reference Station of the Spin GNSS network (Maltese et al., 2021).

3. Methods

3.1 Workflow methodology

At the beginning of the PhD project activity, a prospective research plan was conceived. The plan was structured as follows:

WP 1 'DATA': (wp1.1) Data mining. (wp1.2) Data back analysis. (wp1.3) New data acquisition

WP 2 'Development of innovative methods': (wp2.1) *In-situ* methods for accuracy assessment of remote sensed data. (wp2.2) Methods for hydrological monitoring in a glacial environment. (wp2.3) Application of developed methods

WP 3 'Management': (wp3.1) Improvement of risk assessment. (wp3.2) Sustainable management

While entering the first stages of the research activity, it was realised that some problems would arise in the prospective research plan that was presented. There were mainly two concepts in the 2.1 and 2.2 points that could, potentially, mislead the outcomes of the project owing to:

- Initially the focus of the WP 2.1 was stressing on the *in-situ* measures for the validation of existing remotely sensed datasets. It turned out that the available *in-situ* measurements were on the one hand abundant and presented acceptable uncertainties and coverage for a validation of remote sensed products, but, on the other, available, freely distributed global glacier velocity products obtained from remotely sensed data (Friedl et al., 2021) (Altena et al., 2019) were not suited to the context of alpine glaciers and both data quality and coverage in the areas of interest was none or very limited. Owing to this, we switched the core of the WP towards developing specific methodologies that could produce remotely sensed surface velocity datasets on the small alpine glaciers of our interest in the present study.

- Regarding WP 2.2, the focus was initially set to the methodologies for hydrological monitoring in a glacial environment; the topic is very relevant, mostly linked to the understanding of the processes leading to the destabilisation of temperate glacier tongues, but the approach to the problem highlighted a structure having two demanding advancement steps:

  - The first step would be the time-consuming operation of acquiring and setting up a hydrological measurement network on a specific glacial stream site (Frenierre & Mark, 2014). This task would be feasible in the project's three-year timeframe but this would not account for data processing and analysis, which would indeed be the core of the research activity.

  - The second step would consist in the acquired data analysis; this topic would be very relevant in trying to find correlations between glacier velocities and hydrological variations (Nanni et al., 2020), but in a best possible scenario we could plan one year for conception, one year for the setting up and calibration of instruments and one year of data acquisition. This prospective schedule does not leave any time to perform data analysis during the PhD project. Moreover, the estimation of the hydrological input part would need distributed ablation measurements (or the production of modelled data) that would have economic and human resources costs that go far beyond the possibilities of the present PhD project.

Considering the two abovementioned criticalities, we reworked the prospective research plan and followed an approach that can be summarised in the following workflow scheme:

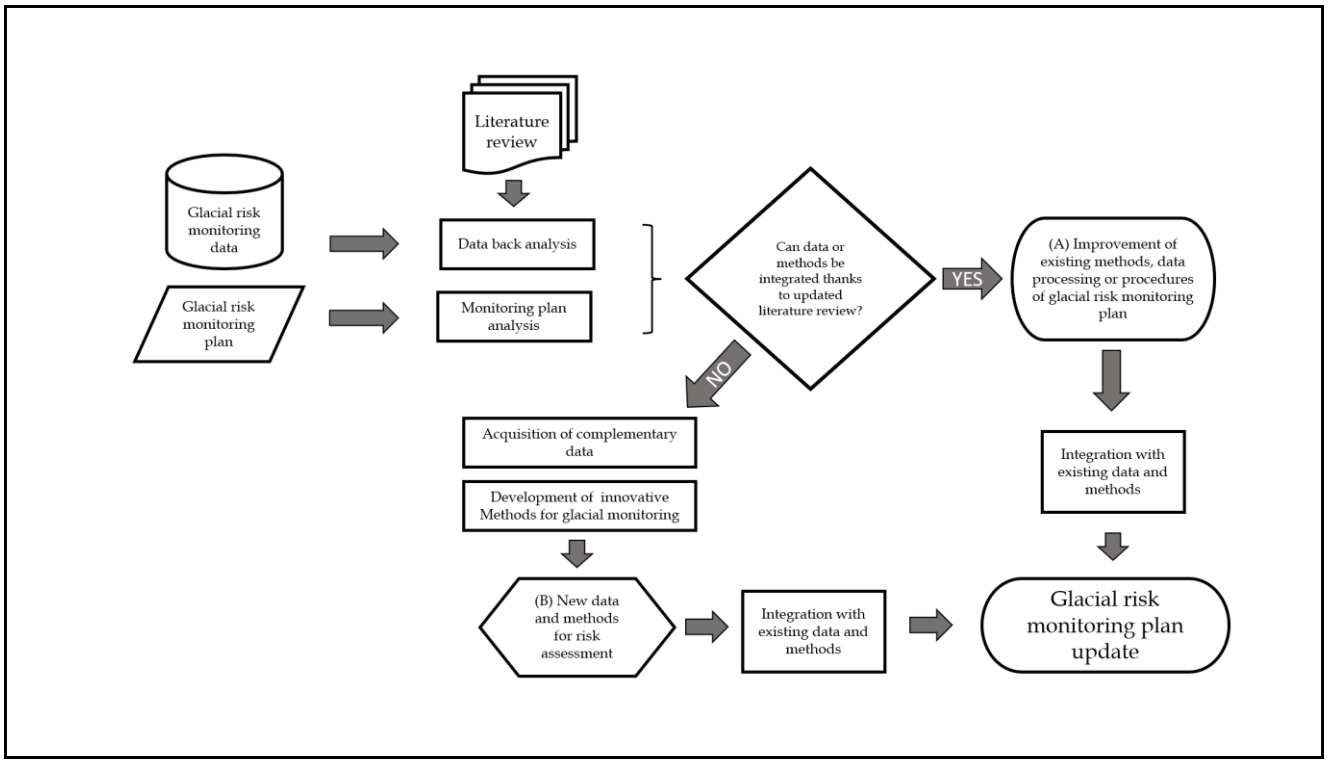

Figure 11. Research Workflow of the PhD project

The general workflow followed in the present study (Figure 11) can be summarised as follows:

- A specific literature review is performed in order to find recent advances in the field of glacial risk studies. We reviewed specific case studies, modelling studies focused on process dynamics and a special focus was centred on the techniques used in the monitoring of glacial instability processes and the current situation in this field.

- An analysis of the actual structure of the regional glacial risk monitoring plan of the Aosta Valley Region was undertaken after the updated literature review. A critical analysis was performed identifying weaknesses and possible improvements in the monitoring plan.

- A specific activity of data organisation and data back analysis was performed on datasets available in the archived data from the monitoring systems and activities of the glacial risk monitoring plan.

- At this stage, a choice of possible research topics to be further investigated was made:

(A) On one hand, activities, methodologies or other possible improvements that were highlighted in the literature review and that could be readily integrated in the glacial risk monitoring plan were summarised and organised for integration with plan. Summarisation and organisation of certain experimental activities that would require more time and finance than is available for the current PhD project activities would come into this category, for possible future further development.

(B) On the other hand, a series of activities that needed consistent experimental activity with the elaboration of new data acquisition and processing and the application of new methods for the monitoring of glacial environments, were chosen on a sustainability basis to possibly achieve some prospected results in the timeframe and economic feasibility of the actual PhD project.

- Research activity was undertaken to acquire and process new data and apply new methods to monitor the glacial environment. A series of results were obtained in the frame of elaborating new methods for glacial risk assessment.

- When possible, the integration of such new methods and the deriving data was integrated in the actual glacial risk monitoring plan.

- The integration of new data and methods in the glacial risk monitoring plan finally converges to an update of the actual monitoring plan.

3.2 Analytic methodologies used in this study

Every manuscript that will be presented in the results section has its own chapter dedicated to the methods used in that specific study, but we hereby highlight some of the methodologies that have been widely applied in a large number of the studies undertaken in the present PhD project.

Structure from Motion technique

Structure from Motion (SfM) is a photogrammetric range-imaging technique for estimating three-dimensional structures from two-dimensional image sequences that may be coupled with local motion signals. It is studied in the fields of computer vision and visual perception. SfM is a technique that sits between photogrammetry and computer vision and which uses overlapping images to reconstruct 3D surface models. It is a valuable research tool in geomorphology and related disciplines. Images can be collected with standard consumer-grade cameras, making SfM a low-cost tool that complements other, more expensive, 3D technologies such as terrestrial and airborne laser scanning (lidar). The high level of automation of SfM processing offers wide possibilities to describe earth surface processes. SfM has been applied to photogrammetric aerial drone acquisitions, helicopter borne acquisitions from digital DSLR cameras and to satellite borne stereo-mode acquisitions. We mainly applied SfM algorithms using two software suites (Agisoft Metashape and PCI Geomatica) that are briefly described in the following paragraphs.

Agisoft Metashape

Agisoft Metashape (previously known as Agisoft PhotoScan) is a tool for photogrammetry pipeline. We used this software when producing Digital Elevation Models (DEMs) and Ortho mosaics from drone or helicopter borne acquisitions of digital imagery. The software is available in Standard and Pro versions: the standard version is sufficient for interactive media tasks while the Pro version is designed for authoring GIS content. The software is developed by Agisoft LLC located in St Petersburg, Russia. The software is widely used in many fields of application from archaeology to earth sciences (Kingsland, 2020).

PCI Geomatica

PCI Geomatica is a remote sensing and photogrammetry desktop software package for processing earth observation data, designed by the PCI Geomatics company. The latest version of the software is Geomatica 2018. Geomatica is aimed primarily at faster data processing and allows users to load satellite and aerial imagery where advanced analysis can be performed.

Geomatica has been used by many educational institutions and scientific programmes throughout the world to analyse satellite imagery and trends, such as the GlobeSAR Program, a programme which was carried out by the Canada Centre for Remote Sensing in the 1990s. The software has been used in this study to perform satellite stereo pair DEM extraction and orthorectification of satellite imagery. This pipeline has already been tested in literature studies in a glacial environment (Berthier et al., 2014)

QGIS

QGIS is a free and open-source cross-platform desktop geographic information system (GIS) application that supports the viewing, editing, printing, and analysis of geospatial data. QGIS functions as geographic information system (GIS) software, allowing users to analyse and edit spatial information, in addition to composing and exporting graphical maps. QGIS supports raster, vector and mesh layers. Vector data is stored as either point, line, or polygon features. Multiple formats of raster images are supported, and the software can georeference images. QGIS integrates with other open-source GIS packages, including PostGIS, GRASS GIS, and MapServer. Plugins written in Python or C++ extend QGIS's capabilities. Plugins can geocode using the Google Geocoding API, perform geoprocessing functions similar to those of the standard tools found in ArcGIS, and interface with PostgreSQL/PostGIS, SpatiaLite and MySQL databases. The QGIS suite sees constant updates and plug-ins development from a huge global community, and specific packages for remote-sensed data analysis already exist (Congedo, 2021).

SAGA GIS

System for Automated Geoscientific Analyses (SAGA GIS) is a geographic information system (GIS) computer programme that is used to edit spatial data. It is free and open-source software, developed originally by a small team at the Department of Physical Geography, University of Göttingen (Germany) and is now being maintained and extended by an international developer community. SAGA GIS is intended to provide scientists with an effective but easily learnable platform for implementing geoscientific methods. This is achieved by the application programming interface (API). SAGA has a fast-growing set of geoscientific methods, bundled in exchangeable module libraries. It implements a wide array of tools for geospatial analysis, one of which is the IMCORR algorithm, widely used in earth sciences for Digital Image Correlation (Jawak et al., 2018)

SNAP

A common architecture for all ESA Sentinel toolboxes is being jointly developed by Brockmann Consult, SkyWatch and C-S: Sentinel Application Platform (SNAP). The SNAP architecture is ideal for Earth Observation processing and analysis due to the technological innovations such as: extensibility, portability, Modular Rich Client Platform, generic EO data abstraction, tiled memory management, and a graph processing framework.

DIC – Digital Image Correlation; GIV toolbox

DIC is a common technique used to measure surface displacements using proximal (Evans, 2000; Ahn & Box, 2010; Schwalbe & Maas, 2017) and remotely sensed imagery (Scambos, 1992; Heid & Kaab, 2012; Marsy et al, 2021; Dematteis et al., 2022). The processing chain performed in the present study uses the open-source Glacier Image Velocimetry (GIV) toolbox (Vries, 2021). GIV uses frequency-based correlation, can process large datasets efficiently and has been shown to perform well on glacier surface velocity measurements at different test sites (Vries, 2021). Co-registration of images is implemented in the GIV process chain using a stable area where

potential shifts are estimated. To measure glacier surface velocities, we adopted the 'multi-pass' option that has proven to produce velocity maps with a high signal-to-noise ratio. The correlation chip size is automatically defined by GIV. Then, the velocities of image pairs are averaged on a monthly basis. A temporal and spatial smoothing function is implemented in the processing algorithm and has been used in the processing of data in this study. To estimate the precision of the DIC measurement in our studies, we analysed the standard deviation of residual displacement on stable terrain (Dehecq et al, 2015).

4. Results

4.1 Literature review

The first result of the research activity was the performing of a wide literature review. This was carried out in order to understand the current situation in both the understanding of the processes involved in glacial hazards and in the techniques and methodologies used for the monitoring of such phenomena. The literature in this topic is not as wide as other fields of glaciology but there is a large number of papers dedicated to glacier destabilisations and glacier lake outburst floods. Many studies focus on the analysis of the processes and the analysis of case studies. Even if a consistent number of publications have dealt with different aspects linked to glacier instabilities, few have been dedicated to risk assessment or to methods or procedures that go in the direction of a real risk assessment framework. Although far from being complete, a short series of papers that can be considered milestones in the field of glacial risk assessment and monitoring are presented in the following chapter with a summary of their contents. The bibliography of each of those works contains extensive references for wider reading on specific subjects: the earlier works have references to historical studies that have been the pillars for the presented works, while the more recent studies may serve as a reference to other works in the same field of interest. A brief synthesis of the contents and the relevance of each article is reported hereby.

Ice avalanches: some empirical information about their formation and reach (Alean 1985)

We consider this study to be a starting point for the description and definition of ice avalanche phenomena, which make up a significant part in the field of glacial hazards. This practical study aimed to predict ice avalanche hazards, documenting approximately 100 ice avalanches, primarily from the Alps. The research categorised starting zones based on terrain features. Ice avalanches originating from lower-altitude zones, with uniformly inclined bedrock planes, were more common in summer and autumn while no such seasonal pattern was observed for other starting zones at higher altitudes or involving abrupt bedrock gradient changes. Testing one- and two-parameter models to estimate run-out distances indicated only modest improvements with the introduction of the second frictional parameter. For shorter run-out distances (several hundred metres), an alternative terrain-based estimation method was suggested.

Assessing risks from glacier hazards in high mountain regions: some experiences in the Swiss Alps (Haeberli 1989)

The relevance of this work resides in it being one of the few studies to date in specific literature dealing with the risk assessment of glacial hazards. Evaluating glacier hazard risks concerning

the safety of settlements and infrastructure in high mountain regions relies on experience from past incidents and simplified rules based on glaciological principles. Estimating the characteristics of steep, largely unmeasured glaciers involves a parameterisation scheme. Factors like glacier length, ice avalanches, and glacier floods must be considered over several years to decades. This systematic assessment leads to the creation of maps indicating potentially hazardous zones. Although Alpine communities have long faced glacier hazards, modern construction, particularly in tourism development, encroaches on previously avoided high-risk areas. Assessing glacier hazards involves comparing them with other mountain hazards such as avalanches, landslides, rockfalls, and storm-induced floods. Determining acceptable risk levels is challenging and is often influenced by political and economic factors rather than purely scientific criteria.

Hazard mapping for ice and combined snow/ice avalanches - two case studies from the Swiss and Italian Alps (Margreth 1999)

What is remarkable and very useful for the present work in this paper, is the presentation of a framework with practical examples in respect to the realisation of both hazard-mapping and consequent safety plans. In September 1996, a glacier ice release from Gutzgletscher in the Bernese Alps caused two large powder avalanches, blocking a road and injuring three people. The avalanche history of Gutzgletscher is well-documented. In another case in January 1997, a section of a hanging glacier in the Mont Blanc Massif broke off, with predictive measurements foreseeing the event. An evacuation was considered due to the potential for snow avalanches triggered by the ice masses. However, the break-off occurred after snow stabilisation, resulting in no further avalanches or damage. Hazard maps and safety plans were prepared by the Swiss Federal Institute for Snow and Avalanche Research (SLF) and the Laboratory for Hydraulics, Hydrology, and Glaciology (VAW). These case studies illustrate the challenges and principles of ice avalanche hazard assessment.

An assessment procedure for glacial hazards in the Swiss Alps (Huggel 2004)

In trying to propose a procedure for the assessment of glacial hazards, this work contains many hints that were integrated in the conception of the glacial risk monitoring plan of Aosta Valley. This text discusses assessing glacial hazards in populated mountain areas like the Swiss Alps, emphasising the importance of considering fundamental glaciological, geomorphological, and hydraulic principles and learning from past events. The proposed approach aims to determine maximum event magnitudes and probabilities. Magnitude analysis draws from empirical data in the Swiss Alps and other mountain regions, while estimating probabilities is challenging due to dynamic glacial systems and infrequent events. Qualitative indicators, like dam features and avalanche patterns, help specify probabilities. Applied to real cases in the Swiss Alps, the results offer reasonable estimates not exceeded by actual events, providing valuable initial hazard assessments for dynamic mountain environments with growing populations and infrastructure.

Assessment principles for glacier and permafrost hazards in mountain regions (Allen 2017) - GAPHAZ

As stated in the introduction, this study is a guide for anyone interested in glacial hazard assessment and, therefore, represents a milestone in this field of studies. This text discusses glacier and permafrost hazards in cold mountain regions, influenced by climate-driven changes in the alpine cryosphere. These hazards range from minor icefalls to major disasters like glacial lake outburst floods (GLOFs), posing risks to downstream communities and infrastructure. The hazard assessment comprises two key aspects: (i) susceptibility and stability assessment, which

involves analysing various factors, including atmospheric, cryospheric, geological, geomorphological, and hydrological elements, to determine the likelihood and origins of these hazards. (ii) Hazard mapping: this component combines process modelling and field mapping to predict potential impacts downstream, forming the basis for decision-making and planning. Historically, glacier and permafrost hazards gained attention after notable disasters in the mid-20th century in places like the Peruvian Andes, Alaska, and the Swiss Alps. Initial assessments were reactive, focused on understanding the causes and mitigating ongoing threats. These incidents underscored the importance of considering complex geosystems and cascading processes, highlighting the cumulative downstream effects. Today, advances in satellite imagery enable a proactive approach to hazard assessment. It starts with a regional-scale susceptibility analysis and modelling to identify unstable slopes or hazardous lakes. Detailed field investigations and hazard mapping concentrate on high-priority areas. Given the rapidly changing mountain environment, forward-looking scenarios are crucial, accounting for emerging threats like new lakes in deglaciating regions. Even though planning for low-probability, high-magnitude events is challenging, they should be considered in comprehensive hazard assessments for effective preparedness.

Avalanching glacier instabilities: review on processes and early warning perspectives (Failletaz 2016)

One of the few studies that exist to date which is focused on the monitoring possibilities of glacial instabilities. Avalanching glacier instabilities, which can lead to significant disasters, have been the subject of extensive study. Recent efforts in monitoring, analysis, and modelling have improved our understanding of destabilisation processes and enhanced early warning capabilities. This paper reviews these advancements. Three types of instability are identified based on the ice/bed interface's thermal properties. In cold conditions, precursory signs such as surface velocity changes and passive seismic activity allow for the prediction of a final break-off event. When meltwater is involved due to partially temperate interfaces, no clear precursory signs exist and monitoring the thermal regime is essential. Steep temperate glacier tongues can switch into an ‘active phase’, with major break-offs occurring rarely, making predictions challenging but identifiable under certain critical conditions.

Glacial lake outburst floods threaten millions globally (Taylor 2023)

Glacial lake outburst floods (GLOFs) pose a significant threat, with an increasing number of glacial lakes appearing globally since 1990. Approximately 15 million people are exposed to potential GLOF impacts, with the highest exposure in High Mountains Asia (HMA), where around a million people live within 10km of glacial lakes. India, Pakistan, Peru, and China collectively account for over half of the globally exposed population. While HMA is most at risk, the Andes region also presents concerns, with significant GLOF potential but comparatively fewer research studies.

The literature review performed was compared to the actual structure and the actual methodologies that are being applied in the glacial risk regional monitoring plan of Aosta Valley. Together with the literature review, a comparison with the guidelines highlighted in the Gaphaz guidance document was performed in order to identify criticalities or points of possible improvement in the existing procedures. An important result of the PhD project was, therefore, the individuation of criticalities in the general workflow as well as in the specific monitoring

regarding the actual structure of the Regional Monitoring Plan of Glacial Risks in the Aosta Valley Region. This analysis is summarised in the following chapter.

4.2 Analysis of the criticalities of the glacial risks monitoring plan and site specific monitoring

Monitoring plan

A first criticality of the large-scale monitoring, in the context of very rapidly evolving glaciers, is the rapid outdating of glacier outlines and the rapid formation and expansion of glacial lakes. The consequence is that when a possible instability is documented, the reference cartography may have large mismatches with the actual situation in the field. A second point is the very low acquisition frequency of the annual helicopter monitoring flight. During a given year, an instability may arise only for a few months and not be seen on the exact day that the survey is undertaken. The monitoring flight should be not eliminated because it can still individuate important indicators of potential instabilities, but an objective of the present study is to evaluate the existence of alternative approaches. The environmental impact of a 3–4-hour helicopter flight should also be considered, as well as its cost.

Grandes Jorasses

The main criticality of the historical monitoring system is the need for costly and dangerous periodical field missions to the top of the serac, at 4200m, to install stakes with reflective prisms. These are used in topographical monitoring via a total station. The predictive methodology applied is known to be effective as long as the basal thermal regime of the serac is of a cold type, as measured in 1997. The second, and possibly major critical point, is the possibility that the actual evolution of climate could be leading to a transition towards a polythermal state of the ice-bedrock interface at the base of the serac, and in the mid-term to a full transition to a temperate basal thermal regime. The basal friction of a temperate based glacier would not be enough to maintain the stability of the serac with such a slope and geometry. Moreover, a failure from the base of the serac would involve a larger volume than was destabilised historically, and the predictive method used historically would not be effective in the prediction of a polythermal of temperate based glacier destabilisation. Last but not least, a warming condition could lead to an accumulation of liquid water inside the serac or in the bergschrund. This could lead to a sudden, unpredictable rupture that would entrain a mixture of ice and water with much larger run-outs than those of an ice avalanche involving ice only.

Planpincieux Glacier

The main criticalities that we found on the monitoring of the Planpincieux Glacier were:

- The monitoring system monitors just a small part of the glacier.

- There is a lack of literature data on the velocity variations of destabilising, avalanching temperate glaciers in the Alpine environment.

- A time-of-failure predictive model has never been successfully tested in literature studies for temperate glacier tongues.

The problem linked to the unpredictability of the failure of a temperate ice mass is assessed in literature studies such as Faillettaz et al. (2015) and Faillettaz et al. (2012). Indications that accelerations can still be indicative of large glacier instabilities in temperate glaciers has been observed at Allalin Gletscher (Faillettaz et al., 2012), Trift Glacier (Meier et al., 2018) and, for the failure of smaller volumes, at Planpincieux Glacier (Giordan, Dematteis, et al., 2020). The problem encountered with the monitoring of accelerations of a temperate glacier is that often a suspect acceleration that provides an indication of an upcoming time of failure may restabilise via a complex equilibrium determined by variations of basal water pressure. This enhances or reduces basal friction and thus velocity of the ice mass. Such behaviour has been documented at Planpincieux Glacier, but there is little data available in literature from potentially unstable temperate glaciers and for monitored temperate glacier destabilisations and failures.

This makes monitoring very challenging, with the persistence of false positive detections of accelerations and very little data to determine velocity thresholds, or acceleration thresholds, for the activation of early warning and civil protection safety plans.

Brenva Rock Spur

The Brenva Rock Spur instability is a good example of a high mountain cascading process. On this specific study site, two very large ice-rock avalanche phenomena have been documented in the last century, causing both damage and casualties in Val Veny, near the hamlet of Entrèves. The events occurred in 1920 and in 1998. Both have been analysed in detail in the literature (Deline, Akçar, et al., 2015) that have carefully reconstructed the sequence of episodes that led the destructive mixture of rock, ice and snow reaching the bottom of the valley. The Regional Geological Survey is in charge of the monitoring of rock instabilities in the Aosta Valley Autonomous Region; nonetheless, as the instabilities on the rock faces on this site can trigger cascading processes involving ice and snow, the Fondazione Montagna Sicura has participated in the conception of the actual monitoring concept and in the dynamic modelling part of the study. The main criticalities of this monitoring were the lack of a specific structural analysis that would identify specific rock volumes potentially prone to failure and the lack of an updated topography of the Brenva Glacier to correctly run the dynamic models of the possible rock failures and subsequent ice-rock avalanches.

Grand Croux GLOF

The active intervention that was realised at Grand Croux lake means that this monitoring site, momentarily, does not top the list of the criticalities in the monitoring plan as, in the present conditions, the actual GLOF events are of a known magnitude. This is slowly increasing and provides a decadal timescale for an implementation of the actual solution; should further intervention be required in the future, the solution will be costly but feasible. It would involve the deeper excavation of a drainage channel or the study of an excavation on the ice dam, a plan which already has been carried out on similar sites around the Alps (Lac de Plaine Morte-CH, Lac des Bossons-FR). (Ogier et al., 2021)

After the critical analysis of the monitoring plan and the specific monitoring sites, a series of prospective research activities that could significantly improve the existing procedures was produced.

We divide the activities into two categories:

A) Improvement of existing methods, data processing or procedures of the glacial risk monitoring plan.

When existing data or existing methodologies could be significantly improved with the application of methods already existing in the literature, we readily structured integrations of the existing plan with updated procedures in the glacial risk monitoring plan.

This did not need specific experimental activity so it is briefly summarised in the following chapter. Although it does not represent the main experimental activity of the PhD project, it nonetheless produced significant improvements with relatively little research effort, so it still is relevant to be introduced here.

Some research activities that are included in this category were identified as being very relevant and readily feasible, but were considered to be too wide-ranging or requiring too much time or financial investment to be accomplished in the course of a three-year PhD; for this reason, we give a brief description of such research activities that were identified and conceived in the preliminary part of the present study but that were then inserted into other research projects in order to secure additional funding and a longer time span in order for them to be accomplished. The writing of the framework of such projects is also a relevant result of the present PhD project.

B) New data and methods for risk assessment

When we did not find a concrete answer to a specific criticality in the monitoring plan that was highlighted, we selected a series of research topics that could be further investigated in the temporal and economic feasibility constraints of the three-year PhD project.

With the abovementioned structure in mind, a critical analysis of the actual monitoring approaches and two distinct approaches to investigate the possible solutions of the identified criticalities were composed: (A) Immediate solutions to be readily integrated without further development and solutions that aren't sustainable in the PhD project, and (B) Solutions that need further research, new data and new methods, to be developed in the present PhD project.

In this framework, a research plan with distinct and well-defined research actions was conceived and is highlighted in the following paragraph.

4.3 Research plan to cope with criticalities of the monitoring plan and site-specific monitoring

Some specific research activities could be planned in order to cope with the criticalities highlighted in chapter 4.2. Prospective specific research actions are synthesised as follows:

Monitoring plan

One of the major objectives of the research activity of this PhD project was the possible integration of remote-sensed data to support the management of the regional glacial risk monitoring plan. The great advantage of remotely sensed data is the simultaneous coverage of very large areas and the much higher frequency of available data acquisitions compared to the annual helicopter flight. To cope with the rapid outdating of glacier outlines in the regional database, the integration of a periodic update by the manual digitisation of glacier outlines based on Sentinel-2 imagery could be planned.

Grandes Jorasses

An initial act that could be carried out to improve the monitoring systems of the Whymper Serac is the coupling of a GBInSAR instrument as well as an analysis of high-resolution time-lapse imagery to monitor the surface velocities of the Whymper Serac ice mass. Radar measurements and digital image correlation measurements could be integrated into the historical topographic monitoring.

As many experimental and monitoring activities had been carried out at different times and by different researchers on the Whymper Serac (including on Planpincieux Glacier, see the paragraph below) we dedicated the first part of the PhD research activity to data re-analysis and data organisation. This part of the work led to the publication of the paper: 'Ten-Year Monitoring of the Grandes Jorasses Glaciers Kinematics. Limits, Potentialities, and Possible Applications of Different Monitoring Systems' (Dematteis et al., 2021), which is the first paper presented in the collection of papers based on the present PhD project. This was a structured methodological approach in order the have a well-organised database of activities, measurements and the relative data on two of the most specifically monitored sites in the monitoring plan.

Planpincieux Glacier

In the frame of the actual monitoring and research actions at Planpincieux Glacier, we identify two main priorities:

(i) To better characterise the variations in velocities of the entire Planpincieux Glacier

(ii) To better characterise the variation in velocities of adjacent and/or similar glaciers to the Planpincieux Glacier.

As for the Whymper Serac, at first, before exploring the research activities of points (i) and (ii), we dedicated an initial part of the PhD research activity to data mining and data organisation (see more in the results chapter (Dematteis et al., 2021)). Moreover, the possibility of the triggering of cascading processes could be a research topic to be integrated in the existing monitoring plan.

Brenva Rock Spur

In order to improve the risk assessment of the Brenva Rock Spur, some actions could be put together to better characterise this specific monitoring site:

- The processing of all the photogrammetrical surveys carried out between 2016 and 2021.

- A structural analysis based on SfM photogrammetrical point clouds and the derivation of possible unstable rock volumes.

- To try to define a volume/frequency relationship for the rockfall volumes calculated by means of multitemporal point cloud analysis.

Grand Croux GLOF

In order to better characterise the Grand Croux lake GLOFs and their evolution, the execution of one yearly drone photogrammetrical survey in order to monitor lake expansion, water volume calculation and characterise the melt rates of the lake's ice dam could be scheduled in the future. GLOFs as a general topic could be tackled with a regional monitoring approach based on the monitoring of NDWI maps obtained by Sentinel-2 satellite imagery on weekly availability (not accounting for cloud cover). This would integrate with existing glacier and glacial lake databases and could monitor the appearance of new supraglacial lakes.

4.4 A) Improvement of existing methods

The integration of existing techniques, data or methods that could be readily integrated into the monitoring plan, or that were considered unsustainable in the present PhD projects, are briefly described in this present chapter.

Integrated in the monitoring plan

- Glacier inventory update based on satellite imagery

The regional glacier inventory is the primordial database on which the glacial risk monitoring plan relies. As glacier national inventories are sporadically updated, one of the first needs identified in the glacial risk monitoring plan had been an update of the glacier inventory whenever an aerophotogrammetric flight was available using state funding. Nowadays, it is well established that freely available datasets such as Sentinel-2 imagery can be successfully used for glacier outline mapping. With 10m ground resolution, such imagery can be ineffective when changes in glacier outlines are of a similar magnitude to the ground resolution. Nonetheless, in the current climate change scenarios, most glaciers undergo length changes of tens to hundreds of metres per year. Thanks to the work carried out in the present study, the glacial risk monitoring plan has introduced the update of glacier outlines of the regional glacier inventory based on Sentinel-2 imagery every two years. The 2019 glacier outlines are available for download on the webGIS (https://geoportale.regione.vda.it/download-old/carte-eo-data/ accessed 20/09/2023) of the Autonomous Region of Aosta Valley (Figure 12).

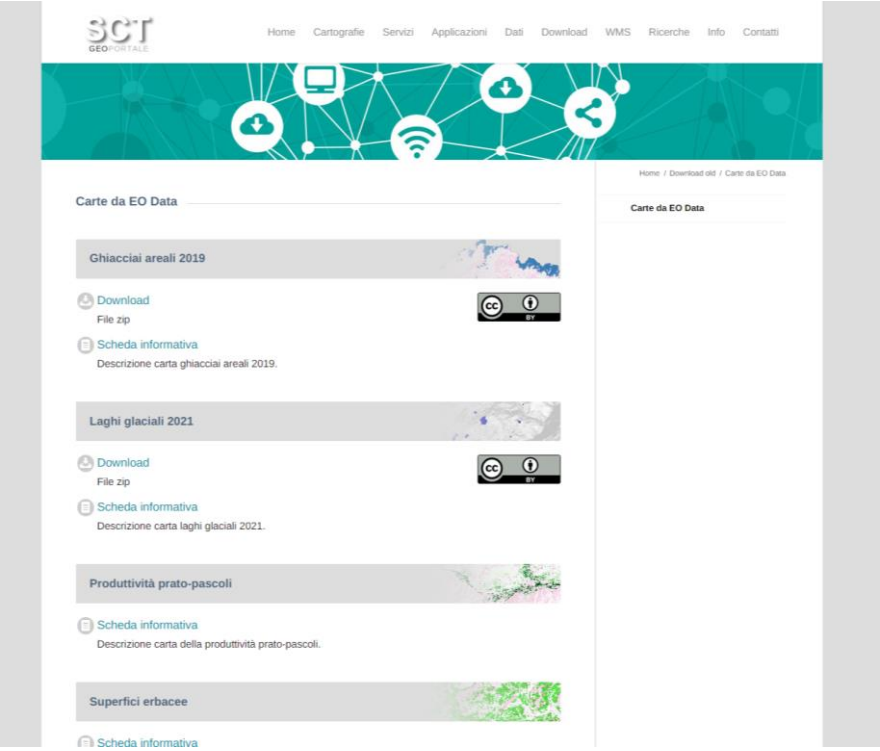

Figure 12. Web interface for the download of glacier outlines of Aosta Valley glaciers updated as of Sentinel-2 imagery dating of 2019.

- Semi-automatic procedure for the monitoring of glacial lakes on satellite imagery

The literature review performed identified certain procedures that have already been tested and applied in bibliographic studies on the possibility to successfully detect water bodies in mountain regions with the use of remotely sensed data. When dealing with freely available datasets, ground resolution and revisit time of Landsat satellites that were available before the Sentinels launch (2015) was not suited to the identification of newly formed glacial lakes in an alpine environment. With the availability of Sentinel-2 datasets, we conceived an experimental activity of a possible semi-automatic classification of newly formed glacial lakes to be possibly integrated into the glacial risk monitoring plan. The draft of the experimental activity was laid down in the framework of the present PhD project. The development of the research plan was inserted into the framework of the WP3 of the Interreg Alcotra 2014-2020 (IT-FR) RISK-ACT-PITEM RISK project. This financed the experiments to validate a procedure based on the analysis of updated NDWI index maps on the regional territory for every low cloud cover percentage image acquired by the Sentinel-2 satellites. The procedure has been integrated in the glacial risk monitoring plan as an experimental monitoring procedure and is currently active and ongoing.

- Integration of Ground Based interferometry for the monitoring of the Whymper Serac

The idea that GbSAR interferometry could be effective for the monitoring of the Whymper Serac clearly emerged from the literature review that was performed in the present study. Nonetheless, experiments were needed in order to understand the reliability and data quality for a site where the distance between the instrument and the target is at the range limit of instrumentation available on the market. Experimental acquisition of data was performed in 2020 and 2021 thanks to financing from the Autonomous Region of Aosta Valley. The studies provided good results and the purchase of an interferometric radar was approved as part of the

FSC national fund for research under the 'Glaciers of the Val Ferret as sentinels of climate change' project. The interferometric measurements of the deformations of the Whymper Serac have now been totally integrated into the glacier monitoring plan procedures and, twice a week, Fondazione Montagna Sicura technicians produce a monitoring report. This integrates the GbSAR measurements that are sent to the Geological Survey of Aosta Valley and the Civil Protection contacts are included, if needed.

<u>To be further investigated in future projects</u>

- Basal thermal regime investigations at the Whymper Serac

During 2020 and 2021, a series of field campaigns for the drilling of boreholes reaching the ice-bedrock interface were performed on Whymper Serac by the Fondazione Montagna Sicura. The work was carried out under my coordination, in cooperation with the University of Grenoble and financed by the Autonomous Region of Aosta Valley. Thermistor chains in the boreholes measured englacial and basal temperatures of the serac and were compared to the measurements obtained by Funk at al. in 1997. This comparison evidenced a general warming of the ice and especially highlighted those one of the six basal points of analysis had switched from the cold state in 1997 to a temperate state in 2020. This analysis underlined that the transition of the Whymper Serac from a cold-based hanging glacier to a polythermal glacier has started and is ongoing. The consequences of a possible destabilisation linked to this phenomenon is of very significant relevance for monitoring activities and safety plans and cannot be tackled as part of the PhD study. A specific modelling activity with the IGE University of Grenoble has begun and further field campaigns and financing for the purchase of new thermistor chains for the future monitoring of the thermal evolution of the Whymper Serac have been proposed and approved as part of the FSC national fund for research 'Glaciers of the Val Ferret as sentinels of climate change' project. The activity carried out in 2020 and 2021 was summarised in a poster presentation (Figure 13) at the 2022 Alpine Glaciology Meeting held in Munich, Germany.

Alpine Glaciology Meeting 2022

Munchen – 25-26 March 2022

Basal thermal regime investigations at Whymper hanging glacier (Aosta Valley – Italy)

Fabrizio Troilo[1], Perret Paolo[1], Simone Gottardelli[1], Luca Mondardini[1], Daniele Giordan[2], Niccolò Dematteis[2], Luc Piard[3], Olivier Gagliardini[3], Adrien Gilbert[3], and Christian Vincent[3]

1 - Mountain Safety Foundation, Glaciers and Permafrost Office, Courmayeur, Italy (ftroilo@fondms.org)

2 - Istituto di Ricerca per la Protezione Idrogeologica - Geohazard Monitoring Group, Consiglio Nazionale Delle Ricerche, Torino, Italy (daniele.giordan@irpi.cnr.it)

3 - Institut des Géosciences de l'Environnement - Departement Glaciologie, Université Grenoble Alpes, Grenoble, France (christian.vincent@univ-grenoble-alpes.fr)

CONTEXT

Fondazione Montagna sicura manages on behalf of the Autonomous region of Aosta Valley, a monitoring of glacial risks on the whole regional territory. In order to do so, some specific monitoring is implemented on some particular glaciers. One of those is the Whymper Serac, on which the present study is focused. This activity has been possible thanx to the collaboration with the Université de Grenoble Alpes, IGE research team and the support of the CNR – Italian research Council.

INTRODUCTION

The Grandes Jorasses Massif culminates at 4203m at the Punta Walker summit on the border between France and Italy. The south slope of Grandes Jorasses is widely glaciated and overlies the Val Ferret, a populated and highly frequented area presenting different hamlets, the most important being Planpincieux village. Located at an altitude between 4000 and 4100 m, the Whymper Serac is a hanging glacier that undergoes periodic gravity-driven instabilities. On 1st June of 1998, 150.000m3 of ice fell, and the resulting ice avalanche reached 1750m, at a distance of about 400m from houses of the Le Pont village and the main road. The monitoring activity started in **1997**: a series of boreholes had been drilled to assess the basal thermal regime of the serac and subsequently install a monitoring system for early warning signs and risk assessment. **All boreholes** showed **negative basal temperature** of the ice mass.

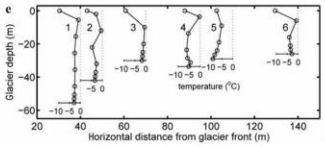

Temperature profiles from the 6 boreholes drilled on the Whymper serac in1997

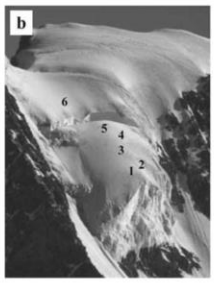

Localization of the 1997 boreholes

MATERIALS

In order to be able to drill 6 boreholes and install thermistor chains in all of them, preliminary topographic and geophysical surveys have been carried out and we can divide 3 different phases of the field campaigns:

1) Topographic surveys: Updated Topograpy of the serac has been performed by UAV digital photogrammetry using Geomax Zenith 25 RTK GPS for GCP measurement, and a DJI Mavic 2 Pro UAV equipped with Hasselblad 20 Mpixel digital camera.
2) Geophysical surveys: Ground penetrating radar has been used to assess glacier thicknesses and therefore plan the drillings and the thermistor chains installation.

3) Temperature measures:
A hot water drill from IGE of Grenoble has been used to drill 6 boreholes and subsequently install 6 Thermistor chains with length comprised between 45 and 60 meters. Thermistors are spaced by 5 meters intervals in the first 30 meters of depth from the surface and 2/3 spacings in the bottom parts of the chains.

Equipment at the drilling site during the 2020 field campaign

METHODS

1) Topographic surveys: data acquired in the aerophotogrammetrical surveys has been processed with Agisoft Metashape software.
2) Geophysical surveys: data from the AIRETH GPR system (2 perpendicular 25 MHz Pulse Ekko antennas) has been processed and coupled to the updated topography of the serac.
3) The temperature measures from the thermistor chains have been downloaded on site at 2 different time intervals from the drilling: a first round of measures about 40 days after drilling and another round of measures at more than 60 days from the drilling. Data from the different campaign measures always showed very good matching. This fact underlines that temperature equilibrium after the hot water drilling had been already reached after 40 days. Because of extreme environmental conditions and a limited expected lifespan of the thermistor chains, no wireless remote access to the temperature data has been setup. Moreover the present study focuses on long term temperature variations at the ice-bedrock interface via comparison of the newly acquired data to those of 1997.

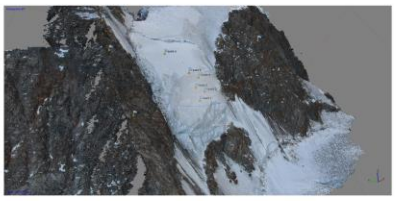

Georeferenced 3D Point Cloud of the Whymper Serac

RESULTS

In September 2020, three thermistor chains in three different boreholes were installed on Whymper Serac. Temperature profiles were measured at different periods between October and November 2020. In September 2021 another three thermistor chains were installed and their temperature profile measured in October 2021. During the same survey, temperature profiles of the 2020 thermistors have been measured again on 2 out of 3 boreholes, (one being too close to the serac front was not safe to reach) confirming data acquired on the 2020 field campaign. The outcome of basal temperature measurements of 2020 and 2021 give good spatial coverage of the serac allowing comparison with data from the 1997 measurements, despite on the fact that most of the ice mass fell in 1998.

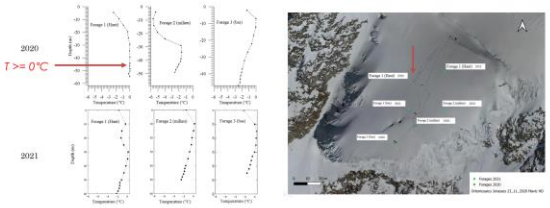

Temperature profiles of the 2020/2021 campaign and their location on the Whymper Serac

A warming trend in most of the temperature profiles of **2020/21** is evident in comparison with 1997 data; averaging the 6 bottom measures from the chains was equal to **-4,2**°C in 1997 and is equal to **-2,2**°C in 2020/21. 5 out of 6 points of measure still show temperatures below 0° C in 2020/21 but remarkably one point of measure shows evidence of **temperate ice** at the ice/bedrock interface.

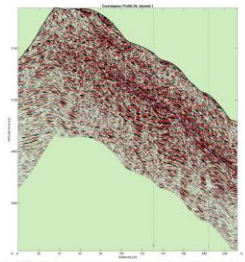

Geophysical surveys have given an updated perspective on the ice-bedrock interface geometry of the Whymper Serac. This is also relevant for the estimation of ice volumes in the occurrence of Ice brake-offs from the Serac. Moreover they have raised questions on the internal structure of the Serac, pointing out that a large part of the serac could be characterized by a quite deep accumulation of firn in its accumulation zone. This assumption needs further research but a first experiment of firn density measurement have given very low values in the first 2.75 meters of depth. Further investigation is planned via an experimental GPR system as well as other classical measures.

Longitudinal Ice Thickness estimation profile from GPR data.

CONCLUSIONS

Whymper Serac measurements provide evidence that the glacier is still frozen to the bedrock, but one part of the serac shows the beginning of a potential transition from cold based regime to temperate based regime. If, on one hand, surface displacements of the ice mass still show low displacements (typical of a cold based glacier), on the other hand, a velocity anomaly was detected on a small portion of the serac corresponding to the temperate based sector. Further research is needed to better understand the evolution of the thermo-mechanical conditions of the Whymper Serac in the current climate change scenarios. Therefore, thermo-mechanical modeling of the Whymper Serac is underway, based on the Elmer/Ice model.

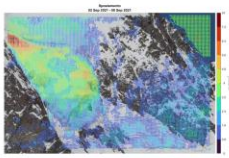

Velocity anomaly detected in September 2021 in the upper right corner of the Serac near the borehole showing temperate basal conditions

Figure 13. Poster presented at the Alpine Glaciology meeting 2022 in Munich.

- Modelling of the thermo-mechanical regime of the Whymper Serac

In understanding the future evolution and scenarios of Whymper Serac destabilisations, a thermo-mechanical modelling experiment (Figure 14) using the Elmer-ice module was performed in cooperation with the IGE University of Grenoble. The reconstruction of a surface point mass balance with the techniques highlighted by Vincent et al. (Vincent et al., 2021) was one of my tasks in this project. This was done thanks to the acquisition, processing and analysis of drone surveys and the obtained DEMs and GNSS measurements of stakes on the serac, coupled with data from the topographic monitoring system and the image analysis on time-lapse imagery from the automated cameras. The modelling activity is due to be completed in 2024 and will possibly include the publication of a dedicated paper.

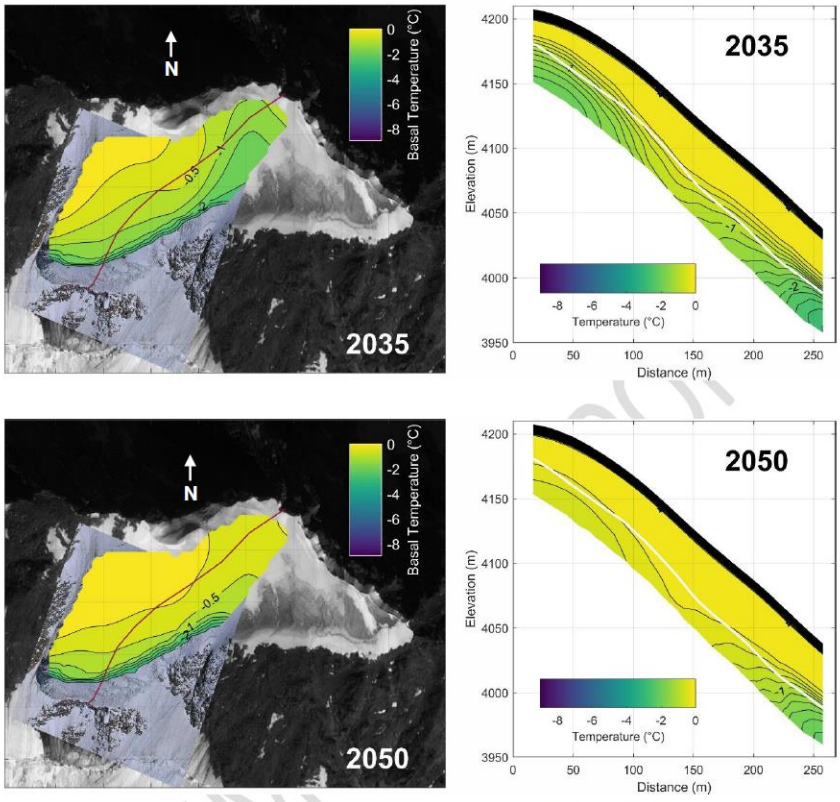

Figure 16 - Temperature modeled in 2035 and 2050 with water percolation in damaged ice. Left side are basal temperature and right side are longitudinal temperature profile along the red line. The white lines on the profiles are the ice-rock interfaces.

Figure 14. Some preliminary results from the initial technical report of the thermo-mechanical modelling of the Whymper Serac; work in progress to be finalised.

- Analysis of hydrological data and regimes of a destabilising temperate glacier

Owing to a great knowledge gap that was evidenced thanks to the literature review performed in this PhD project, the further investigation of the hydrological regimes of the subglacial drainage system, and their influence and glacier motion and destabilisation, was identified as a major goal for the future of glacial risk assessment and management. As the issue is very wide-ranging and difficult to be investigated, a large part of the project FSC national fund for research 'Glaciers of the Val Ferret as sentinels of climate change' project was dedicated to this specific topic. As part of this project, a series of four boreholes reaching the bedrock of the central part of the Planpincieux Glacier are due to be drilled during summer 2024. The objective of this

campaign will be the measurement of deformations and basal sliding throughout the whole glacier, from the surface to the ice-bedrock interface. Another aim is the measurement of the presence and the pressure of basal water, inferring the activity of the basal drainage network via seismic monitoring and relating this data to the input and output of water by the continuous measurement of ablation. There will be the installation of an on-site AWS and the analysis of data from the already installed (2023) radar hydrometric station on the glacial stream coming from the Montitaz lobe of the Planpincieux Glacier (Montitaz Stream). These will be the main aims of the project activity in 2024.

4.5 B) New methods for risk assessment

We decided to pursue certain specific objectives amongst all the criticalities and the open research questions highlighted in the precedent chapter of the present PhD project. The possible outcomes of these research actions could possibly be new methodologies for glacial risk assessment to be later integrated into the current glacial risk monitoring plan. The specific topics are summarised as follows:

1) To start an organised review of the existing monitoring data on the two most studied glaciers in the Aosta Valley: Whymper Serac and Planpincieux Glacier.
2) To review the current state of glacier displacements monitoring in the literature.
3) To review existing data of glacier displacements in the Mont Blanc Massif in order to contextualise the monitored Planpincieux Glacier displacement and acceleration at the Massif scale.
4) To study the possibility to obtain time series of glacier velocity of the full extent of the Planpincieux Glacier, and possibly of neighbouring glaciers, to better understand displacements and accelerations of the Planpincieux Glacier.
5) To analyse the morphometry of the destabilising areas of the Planpincieux Glacier, determine a recurrency in the kinematic sectors formation and a possible relationship with bedrock morphology.
6) To analyse the possibility of the triggering of cascading events at Planpincieux Glacier.
7) To determine possible failure scenarios of the Brenva Rock Spur.
8) To analyse a larger context of current degradation of high-altitude rock outcrops in order to understand future scenarios of possible large rock ice avalanche formations.

A series of manuscripts summarise the main research activities that have been carried out around the above-mentioned research objectives and are reported in the following paragraphs.

Ten-Year Monitoring of the Grandes Jorasses Glaciers Kinematics. Limits, Potentialities, and Possible Applications of Different Monitoring Systems

Short summary

The publication of the technical note 'Ten-Year Monitoring of the Grandes Jorasses Glaciers Kinematics. Limits, Potentialities, and Possible Applications of Different Monitoring Systems' (Dematteis et al., 2021), summarises the history and the ongoing main activities linked to the monitoring of both the Planpincieux Glacier and the Whymper Serac. This served as a base of knowledge to build up further research activities on these two specific monitoring sites.

Main findings

The main findings of this publication are:

- Combining discontinuous and permanent monitoring data into one database.
- Highlighting limits and potentialities of the adopted monitoring systems.
- Analysing the early warning capabilities of each system.
- Proposing data integration strategies.

Contributions of the PhD candidate

Conceptualisation of the research activity with the co-authors. Data retrieval and organisation. Analysis and interpretation of the data. Collection of the data and maintenance of the measurement networks. Contribution in the preparation and writing of the manuscript and the figures with the co-authors.

Data availability

The data are available from the authors, upon request.

Journal

Remote Sensing (ISSN 2072-4292) publishes regular research papers, reviews, technical notes and communications covering all aspects of remote sensing science, from sensor design, validation/calibration, to its application in geosciences, environmental sciences, ecology and civil engineering. The journal's aim is to publish novel/improved methods/approaches and/or algorithms of remote sensing to benefit the community, open to everyone in need of them. 2022 JCR Impact factor: 5.0

remote sensing

MDPI

Technical Note

Ten-Year Monitoring of the Grandes Jorasses Glaciers Kinematics. Limits, Potentialities, and Possible Applications of Different Monitoring Systems

Niccolò Dematteis [1], Daniele Giordan [1,*], Fabrizio Troilo [2], Aleksandra Wrzesniak [1] and Danilo Godone [1]

[1] Italian National Research Council, Research Institute for Geo-Hydrological Protection (CNR-IRPI), Strada delle Cacce 73, 10135 Torino, Italy; niccolo.dematteis@irpi.cnr.it (N.D.); aleksandra.wrzesniak@irpi.cnr.it (A.W.); danilo.godone@irpi.cnr.it (D.G.)

[2] Fondazione Montagna Sicura, Località Villard de la Palud, 1, 11013 Courmayeur, Italy; ftroilo@fondms.org

* Correspondence: daniele.giordan@irpi.cnr.it

Abstract: In the Ferret Valley (NW Italy), anthropic activities coexist close to the Grandes Jorasses massif's glaciological complex. In the past, break-off events have caused damage to people and infrastructure. These events concerned two specific sectors: the Montitaz Lobe (Planpincieux Glacier) and the Whymper Serac (Grandes Jorasses Glacier). Since 2010, permanent and discontinuous survey campaigns have been conducted to identify potential failure precursors, investigate the glacier instability processes, and explore different monitoring approaches. Most of the existing terrestrial apparatuses that measure the surface kinematics have been adopted in the Grandes Jorasses area. The monitoring sites in this specific area are characterized by severe weather, complex geometry, logistic difficulties, and rapid processes dynamics. Such exceptional conditions highlighted the limitations and potentialities of the adopted monitoring approaches, including robotic total station (RTS), GNSS receivers, digital image correlation applied to time-lapse imagery, and terrestrial radar interferometry (TRI). We examined the measurement uncertainty of each system and their monitoring performances. We discussed their principal limitations and possible use for warning purposes. In the Grandes Jorasses area, the use of a time-lapse camera appeared to be a versatile and cost-effective solution, which, however is not suitable for warning applications, as it does not guarantee data continuity. RTS and GNSS have warning potentialities, but the target installation and maintenance in remote environments remain challenging. TRI is the most effective monitoring system for early warning purposes in such harsh conditions, as it provides near-real-time measurements. However, radar equipment is very costly and requires extreme logistic effort. In this framework, we present data integration strategies to overcome the abovementioned limits and we demonstrate that these strategies are optimal solutions to obtain data continuity and robustness.

Keywords: glaciers; monitoring; natural hazards; data integration; glacier flow

Citation: Dematteis, N.; Giordan, D.; Troilo, F.; Wrzesniak, A.; Godone, D. Ten-Year Monitoring of the Grandes Jorasses Glaciers Kinematics. Limits, Potentialities, and Possible Applications of Different Monitoring Systems. *Remote Sens.* **2021**, *13*, 3005. https://doi.org/10.3390/rs13153005

Academic Editors: Davide Fugazza, Roberto Sergio Azzoni, Antonella Senese and Giovanni Baccolo

Received: 16 June 2021
Accepted: 22 July 2021
Published: 30 July 2021

1. Introduction

Mountain glaciers are a crucial element for the local economy in terms of freshwater supply, hydroelectric production, and tourist activities [1]. Glacier surface mass balance, elevation change, and terminus retreat are often quantitatively surveyed to evaluate their current state and recent evolution [2]. However, such monitoring activities are usually conducted periodically (e.g., with seasonal or annual revisit time) due to the investigated processes' relatively slow dynamics.

Conversely, glacial phenomena such as ice avalanches and glacier lake outburst floods develop and evolve more rapidly, with a time scale from days to minutes. They represent a potential risk for infrastructure and the population [3–5]. Therefore, high temporal frequency monitoring is necessary to observe such rapid processes and acquire a detailed sequence of physical parameters that allows correct data analysis. Thereby, it is possible to

provide insight into the investigated phenomena and support decision-makers in managing glacial risk.

The majority of efforts dedicated to technological development have focused on new technologies and methodologies to measure surface displacement, as the surface kinematic is the most connected variable to potential failures. Spaceborne surveys cover wide areas, providing data without great human effort and the recent Sentinel program has notably reduced the revisit time. Nevertheless, their frequency is not yet sufficient to observe rapid processes and complex geometries typical of mountain glaciers, hampering the spaceborne measurement.

Only terrestrial systems can provide a sufficiently temporally dense dataset. However, they have the disadvantage of observing relatively small areas and requiring significant human and financial input. Glaciers are usually located in remote and challenging environments and the existing commercial instrumentations were not designed for glaciological surveys specifically. Therefore, continuous glaciological long-term monitoring campaigns are not common.

According to Watson and Quincey [6], terrestrial measurement techniques of glacier movement include total station/theodolites, GNSS receivers (hereafter GNSS) and time-lapse cameras (TLC) using the digital image correlation (DIC) method. Additionally, terrestrial radar interferometry (TRI) proved to be a valuable tool in this regard [7].

Theodolites for surveying glacier flow have been used in the past century [8,9]. Typically, a series of stacks or stones were periodically measured and replaced in their original positions. Recently, the adoption of robotic total station (RTS) allowed us to obtain long-term continuous surveys of glaciers [10,11]. The RTS combines an electronic theodolite and a laser range finder to measure the three-dimensional position of a given target with millimetric sensitivity. The RTS autonomously acquires during day and night, but dense fog or clouds hamper its performance. The RTS system requires the installation of reflective prisms within the monitored area, while prisms placed in stable areas are used to reduce the atmospheric artefacts on the measurements and determine angular offsets. A network of passive targets entails the necessity of periodic maintenance, which can be complicated in challenging areas.

GNSS measure their own three-dimensional position with centimeter to millimeter precision. They are composed of an antenna and an L-band microwave receiver. More sophisticated GNSS acquire multiple frequencies to filter the ionospheric and atmospheric influence better. Currently, the use of geodetic sensors is common in glaciology [12–15] due to their light portability and simple use. However, most of the applications concern discontinuous manual surveys, involving human access into the glacierized area. Permanent GNSS networks are less frequent because they need periodic maintenance and a continuous on-site power supply. Examples can be found in [10,16,17].

One of the first applications of terrestrial DIC to glacier motion was described by Evans [18], who used digitalized image negatives of the Godley Glacier (New Zealand). Subsequently, terrestrial DIC has been adopted in a number of glaciological studies [19–22]. Typically, DIC is applied to time-lapse cameras deployed on stable ground/surfaces to minimize image misregistration. The principle of DIC is to search for the position of a given patch between two images. Thereby, DIC detects the spatially distributed displacement components orthogonal to the line of sight (LOS). The pixel's footprint is typically of the order of centimeters and depends on camera specifications and camera-to-target distance. In optimal contexts, DIC can provide sub-pixel measurements. However, reliable results are more frequent for displacement larger than a few pixels. The major limitation of DIC is the need for favorable visibility and illumination conditions. This often requires the manual selection of the images to be processed in order to discard the corrupted ones [23]. For these reasons, the temporal frequency of the results is often on a daily basis.

The first TRI surveys of a glacier were conducted experimentally in the Belvedere Glacier (Italy) [7,24] and Gorner Glacier (Switzerland) [25]. The authors adopted prototypes of two interferometric apparatuses (i) ground-based synthetic aperture radar (GBSAR)

and (ii) real aperture radar (RAR), respectively. The GBSAR is the commonest TRI system. It is composed of small transmitting and receiver antennas that slide onto a linear rail, typically 2–3 m long. This movement has a twofold effect: first, it allows us to obtain an aerial distribution of the surveyed displacement, and second, it simulates a wider antenna to obtain a finer spatial resolution. Differently, a RAR system uses large antennas that rotate about a vertical axis to scan the whole scene. The increased antenna dimension entails a better signal-to-noise ratio (SNR), which permits a longer operational range (up to 10–15 km), but the financial cost is usually higher than the GBSAR. Subsequently, TRI has occasionally been adopted in short-term surveying campaigns [26–28]. TRI measures the phase difference between two electromagnetic pulses, which is directly linked to the target displacement parallel to the LOS. Usually, terrestrial radars operate in Ku-band, which corresponds approximately to a wavelength of λ = 15–20 mm. Therefore, the TRI measurement sensitivity is submillimeter. However, the maximum displacement detected between two acquisitions is $\lambda/2 < 10$ mm [29]. Typical acquisition frequencies vary from seconds to minutes. TRI surveys can be conducted continuously during day and night and in all meteorological conditions. Nevertheless, atmospheric changes affect the measurement [30]. In glacial environments, severe weather frequently occurs [31]. Specific methods must be adopted to filter the atmospheric influence properly [31–33]. TRI systems require a considerable power supply and logistic efforts. Therefore, long-term surveys are difficult to conduct in remote environments, like that of the Mont Eiger (Switzerland) [32].

Typically, the scope of terrestrial glaciological campaigns focuses on the investigation of glacial processes, but the metrological effectiveness of survey sensors and techniques has seldom been analyzed in recent years [6,33,34].

In this paper, we present applications and results of the abovementioned monitoring techniques that have been adopted in the glacial complex of the Grandes Jorasses (Italy) during the last decade. We conducted various campaigns using RTS, GNSS, DIC and TRI. These surveys had multiple objectives. Since the Grandes Jorasses is an area where glacial hazards are frequent and can menace the population, the first objective was the glacier monitoring for potential failure precursor identification [35] and for glacial risk evaluation [36]. The second objective was the glacier behavior investigation to enhance our understanding of the instability processes [37]. The third objective was to explore existing and innovative approaches for effective continuous glacier monitoring [23,38–41]. The presented work focuses of the latter topic.

More than 10 years of monitoring in a high-mountain glacial environment with exceptional characteristics of meteorology, geometry, and process dynamics allowed for the exploration of the effectiveness, limits, and potentialities of various surveying methods. In this paper, we present these limits and potentialities in a comprehensive view, and we discuss the use of RTS, GNSS, DIC, and TRI for glacier observation, investigation, and glacial hazard warning.

Section 2 presents the study area of the Grandes Jorasses glacial complex, while Section 3 provides the technical specification of the survey systems and describes their operative applications, including the strategies adopted to take advantage of their measurement capability. Section 4 pertains to the description of the kind of data that can be provided by the various systems and briefly presents the related uncertainties. Sections 5 and 6 discuss the findings of more than 10 years of glacial monitoring.

2. Area of Interest: The Grandes Jorasses Glacial Complex

The Planpincieux Glacier (WGI # IT4L01517018) and Grandes Jorasses Glacier (WGI #IT4L01517019) [42] are located in Ferret Valley on the Italian side of the Grandes Jorasses massif (Figure 1). These two glaciers form a unique glacial complex (GLIMS ID G006977E45859N) [43] extended between 2600 m a.s.l. and 4206 m a.s.l. with a mean South-East aspect.

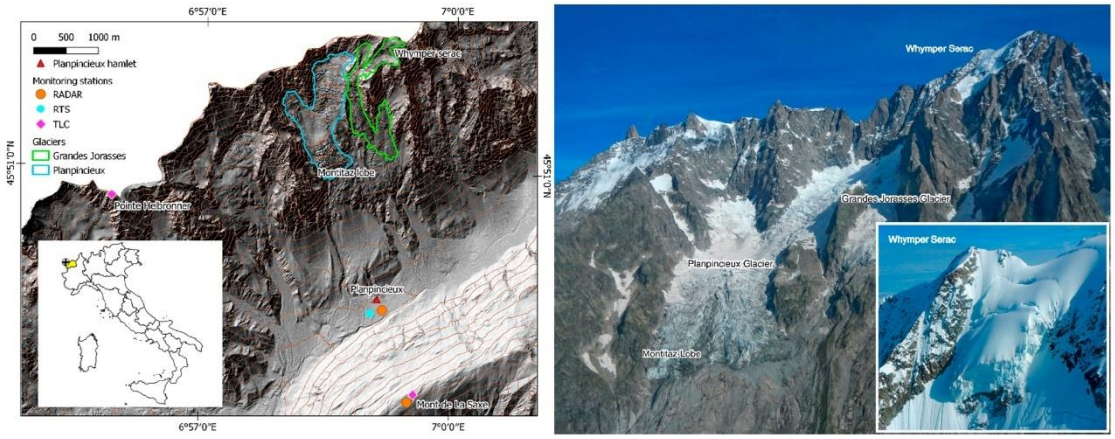

Figure 1. Left panel: overview of the study area. Right panel: Planpincieux and Grandes Jorasses glaciers. In the white box, a closer perspective of the Whymper Serac is shown.

The total glacierised surface of the glacial complex is 1.594 km^2 divided into 1.008 km^2 for the Planpincieux Glacier and 0.586 km^2 for the Grandes Jorasses Glacier (Regional glacier inventory of Aosta Valley, update 2019). The Ferret Valley is a renowned tourist locality in the Mont Blanc area and it is a clear example of the relationship between glaciers and human infrastructure. As is common in the Alpine region, the anthropic pressure in this area has progressively augmented in the last fifty years. The vulnerability of the infrastructure in the valley currently represents a critical factor that requires the correct management of glacial hazards. Frequent and recurrent break-off events from the Montitaz Lobe (ML) of the Planpincieux Glacier and the Whymper Serac (WS) of the Grandes Jorasses Glacier cause damage to the underlying Planpincieux hamlet [36,37]. Major survey efforts have been dedicated to monitoring these two glacial sectors.

The ablation area of the Planpincieux Glacier is composed of two lobes. The ML (Figure 1) is a 32°-steep icefall whose terminus lies at 2600 m a.s.l. and ends in correspondence with a bedrock cliff that induces frequent calving [37].

The WS is located in the upper part of the Grandes Jorasses Glacier (Figure 1), at approximately 4000 m a.s.l. Six boreholes drilled in January 1998 showed basal temperatures below 0° [44]. Recent observations indicate that the basal temperature has risen (Vincent, 2020, personal communication). The serac is 45°-steep and it is classified as an unbalanced hanging glacier [44]. The WS follows an evolution cycle characterized by its progressive volume increase until its shape and mass reach unstable conditions, and consequently, it collapses [35,44,45]. The last break-offs occurred in August 1993 (causing the fatality of eight mountaineers), in June 1998 [36], in September 2014 [35] and during the Autumn of 2020.

3. Implementation: Survey Methods

In the last decade, the surveys in the Grandes Jorasses area were conducted by various technologies and techniques [41]. Since one goal was to monitor the glacier kinematics to detect potential hazards, particular attention was dedicated to systems that survey the surface displacement. In the following, we present these systems and briefly describe the procedures of monitoring system management. In Table 1, we report the details of the survey campaigns conducted in the Grandes Jorasses area.

Table 1. Survey campaigns in the Grandes Jorasses glacial complex since 2010 (TLC = time-lapse camera; GNSS = global navigation satellite system; RTS = robotic total station; TRI = terrestrial radar interferometry).

Apparatus	Monitored Area	Survey Period	Operative Range	Reference
RTS	Whymper Serac	October 2010–in activity	4800 m	[35]
GNSS	Whymper Serac	October 2010–2012	—	[46]
TLC	Montitaz Lobe	August 2013–in activity	3800 m	[37,40]
TLC	Whymper Serac	August 2016–in activity	4800 m	[41]
TRI	Montitaz Lobe	9 August 2013 (2 h) 7 August 2014 (2 h)	2500 m/3800 m *	[47]
TRI	Whymper Serac	9 August 2013 (2 h) 8 August 2014 (3 h)	4800 m/5400 m *	[47]
TRI	Montitaz Lobe	2 September–14 October 2015	2500 m	[38]
TRI	Montitaz Lobe	13-19 June 2016	2500 m	
TRI	Montitaz Lobe	26 September 2019–in activity	2500 m	
TRI	Whymper Serac	16 January 2020–in activity	4800 m	

* Operative range in terms of distance from Planpincieux hamlet/Mont de La Saxe crest.

3.1. Robotic Total Station

An RTS Leica TM30 was installed in the Planpincieux hamlet in 2010 (Figure 1) to monitor the WS, acquiring a measurement every 2 h. The WS is approximately 4800 m-distant from the RTS and the elevation difference is 2400 m. This distance is beyond the declared operational range for the automatic target recognition acquisition mode, which is 3000 m for standard prisms (Leica TM30 technical data [48]). For this reason, often, not all targets were detected during a single measurement session. The declared accuracy by the manufacturer at the distance of 4800 m is approximately 8 mm.

A network of several prisms (with an optimal view angle of 40° for both the horizontal and vertical axes) has been arranged on the WS with the aid of alpine guides (Figure 2). To minimize the risk of losing the prism visibility for the tilting/rotation of the supporting pole, we adopted V-shaped bars that prevent the rotation along the z-axis; furthermore, in October of 2020 we installed a prism with 360° and 120° view angles along the z- and x-axes, respectively. Due to logistic difficulties, only two reference prisms were installed in the surrounding bedrock. The exceptional high-mountain conditions caused a frequent loss of prisms, and in-field interventions to replace or substitute missing targets were often necessary. A total of 42 prisms have been installed on the WS surface since 2010. Over this period, on average, 2–5 prisms were concurrently present. The RTS collected more than 26,000 measurement epochs and approximately 15,000 had at least one reference prism available. The RTS dataset of the WS is likely one of the longest continuous time series of a glacier worldwide.

The extreme weather conditions and the critical operational range introduced high noise to the RTS measurement. To analyze the RTS data before the 2014 break-off, Faillettaz and others (2016) used a robust method to filter most of the artefacts in the data [49].

Figure 2. (**a**) Alpine guides install reflective prisms onto the Whymper Serac on 5 March 2020. (**b**) GNSS equipped with datalogger, solar panels, and batteries [46]. Reflective prisms were placed on the metallic bars that supported the GNSS for comparison. (**c**) TLC station that monitors the Montitaz Lobe, with the Planpincieux and Grandes Jorasses glaciers visible in the background. (**d**) TLC station that monitors the Whymper Serac from Pointe Helbronner. (**e**–**g**) the RAR GPRI and the GBSARs IBIS-L and FastGBSAR, respectively.

3.2. GNSS

Within the GlaRiskAlp project (http://www.glariskalp.eu/ accessed on 1 February 2021) [46], three prototypal GNSS were installed on the WS surface (Figure 2) in October 2010 and remained operative until 2012. Low-cost, single-channel receivers were adopted (AC12 Magellan), as break-offs, snow avalanches, and intense snowfall could have caused their loss. Each device was equipped with a solar panel, a small backup battery and a prototypal datalogger. The stored data were Wi-Fi transmitted to a radio repeater every 30 min, which was connected to the processing station in the Planpincieux hamlet [50]. The GNSS was acquired every 15 s and the data were processed using the differential GPS method, using three GNSS reference receivers located in the Ferret Valley. Unfortunately, serious hardware issues and the snow cover strongly limited correct data acquisition. Nevertheless, between July 2011 and January 2012, the data quality was satisfactory.

3.3. Time-Lapse Imagery

Time-lapse cameras (TLCs) were installed in August 2013 and 2016 to monitor the ML [40] and WS, respectively. The TLCs were placed on the Mont de La Saxe crest (2300 m a.s.l.) and at Pointe Helbronner (3400 m a.s.l.) (Figure 1). The TLC distances from the respective glaciers are approximately 3800 m and 4800 m, respectively.

The monitoring station of ML (Figure 2) comprises a UMTS modem, a DSLR Canon EOS 700D equipped with a 297 mm-lens (another TLC targets the Planpincieux Glacier with 120 mm-lens), a Raspberry-Pi 3 computer, a fan heater, a power module composed of several solar panels and a backup battery and two surveying webcams. The TLCs are mounted on a cemented pillar independent from the shelter box. This allows minimum misregistration, even in the presence of strong wind. Occasionally, bad weather and snow cover cause system stand-by, but it reactivates autonomously. The monitoring station is completely autonomous, and it is remotely accessible. The TLCs acquire with hourly frequency and the images are transmitted using a UMTS connection. We experimented with both auto and manual focus modalities for image acquisition. The advantage of the former solution is that, in general, the photographs are sharper, while using manual focus they are frequently blurred. On the other hand, autofocus can fail in the presence of slight condensation on the viewing window. To solve this issue, we equipped the monitoring station with a fan heater that eliminates the condensation. In the end, we opted for the autofocus acquisition mode, because image blurring affects DIC results [51]. Since DIC suffers surface shadow pattern change [22,52], we implemented an automatic machine

learning-based procedure to autonomously select and process the images acquired in diffuse illumination conditions [23]. Thereby, we strongly reduced the human efforts required to monitor the glacier continuously. During the years 2014–2019, we applied the DIC using the spatial cross-correlation calculated in the Fourier space. In 2020, we adopted the zero-mean normalized cross-correlation metrics. This latter method is computationally demanding, but it is less affected by environmental noise [51].

The TLC that targets the WS is a DSLR Canon EOS 1200D equipped with a 400 mm-lens. The TLC acquires photos in auto-focus mode. The monitoring system is connected to the power grid and transmits, depending on the season, one to four images per hour via a WiFi connection. The shelter box is mounted on the metallic pillars of the Skyway cable car station of Pointe Helbronner. We observed strong image misregistration. The image registration was hampered by the presence/absence of snow on the stable surfaces that were adopted as reference. To partially reduce this hindrance, we adopted the cosine similarity method [51], which proved to be less affected by this issue.

The pixel footprints of the TLCs are approximately 54 mm px^{-1} and 52 mm px^{-1} (ML and WS images, respectively).

The TLC that monitors the ML acquired more than 23,500 photographs between August 2013 and December 2020, while that of the WS acquired more than 10,500 images between August 2016 and December 2020. The time-lapse time series of ML and WS are among the longest continuous glaciological TLC surveys worldwide.

3.4. Terrestrial Radar Interferometry

In the Grandes Jorasses area, six experimental TRI campaigns have been conducted since 2013. Among the different typologies of TRI apparatuses, three models of GBSAR: IBIS-L (IDS GeoRadar), FastGBSAR (Metasensing), and GBinSAR LiSALab (LiSALab), and one RAR: GPRI (Gamma Remote Sensing), were adopted (Figure 2). All the radars operated in Ku-band and provided VV polarisation; FastGBSAR additionally had fully polarimetric capability.

All radars were installed in the Planpincieux hamlet to have the apparatuses connected to the power grid. The distances from ML and WS were of 2500 m and 4800 m, respectively. Using the RAR, we also experimented with the positioning on the Mont de La Saxe crest, near the TLC monitoring system of the ML (Figure 1). In this case, the sensor-to-distance increased (Table 1).

The exceptional mountain environment introduced a series of data processing issues [29,31]. The variable atmospheric conditions and the large elevation difference caused a strong disturbance. Liquid and solid precipitation modified the surface scattering properties and caused data degradation. Therefore, we implemented specific methods to minimize the atmospheric effects and to remove corrupted data effectively [38]. A further critical issue concerned the sensor-to-target distance. GBSAR devices have a limited operational range, up to 4–5 km. Therefore, ad hoc software/hardware adjustments were applied to monitor WS, e.g., the adoption of high-gain antennas. The long distances also affected the results' spatial resolution. The azimuth resolution linearly decreases with the range. Using the GBSARs, the resolution was approximately 10–15 m for ML and 15–20 m for WS. Unlike the GBSAR systems, the RAR suffered the operational range less, due to its higher SNR, but its azimuth resolution was twice as coarse.

Another issue concerned the radargrams' georeferencing, which was fundamental to evaluate the active glacier portions precisely. Therefore, we proposed a method based on the spatial correlation between amplitude maps and a digital terrain model, obtaining high georeferencing precision [39].

3.5. Data Integration

Besides the independent analysis of single monitoring data, we implemented data integration methods. The use of many systems surveying the same area provided data redundancy that served multiple scopes. First, the data were validated to strengthen

their reliability and to recognize potential outliers. Second, the probability of losing data because of system failure was reduced. Third, each surveying sensor detected different components of surface displacement. This allowed for the development of a technique to fuse the DIC and TRI results [39]. Since DIC and TRI detect complementary displacement components, their merging provided the spatially distributed three-dimensional surface kinematics. The procedure involved first the radar data geocoding, which was conducted by applying a spatial correlation between the DTM and the radar amplitude map, and the orthorectification of the oblique image, using recognizable natural features on both the photographs and the available DTM as ground-control points. Second, the measurement data of both instruments were projected into a common coordinate system (CS) by applying three-dimensional rototranslation.

Finally, the independent displacement components were summed to obtain the three-dimensional displacement vector. In our case, we projected the TRI data onto the images of CS and we summed the projected LOS-parallel displacement component with the two displacement components orthogonal to the LOS obtained with the DIC.

4. Results

4.1. Robotic Total Station and GNSS

In this section, we present the results of the topographic network installed on the WS. As mentioned before, the GNSS installed in 2010 suffered technical failures that reduced the number of correct acquisitions. However, in the period between July 2011 and January 2012, the GNSS provided displacement values in good agreement with the RTS data between July–December 2011 and (monthly averages have correlation coefficient 0.73, p-value < 10^{-4} and mean absolute difference 4.5 mm day^{-1}) (Figure 3) [46].

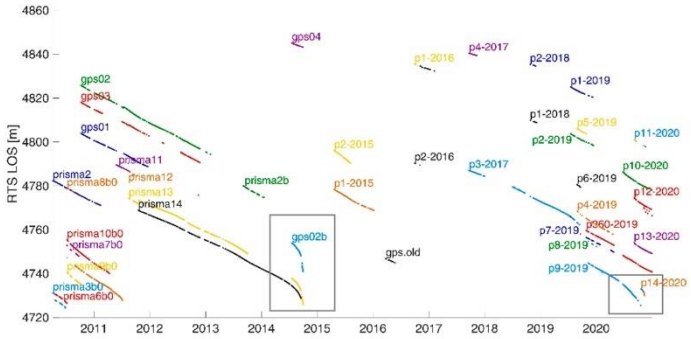

Figure 3. Reflective prisms installed onto the WS since 2010. The labels "gps" refer to prisms too. The ordinates report the evolution of the distance between every prism and the RTS. In September 2014 and November 2020, the acceleration of several prisms is visible in the grey boxes, which corresponds to ice break-offs.

The analysis of RTS data showed that the usual WS surface velocity follows a seasonal trend. This velocity varies between ~20–30 mm day^{-1} in the cold season and 40–50 mm day^{-1} during the warm period (Figure 3) [45]. The RTS time series of the second halves of 2014 and 2020 showed the serac acceleration before the ice break-offs that occurred on 23 and 29 September 2014 and 17 October and 11 November 2020 (Figure 4).

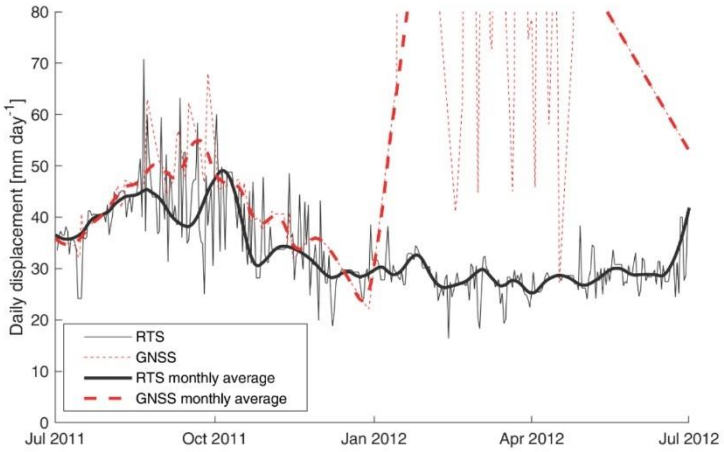

Figure 4. Whymper Serac's daily surface 3D displacement measured by GNSS (dashed red line) and RTS (solid black line). Thick lines refer to the monthly averages. The displacement values are the averaged values of the available three GNSS and three to five RTS measured prisms.

The displacement trend in 2014 followed the combination of power-law and log-oscillation behavior proposed by Pralong et al. [53]. Integrating this method in data post-processing, Faillettaz et al. [35] showed that it would be possible to predict the instant of failure almost two weeks before the event.

4.2. Time-Lapse Camera

Commonly, monitoring with the DIC technique provides at most daily kinematic maps, because the processed images should be acquired with similar illumination conditions. Such a temporal frequency is sufficient to detect relatively fast processes. For example, we observed a few periods of strong acceleration of the ML every year, culminating with relatively large break-offs [37]. Such a phenomenon has a temporal development of 5–10 days (Figure 5).

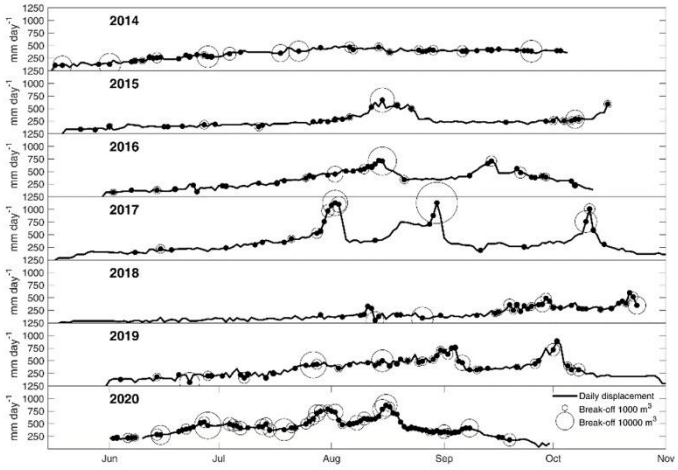

Figure 5. DIC time series of the daily velocity of the ML snout. The solid black circles represent the break-offs, while the white circle size is proportional to the break-off volume. Modified from [37].

Moreover, the analysis of surface displacement maps and the photographs' visual investigation permitted the identification of potentially unstable sectors. In the Summer of 2019 and 2020, we identified wide fractures that isolated ice portions characterized by notable acceleration. These portions had an estimated volume of 250,000 m^3 and 500,000 m^3 [54]. Run out simulations showed that potential break-offs could have reached the Planpincieux hamlet [55]. Emergency plans were activated, but fortunately, large collapses did not occur.

Besides the kinematics measurement, the availability of high-frequency images allowed the identification and classification of the break-offs from the ML snout. Three main processes usually cause collapses: (i) disaggregation: detachments of relatively small ice fragments (volume < 10^3 m^3); (ii) water tunnelling: collapse due to the outburst of water pockets and/or collapse of the empty cavities; and (iii) slab failure: detachment of large ice lamella due to development of a fracture along the entire ice thickness (volume > 10^4 m^3). The largest break-off was observed on 29 August 2017 with a volume of approximately 55,000 m^3 [37].

In 2020, we applied the DIC processing to the photographs of the WS. The expected motion was approximately 20–50 mm day^{-1}, which corresponded to less than one pixel. We applied the DIC processing to images separated by time gaps of a few days to a couple of weeks to ensure larger SNR. Such an approach allowed us to observe the acceleration of the ice chunks that collapsed on 17 October and 11 November 2020 (Figure 6).

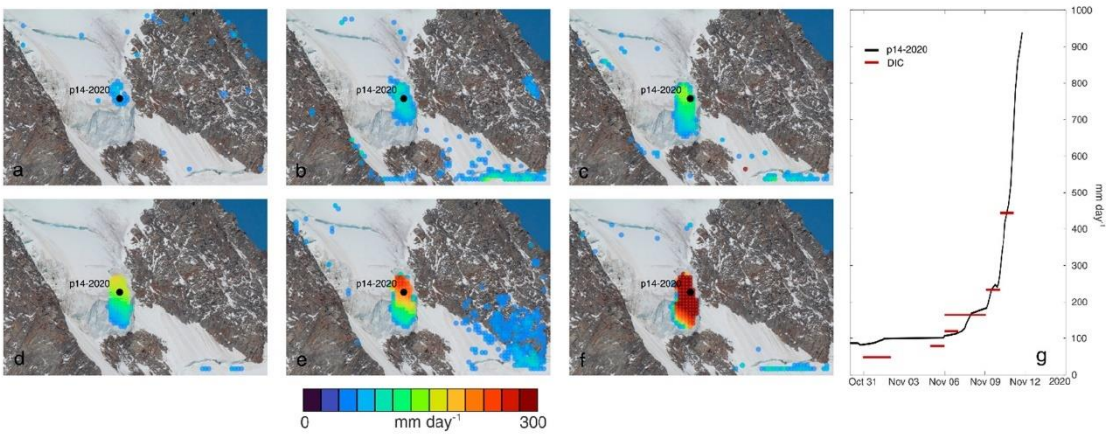

Figure 6. (**a**–**f**) Mean daily velocity (calculated as the sum of the two displacement components orthogonal to the LOS) of the Whymper Serac measured with DIC. The results were obtained by processing the images between 31 October–2 November; 5–6 November; 6–7 November; 6–9 November; 9–10 November; and 10–11 November 2020, respectively. (**g**) The black line refers to the velocity of the prism p14-2020 that was placed onto the surface of the ice chunk of approximately 20,000 m^3 that broke-off on 11 November 2020, while the horizontal red lines indicate the mean daily velocity obtained with the DIC in correspondence of the prism. Both DIC and RTS data evidenced the acceleration of the ice chunk. The height of the serac face is approximately 40 m.

4.3. Terrestrial Radar Interferometry

The experimental campaigns conducted between 2013 and 2016 were used to assess the limits and potentiality of the TRI in surveying the Grandes Jorasses glaciers. During the RAR campaigns in 2013 and 2014, we examined the influence of radar positioning (Figure 1). The installation in the Planpincieux hamlet offered a LOS perspective almost parallel to the displacement direction. Therefore, the measured displacement represented most of the real movement. However, the visibility of glacier portions was limited.

Conversely, almost the whole glaciated area was detectable from the crest of Mont de La Saxe, but a lower fraction of the actual displacement was observed due to the higher

angle between the LOS and the main motion direction. Figure 7 shows the surface velocity maps of the surveys of 7 and 8 August 2014. In the areas visible by both radar positions, one can note the difference in measured velocities due to the different LOS orientations.

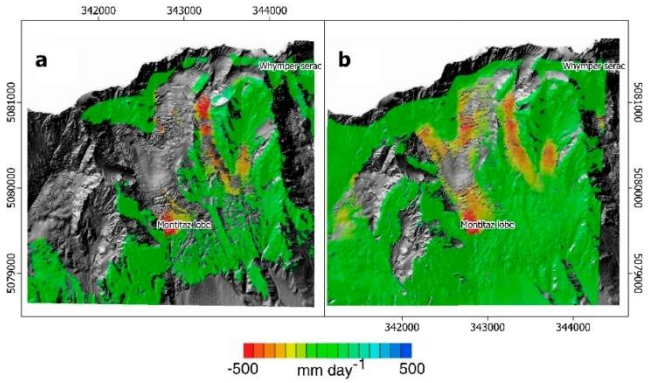

Figure 7. Velocity maps obtained with terrestrial interferometric radar installed (**a**) in the Planpincieux hamlet and (**b**) on the opposite ridge of the valley. The two campaigns lasted for 2 h and were conducted on 7 and 8 August 2014, respectively. Modified from [47].

In 2015, the measurements were conducted with an acquisition frequency of approximately 15 min. In that period, the daily glacier displacement was of the order of 400–500 mm day^{-1}. The Ku-band adopted radar had a maximum detectable displacement capability between two acquisitions of 8.5 mm, which corresponded approximately to 400 mm day^{-1}, i.e., comparable to the glacier velocity. Therefore, phase wrapping often occurred. To avoid it, we adopted a shorter temporal baseline in the subsequent surveys.

In 2016, we conducted a campaign with an acquisition frequency of 10 s. This allowed us to minimize the atmospheric disturbance and to avoid phase ambiguity. However, the signal amplitude was low due to the shorter duration of the acquisition, thus, the surveyed area was reduced. Additionally, we explored the possible application of different polarimetric configurations, which help in land cover classification [56]. Unfortunately, the quality of the results was low, likely because the Ku band is not suitable for polarimetric measurements on temperate glaciers, as also observed by Baffelli et al. [57].

Since September 2019 and January 2020, two permanent GBSARs have been arranged to survey the ML and WS, respectively. These monitoring systems are still in activity and serve early warning purposes. For legal reasons, the possibility of publishing their data is limited.

4.4. Data Integration

The concurrent use of various surveying systems provided data redundancy that minimized data loss. Figure 6 shows the WS daily velocity obtained with DIC and RTS. As one can note, the DIC data were not continuous, while the RTS acquired several epochs every day. However, their integration provided wider information on the glacier kinematics. Since DIC detected spatially distributed data, it was possible to observe the vertical gradient of the ice chunk motion before the break-off. On the other hand, using only RTS data, such a toppling process could not have been observed. It is worth noting that the RTS displacement values were higher than the DIC ones. This happened because the RTS detected three-dimensional displacement, while the DIC detected only the two displacement components orthogonal to its LOS.

Another advantage of data integration is the measurement validation. During April–May 2020, TRI, DIC, and RTS observed different velocity trends to the WS. The RTS detected an acceleration because the reflective prism was located on an ice chunk isolated from the main serac body, while the TRI measured an overall deceleration. Analyzing the DIC

results, we noticed the presence of an isolated ice chunk, while the rest of the serac was constantly moving. Additionally, the TRI data were probably affected by atmospheric artefacts, which were corrected using the other sensors' data for calibration.

Another developed data integration approach was the coupling of TRI and DIC measurements. We tested this method between 4 and 27 September 2015 and in the 2020 warm season (Figure 8) [39]. In these cases, we used a GBSAR installed in the Planpincieux hamlet and the TLC of the Mont de La Saxe (Figure 1). The data coupling provided spatially distributed three-dimensional surface kinematics in the areas visible by both apparatuses, which depended on the positioning of the monitoring systems. These three-dimensional displacement maps allowed us to observe that the motion direction was not uniformly parallel to the local slope. The steep faces of the seracs moved as a single rigid body showing a relevant horizontal component of the movement [39].

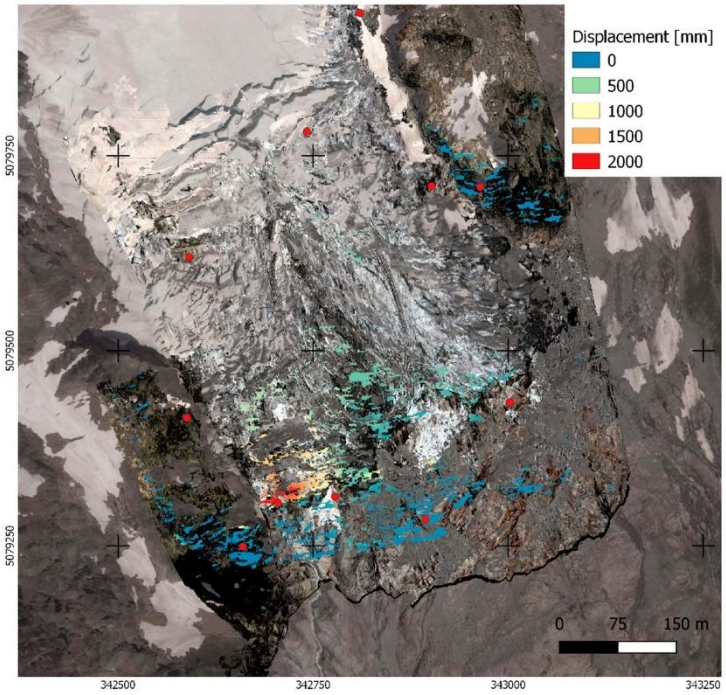

Figure 8. Three-dimensional daily displacement of the Planpincieux glacier between 31 July and 1 August 2020 obtained from the fusion of DIC and TRI results. The orthorectified oblique photographs is overlain on a Google Earth image. The red dots indicate the ground control points adopted to orthorectify the oblique picture.

4.5. Uncertainty Analysis

The GNSS uncertainty was estimated during field tests. The GNSS were deployed in two different positions, which were measured for periods of two hours each. The residuals adopted as reference had a standard deviation of 20 mm compared with the measurement of a total station.

We estimated the measurement uncertainty of the other monitoring systems according to the following approach: we examined the displacement calculated on the stable areas, which is assumed to be null, and we considered the standard deviation of the residuals as the uncertainty.

In the case of RTS, we considered the corrected values of the reference prisms since 2010, whose standard deviation was 106 mm.

We calculated the uncertainty of DIC applied to ML and WS photographs separately. For ML, we considered the daily displacement measured in bedrock areas between 4 and 27 September 2015 (11,700 points), while for WS, we used the dataset shown in Figure 6 (5600 points). For these datasets, we obtained a standard deviation of 18 mm and 17 mm, respectively. However, in WS, misregistration caused large errors, thus, the corresponding uncertainty refers only to the measurement obtained in optimal conditions.

In the case of the GBSAR, we considered 6300 measurements between 4–27 September 2015. These data were acquired every 15 min on a rocky area. For this dataset, we obtained a standard deviation of 1 mm.

Concerning the DIC-TRI fusion, a source of error pertained to the data georeferencing. We estimated a geocoding uncertainty between 1–2 m and ~4 m for the DIC and TRI results [39].

5. Discussion

The monitoring systems adopted in the Grandes Jorasses glacial complex cover most of the existing terrestrial apparatuses to survey the surface glacier kinematics:, i.e., RTS, GNSS, TLC, and terrestrial radar interferometer. Such a wide range of sensors in a limited area makes the Grandes Jorasses an open-air laboratory, where the limits and potentialities of monitoring systems in an environment with extreme weather, accessibility, and geometric characteristics can be explored. Table 2 summarizes the main characteristics of every monitoring system, as well as their main advantages and limitations.

Table 2. Main characteristics, advantages, and limitations of the considered survey systems.

Survey System	Measurement	Measurement Uncertainty	Acquisition Frequency	Financial Cost [10^3 €]	Advantages	Limitations
RTS	Point 3D displacement	~100 mm	Hour	30–50	Long-life	Uncertainty increasing with range Need for on-site access Weather sensitive
GNSS	Point 3D displacement	~20 mm	Hour	1–10 each	Continuous survey Weather insensitive	Need for on-site access Need for on-site power supply Possible sensor loss
TLC	Area 2D components orthogonal to LOS	~20 mm	Day	5–10	Low-cost Long life Remote sensing	Low sensitivity Weather sensitive No nocturnal acquisition Non-geocoded measurement
TRI	Area 1D component parallel to LOS	~1 mm	Minute	150–350	High acquisition frequency Continuous survey Remote sensing	Expensive Complex processing Difficult logistics

The RTS provided punctual, three-dimensional measurements with millimetric sensitivity. The RTS technology is consolidated, and its limitations and advantages are known. In optimal conditions, it offers continuous hourly data. The RTS requires little processing effort and has good endurance and reliability. The network's financial cost is mainly related to the instrument, whose price is in the range of 20,000–40,000 €; the cost of the targets is negligible. The principal disadvantage of this system is the need for physical installation and maintenance of passive targets in the investigated area. This can be impossible in inaccessible areas like the ML, or very challenging, like in the WS, where the support of alpine guides is necessary. The data continuity may be hampered by target loss or by small changes in the view angle of the reflective prisms caused by strong wind, avalanches, or rapid glacier movement. All these factors can prevent target localization by the RTS. Therefore, target replacement is often necessary. A possible solution is the use of prisms with a full view angle (i.e., 360° on the vertical axis and 120° on the horizontal axis). However, the cost of such a prism is in the order of 1000 €. Moreover, severe weather may hinder the survey, especially when the sensor-to-target distance is high. In the Grandes Jorasses case, the RTS measurement uncertainty is high (approximately 100 mm). A robust network of reference prisms should solve this issue; however, this could be challenging to achieve in

exceptional contexts such as WS. Despite its limitations, the RTS of the WS proved to be an effective solution for continuous monitoring. This RTS system, active since 2010, allowed for the identification of precursors of the collapses of 2014 and 2020 [35], thus confirming its suitability for warning purposes.

GNSS share some peculiarities with the RTS. They also provide punctual, high-frequency, three-dimensional measurements with millimetric sensitivity. Additionally, they acquire data in every meteorological condition. An important GNSS advantage is that they do not require direct visibility from the master station because they are connected to it using radio protocol. In the case of WS, visibility is one of the most serious limitations of acquisition continuity. The cost of high-performing multi-channel GNSS can reach up to 10,000 € per device. Therefore, a potential sensor loss represents a relevant financial waste. However, low-cost solutions can be adopted with acceptable reliability [58], as in the case of WS, where the cost of a single GNSS was approximately 1000 €, including the power supply and the data transmission equipment [50]. GNSS, like the RTS, require direct access to the investigated area for the receiver installation. However, GNSS sensor maintenance has to be done on site, requiring further efforts, particularly if installed in areas not easy to reach with bad meteorological conditions. Moreover, the need for an autonomous power supply is an additional constraint of this system, making it a less robust solution.

The TLC provided a photographic dataset that facilitates the phenomena investigation, such as the break-off and fracture identification and the instability process evolution. The operational distance can easily reach several km with the adoption of entry-level equipment. In addition, the adoption of the DIC technique offers spatially distributed two-dimensional maps of surface kinematics. The data's spatial resolution depends on the adopted hardware, the sensor-to-target distance, and the processing parameters. Spatial data facilitate the understanding of the investigated process. For example, in the ML, we identified different kinematic domains, which corresponded to potentially unstable sectors [37], while in WS, we observed the toppling process before the break-off occurred on 11 November 2020 (Figure 6). The DIC uncertainty is sub-pixel in optimal conditions, which corresponded to less than 20 mm in ML and WS cases. However, snow pattern changes hamper co-registration and measurement. Reliable results are obtained only with favorable weather and suitable illumination conditions. Moreover, the temporal baseline should correspond to a displacement of a few pixels to enhance the SNR. Consequently, the optimal temporal frequency is to process one image per day. The occurrence of bad weather can limit the number of usable images and increase the time gaps between the images suitable for processing [59]. Nevertheless, such periods rarely last more than several days. Such a frequency is usually sufficient to observe rapid glaciological phenomena successfully. For example, we observed the speed-up phases of the ML snout, which lasted several days (Figure 5), or the acceleration of the collapsed ice chunk in the WS on 11 November 2020 (Figure 6). A TLC monitoring system has a high benefit–cost ratio thanks to the photographic time-lapse dataset's characteristics and the financial costs of the involved equipment (approximately 5000–10,000 €). It is suitable to investigate rapid glacial processes and, to a lesser extent, it can help in warning activities, even though it cannot be a primary tool for this purpose, because it operates at daily temporal frequency and needs favorable weather to provide results.

TRI offers spatially distributed maps of the displacement component that is parallel to the LOS. The apparatus positioning has to be carefully identified to maximize the displacement fraction that can be measured. Terrestrial radars have the advantage of operating continuously with minute frequency, even in the presence of unfavorable weather. TRI measurements have millimeter uncertainty, but they are sensitive to many sources of noise. In glacial areas, environmental disturbances complicate the data processing. The results interpretation is not trivial, and specific expertise is necessary. Elevated sensor-to-target distances coarsen the spatial resolution and may require non-standard hardware. The equipment is cumbersome and power demanding; consequently, logistic efforts are necessary. Additionally, the financial costs of the apparatus are relevant and vary from

150,000 € to 350,000 €. Despite these limitations, a terrestrial radar interferometer is the best performing solution for continuous near-real-time monitoring that is also suitable for early warning purposes. For this reason, in the Winter of 2019/2020, two permanent GBSARs were arranged to survey the ML and WS for early warning purposes. In these cases, the TRI technique was adopted due to its measurement capability in every meteorological condition and its high temporal frequency.

Finally, we showed that the concurrent adoption of different monitoring systems has various advantages. First, it avoids data loss in the case of a single system failure; second, it provides data redundancy for measurement validation; third, it allows DIC and TRI data coupling to obtain the three-dimensional surface kinematics.

6. Conclusions

The Grandes Jorasses glacial complex comprises different typologies of glaciers located close to a touristic area. Two sectors of these glaciers (i.e., the ML and the WS) menace the population due to regular break-offs that could reach hundreds of thousands of cubic meters. In the last decade, a complex monitoring network has been arranged to enhance our understanding of the glacier dynamics and control their evolution to identify potential failure precursors.

We presented several strategies adopted to monitor the WS and ML. In the last decade, we conducted surveys employing a wide range of sensors that detected the surface kinematic. In particular, this paper presented the use of RTS, GNSS, TLC, and TRI. We reported the most relevant results obtained and illustrated the main potentialities and limits of the single monitoring apparatuses. We discussed their possible uses in the complex and challenging glacial environment. Limited accessibility, bad weather conditions, low temperatures, and the need for long-range measurement systems make glacier monitoring a critical challenge from the technical point of view. The open-air laboratory of the Grandes Jorasses offers the opportunity to develop and test different monitoring solutions.

Considering the aims of process investigation and warning activities, we showed that warning systems should acquire data in every meteorological condition and early warning can be achieved only by using apparatuses that provide near-real-time data. Therefore, TRI is likely the best approach, even though it requires high financial costs. In simpler contexts, RTS and GNSS have often been adopted for early warning due to their lower financial cost. Nevertheless, logistic issues of accessibility and maintenance are critical elements in the WS and the extreme weather and geometry do not guarantee data continuity. A possible solution is the adoption of redundant monitoring systems to minimize data loss.

Conversely, photographic data allow for an immediate vision of the monitored area. Accordingly, TLC is a valuable tool for understanding glaciological processes. Moreover, the DIC technique produces quantitative displacement results. The combined use of different monitoring systems to acquire complementary data is a promising approach that provides further opportunities for scientific investigation and early warning activities.

Author Contributions: Conceptualization, formal analysis, investigation, writing—original draft, N.D.; conceptualization, supervision, investigation, writing—review and editing, D.G. (Daniele Giordan); investigation, writing—review and editing, F.T.; formal analysis, Writing—Review and editing, A.W.; writing—review and editing, D.G. (Danilo Godone). All authors have read and agreed to the published version of the manuscript.

Funding: This research received no external funding.

Institutional Review Board Statement: Not applicable.

Informed Consent Statement: Not applicable.

Data Availability Statement: Datasets for this research is published in Dematteis et al. (2020) Multisource data of glacier kinematics. 4TU. Centre for Research Data doi:10.4121/uuid:688ae25c-0fa0-463c-baf3-34ebdf9fdbd.

Conflicts of Interest: The authors declare no conflict of interest.

References

1. Barnett, T.P.; Adam, J.C.; Lettenmaier, D.P. Potential impacts of a warming climate on water availability in snow-dominated regions. *Nature* **2005**, *438*, 303–309. [CrossRef]
2. López-Moreno, J.I.; Alonso-González, E.; Monserrat, O.; Del Río, L.M.; Otero, J.; Lapazaran, J.; Luzi, G.; Dematteis, N.; Serreta, A.; Rico, I.; et al. Ground-based remote-sensing techniques for diagnosis of the current state and recent evolution of the Monte Perdido Glacier, Spanish Pyrenees. *J. Glaciol.* **2019**, *65*, 85–100. [CrossRef]
3. Deline, P.; Gruber, S.; Delaloye, R.; Fischer, L.; Geertsema, M.; Giardino, M.; Hasler, A.; Kirkbride, M.; Krautblatter, M.; Magnin, F.; et al. Ice Loss and Slope Stability in High-Mountain Regions. In *Snow and Ice-Related Hazards, Risks, and Disasters*; Academic Press: Cambridge, MA, USA, 2014; pp. 521–561, ISBN 9780123964731.
4. Kääb, A.; Huggel, C.; Fischer, L.; Guex, S.; Paul, F.; Roer, I.; Salzmann, N.; Schlaefli, S.; Schmutz, K.; Schneider, D.; et al. Remote sensing of glacier- and permafrost-related hazards in high mountains: An overview. *Nat. Hazards Earth Syst. Sci.* **2005**, *5*, 527–554. [CrossRef]
5. Shugar, D.H.; Jacquemart, M.; Shean, D.; Bhushan, S.; Upadhyay, K.; Sattar, A.; Schwanghart, W.; McBride, S.; de Vries, M.V.W.; Mergili, M.; et al. A massive rock and ice avalanche caused the 2021 disaster at Chamoli, Indian Himalaya. *Science* **2021**, *373*, 300–306.
6. Watson, C.S.; Quincey, D. Glacier Movement. In *Geomorphological Techniques*; British Society for Geomorphology: London, UK, 2015.
7. Luzi, G.; Pieraccini, M.; Mecatti, D.; Noferini, L.; Macaluso, G.; Tamburini, A.; Atzeni, C. Monitoring of an alpine glacier by means of ground-based SAR interferometry. *IEEE Geosci. Remote Sens. Lett.* **2007**, *4*, 495–499. [CrossRef]
8. Hewitt, K.; Wake, C.P.; Young, G.J.; David, C. Hydrological investigations at Biafo Glacier, Karakoram range, Himalaya: An important source of water for the Indus River. *Ann. Glaciol.* **1989**, *13*, 103–108. [CrossRef]
9. Stocker-Waldhuber, M.; Fischer, A.; Helfricht, K.; Kuhn, M. Long-term records of glacier surface velocities in the Ötztal Alps (Austria). *Earth Syst. Sci. Data* **2019**, *11*, 705–715. [CrossRef]
10. Huss, M.; Bauder, A.; Werder, M.; Funk, M.; Hock, R. Glacier-dammed lake outburst events of Gornersee, Switzerland. *J. Glaciol.* **2007**, *53*, 189–200. [CrossRef]
11. Sugiyama, S.; Bauder, A.; Weiss, P.; Funk, M. Reversal of ice motion during the outburst of a glacier-dammed lake on Gornergletscher, Switzerland. *J. Glaciol.* **2007**, *53*, 172–180. [CrossRef]
12. Diolaiuti, G.; Kirkbride, M.P.; Smiraglia, C.; Benn, D.I.; D'Agata, C.; Nicholson, L. Calving processes and lake evolution at Miage glacier, Mont Blanc, Italian Alps. *Ann. Glaciol.* **2005**, *40*, 207–214. [CrossRef]
13. Dunse, T.; Schuler, T.V.; Hagen, J.O.; Reijmer, C.H. Seasonal speed-up of two outlet glaciers of Austfonna, Svalbard, inferred from continuous GPS measurements. *Cryosphere* **2012**, *6*, 453–466. [CrossRef]
14. Einarsson, B.; Magnússon, E.; Roberts, M.J.; Pálsson, F.; Thorsteinsson, T.; Jóhannesson, T. A spectrum of jökulhlaup dynamics revealed by GPS measurements of glacier surface motion. *Ann. Glaciol.* **2016**, *57*, 47–61. [CrossRef]
15. Manson, R.; Coleman, R.; Morgan, P.; King, M. Ice velocities of the Lambert Glacier from static GPS observations. *Earth Planets Sp.* **2000**, *52*, 1031–1036. [CrossRef]
16. Fallourd, R.; Trouvé, E.; Roşu, D.; Vernier, F.; Bolon, P.; Harant, O.; Gay, M.; Bombrun, L.; Vasile, G.; Nicolas, J.M.; et al. Monitoring Temperate Glacier Displacement by Multi-Temporal TerraSAR-X Images and Continuous GPS Measurements. *IEEE J. Sel. Top. Appl. Earth Obs. Remote Sens.* **2011**, *4*, 372–386. [CrossRef]
17. Sugiyama, S.; Gudmundsson, G.H. Short-term variations in glacier flow controlled by subglacial water pressure at Lauteraargletscher, Bernese Alps, Switzerland. *J. Glaciol.* **2004**, *50*, 353–362. [CrossRef]
18. Evans, A.N. Glacier surface motion computation from digital image séquences. *IEEE Trans. Geosci. Remote Sens.* **2000**, *38*, 1064–1072. [CrossRef]
19. Ahn, Y.; Box, J.E. Glacier velocities from time-lapse photos: Technique development and first results from the Extreme Ice Survey (EIS) in Greenland. *J. Glaciol.* **2010**, *56*, 723–734. [CrossRef]
20. Brinkerhoff, D.; O'Neel, S. Velocity variations at Columbia Glacier captured by particle filtering of oblique time-lapse images. *arXiv* **2017**, arXiv:1711.05366.
21. Messerli, A.; Grinsted, A. Image georectification and feature tracking toolbox: ImGRAFT. *Geosci. Instrum. Methods Data Syst.* **2015**, *4*, 23–34. [CrossRef]
22. Schwalbe, E.; Maas, H.G. The determination of high-resolution spatio-temporal glacier motion fields from time-lapse sequences. *Earth Surf. Dyn.* **2017**, *5*, 861–879. [CrossRef]
23. Dematteis, N.; Giordan, D.; Allasia, P. Image Classification for Automated Image Cross-Correlation Applications in the Geosciences. *Appl. Sci.* **2019**, *9*, 2357. [CrossRef]
24. Noferini, L.; Mecatti, D.; Macaluso, G.; Pieraccini, M.; Atzeni, C. Monitoring of Belvedere Glacier using a wide angle GB-SAR interferometer. *J. Appl. Geophys.* **2009**, *68*, 289–293. [CrossRef]
25. Riesen, P.; Strozzi, T.; Bauder, A.; Wiesmann, A.; Funk, M. Short-term surface ice motion variations measured with a ground-based portable real aperture radar Interferometer. *J. Glaciol.* **2011**, *57*, 53–60. [CrossRef]
26. Allstadt, K.E.; Shean, D.E.; Campbell, A.; Fahnestock, M.; Malone, S.D. Observations of seasonal and diurnal glacier velocities at Mount Rainier, Washington, using terrestrial radar interferometry. *Cryosphere* **2015**, *9*, 2219–2235. [CrossRef]

27. Gundersen, R.; Norland, R.; Denby, C.R. Monitoring glacier flow in Ny-Ålesund with a high temporal resolution ground-based interferometric-phased array radar. *Polar Res.* **2019**, *38*. [CrossRef]
28. Liu, L.I.N.; Jiang, L.; Sun, Y.Y.; Wang, H.; Sun, Y.Y.; Xu, H. Diurnal fluctuations of glacier surface velocity observed with terrestrial radar interferometry at Laohugou No. 12 Glacier, western Qilian mountains, China. *J. Glaciol.* **2019**, *65*, 239–248. [CrossRef]
29. Monserrat, O.; Crosetto, M.; Luzi, G. A review of ground-based SAR interferometry for deformation measurement. *ISPRS J. Photogramm. Remote Sens.* **2014**, *93*, 40–48. [CrossRef]
30. Luzi, G.; Pieraccini, M.; Mecatti, D.; Noferini, L.; Guidi, G.; Moia, F.; Atzeni, C. Ground-based radar interferometry for landslides monitoring: Atmospheric and instrumental decorrelation sources on experimental data. *IEEE Trans. Geosci. Remote Sens.* **2004**, *42*, 2454–2466. [CrossRef]
31. Luzi, G.; Dematteis, N.; Zucca, F.; Monserrat, O.; Giordan, D.; López-Moreno, J.I. Terrestrial radar interferometry to monitor glaciers with complex atmospheric screen. In Proceedings of the International Geoscience and Remote Sensing Symposium (IGARSS), Valencia, Spain, 22–27 July 2018; pp. 6243–6246.
32. Margreth, S.; Funk, M.; Tobler, D.; Dalban, P.; Meier, L.; Lauper, J. Analysis of the hazard caused by ice avalanches from the hanging glacier on the Eiger west face. *Cold Reg. Sci. Technol.* **2017**, *144*, 63–72. [CrossRef]
33. Avian, M.; Bauer, C.; Schlögl, M.; Widhalm, B.; Gutjahr, K.H.; Paster, M.; Hauer, C.; Frießenbichler, M.; Neureiter, A.; Weyss, G.; et al. The status of earth observation techniques in monitoring high mountain environments at the example of Pasterze Glacier, Austria: Data, methods, accuracies, processes, and scales. *Remote Sens.* **2020**, *12*, 1251. [CrossRef]
34. De Sanjosé, J.J.; Berenguer, F.; Atkinson, A.D.J.; De Matías, J.; Serrano, E.; Gómez-Ortiz, A.; González-García, M.; Rico, I. Geomatics techniques applied to glaciers, rock glaciers, and ice patches in Spain (1991–2012). *Geogr. Ann. Ser. A Phys. Geogr.* **2014**, *96*, 307–321. [CrossRef]
35. Faillettaz, J.; Funk, M.; Vagliasindi, M. Time forecast of a break-off event from a hanging glacier. *Cryosphere* **2016**, *10*, 1191–1200. [CrossRef]
36. Margreth, S.; Faillettaz, J.; Funk, M.; Vagliasindi, M.; Diotri, F.; Broccolato, M. Safety concept for hazards caused by ice avalanches from the Whymper hanging glacier in the Mont Blanc Massif. *Cold Reg. Sci. Technol.* **2011**, *69*, 194–201. [CrossRef]
37. Giordan, D.; Dematteis, N.; Allasia, P.; Motta, E. Classification and kinematics of the Planpincieux Glacier break-offs using photographic time-lapse analysis. *J. Glaciol.* **2020**, *66*, 188–202. [CrossRef]
38. Dematteis, N.; Luzi, G.; Giordan, D.; Zucca, F.; Allasia, P. Monitoring Alpine glacier surface deformations with GB-SAR. *Remote Sens. Lett.* **2017**, *8*, 947–956. [CrossRef]
39. Dematteis, N.; Giordan, D.; Zucca, F.; Luzi, G.; Allasia, P. 4D surface kinematics monitoring through terrestrial radar interferometry and image cross-correlation coupling. *ISPRS J. Photogramm. Remote Sens.* **2018**, *142*, 38–50. [CrossRef]
40. Giordan, D.; Allasia, P.; Dematteis, N.; Dell'Anese, F.; Vagliasindi, M.; Motta, E. A low-cost optical remote sensing application for glacier deformation monitoring in an alpine environment. *Sensors* **2016**, *16*, 1750. [CrossRef]
41. Giordan, D.; Dematteis, N.; Troilo, F.; Segor, V.; Godone, D. Close-Range Sensing of Alpine Glaciers. In *Glaciers and Polar Environment*; IntechOpen: London, UK, 2020; ISBN 978-1-83962-593-0.
42. World Glacier Monitoring Service (WGMS). *World Glacier Inventory: Status 1988*; Haeberli, W., Bösch, H., Scherler, K., Østrem, G.W., Eds.; IAHS(ICSI)/UNEP/UNESCO, World Glacier Monitoring Service: Zurich, Switzerland, 1989.
43. Raup, B.; Racoviteanu, A.; Khalsa, S.J.S.; Helm, C.; Armstrong, R.; Arnaud, Y. The GLIMS geospatial glacier database: A new tool for studying glacier change. *Glob. Planet. Chang.* **2007**, *56*, 101–110. [CrossRef]
44. Pralong, A.; Funk, M. On the instability of avalanching glaciers. *J. Glaciol.* **2006**, *52*, 31–48. [CrossRef]
45. Faillettaz, J.; Funk, M.; Vincent, C. Avalanching glacier instabilities: Review on processes and early warning perspectives. *Rev. Geophys.* **2015**, *53*, 203–224. [CrossRef]
46. GlaRiskAlp. Available online: http://www.glariskalp.eu/ (accessed on 1 February 2021).
47. Strozzi, T. *Monitoraggio del ghiacciaio di Planpincieux in Valle d'Aosta (Italia)*; Istituto di Ricerca per la Protezione Idrogeologica: Gumligen, Switzerland, 2014.
48. Leica TM30 Technical Data. Available online: https://w3.leica-geosystems.com/downloads123/zz/tps/tm30/brochures-datasheet/tm30_technical_data_en.pdf (accessed on 1 February 2021).
49. Faillettaz, J.; Pralong, A.; Funk, M.; Deichmann, N. Evidence of log-periodic oscillations and increasing icequake activity during the breaking-off of large ice masses. *J. Glaciol.* **2008**, *54*, 725–737. [CrossRef]
50. Lucianaz, C.; Rorato, O.; Allegretti, M.; Mamino, M.; Roggero, M.; Diotri, F. Low cost DGPS wireless network. In Proceedings of the 2011 IEEE-APS Topical Conference on Antennas and Propagation in Wireless Communications, Torino, Italy, 12–16 September 2011; pp. 792–795.
51. Dematteis, N.; Giordan, D. Comparison of digital image correlation methods and the impact of noise in geoscience applications. *Remote Sens.* **2021**, *13*, 327. [CrossRef]
52. Travelletti, J.; Delacourt, C.; Allemand, P.; Malet, J.P.; Schmittbuhl, J.; Toussaint, R.; Bastard, M. Correlation of multi-temporal ground-based optical images for landslide monitoring: Application, potential and limitations. *ISPRS J. Photogramm. Remote Sens.* **2012**, *70*, 39–55. [CrossRef]
53. Pralong, A.; Birrer, C.; Stabel, W.A.; Funk, M. On the predictability of ice avalanches. *Nonlinear Process. Geophys.* **2005**, *12*, 849–861. [CrossRef]

54. Sevestre, H. Extreme Summer Impacts Ice Shelves and Glaciers. Available online: https://public.wmo.int/en/media/news/extreme-summer-impacts-ice-shelves-and-glaciers (accessed on 1 October 2020).
55. Schweizer, J.; Margreth, S. *Evaluation of Hazard Caused by Ice Avalanches from the Planpincieux Glacier, Val Ferret, Courmayeur, Italy*; Update 2020; Part 1: Summer Scenarios; European Geosciences Union: Davos, Switzerland, 2020; Available online: https://meetingorganizer.copernicus.org/EGU2020/EGU2020-9717.html?pdf (accessed on 10 June 2021).
56. Cloude, S.R.; Pottier, E. An entropy based classification scheme for land applications of polarimetric SAR. *IEEE Trans. Geosci. Remote Sens.* **1997**, *35*, 68–78. [CrossRef]
57. Baffelli, S.; Frey, O.; Hajnsek, I. Polarimetric analysis of natural terrain observed with a ku-band terrestrial radar. *IEEE J. Sel. Top. Appl. Earth Obs. Remote Sens.* **2019**, *12*, 5268–5288. [CrossRef]
58. Notti, D.; Cina, A.; Manzino, A.; Colombo, A.; Bendea, I.H.; Mollo, P.; Giordan, D. Low-cost GNSS solution for continuous monitoring of slope instabilities applied to Madonna del Sasso Sanctuary (NW Italy). *Sensors* **2020**, *20*, 289. [CrossRef]
59. Lenzano, M.G.; Lannutti, E.; Toth, C.; Rivera, A.; Lenzano, L. Detecting glacier surface motion by optical flow. *Photogramm. Eng. Remote Sens.* **2018**, *84*, 33–42. [CrossRef]

Morphodynamics of the Mont Blanc glaciers and their recent evolution

In order to further investigate topics (2) (3) (4) highlighted in the previous chapter, we concentrated on a first part of literature review, coming to the resolution that: (i) state of the art monitoring techniques are already in use at Planpincieux and Grandes Jorasses for the measurement of surface velocities of glaciers. (ii) Continuous monitoring of glacier displacements is seldom carried out and achieved worldwide. The Argentière Glacier in the Mont Blanc Massif represents a unique site for glacier displacement measurements around the globe (Vincent et al., 2022; Vincent & Moreau, 2016). (iii) An extension of the velocity measurements from a small part of the glacier to its full extent, and a region-wide assessment of seasonal and interannual variations in velocities could possibly be carried out with the use of satellite-borne remote-sensed data, but this has still not been the subject of literature studies on the Mont Blanc area or on other Alpine massifs. The outcomes of the research activities on this topic are summarised in the 'Morphodynamics of the Mont Blanc glaciers and their recent evolution' manuscript. The paper has been submitted to the journal "The Cryosphere" and has been published online as a Pre-print for open discussion and review.

Short summary

In the present manuscript, we reconstructed a seven year-long time series of surface displacements from a set of thirty glaciers on the Mont Blanc Massif. We validated results via comparison with other remotely sensed datasets and with ground-based measurements. We analysed the results highlighting remarkable trends and, finally, we proposed a classification of the different glacial bodies based on their morphometric analysis and their kinematic behaviour.

Main findings

The main findings of this publication are:

• Testing an experimental procedure to retrieve monthly surface displacements for Alpine glaciers with the use of freely available satellite imagery.

• Analysing the trends and characteristics of the obtained velocity time series.

• Proposing a classification of the analysed glaciers based on morphometric and kinematic characteristics.

• Highlighting limits and potentialities of the adopted methodologies.

Contributions of the PhD candidate

Conceptualisation of the research activity. Literature review. Archive data retrieval and organisation. Pre-processing of imagery. Digital image correlation analysis of the image stacks. Extraction of time series. Data organisation. Data analysis. Manuscript writing and figure elaboration.

Data availability

The data are available from the authors, upon request.

Journal

The Cryosphere (TC) is a not-for-profit international scientific journal dedicated to the publication and discussion of research articles, short communications, and review papers on all aspects of frozen water and ground on Earth and on other planetary bodies.

The main subject areas are the following:

- ice sheets and glaciers;
- planetary ice bodies;
- permafrost and seasonally frozen ground;
- seasonal snow cover;
- sea ice;
- river and lake ice;
- remote sensing, numerical modelling, in situ and laboratory studies of the above and including studies of the interaction of the cryosphere with the rest of the climate system.

The actual Journal Impact Factor is rated as 5.2.

The Cryosphere has an innovative two-stage publication process which involves interactive scientific discussion of preprints and utilizes the full potential of the Internet to do the following:

- foster scientific discussion;
- enhance the effectiveness and transparency of scientific quality assurance;
- enable rapid publication;
- make scientific publications freely accessible.

https://doi.org/10.5194/egusphere-2023-2771
Preprint. Discussion started: 4 December 2023

Morphodynamics of the Mont Blanc glaciers and their recent evolution

Fabrizio Troilo[1,4], Niccolò Dematteis[3], Francesco Zucca[4], Martin Funk[2], Daniele Giordan[3].

[1]Fondazione Montagna sicura, Glaciers, snow and avalanche research area, Courmayeur, 11013, Italy.
[2]ETH-VAW, Versuchsanstalt für Wasserbau, Hydrologie und Glaziologie, Zurich, CH-8092, Switzerland.
[3]Research Institute for Geo-Hydrological Protection IRPI, Italian National Research Council, Turin, 10135, Italy.
[4]University of Pavia, Department of Earth and Environmental Sciences, Pavia, 27100, Italy.

Correspondence to: Niccolò Dematteis (niccolo.dematteis@irpi.cnr.it); Fabrizio Troilo (ftroilo@fondms.org).

Abstract. The surface velocity of glaciers is a key parameter that provides fundamental information on glacier dynamics and their adaptation to changes in climate; moreover, ice velocity measurements are a very important parameter for modelling glacier physics and their evolution. While a few decades ago ice velocity would rely on point measurements performed in the field, the processing of high temporal and spatial resolution information from satellites nowadays provides new insights and a vast quantity of data, on a global scale, for the measurement of ice velocity. As of today, few studies have been performed in Alpine regions, and rarely has the focus been on ice velocity evolution. In the present study, we analyse the average monthly velocities on Alpine glaciers in the Mont Blanc massif. Seven years of Sentinel-2 optical satellite imagery have been processed to obtain ice velocity data. The main objectives of the study are: (i) to characterise the variability of the velocity fields of such glaciers, referring both to their temporal (seasonal and interannual) and spatial variations; (ii) to find relationships between the morphology of glaciers and their kinematics. We measured the monthly velocities of thirty glaciers varying from 18.0 m yr^{-1} to 436.3 m yr^{-1}, highlighting a breakpoint in the trends in 2020. This led to the identification of 13 glaciers showing variation of more than 20.0 m yr^{-2} between 2020 and 2022 compared to the previous years. We identified five clusters of morpho-dynamic characteristics, thus describing five different glacier type classes.

1 Introduction

Glacier flow has been one of the early drivers of glaciological interest and research since it was first studied. Its understanding and modelling evolved via the observations and findings of Somigliana in the early 1900s, Glen's laboratory experiments (Glen, 1952), followed by the interpretations of Nye (Nye, 1952) during the 1950s, to cite just a few, and have explained that the two main mechanisms of glacier flow rely on ice deformation and basal sliding. However, the motion of Alpine glaciers is largely related to basal sliding (Willis, 1995). Continuous monitoring of sliding velocities is extremely difficult and rarely achieved (Vincent and Moreau, 2016), but also the continuous monitoring of surface velocities of Alpine glaciers is complex on specific study sites, and very rarely has it been performed on a spatially distributed scale.

The flow of glaciers generally depends on a variety of physical parameters: ice thickness, which is the main driver of ice flow (Jiskoot 2011), and is related indirectly to the glacier trend in mass balance as it determines an evolution towards increase or decrease in glacier thickness; the glacier surface slope which is the other fundamental driver of ice flow; other parameters that influence ice flow are: ice properties (temperature, density), bedrock conditions (hard, soft, frozen or thawed ice-bed contact), topography, the glacier's terminal area type (land, sea, ice shelf), but also air temperature and precipitation and their seasonality that influences subglacial hydrology (Jiskoot, 2011; Humbert et al., 2005; Cuffey and Paterson, 2010; Benn and Evans, 2014; Bindschadler, 1983).

https://doi.org/10.5194/egusphere-2023-2771
Preprint. Discussion started: 4 December 2023

The analysis of glacier surface displacements is often measured as a proxy of ice flow and has a wide array of applications: it is a powerful climate change indicator (Beniston et al., 2018). It is also an important input data for global ice thickness models (Millan et al., 2022; Samsonov et al., 2021) which estimate global freshwater resources and global mass balance models that can also approximate sea-level rise contribution by glaciers (Zekollari et al., 2019). In the field of glacial hazards, it is used as a proxy for the detection of glacier surges (Kamb, 1987; Kääb et al., 2021), and accelerations that can result in glacier-related hazards (Pralong and Funk, 2006; Giordan et al., 2020). Measurements of the surface velocity of glaciers can be achieved by terrestrial techniques (Dematteis et al., 2021) such as topographic measurements of stakes or fixed points on the glacier (Stocker-Waldhuber et al., 2019), GNSS repeated or continuous surveys (Einarsson et al., 2016), digital image correlation of oblique photographs (Evans, 2000; Ahn and Box, 2010) and terrestrial radar interferometry (Luzi et al., 2007; Allstadt et al., 2015).

Considering remote sensing solutions, glacier surface velocities can be measured by a variety of aerial and space borne sensors. In recent decades, public access to satellite optical and radar data (especially from Sentinel and Landsat constellation satellites), as well as the commercial availability of very high resolution (30 cm to 1 m ground resolution) optical imagery (Deilami and Hashim, 2011) and radar data (Rankl et al., 2014), have given great input to glaciological research. In particular, Sentinel-2 optical imagery is widely used in glaciological studies and has been tested in literature on various environments (Paul et al., 2016; Millan et al., 2019). Nowadays, the automated processing of ice velocity maps with global coverage from satellite imagery is freely available online from web-based platforms such as the Golive datasets (Fahnestock et al., 2016), the ITS Live dataportal (https://its-live.jpl.nasa.gov/) or the FAU-Glacier portal (RETREAT, 2021 Ice surface velocities derived from Sentinel-1, Version 1; http://retreat.geographie.uni-erlangen.de/search). The availability of such datasets is very relevant globally, but its application to Alpine glaciers is limited due to its relatively coarse spatial resolution - e.g., 300x300 m (GOlive), 120x120 m (ITS live) - which can provide data on just few of the largest Alpine glaciers. The adopted resolution is a trade-off between computational effort and best resolution of the output that must cope with the global availability of the analysis. Limiting the processing of images at a regional scale decreases the computational effort compared to global products and makes it easier to obtain higher resolution velocity maps that allows Alpine glaciers to be investigated (Berthier et al., 2005), even though very small glaciers (i.e., width <250 m) are still difficult to analyse (Millan et al., 2019).

Recent studies using different techniques have measured spatio-temporal variations of ice velocity on large valley glaciers in an Alpine environment (Argentière Glacier) (Vincent and Moreau, 2016) (Miage Glacier) (Fyffe, 2012) as well as on steep glacier snouts (Planpincieux Glacier) (Giordan et al., 2020) but a spatially distributed analysis, at a regional scale, of the variations of velocities over glaciers with different morphological characteristics is, as of today, still lacking in the Alpine environment.

The main purposes of this study are the production of seven year-long velocity time series of surface velocity of thirty glaciers at a massif scale, as well as an integrated analysis of morphological and kinematic features of such glaciers. The identification of possible trends in the velocity time series, and a classification based on kinematic and morphological features, are major objectives of the present study. We analysed seven years of Sentinel-2 optical imagery to retrieve monthly velocity data on thirty glaciers in the Mont Blanc massif. We describe different patterns and behaviours of surface; subsequently, a classification based on velocity and morphometric features is proposed.

2 Area of study

The study area is the Mont Blanc massif. It is located in the western part of the European Alps bordering France, Italy and Switzerland (Figure 1) and culminating at 4809 m with the Mont Blanc summit; the highest peak in Central Europe. Many

https://doi.org/10.5194/egusphere-2023-2771
Preprint. Discussion started: 4 December 2023

other peaks in the Mont Blanc massif reach well above 4000 m and the entire area is very highly frequented with famous tourist resorts such as Courmayeur and Chamonix attracting thousands of tourists every year.

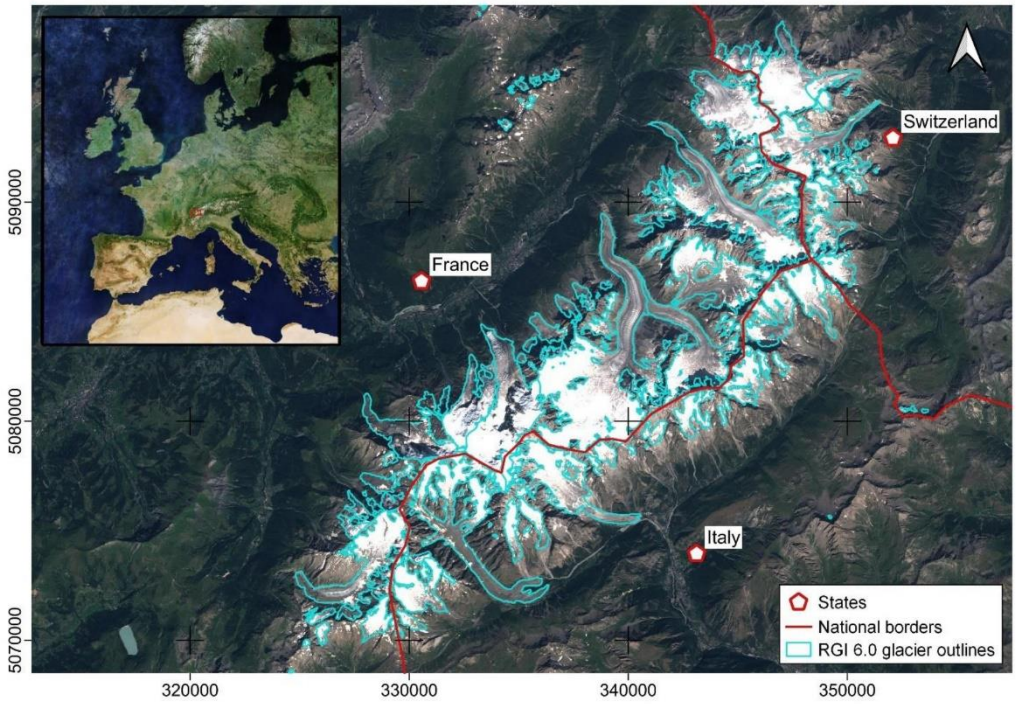

Figure 1. Study area of the Mont Blanc massif. Background: true colour image (cloud-free Europe mosaic in upper left panel), courtesy of the Copernicus Open Access Hub (https://scihub.copernicus.eu, last access: 10 September 2023).

The total surface of glaciers in the Mont Blanc massif is equal to 169 km^2 and totals 116 glaciers, according to the Randolph glacier inventory (RGI) 6.0 data which refers to 2003 (Pfeffer et al., 2014; Arendt et al., 2017). Seventy-six glaciers are very small, covering an area of less than 0.1 km^2, twenty-eight glaciers fall in the range between 1 km^2 and 5 km^2, and twelve glaciers have surface areas of more than 5 km^2.

The geological setting and the geomorphology of the Mont Blanc massif forms a high mountain range with its main ridge line oriented in a south-west/north-east direction along the French-Italian border. The valley floors flanking the massif have low altitudes - in the range of 1000-1500 m - resulting in steep slopes originating from the highest peaks with large vertical altitudinal differences. The meteo-climatic local conditions on the massif are of a continental type, but orographic effects on the predominant incoming weather fronts mean larger amounts of local precipitation compared to nearby regions (Gottardi et al., 2012).

The Argentière Glacier is the only glacier with regular mass balance measurements included in the WGMS 'Reference Glaciers' dataset in the Mont Blanc massif (Zemp et al., 2009). The Argentière Glacier has shown a general negative mass

https://doi.org/10.5194/egusphere-2023-2771
Preprint. Discussion started: 4 December 2023

balance trend since the early 1990s, in line with mass balances of other Alpine glaciers and glaciers from other mountain ranges across the globe. Geodetic mass balance measurements of the Thoula Glacier, a small glacier on the border between France and Italy at altitudes between 2900 and 3300m, represent well the local meteo-climatic conditions that result in slightly less negative mass balance trends compared to other glaciers in the Alps (Zemp et al., 2021; Zemp et al., 2020; Mondardini et al., 2021).

A more spatially distributed analysis of mass balances in the Mont Blanc region has also been outlined in the literature by means of geodetic mass balances of the whole Mont Blanc massif using stereo satellite imagery from the Pléiades and Spot satellite constellations (Berthier et al., 2014; Beraud et al., 2023). The trend outlined by Berthier (2014) at the massif scale, reflects data trends comparable to the glaciological mass balances of WGMG reference glaciers in the Alps. Locally, glaciers at a very low altitude show large ice volume losses and subsequent substantial glacier front retreats (Paul et al., 2020), while glaciers at higher altitudes suffer less acute volume loss and shrinkage. Large differences in the glacier frontal position, especially for the lower altitude terminating glaciers, can be well assessed by the difference of the terminus position in recent satellite imagery compared to the position outlined on the Randolph Glacier Inventory (RGI).

3 Materials

In this paper, we analysed the Copernicus - ESA Sentinel-2 optical satellite imagery dataset available for the study area. In addition to the above-mentioned dataset, we used Airbus Pleiades Stereo derived digital elevation models (DEMs) for the morphometric analysis of glaciers, and publicly available modelled ice thickness data from Millan et al. (Millan et al., 2022).

3.1 Sentinel-2 optical satellite imagery

The Sentinel-2 mission is composed of twin satellites - Sentinel-2A and Sentinel-2B - orbiting on sun-synchronous orbits at an altitude of 786 km. Free availability of thirteen multispectral bands (443 nm-2190 nm central wavelengths) with ground resolutions ranging between 10 m and 60 m, and a revisit time as low as three days for some areas (five days for most areas), as well as global coverage, make this product a very important resource for glaciological studies. In particular, Sentinel-2 near infrared band B08 processing level L1C is used for the application of feature tracking on glacial surfaces, as suggested by previous studies (Kääb et al., 2016). Based on different publications (Kääb et al., 2016; Millan et al., 2019), the geometric error of Sentinel-2 can show up to 1.5 pixel offsets in the horizontal plane. Therefore, an image co-registration process is normally needed for multitemporal analyses.

In the present study, a set of 108 images between 5 February 2016 and 10 November 2022, covering the whole study area, was adopted (GRANULE T32TLR, relative orbit 108). Such images, named 'tiles', are ~110x110 km^2 ortho-images in UTM/WGS84 projection.

3.2 Morphometric analysis data

Morphometric analysis of sample glaciers was performed using altitudinal data from a 1m resolution DEM obtained by the processing of Pleaides stereo pairs from August 2018 (Berthier et al., 2014). Mean glacier thicknesses were extrapolated from globally modelled ice thickness data published by Millan et al. (Millan et al., 2022).

https://doi.org/10.5194/egusphere-2023-2771
Preprint. Discussion started: 4 December 2023

4 Methods

We used digital image correlation to produce monthly-averaged and multi-year averaged velocity maps to investigate variations of glacier surface velocity in time and in space over the selected glaciers. We can hereby summarize the workflow that was used (Figure 2):

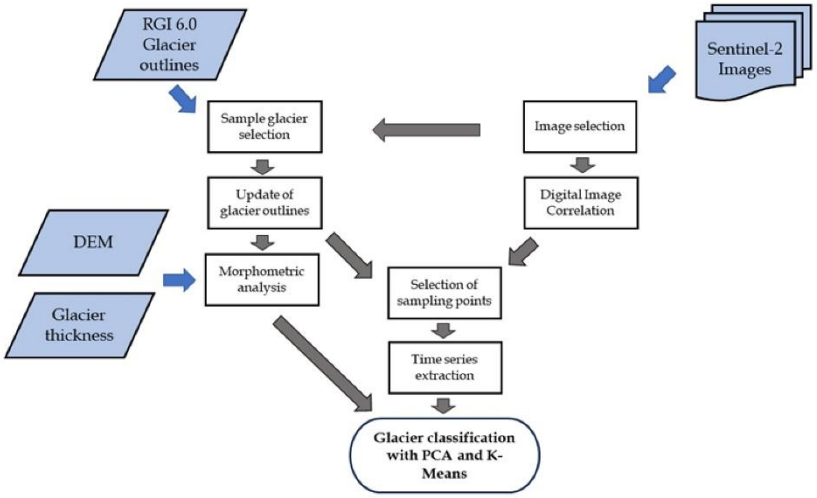

Figure 2. Workflow of the present study. The input datasets are evidenced in light blue while the processing steps are indicated in grey.

The input data are a DEM of the area of study, the RGI glacier outlines, the modelled glacier thickness and the stack of Sentinel-2 images in the reference period. The input DEM is used to obtain morphometric parameters of the glacier while the RGI glacier outlines are used, together with the selected satellite imagery, to choose suitable glaciers for surface glacier velocity analysis. After the glacier selection, we updated the RGI glacier outlines. Selected imagery is processed with digital image correlation to obtain glacier velocities. The glacier surface velocity maps are then used, together with the updated glacier outlines, to identify suitable areas and sampling points to extract velocity time series. Time series are analysed to identify general trends, seasonal patterns or particular kinematic behaviours. Finally, the velocity dataset and the morphometric parameters are analysed with a principal component analysis (PCA); subsequently, the principal components (PCs) are clustered using a K-means analysis to determine different classes of glacier based on their morpho-dynamic features.

4.1 Sentinel-2 image selection

To select the images, we considered two elements: (i) to maximize the geometric and geo-referencing precision, we adopted images acquired from the same orbit; (ii) to reduce the impact of clouds, we carried out a visual check of all images with a cloud cover percentage lower than 90% (as detected by the Copernicus cloud cover estimation algorithm) on the whole tile. We adopted this manual selection to maximize the number of available images; in the case of the Mont Blanc massif (like in

https://doi.org/10.5194/egusphere-2023-2771
Preprint. Discussion started: 4 December 2023

most mountainous areas worldwide), the local distribution of clouds can be extremely variable; in many cases, this can contribute to a considerable cloud percentage, even though high altitude areas may still be cloud-free.

4.2 Glacier selection

In the Mont Blanc massif, the presence of high-altitude accumulation areas, together with steep slopes, results in a significant number of very active glaciers with high average velocities in a relatively small region. In the present study, we selected a set of glaciers and investigated their surface velocity.
To minimize the presence of noisy and unreliable velocity data, we performed a selection of glaciers from the RGI 6.0 dataset. In particular, we did not include in our study:
A) glaciers with area < 0.1 km^2, as those glaciers would be too small for the reliable extraction of velocity maps with 10 m resolution optical satellite imagery (Millan et al., 2019).
B) glaciers showing strong variations of cast shadow.
C) glaciers that lack surface features to be tracked (e.g., ice caps).
Selection of point B) was made by creating a stack of images acquired between October and March, when cast shadows appear on satellite imagery, especially on north facing slopes. Subsequently, we manually individuated glaciers that are subject to large variations of shadow on their surface. We used the scene classification map (SCL) class 11 (cast shadows), available in processing level L2A of the Sentinel-2 images. However, since shadows on glaciers may often be misclassified in wintry conditions, we conducted a manual check to correct potential errors.
Selection of point C) is made manually by selecting glaciers that show very even surfaces on Sentinel-2 images. This is normally noted in ice caps at higher altitudes.

4.3 Glaciers' outline delineation

To analyse glacier areas and have an up-to-date mapping of glacier areas, we updated RGI 6.0 glacier outlines in order to fit with the glacier extensions that can be observed and manually outlined from Sentinel-2 imagery. We selected a cloud-free scene acquired on 28 August 2018 that represents well the conditions of the glaciers in the study period; True Color Image was used for this purpose. In some cases, a morphological indication that some parts of the glaciers could be considered independently from others in a division of kinematic domains was individuated (Paul et al., 2022; Zemp et al., 2021). As the kinematic analysis confirmed distinct behaviours of some glacier parts, those glaciers were mapped accordingly. The main examples of this are the tributary glaciers of the larger Miage Glacier complex, which all have distinct kinematic behaviour, well differentiated from the slow-moving, debris-covered main central valley tongue. Another example is present at Talèfre Glacier, where, over the past twenty years, the western part of the glacier has become totally independent from the eastern section so it made sense to consider it as a single glacier as of the RGI mapping of 2003. However, it should be considered independently in this study and consequently mapped.

4.4 Glaciers' morphometric analysis

The morphology that characterizes the glaciers selected in this study was analysed with the individuation of a series of key morphometric parameters:
1) the glacier planimetric surface (*Area*),
2) the glacier mean slope (*Slope*),
3) the glacier mean thickness (*Thickness*), obtained using the free dataset of Millan et al (Millan et al., 2022).

https://doi.org/10.5194/egusphere-2023-2771
Preprint. Discussion started: 4 December 2023

4) the glacier elongation evaluated as the ratio between glacier length and area (Shape).
5) the accumulation area ratio (*AAR*). The AAR is a common parameter used in glaciological studies to define the ratio between a snow-covered accumulation area and a bare ice ablation area of a specific glacier, at the end of the summer season. This gives an indication of the tendency of a glacier to tend towards stable or mass gain conditions or towards a mass loss condition (Cuffey and Paterson, 2010). AAR was obtained by mapping the snow accumulation areas on Sentinel-2 satellite images for every year between 2016 and 2022 at the end of the melting season. Subsequently, we calculated the average AAR for the study period.

4.5 Glaciers' surface velocity mapping

Digital image correlation is a common technique used to measure surface displacements using proximal (Evans, 2000; Ahn and Box, 2010; Schwalbe and Maas, 2017) and remotely sensed imagery (Scambos et al., 1992; Heid and Kääb, 2012b; Marsy et al., 2021; Dematteis and Giordan, 2021). The processing chain performed in the present study uses the open-source Glacier Image Velocimetry (GIV) toolbox (Van Wyk De Vries and Wickert, 2021). GIV uses frequency-based correlation, can process large datasets efficiently way and has been shown to perform well on glacier surface velocity measurements at different test sites (Van Wyk De Vries and Wickert, 2021). Co-registration of images is implemented in the GIV process chain using a stable area where potential shifts are estimated. To measure glacier surface velocities, we adopted the 'multi-pass' option which updates displacement estimates over multiple iterations, refining initial coarse chip size displacement calculations using progressively smaller chip sizes. The initial chip size is automatically defined by GIV and cannot be smaller than 32x32 px. Velocities higher than 1500 m yr^{-1} were considered as unrealistic and discarded. Grid spacing of the nodes in the displacement maps was set to 40 m. To produce the time series, given a specific image, we processed the first and second subsequent images (GIV order 2 time-oversampling). Then, the velocities of image pairs were averaged on a monthly basis. A temporal and spatial smoothing function was implemented in the processing algorithm and was used in the processing of data in this study.

4.6 Selection of sampling points

To analyse the time series that are representative of velocity variations of the selected glaciers, sampling points were identified on the velocity maps. The selection of sampling points for the time series extraction was carried out manually on the glacier surface, focusing on areas where velocity maps show high spatial coherence (Altena et al., 2019).
In some cases, the sampling points are not evenly distributed; when this occurred, the sampling points were located in areas that highlight velocity peaks (areas that show larger displacements than the surrounding areas) and high spatial coherence and that show no data voids (areas with unsuccessful image pair matching results in missing values). For each of the selected glaciers we analysed representative sectors: we extracted a variable number of sampling points ranging from 10 to 30 according to the glacier size and morphology.

4.7 Velocity time series extraction

Once we defined the sampling points for every selected glacier, we extracted the monthly time series of velocity by averaging the values of all the sampling points. Outliers' removal in the time series was performed via a manual check of the data.
We derived the velocity trend using an iteratively re-weighted least squares linear fit. To evaluate the significance of the fit coefficient, we consider the ratio between the coefficients and their standard errors; this equates to the t-statistics to test the null hypothesis that the corresponding coefficient is zero against the alternative that it is different from zero. That is, the lower the t-statics is, the lower the statistical significance of the obtained coefficient is.

https://doi.org/10.5194/egusphere-2023-2771
Preprint. Discussion started: 4 December 2023

Subsequently, we analysed a set of specific parameters:
A) GlobalAvg: the median global velocity during the whole considered period.
B) GlobalVar: the velocity min/max range (excluding the outliers $v < Q_1 - 1.5(Q_3 - Q_1)$ or $v > Q_3 + 1.5(Q_3 - Q_1)$, where Q1 are the first and third quartiles of monthly velocity)
C) SeasonalVar: the mean difference between the average velocities during the ablation season (i.e., from July to September) and the during the accumulation season (i.e., from December to April). The reference periods were chosen according to periods of acceleration and slow down measured at Planpincieux Glacier by Giordan et. Al (2020).
D) MaxAnom: the ratio between the maximum monthly velocity and GlobalAvg.

4.8 Glacier classification

We investigated the presence of distinct classes of glacier based on their morphodynamics using PCA and K-means clustering. PCA is a multivariate analysis technique that allows a reduction in the dimensionality of a given dataset, increasing interpretability but minimising information loss. This is achieved by creating new, uncorrelated variables that successively maximise the variance of the dataset (Jolliffe and Cadima, 2016). We applied PCA to the morphometric and kinematic features listed in Sections 4.3 and 4.7, respectively. Since PCA performs better with data of similar magnitude, we normalized the data by subtracting the mean and dividing it by the standard deviation (Figure S2).
The K-means clustering method is an unsupervised machine-learning technique used to identify clusters of data objects in a dataset. It is largely used in the analysis of remote-sensed data and earth observation data (Paradis, 2022). We applied the K-means algorithm to the two principal components (PCs), considering five classes.

5 Results

We obtained detailed kinematic data from thirty glaciers in the Mont Blanc massif. Different kinematic behaviours were analysed and compared to the morphometrics of the glaciers studied. Some particular seasonal kinematics were highlighted, and particularities in the average velocity trends observed. A brief description of all the glaciers we analysed is found in Appendix 1 to describe the location and geomorphological setting of the glaciers as well as highlight when a single glacier complex from the RGI inventory was divided into independent glacial bodies because of very distinct kinematic behaviour. We therefore detail all the results obtained in the present study in the following sections.

5.1 Sentinel-2 image selection

To select the Sentinel-2 images for glacier analysis, we discarded tiles with cloud cover, as detected by the Copernicus scene classification, of higher than 90% due to the low possibility of having cloud-free conditions in the study area. From 1 January 2016 to 31 December 2022, a total of 295 images with a could cover percentage lower than 90% was analysed. Of these images, 135 derive from Sentinel S2B and 160 from Sentinel S2A. From this dataset, we extracted a subset of 105 images that are cloud free on the selected glacier areas via the visual inspection of the individual images. The number of suitable images that are available per year varies from 10 to 21 with a yearly mean of 15 images in the following distribution: 2016: 10; 2017: 18; 2018: 10; 2019: 14; 2020: 11; 2021: 21; 2022: 21.
Year 2016, and partially 2017, is influenced by the lack of Sentinel 2B images. In fact, while Sentinel 2A was launched on 23 June 2015, Sentinel 2B was launched on 7 March 2017; image availability variations on the following years is influenced by

https://doi.org/10.5194/egusphere-2023-2771
Preprint. Discussion started: 4 December 2023

cloud cover at the time of scene acquisition. We chose to start the analysis from 2016 because it was the first full year of acquisition from the satellite.

5.2 Glacier velocity mapping and selection, outline delineation and morphometric analysis

The glacier selection process identified thirty glaciers with a total glacierised surface of 85.8 km^2. Compared to the total glacierised surface of the massif from RGI 6.0, this represents the covering of 50.8% of the total 169 km^2 and 25.9% in terms of number of glaciers; this rises to 39.5% if we consider the subset of seventy-six glaciers having a glacierised surface of more than 0.1 km^2. The selected glaciers are highlighted in Figure 3 and listed in Table 1, while a short description of each glacier is provided in the Supplementary. Two of the selected glaciers are located in Switzerland, ten are located in France and eighteen in Italy. This distribution is mainly due to a small portion of the massif being located in Switzerland and the presence of more fragmented glacierised bodies on the Italian side. Of the thirty glaciers, seven have been mapped as sub-areas in comparison to RGI individual glacier bodies.

In Figure 3 we present a velocity map with a resolution of 40 m (an masked over free-ice terrain in provided in Figure S1). This was obtained by averaging all the single monthly averaged velocity maps in the study period (2016-2022).

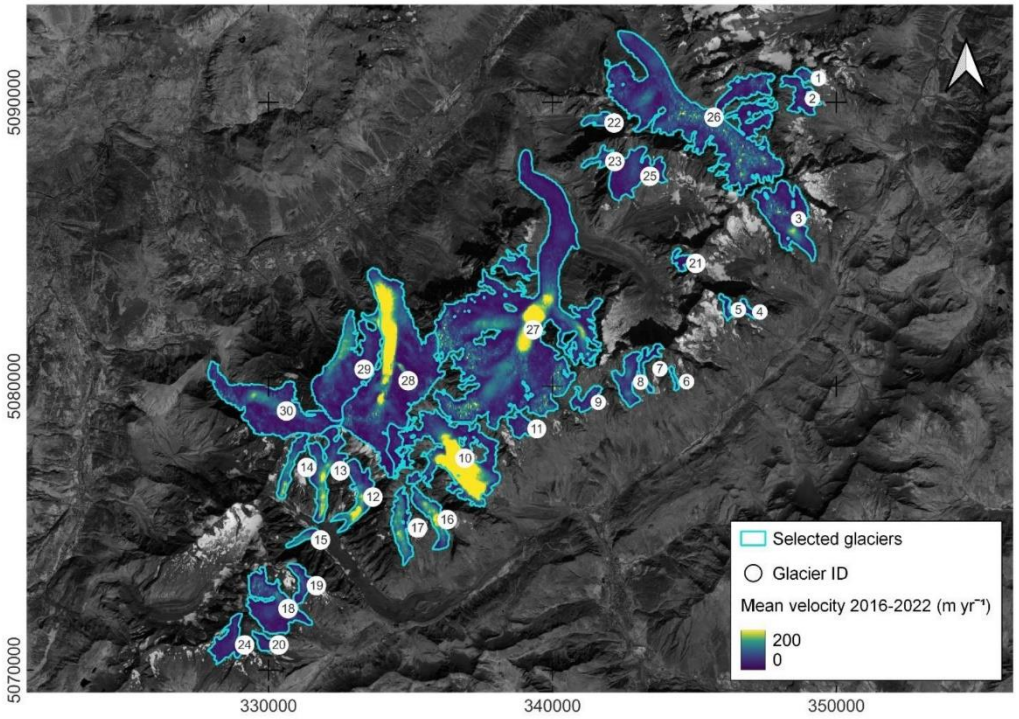

Figure 3. Surface glacier velocity map averaged in the 2016-2022 period. Selected glaciers for specific analyses are outlined in cyan. Background: Sentinel-2 image (B08 band), courtesy of the Copernicus Open Access Hub (https://scihub.copernicus.eu, last access: 10 September 2023).

https://doi.org/10.5194/egusphere-2023-2771
Preprint. Discussion started: 4 December 2023

276

277 **Table 1. Name and identification codes of glaciers selected for analysis in the present study. Codes from RGI and IDs used for**
278 **simplicity in this study together with main morphometric parameters analysed in this study.**

Glacier name	ID	RGI 6.0 ID	Area (km^2)	Length (m)	Min alt (m asl)	Max alt (m asl)	Avg slope (°)	Mean ice thickness (m)	Elongation ratio
A Neuve N	1	RGI60-11.02859	0.269	793	3084	3454	25.0	23.60	2.95
A Neuve Central	2	RGI60-11.02864	0.889	1800	2664	3554	26.3	26.29	2.02
Pre de Bard	3	RGI60-11.02916	3.011	3300	2360	3641	21.2	62.95	1.10
Greuvettaz E	4	RGI60-11.02978	0.196	985	2948	3582	32.8	11.88	5.03
Greuvettaz W	5	RGI60-11.02981	0.169	837	2704	3291	35.0	11.67	4.95
Planpincieux	6	RGI60-11.02991	1.013	2050	2627	3650	26.5	44.52	2.02
Grandes Jorasses	7	RGI60-11.02991	0.482	2110	2701	4206	35.5	15.27	4.38
Pra Sec	8	RGI60-11.02996	0.119	873	2536	3190	36.8	9.12	7.34
Rochefort	9	RGI60-11.03000	0.558	995	2720	3301	30.3	24.48	1.78
Brenva	10	RGI60-11.03001	6.579	4492	2374	4766	28.0	80.30	0.68
Thoula	11	RGI60-11.03002	0.58	1075	2880	3416	26.5	25.26	1.85
Mont Blanc	12	RGI60-11.03005	0.764	2486	2776	3773	21.9	46.85	3.25
Dome	13	RGI60-11.03005	1.973	3553	2453	4121	25.1	51.03	1.80
Bionassay (IT)	14	RGI60-11.03005	1.354	2926	2467	3816	24.8	52.69	2.16
Aiguille de Tre la tete N	15	RGI60-11.03005	0.312	1355	2408	3010	24.0	78.47	4.34
Freney	16	RGI60-11.03013	1.017	2623	2420	3698	26.0	60.74	2.58
Brouillard	17	RGI60-11.03014	1.166	2733	2499	3972	28.3	52.28	2.34
Lex Blanche	18	RGI60-11.03020	2.64	2450	2467	3757	27.8	41.40	0.93
Petit Mont Blanc	19	RGI60-11.03020	0.556	1767	2863	3580	22.1	26.31	3.18
Estelette	20	RGI60-11.03022	0.291	950	2716	3214	27.7	23.74	3.26
Pierre Joseph	21	RGI60-11.03258	0.275	710	2920	3409	34.6	14.77	2.58
Nant Blanc	22	RGI60-11.03263	0.363	1150	2600	3351	33.1	33.23	3.17
Charpoua	23	RGI60-11.03284	0.322	1211	2650	3479	34.4	25.41	3.76
Des Glaciers	24	RGI60-11.03339	1.091	2050	2735	3815	27.8	31.19	1.88
Talèfre N	25	RGI60-11.03466	2.037	1950	2700	3550	23.6	39.24	0.96
Argentière	26	RGI60-11.03638	13.109	7850	2178	3847	12.0	88.90	0.60
Mer de Glace	27	RGI60-11.03643	23.556	12090	1774	4025	10.5	103.75	0.51
Bossons	28	RGI60-11.03646	11.319	6795	1691	4776	24.4	59.66	0.60
Taconnaz	29	RGI60-11.03647	4.994	4291	2043	4286	27.6	40.15	0.86
Bionassay (FR)	30	RGI60-11.03648	4.774	5241	1835	4287	25.1	39.83	1.10

279 **5.3 Spatial distribution of velocity patterns**

280 Most glaciers can show seasonal velocity changes, as well as less markedly interannual velocity variations. Despite those
281 variations, they maintain a constant spatial distribution of the velocity patterns on the velocity maps. To detect possible
282 variations of the spatial distribution of velocities, we analysed single monthly maps on the selected glaciers for both winter

https://doi.org/10.5194/egusphere-2023-2771
Preprint. Discussion started: 4 December 2023

and summer months. This analysis led to the individuation of one glacier in particular - Charpoua Glacier (ID:23) - on which the spatial distribution of velocities can be significantly different (Figure 4). In fact, years that present surge-like behaviour show higher velocities towards the frontal part of the glacier while years that do not show surge-like activity show higher velocities in the higher part of the glacier (Figure 4).

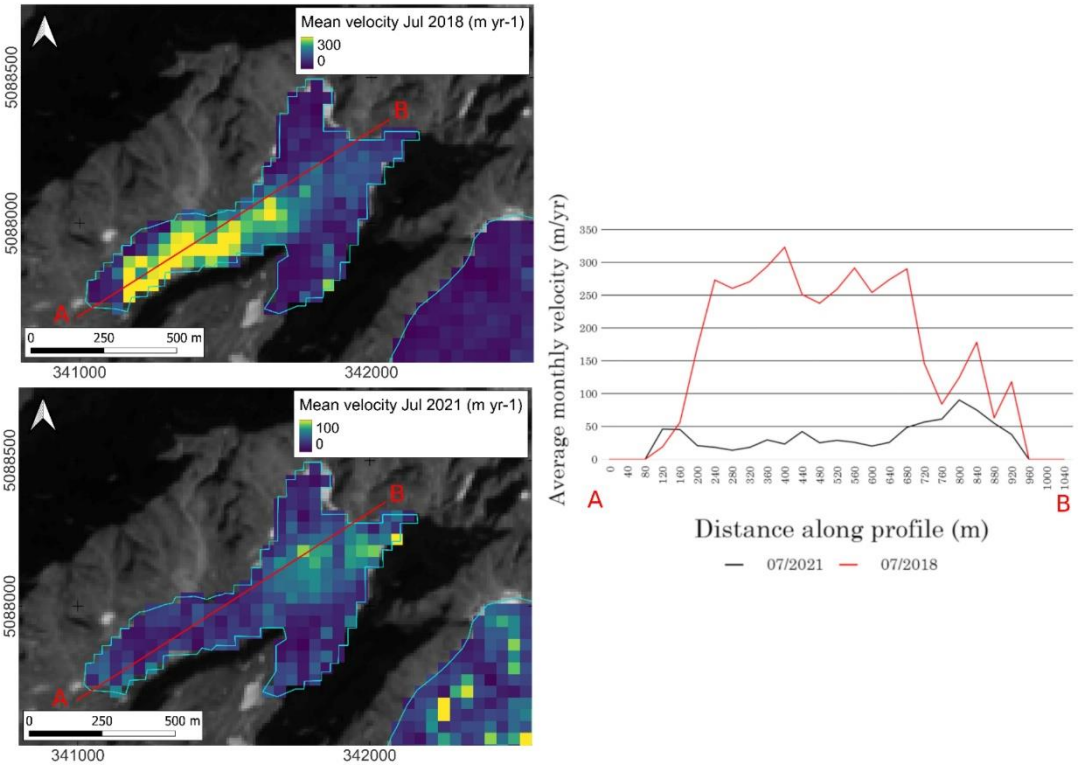

Figure 4. Charpoua Glacier (ID: 23) monthly surface velocity maps showing spatial variation of the velocity patterns in between July 2018 (upper left) and July 2021 (lower left); note the different colour scales to highlight spatial distribution of values. The right panel shows the average monthly velocity profile along a longitudinal west-east profile (in red on the maps, the profile start at A is altitudinally lower) with July 2018 values in red and July 2021 values in black. Sentinel-2 imagery base map (B08 band), courtesy of the Copernicus Open Access Hub (https://scihub.copernicus.eu, last access: 10 September 2023)

5.4 Selection of sampling points

Within every selected glacier, we manually identified ten to thirty points, depending on the glacier size, to extract velocity time series. The points were distributed on the glacier surface evenly when possible, or avoiding areas with low spatial coherence in the velocity maps which could be linked to local areas that suffered unsuccessful image matching. The presence of cloud or snow on the glacier surface made it impossible to extract reliable data in the following periods: i) January 2017 ii) December 2020, January and February 2021. However, the gaps represent only four months of no data out of the seven years

https://doi.org/10.5194/egusphere-2023-2771
Preprint. Discussion started: 4 December 2023

299 considered in the study (i.e., <5%). In Figure 5, we present an example of the obtained velocity map and the distribution of
300 sampling points over several chosen glaciers.

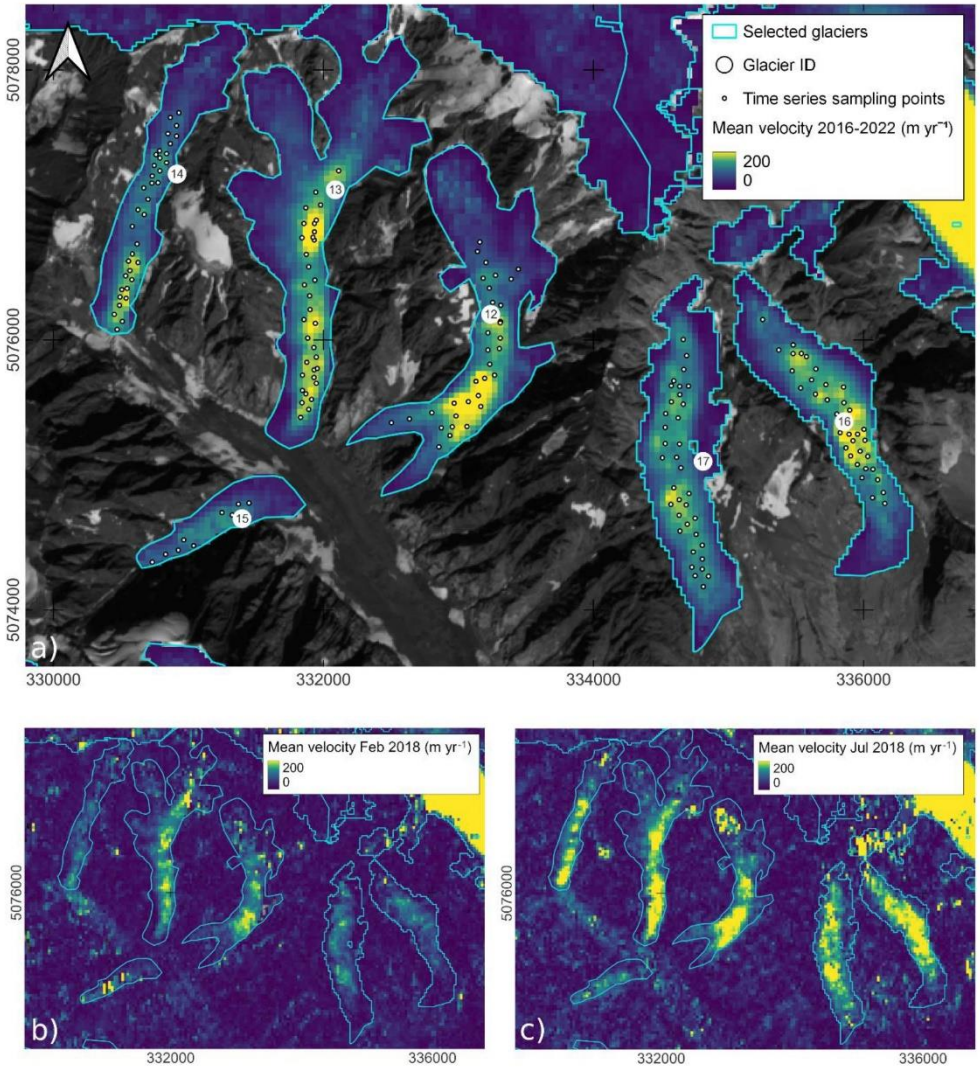

301
302 **Figure 5. a) Details of glacier surface velocity map averaged in the 2016-2022 period and sampling points of selected sample glaciers.**
303 **From left to right: Bionassay (IT) Glacier – ID 14; Tre la Tete N Glacier – ID 15; Dome Glacier – ID 13; Mont Blanc Glacier – ID**
304 **12, Brouillard Glacier - ID 17; Freney Glacier – ID 16. Note that on smaller glaciers there is a limited number of sampling points**
305 **because of their limited area; on medium glaciers there is a distribution of points over all areas that show velocity maps with high**

https://doi.org/10.5194/egusphere-2023-2771
Preprint. Discussion started: 4 December 2023

spatial coherence. Sentinel-2 imagery base map (B08 band), courtesy of the Copernicus Open Access Hub (https://scihub.copernicus.eu, last access: 10 September 2023). Lower left (b) and right panels (c) show single average monthly velocity maps of February and July 2018 respectively.

5.5 Velocity time series extraction

On the thirty glacial bodies we investigated in this study, the monthly velocity values range from 30-40 m yr^{-1}, typically reached during winter months, to 350 and 400 m yr^{-1}, typically reached in summer/late summer. Such high velocity values are attained by just a few of the largest glaciers in the dataset. In particular, monthly extreme values vary from 18.0 m yr^{-1} reached on January 2020 by the Greuvettaz E Glacier, to 436.3 m yr^{-1} reached by the Brenva Glacier in July 2016.
Figure 6 presents the distributions of the monthly velocity of the considered glaciers. The mean surface velocities averaged over the whole period range from 33.7 m yr^{-1} at the Pierre-Joseph Glacier to 309.7 m yr^{-1} at the Bossons Glacier. The standard deviation of the velocity time series of single glaciers varies from 8.9 m yr^{-1} at Pierre Joseph Glacier to 57.7 and 62.6 m yr^{-1} at the Pra Sec and Charpoua glaciers, respectively.

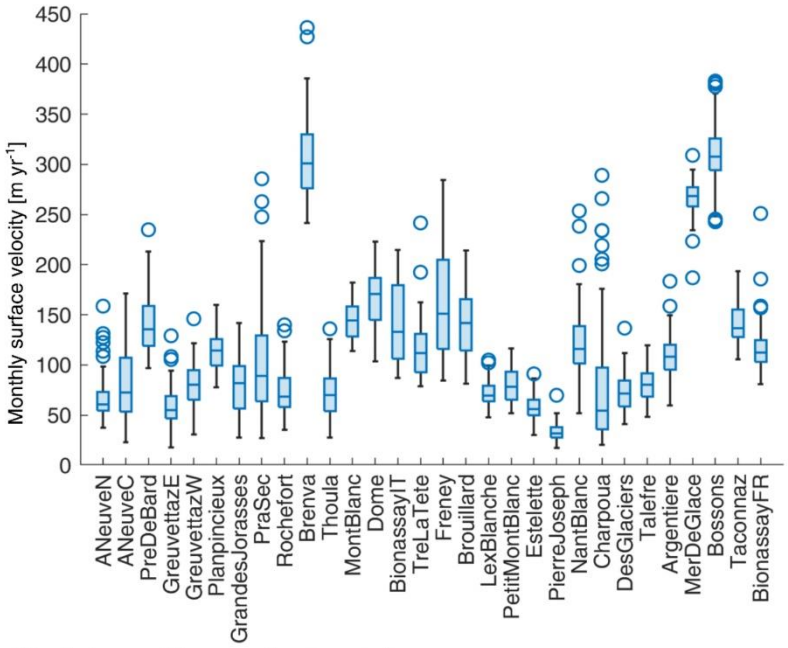

Figure 6. Boxplot of the glaciers monthly averaged surface velocity.

Velocity time series of the 30 analysed glaciers are represented in Figure 7. Glaciers such as the Freney, Brouillard, Dome, Mont Blanc and Bionassay (IT) show large seasonal variability while others, such as the Taconnaz, Mer de Glace, or smaller glaciers such as Pierre Joseph or Aiguille des Glaciers, show steadier values. Most glaciers with strong seasonality show distinct high velocity peaks that appear in summer/late summer (July to October) and minima that normally occur during mid-

https://doi.org/10.5194/egusphere-2023-2771
Preprint. Discussion started: 4 December 2023

winter (January to April). Some of the series show stronger interannual variations and this is particularly noticeable on Brenva Glacier and Charpoua Glacier.

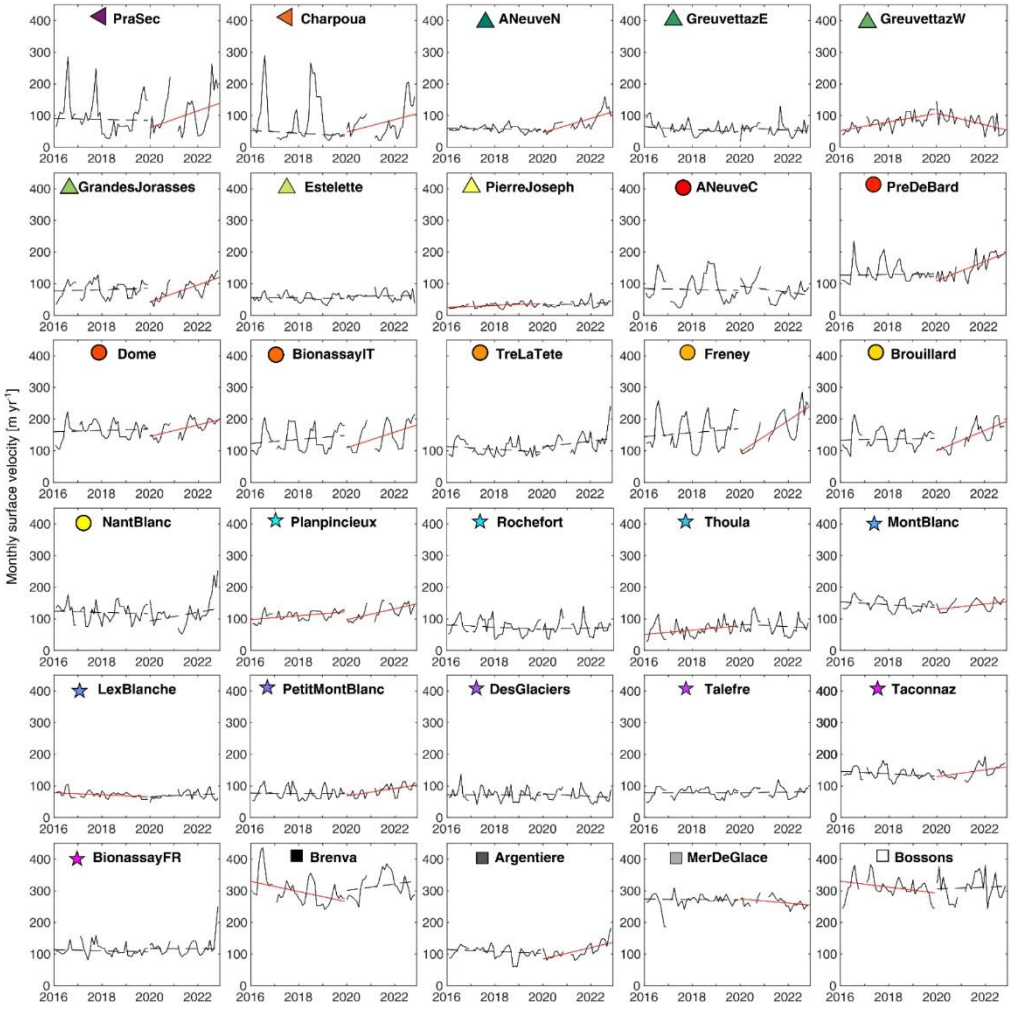

Figure 7. Time series of monthly glacier surface velocities over the 2016-2022 period. Robust linear trends calculated on each full period (i.e.: 2016-2019 and 2020-2022) are highlighted in solid red (*t*-statistics > 2) and dashed black (*t*-statistics < 2) lines. Coloured markers refer to the glacier classification.

Pra Sec and Charpoua, in particular, show very low minimum velocities (in the range of 25 m yr^{-1} to 50 m yr^{-1}) but very high peaks with a max/min ratio that can reach a 7:1 value. These velocity peaks seem to appear in summer/late summer and extreme velocity changes from winter to summer velocities can be noticed (Pra Sec 2022, Charpoua 2018). Charpoua Glacier shows

https://doi.org/10.5194/egusphere-2023-2771
Preprint. Discussion started: 4 December 2023

seasons with high summer peaks (2016, 2018) and other summer seasons that maintain particularly low displacements throughout the entire summer (2017, 2019, 2021). Pra Sec Glacier seems to display more regular annual summer speed ups: in the period analysed, every summer had a strong velocity peak only, except 2018.

The analysis of the time series shows that many glaciers had a positive trend of velocity starting from 2020, which is particularly evident in some glaciers like Argentière, Biossanay (IT), Brouillard, Freney, Pré de Bard. To statistically and quantitatively estimate this behaviour, we divided the full timespan into two periods: a first period between 2016 and 2019, and a second one between 2020 and 2022 (Figure 7). Subsequently, we applied a robust linear regression to each full period (i.e., considering all the monthly data) and only to winter (i.e., from December to April) and summer (i.e., from July to September) months. Figure 8 shows the linear trends of the first vs second period in the three cases. Considering the winter months, a well-defined general behaviour is not clearly noticeable. In the first period, most velocity trends are included in the range $\pm$10 m yr^{-2}, 11 have negative trends and 19 positives; the trends in the second period are in general similar to those of the first, with exception of six glaciers that show an increase compared to the first period (i.e., Trend in 2019–2022 minus Trend in 2016–2019, t_2-t_1), of t_2-t_1>10 m yr^{-2}, and three with a decrease t_2-t_1<10 m yr^{-2} (Figure 8a). Considering the full year, in the first period, the velocity trends are basically the same as those of the winter case; while in the second period, 17 glaciers showed a velocity increase of >10 m yr^{-2} and seven glaciers an increase of >20 m yr^{-2}. Overall, 24 glaciers showed an acceleration (or a decrease of deceleration, i.e., t_2-t_1>0) between the first and second periods, of which 17 glacier t_2-t_1>10 m yr^{-2} and 9 glacier t_2-t_1>20 m yr^{-2} (Figure 8b). Considering the summer months, in the first period, most glaciers (26 of 30) have negative velocity trends, while in the second period, 23 glaciers show positive acceleration of which 17 glaciers have trends >10 m yr^{-2} and 12 glaciers >20 m yr^{-2}. Overall, 27 glaciers have a velocity trend in the second period greater than in the first period, in 20 glaciers, the difference between second and first period is at least t_2-t_1>10 m yr^{-2}, and in 13 cases the difference is t_2-t_1>20 m yr^{-2} (Figure 8c). Overall, we observed that the trends included in the range $\pm$10 m yr^{-2} had *t*-statistics (i.e., linear slope divided by its standard error) <2, thus they were less statistically significative.

https://doi.org/10.5194/egusphere-2023-2771
Preprint. Discussion started: 4 December 2023

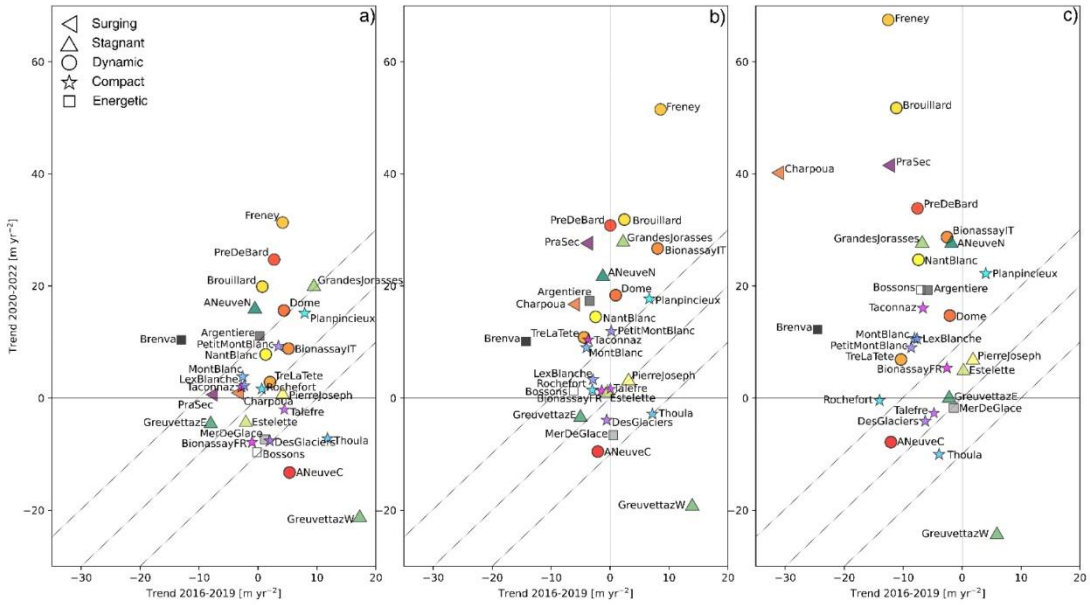

Figure 8. Annual velocity variations of the glaciers during the period 2016-2019 (x-axis) and 2020-2022 (y-axis). Trends have been calculated using: in a) cold months (from November to April); in b) every month (i.e., From January to December), while in c) warm months (from June to September). The oblique lines indicate the boundary where the difference between the trends of the two periods (second minus first period) is +10 m yr^{-2}, 0 m yr^{-2} and -10 m yr^{-2}, respectively from the upper to the lower line. Markers indicate the glacier class.

5.6 Glacier classification

The investigation of the possible presence of distinct classes of glacier based on their morphodynamics using PCA and K-means clustering is hereby presented. Figure 9 shows the biplot of the two principal components (PCs). The first PC (PC1) accounts for 42% of the explained variance of the dataset. It is principally composed of the morphological features - Area and Thickness contribute positively; Shape and Slope negatively - and glacier flow velocity (GlobalAvg). Accordingly, wide, compact (i.e., non-elongated), gentle and fast glaciers have PC1 high positive values. On the other hand, PC2 explains 26% of the dataset variance and is mainly formed of kinematic features and AAR, which contributes negatively. In this case, glaciers with high velocity variability and small accumulation areas assume PC2 high positive values. Based on the two first PCs, an unsupervised K-mean clustering identified five classes of glacier.

https://doi.org/10.5194/egusphere-2023-2771
Preprint. Discussion started: 4 December 2023

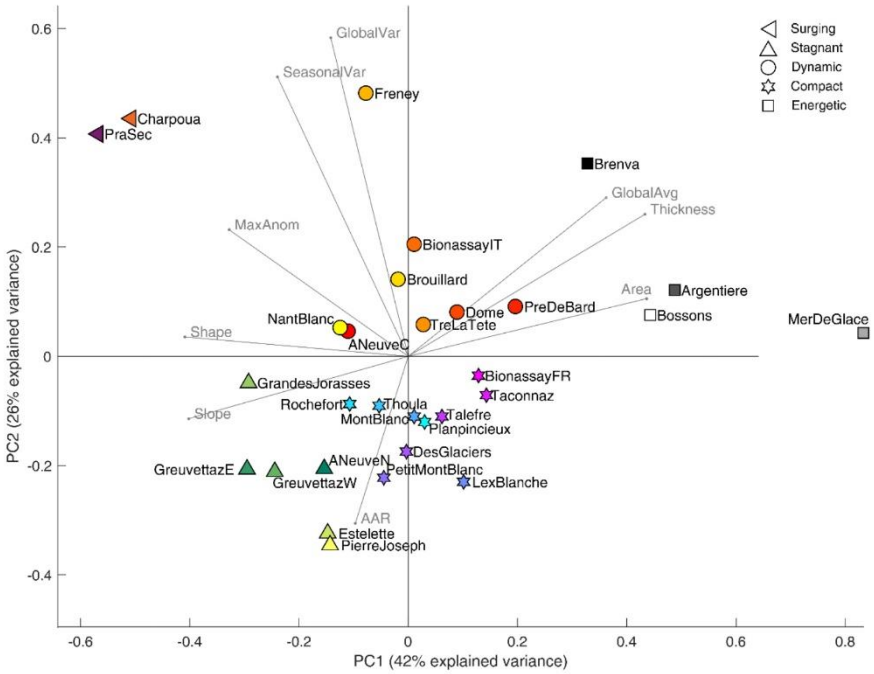

Figure 9. Biplot of the two principal components describing the variance of the dataset. Five clusters of glaciers are identified and highlighted by different markers.

6 Discussion

6.1 Velocity trends and comparison with other regional studies

Concerning the time series analysis, we compared our observations with similar existing studies in this region considering two long-term glacier velocity records in the Argentière Glacier (Vincent and Moreau, 2016) and Miage Glacier (Smiraglia et al., 2000; Fyffe, 2012). At Argentière Glacier, a unique series of continuous basal sliding measurements exist from 1997 and was still active as of 2022 (Vincent et al., 2022; Nanni et al., 2020). The whole series indicates a general decrease in basal sliding velocities (Vincent and Moreau, 2016) since the end of the 1990s. This general decrease has shown a strong correlation with the negative mass balance of the glacier, which agrees with the conceptual model from Span and Kuhn (Span and Kuhn, 2003), in which the glacier flow variation is primarily driven by the mass balance of the accumulation area in the previous year (as it determines glacier thickness variations). Seasonal field surveys conducted at Argentière Glacier from the 1950s document a longer data series than the basal sliding measurements started in 1997, and an increase of surface velocities was clearly measured during a period of positive mass balances in the early 1980s (Vincent and Moreau, 2016). The same trend was highlighted by Span and Kuhn (Span and Kuhn, 2003) for at least six other glaciers: Saint Sorlin in France, Gietro and Corbassiere in Switzerland, and Pasterze, Vernagtferner and Odenwinkelkees in Austria. At Miage Glacier, surface velocities

https://doi.org/10.5194/egusphere-2023-2771
Preprint. Discussion started: 4 December 2023

have been measured historically by different authors (Diolaiuti et al., 2005; Smiraglia et al., 2000; Fyffe, 2012; Lesca, 1974; Pelfini et al., 2007; Deline, 2002) and also show a general velocity decrease in recent decades. (Smiraglia et al., 2000; Fyffe, 2012). Globally, glacier slowdown linked to negative mass balance trend was also shown for six different regions around the globe and dates spanning from 1953 to 2009 by Heid and Kaab in 2012 (Heid and Kääb, 2012a) by an analysis of remotely-sensed optical images. Specific analysis of velocity trends and glacier mass loss showed generalized decreasing velocity trends over different regions of High Mountain Asia between 2000 and 2017 and a strong correlation with the negative mass balance trend (Dehecq et al., 2019).

According to the observations at the Argentière and Miage glaciers, the signal of velocity decrease from the early 2000s can be linked to continuous negative mass balances (Vincent and Moreau, 2016) of most Alpine glacier since the 2000s (Zemp et al., 2021). The results of our study agree with this negative trend in the first part of the considered period (i.e., 2016–2019), but we detected an inverse trend and a velocity rise from 2020 occurring in most glaciers under study. Notably, the velocity trend inversion in the recent years is most visible during the warm season, while there is not a clear signal in winter. An accelerating trend (+5 m yr^{-2} between 2015-2021) has recently been shown for the Brenva Glacier by an analysis of remotely-sensed optical images (Rabatel et al., 2023). Besides, (Rabatel et al., 2023) observed a slight ice thickening (~1 m between 2000 and 2019) in an upper sector of the Brenva Glacier. They proposed three hypotheses to explain the acceleration of the Brenva: a) a glacier thickening; b) a change in thermal regime; and c) a change in subglacial hydrology, possibly related to an increased ablation in the upper reaches of the glacier (Rabatel et al., 2023). Even though the hypothesis of glacier thickening could explain the specific case of Brenva, the glacier surface elevation change across the Mont Blanc massif has been generally negative in the last years, as evidenced by the negative mass balance of the reference glaciers in the area (Zemp et al., 2021; Zemp et al., 2009). Local anomalies of positive mass balance could explain an increase of velocity but the lack of measurements at higher altitudes does not allow us to confirm this behaviour at present. However, the meteorological conditions in the recent years have remained approximately constant, with slight trends of increasing temperature and decreasing precipitation between 2020-2022 that make unlikely a general glacier thickening in the region (Figure S3). Localized high rates of accumulation due to increased avalanche activity and wind accumulation should also contribute to the ice thickening (thus yielding an acceleration), but cannot be investigated at this stage. In any case, these hypotheses can be valid for specific sectors of glaciers, while we observed a generalised acceleration across the region; thus, glacier thickening seems not to be the most relevant forcing of velocity increase. A variation of the hydrology of groups of glaciers could be more reasonable, especially if they lie in neighbouring basins, but is unlikely to occur contemporary over the whole region. On the other hand, the distribution of the acceleration trend over different areas of the massif and regarding different classes of glaciers suggest the existence of a climatic driver of the phenomenon. Therefore, a thermal regime change could explain the velocity rise. The fact that the acceleration is most evident during the warm season seems to corroborate this hypothesis, even though the mean summer temperature was slightly lower (-0.2°C) in 2020-2022 than in 2016-2019 (Table S1). In the end, a definitive answer cannot be formulated so far and further research is necessary to understand the processes involved in this trend.

The general acceleration detected in the study should be monitored in the future. In fact, if this trend continues, it should be also considered that an acceleration trend over few years (2012-2016) has been measured before the large destabilization of Aru 1 Glacier (Gilbert, 2018). However, the trend highlighted in our study is detected over a short period (2020-2022) and could be a fluctuation onset on a generally decreasing trend at a decadal scale. In any case, the causes of such an anomaly should be a matter of further research.

6.2 Glacier classification

In regard to glacier classification, we individuated five groups:

https://doi.org/10.5194/egusphere-2023-2771
Preprint. Discussion started: 4 December 2023

'*Surging glaciers*': only two glaciers belong to this group: Charpoua and Pra Sec. They are thin small steep elongated glaciers. Their average velocity is rather low but they feature a much stronger annual cycle with periods of surge-like dynamics during which they occasionally show accelerations of almost one order of magnitude. Possible glacier advances are prevented by the steep bedrock cliff at the snout, which causes the disintegration of the glacier by repeated ice falls from the glacier front (Giordan et al., 2020; Pralong and Funk, 2006). Both glaciers have had documented ice avalanche activity from their frontal areas (Buisson et al., 1999; Mourey and Ravanel, 2017; Ravanel, 2009; Deline et al., 2010). Ice avalanches from the Pra Sec Glacier occurred in the 1930s, in August 1981 (Deline et al., 2010), and repeatedly in 2020 and 2021 (Forestry Service of Aosta Valley, personal communication). Ice avalanches from the Charpoua snout between 40000 and 60000 m^3 occurred in 1997 (Deline et al., 2010; Deline et al., 2012) and 2018 (Lehmann, 2018 - https://news.unil.ch/display/1536777918113, accessed online 11 October 2023). During 2018, a strong summer acceleration was highlighted in the present study at Charpoua Glacier. The precursory acceleration before a failure has been investigated and measured in landslides and rockfalls (Fukuzono, 1985), cold-based glaciers (Faillettaz et al., 2016) and, in a few cases, temperate or polythermal glaciers (Giordan et al., 2020; Faillettaz et al., 2012).

Elevation changes typical of surging glaciers should be investigated to better describe such processes but, presently, such data is not available. As far as we know, to date, such surge-like behaviour on small steep temperate Alpine glaciers have not been documented.

'*Stagnant glaciers*': they are morphologically similar to *surging glaciers* (i.e., small, steep and elongated). *Stagnant glaciers* lie, in general, at high altitudes, thus they have a larger AAR compared to other glaciers (in particular *surging glaciers*). The velocity seasonal cycle is modest or even non-detectable since the velocity in winter is close to the measurement uncertainty (besides the Grandes Jorasses, which has a relatively pronounced seasonal cycle). It is worth highlighting that signals of potential velocity fluctuations could exist but remotely-sensed data are not currently suited for the analysis of such small glaciers.

'*Dynamic glaciers*': the morphology of these glaciers is less homogeneous, even though most are generally gentler and thicker than average. They all feature strong kinematic activity, their velocity is higher than average with marked variability and they often show a pronounced regular annual cycle, as in the case of the Bionassay (IT) and Freney glaciers. A large ice avalanche event was documented in 1956 at Freney Glacier (Chiarle et al., 2023), which is one of the glaciers displaying some of the largest velocity variations in this group. A possible correlation between summer accelerations and glacier destabilisations that can lead to ice avalanche processes would need further research; in any case, this would be more site-specific research and goes beyond the scope of the present study.

'*Compact glaciers*': gentle, medium-sized glaciers that are not very elongated. Morphologically similar to *dynamic glaciers* but generally thinner, they are markedly less active. In particular, even though some display a regular seasonal cycle (e.g., Planpincieux, Mont Blanc, Rochefort), their velocity variability and average thickness are much lower, comparable to the *stagnant glaciers*. Since their extension is limited, the areas suitable for the analysis presented in this study can also be small and influence the quality of the output. This group of glaciers would probably be better analysed using higher resolution imagery and higher frequency image acquisition.

'*Energetic glaciers*': this group includes large and thick glaciers which are not very elongated. *Energetic glaciers* have accumulation areas located at high altitudes; they show high surface velocities across the whole year and seldom display seasonal variations (except Brenva, which follows an evident seasonal cycle). Their morphology is complex - e.g., the slope varies considerably. In the present study, we concentrated the analyses on the middle sectors of the glaciers where the quality of the velocity data was higher. Since they are large, reach a low altitude and have flat and little crevassed valley tongues, they have often been historically chosen for glaciological field surveys (Span and Kuhn, 2003). Therefore, the knowledge of Alpine

https://doi.org/10.5194/egusphere-2023-2771
Preprint. Discussion started: 4 December 2023

glaciers kinematics is generally mostly related to this type of glacier, which can be significantly different compared to the other glacier groups analysed in this study.

6.3 Uncertainty analysis

To estimate the quality of our data, we performed two investigations. First, following the method proposed by (Millan et al., 2019), we calculated the standard deviation of the monthly time series during the whole period 2016–2022 on a set of 155 points selected on stable terrain; subsequently, we consider the median of these standard deviations, obtaining an uncertainty of 10.9 m yr^{-1}. In their study, (Millan et al., 2019) estimated the nominal precision according to the temporal baseline between the correlated images, which they found being between 6–16 m yr^{-1} for baselines respectively of 40 and 20 days, which is the typical range of temporal gaps between images used in our study. Moreover, the value of 10.9 m yr^{-1} is in close agreement with the uncertainty found by (Mouginot et al., 2023), which obtained a root mean squared error of 10.5 m yr^{-1} between glacier velocities measured over the Mer de Glace and Argèntiere glaciers using image correlation of Sentinel2 images and GNSS in situ data (https://glacioclim.osug.fr/).
Second, we considered the glacier velocity from (Millan et al., 2019), who published mean annual velocity in the period 2017–2018 on a 50x50 m regular grid. They adopted normalised cross-correlation and chip size refinement (initial size of 16x16 px). They estimated an overall uncertainty of glacier surface velocity time series of ~12 m yr^{-1} over the Mont Blanc glaciers, and, specifically at Brenva and Bosson glacier, an uncertainty of 15–20 m yr^{-1}. We compared these data and ours along four glacier longitudinal central lines (i.e., in Bossons, Brenva, Freney and Taconnaz), obtaining good agreement (Figure 10). The largest differences (>50 m yr^{-1}) where found in a specific sector of the Taconnaz Glacier (Figure 10d), where the flux is highly channelized in a narrow passage. There, the data of (Millan et al., 2019) show a velocity decrease that seems unlikely considering the geometry of the site. However, the velocity profiles are similar elsewhere. On average, the surface velocities that we obtained are slightly higher, with difference mean +6.6 m yr^{-1} and root mean squared deviation (RMSD) of 28.2 m yr^{-1} (Table 2). The slightly higher RMSD compared to the expected uncertainty can be due to the fact that the precision in glacierized areas is probably larger (less precise) than in ice-free zones because the surface texture is different and changes (e.g., snow precipitation, surface melt, glacier movement) occur more rapidly, therefore causing more decorrelation (Millan et al., 2019).

https://doi.org/10.5194/egusphere-2023-2771
Preprint. Discussion started: 4 December 2023

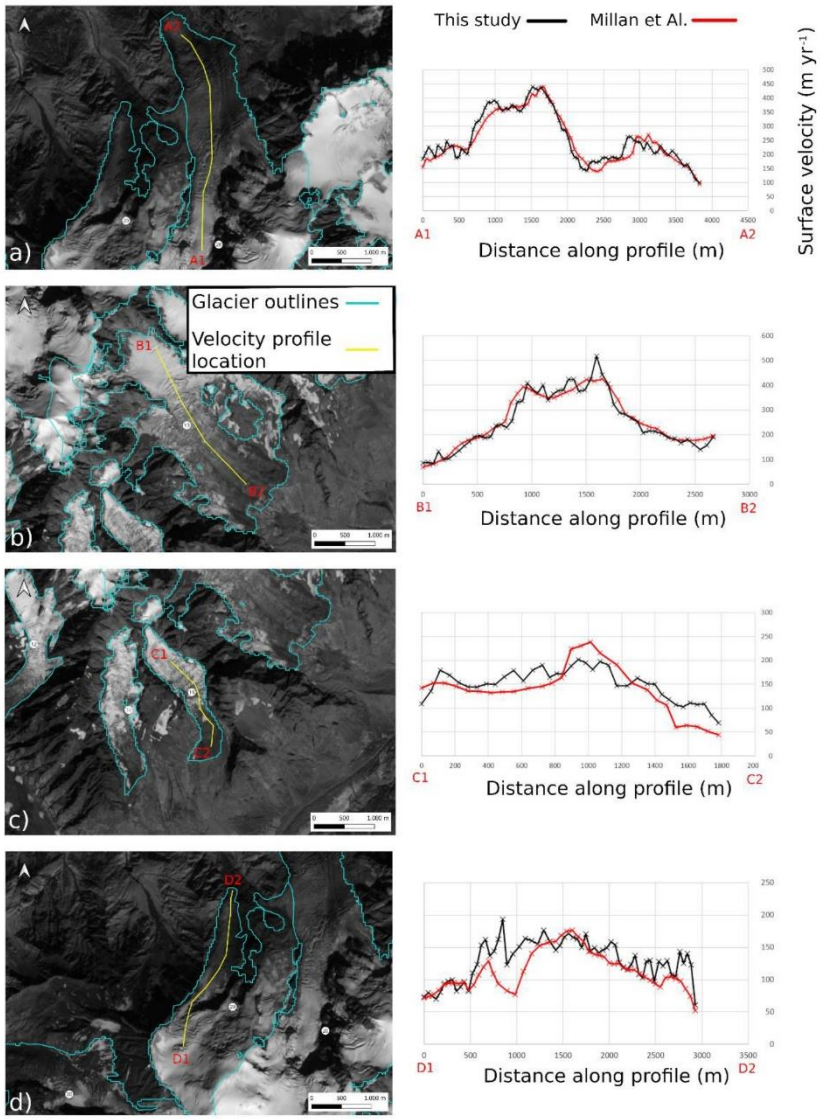

496

497 **Figure 10. Comparison of velocity profiles from Millan et al. (2022) (red) and from this study (black) at: (a) Bossons Glacier, (b)**
498 **Brenva Glacier, (c) Freney Glacier and (d) Taconnaz Glacier. Higher altitude to the left, lower altitude to the right, traced along**
499 **profiles in yellow on the corresponding maps. Sentinel-2 image base map (B08 band), courtesy of the Copernicus Open Access Hub**
500 **(https://scihub.copernicus.eu, last access: 10 September 2023).**

https://doi.org/10.5194/egusphere-2023-2771
Preprint. Discussion started: 4 December 2023

Table 2. Mean difference and root mean squared deviation (RMSD) between this study and Millan et al. (2022) along velocity longitudinal profiles.

	Bossons	Brenva	Freney	Taconnaz	Mean all profiles
Mean [m yr^{-1}]	3.2	5.9	6.7	10.7	6.6
RMSD [m yr^{-1}]	28.9	33.3	30.2	20.6	28.2

6.4 Limits of the proposed methodology

The methodology presented in this study allow the detection of anomalous accelerations of glaciers, which can be precursors of ice avalanches (Pralong et al., 2005; Faillettaz et al., 2008; Giordan et al., 2020). In this frame, it would be very relevant to measure and know typical velocity fluctuations of specific glaciers in stable conditions. This could allow an assessment and to what extent a suspect acceleration may be anomalous and potentially destabilising, bearing in mind that high-rate monitoring is essential to detect glacial instabilities, since the expected sharp increase in velocity in the weeks before the failure (Pralong and Funk, 2006) could be hardly detectable from remote sensing (e.g., due to scarce visibility, image decorrelation, low resolution).

Limits of the methodology presented in this study should also be considered: considering the estimated precision of ~11 m yr^{-1} and the usual revisiting time between available images (i.e., with sufficient visibility), which typically ranged between 20 to 40 days, the minimum measurable velocity is approximatively 40 m yr^{-1}. Glacier moving at slower rates can be surveyed using larger temporal baselines (Millan et al., 2019; Mouginot et al., 2023), but this implies reducing the ability to catch short-term velocity fluctuations, like those observed at Charpoua and Pra Sec glaciers. Another known issue pertains to the lack of features of the glacier surface that makes it impossible to track movements using optical imagery. Satellite optical imagery is limited and can be strongly influenced by the presence of clouds that could yield extensive periods without data acquisition, even though, in the present study, few limiting conditions have occurred (four months with no data out of eighty processed months of available imagery). Anomalies due to image decorrelation for the presence of shadows, snow or morphological surface modifications can occur and an expert-based visual check may be required to discriminate anomalous velocities.

7 Conclusions

In the present study, we produced ice velocity maps and time series of thirty glaciers of the Mont Blanc massif during the period 2016–2022. The existing publicly available automatically processed velocity datasets, normally have coarse velocity maps (i.e., >100 m), which cannot detect correctly the kinematics of most Alpine glaciers, due to their small size. Therefore, specific processing and studies are needed to characterize the surface kinematics of Alpine glaciers. We used Sentinel-2 imagery due to its free availability, ground resolution and revisit time in the study area. Using PCA and unsupervised K-means clustering, we proposed a classification of five groups of glaciers based on their morpho-kinematic features. Plus, we observed a significative acceleration trend in most of the studied glaciers in the last years (2020–2022), but the causes are still not well understood.

Processing and analysis of such datasets around other massifs in the Alps, and globally, should be a base for stimulating research on high resolution spatiotemporal variations of velocities on Alpine glaciers and, especially, on understanding the variations in the motion of mountain glaciers. A large research question remains open and deals in understanding and

https://doi.org/10.5194/egusphere-2023-2771
Preprint. Discussion started: 4 December 2023

measuring the drivers of change in motion of alpine glaciers. This implicates the complex acquisition of data related to the possible drivers of the variations such as mass balances, water inputs and the temporal variations in subglacial hydrology of single glaciers. However, in order to delve further into these investigations, more complete and widespread glacier surface velocity databases such as that presented in this study, are needed to build future research on the topic.

Acknowledgments

The authors would like to thank Jean Pierre Fosson, Raffaele Rocco, Valerio Segor, Guido Giardini for their support and their will to stimulate cryospheric research activities in the Aosta Valley region and on the Italian side of Mont Blanc massif. We thank all the staff at Fondazione Montagna sicura for supporting all the research activities of the research team. Dr Etienne Berthier supplied a processed 2018 Pleaides stereo DEM on which retrieving altitudinal data that was presented in this paper. We thank Prof. Christian Vincent for his advice on research activity and for supplying useful additional information, especially on the French glaciers of Mont Blanc.

Data availability

Glacier outlines shapefiles can be requested by contacting the lead author. Sentinel-2 imagery is available from the Copernicus Open Access Hub (https://scihub.copernicus.eu, Copernicus, 2022). The GIV toolbox is freely available online (https://github.com/MaxVWDV/glacier-image-velocimetry). The original glacier surface velocity dataset is available for download as a supplement.

Competing interests. The authors declare that they have no conflict of interest.

Author contributions. Fabrizio Troilo: Conceptualization, writing – original draft preparation, investigation, methodology, data curation, formal analysis, visualization; Niccolò Dematteis: Writing – review & editing, data curation, methodology, formal analysis, validation, visualization; Francesco Zucca Writing – review & editing, methodology, supervision, validation; Martin Funk Writing – review & editing, supervision; Daniele Giordan: Writing – review & editing, methodology, supervision, validation.

References

Ahn, Y. and Box, J. E.: Glacier velocities from time-lapse photos: technique development and first results from the Extreme Ice Survey (EIS) in Greenland, Journal of Glaciology, 56, 723-734, 2010.
Allstadt, K., Shean, D., Campbell, A., Fahnestock, M., and Malone, S.: Observations of seasonal and diurnal glacier velocities at Mount Rainier, Washington, using terrestrial radar interferometry, The Cryosphere, 9, 2219-2235, 2015.
Altena, B., Scambos, T., Fahnestock, M., and Kääb, A.: Extracting recent short-term glacier velocity evolution over southern Alaska and the Yukon from a large collection of Landsat data, The Cryosphere, 13, 795-814, 2019.
Arendt, A., Bliss, A., Bolch, T., Cogley, J., Gardner, A., Hagen, J.-O., Hock, R., Huss, M., Kaser, G., and Kienholz, C.: Randolph Glacier inventory–A dataset of Global glacier outlines: Version 6.0: Technical report, Global land ice measurements from space, 2017.
Beniston, M., Farinotti, D., Stoffel, M., Andreassen, L. M., Coppola, E., Eckert, N., Fantini, A., Giacona, F., Hauck, C., and Huss, M.: The European mountain cryosphere: a review of its current state, trends, and future challenges, The Cryosphere, 12, 759-794, 2018.
Benn, D. I. and Evans, D. J.: Glaciers & glaciation, Routledge 2014.

https://doi.org/10.5194/egusphere-2023-2771
Preprint. Discussion started: 4 December 2023

574 Beraud, L., Cusicanqui, D., Rabatel, A., Brun, F., Vincent, C., and Six, D.: Glacier-wide seasonal and annual geodetic mass
575 balances from Pléiades stereo images: application to the Glacier d'Argentière, French Alps, Journal of Glaciology, 69, 525-
576 537, 2023.
577 Berthier, E., Vadon, H., Baratoux, D., Arnaud, Y., Vincent, C., Feigl, K., Remy, F., and Legresy, B.: Surface motion of mountain
578 glaciers derived from satellite optical imagery, Remote Sensing of Environment, 95, 14-28, 2005.
579 Berthier, E., Vincent, C., Magnússon, E., Gunnlaugsson, Á., Pitte, P., Le Meur, E., Masiokas, M., Ruiz, L., Pálsson, F., and
580 Belart, J.: Glacier topography and elevation changes derived from Pléiades sub-meter stereo images, The Cryosphere, 8, 2275-
581 2291, 2014.
582 Bindschadler, R.: The importance of pressurized subglacial water in separation and sliding at the glacier bed, Journal of
583 Glaciology, 29, 3-19, 1983.
584 Buisson, A., Dumas, C., Reynaud, L., and Valla, F.: Les risques naturels d'origine glaciaire: inventaire dans les Alpes françaises
585 et typologie, La Houille Blanche, 47-53, 1999.
586 Chiarle, M., Viani C., Mortara G., Deline P., Tamburini A. and Nigrelli G.,: Large glacier failures in the Italian Alps over the
587 last 90 years, Geografia Fisica e Dinamica Quaternaria, 45, 19-40, 2022.
588 Cuffey, K. M. and Paterson, W. S. B.: The Physics of Glaciers, Academic Press2010.
589 Dehecq, A., Gourmelen, N., Gardner, A. S., Brun, F., Goldberg, D., Nienow, P. W., Berthier, E., Vincent, C., Wagnon, P., and
590 Trouvé, E.: Twenty-first century glacier slowdown driven by mass loss in High Mountain Asia, Nature Geoscience, 12, 22-27,
591 2019.
592 Deilami, K. and Hashim, M.: Very high resolution optical satellites for DEM generation: a review, European Journal of
593 Scientific Research, 49, 542-554, 2011.
594 Deline, P.: Étude géomorphologique des interactions entre écroulements rocheux et glaciers dans la haute montagne alpine: le
595 versant sud-est du massif du Mont-Blanc (Vallée d'Aoste, Italie), Chambéry, 2002.
596 Deline, P., Gardent, M., Magnin, F., and Ravanel, L.: The morphodynamics of the Mont Blanc massif in a changing cryosphere:
597 a comprehensive review, Geografiska Annaler: Series A, Physical Geography, 94, 265-283, 2012.
598 Deline, P., Bolon, P., Chiarle, M., Fioraso, G., Fosson, J. P., Gay, M., Gardent, M., Di Cella, U. M., Ott, L., and Pogliotti, P.:
599 GlaRiskAlp, a French-Italian project (2010-2013) on glacial hazards in the Western Alps in relation with the glacier retreat,
600 14th Alpine Glaciological Meeting,
601 Dematteis, N. and Giordan, D.: Comparison of digital image correlation methods and the impact of noise in geoscience
602 applications, Remote Sensing, 13, 327, 2021.
603 Dematteis, N., Giordan, D., Troilo, F., Wrzesniak, A., and Godone, D.: Ten-Year Monitoring of the Grandes Jorasses Glaciers
604 Kinematics. Limits, Potentialities, and Possible Applications of Different Monitoring Systems, Remote Sensing, 13, 3005,
605 2021.
606 Diolaiuti, G., Kirkbride, M., Smiraglia, C., Benn, D., D'agata, C., and Nicholson, L.: Calving processes and lake evolution at
607 Miage glacier, Mont Blanc, Italian Alps, Annals of Glaciology, 40, 207-214, 2005.
608 Einarsson, B., Magnússon, E., Roberts, M. J., Pálsson, F., Thorsteinsson, T., and Jóhannesson, T.: A spectrum of jökulhlaup
609 dynamics revealed by GPS measurements of glacier surface motion, Annals of Glaciology, 57, 47-61, 2016.
610 Evans, A. N.: Glacier surface motion computation from digital image sequences, IEEE Transactions on Geoscience and Remote
611 Sensing, 38, 1064-1072, 2000.
612 Fahnestock, M., Scambos, T., Moon, T., Gardner, A., Haran, T., and Klinger, M.: Rapid large-area mapping of ice flow using
613 Landsat 8, Remote Sensing of Environment, 185, 84-94, 2016.
614 Faillettaz, J., Funk, M., and Sornette, D.: Instabilities on Alpine temperate glaciers: new insights arising from the numerical
615 modelling of Allalingletscher (Valais, Switzerland), Natural Hazards and Earth System Sciences, 12, 2977-2991, 2012.
616 Faillettaz, J., Funk, M., and Vagliasindi, M.: Time forecast of a break-off event from a hanging glacier, The Cryosphere, 10,
617 1191-1200, 2016.
618 Faillettaz, J., Pralong, A., Funk, M., and Deichmann, N.: Evidence of log-periodic oscillations and increasing icequake activity
619 during the breaking-off of large ice masses, Journal of Glaciology, 54, 725-737, 2008.
620 FUKUZONO, T.: A method to predict the time of slope failure caused by rainfall using the inverse number of velocity of
621 surface displacement, Landslides, 22, 8-13_11, 1985.
622 Fyffe, C. L.: The hydrology of debris-covered glaciers, University of Dundee, 2012.

https://doi.org/10.5194/egusphere-2023-2771
Preprint. Discussion started: 4 December 2023

Giordan, D., Dematteis, N., Allasia, P., and Motta, E.: Classification and kinematics of the Planpincieux Glacier break-offs using photographic time-lapse analysis, Journal of Glaciology, 66, 188-202, 2020.
Glen, J.: Experiments on the deformation of ice, Journal of Glaciology, 2, 111-114, 1952.
Gottardi, F., Obled, C., Gailhard, J., and Paquet, E.: Statistical reanalysis of precipitation fields based on ground network data and weather patterns: Application over French mountains, Journal of hydrology, 432, 154-167, 2012.
Heid, T. and Kääb, A.: Repeat optical satellite images reveal widespread and long term decrease in land-terminating glacier speeds, The Cryosphere, 6, 467-478, 2012a.
Heid, T. and Kääb, A.: Evaluation of existing image matching methods for deriving glacier surface displacements globally from optical satellite imagery, Remote Sensing of Environment, 118, 339-355, 2012b.
Humbert, A., Greve, R., and Hutter, K.: Parameter sensitivity studies for the ice flow of the Ross Ice Shelf, Antarctica, Journal of Geophysical Research: Earth Surface, 110, 2005.
Jiskoot, H.: Dynamics of Glaciers, physical Research, 92, 9083-9100, 2011.
Jolliffe, I. T. and Cadima, J.: Principal component analysis: a review and recent developments, Philosophical transactions of the royal society A: Mathematical, Physical and Engineering Sciences, 374, 20150202, 2016.
Kääb, A., Winsvold, S., Altena, B., Nuth, C., Nagler, T., and Wuite, J.: Glacier Remote Sensing Using Sentinel-2. Part I: Radiometric and Geometric Performance, and Application to Ice Velocity, Remote Sensing, 8, 2016.
Kääb, A., Jacquemart, M., Gilbert, A., Leinss, S., Girod, L., Huggel, C., Falaschi, D., Ugalde, F., Petrakov, D., and Chernomorets, S.: Sudden large-volume detachments of low-angle mountain glaciers–more frequent than thought?, The Cryosphere, 15, 1751-1785, 2021.
Kamb, B.: Glacier surge mechanism based on linked cavity configuration of the basal water conduit system, Journal of Geophysical Research: Solid Earth, 92, 9083-9100, 1987.
Lesca, C.: Emploi de la photogrammetrie analytique pour la determination de la vitesse superficielle des glaciers et des profondeurs relatives, 1974.
Luzi, G., Pieraccini, M., Mecatti, D., Noferini, L., Macaluso, G., Tamburini, A., and Atzeni, C.: Monitoring of an alpine glacier by means of ground-based SAR interferometry, IEEE Geoscience and Remote Sensing Letters, 4, 495-499, 2007.
Marsy, G., Vernier, F., Trouvé, E., Bodin, X., Castaings, W., Walpersdorf, A., Malet, E., and Girard, B.: Temporal Consolidation Strategy for Ground-Based Image Displacement Time Series: Application to Glacier Monitoring, IEEE Journal of Selected Topics in Applied Earth Observations and Remote Sensing, 14, 10069-10078, 2021.
Millan, R., Mouginot, J., Rabatel, A., and Morlighem, M.: Ice velocity and thickness of the world's glaciers, Nature Geoscience, 15, 124-129, 2022.
Millan, R., Mouginot, J., Rabatel, A., Jeong, S., Cusicanqui, D., Derkacheva, A., and Chekki, M.: Mapping surface flow velocity of glaciers at regional scale using a multiple sensors approach, Remote Sensing, 11, 2498, 2019.
Mondardini, L., Perret, P., Frasca, M., Gottardelli, S., and Troilo, F.: Local variability of small Alpine glaciers: Thoula Glacier geodetic mass balance reconstruction (1991-2020) and analysis of volumetric variations, Geografia Fisica e Dinamica Quaternaria, 44, 29-38, 2021.
Mouginot, J., Rabatel, A., Ducasse, E., and Millan, R.: Optimization of Cross Correlation Algorithm for Annual Mapping of Alpine Glacier Flow Velocities; Application to Sentinel-2, IEEE Transactions on Geoscience and Remote Sensing, 61, 1-12, 2023.
Mourey, J. and Ravanel, L.: Evolution of access routes to high mountain refuges of the Mer de Glace Basin (Mont Blanc Massif, France). An example of adapting to climate change effects in the Alpine High mountains, Journal of Alpine Research| Revue de géographie alpine, 2017.
Nanni, U., Gimbert, F., Vincent, C., Gräff, D., Walter, F., Piard, L., and Moreau, L.: Quantification of seasonal and diurnal dynamics of subglacial channels using seismic observations on an Alpine glacier, The Cryosphere, 14, 1475-1496, 2020.
Nye, J. F.: The mechanics of glacier flow, Journal of Glaciology, 2, 82-93, 1952.
Paradis, E.: Probabilistic unsupervised classification for large-scale analysis of spectral imaging data, International Journal of Applied Earth Observation and Geoinformation, 107, 102675, 2022.
Paul, F., Winsvold, S. H., Kääb, A., Nagler, T., and Schwaizer, G.: Glacier remote sensing using Sentinel-2. Part II: Mapping glacier extents and surface facies, and comparison to Landsat 8, Remote Sensing, 8, 575, 2016.
Paul, F., Piermattei, L., Treichler, D., Gilbert, L., Girod, L., Kääb, A., Libert, L., Nagler, T., Strozzi, T., and Wuite, J.: Three different glacier surges at a spot: what satellites observe and what not, The Cryosphere, 16, 2505-2526, 2022.

https://doi.org/10.5194/egusphere-2023-2771
Preprint. Discussion started: 4 December 2023

673 Paul, F., Rastner, P., Azzoni, R., Diolaiuti, G., Fugazza, D., Le Bris, R., Nemec, J., Rabatel, A., Ramusovic, M., and Schwaizer,
674 G.: Glacier shrinkage in the Alps continues unabated as revealed by a new glacier inventory from Sentinel-2, Earth Syst. Sci.
675 Data, 12, 1805–1821, 2020.
676 Pelfini, M., Santilli, M., Leonelli, G., and Bozzoni, M.: Investigating surface movements of debris-covered Miage glacier,
677 Western Italian Alps, using dendroglaciological analysis, Journal of Glaciology, 53, 141-152, 2007.
678 Pfeffer, W. T., Arendt, A. A., Bliss, A., Bolch, T., Cogley, J. G., Gardner, A. S., Hagen, J.-O., Hock, R., Kaser, G., and Kienholz,
679 C.: The Randolph Glacier Inventory: a globally complete inventory of glaciers, Journal of glaciology, 60, 537-552, 2014.
680 Pralong, A. and Funk, M.: On the instability of avalanching glaciers, Journal of Glaciology, 52, 31-48, 2006.
681 Pralong, A., Birrer, C., Stahel, W. A., and Funk, M.: On the predictability of ice avalanches, Nonlinear Processes in Geophysics,
682 12, 849-861, 2005.
683 Rabatel, A., Ducasse, E., Ramseyer, V., and Millan, R.: State and Fate of Glaciers in the Val Veny (Mont-Blanc Range, Italy):
684 Contribution of Optical Satellite Products, Journal of Alpine Research| Revue de géographie alpine, 2023.
685 Rankl, M., Kienholz, C., and Braun, M.: Glacier changes in the Karakoram region mapped by multimission satellite imagery,
686 The Cryosphere, 8, 977-989, 2014.
687 Ravanel, L.: Évolution géomorphologique de la haute montagne alpine dans le contexte actuel de réchauffement climatique,
688 2009.
689 Samsonov, S., Tiampo, K., and Cassotto, R.: SAR-derived flow velocity and its link to glacier surface elevation change and
690 mass balance, Remote Sensing of Environment, 258, 112343, 2021.
691 Scambos, T. A., Dutkiewicz, M. J., Wilson, J. C., and Bindschadler, R. A.: Application of image cross-correlation to the
692 measurement of glacier velocity using satellite image data, Remote sensing of environment, 42, 177-186, 1992.
693 Schwalbe, E. and Maas, H.-G.: The determination of high-resolution spatio-temporal glacier motion fields from time-lapse
694 sequences, Earth Surface Dynamics, 5, 861-879, 2017.
695 Smiraglia, C., Diolaiuti, G., Casati, D., and Kirkbride, M. P.: Recent areal and altimetric variations of Miage Glacier (Monte
696 Bianco massif, Italian Alps), IAHS-AISH publication, 227-233, 2000.
697 Span, N. and Kuhn, M.: Simulating annual glacier flow with a linear reservoir model, Journal of Geophysical Research:
698 Atmospheres, 108, 2003.
699 Stocker-Waldhuber, M., Fischer, A., Helfricht, K., and Kuhn, M.: Long-term records of glacier surface velocities in the Ötztal
700 Alps (Austria), Earth system science data, 11, 705-715, 2019.
701 Van Wyk De Vries, M. and Wickert, A. D.: Glacier Image Velocimetry: an open-source toolbox for easy and rapid calculation
702 of high-resolution glacier velocity fields, The Cryosphere, 15, 2115-2132, 10.5194/tc-15-2115-2021, 2021.
703 Vincent, C. and Moreau, L.: Sliding velocity fluctuations and subglacial hydrology over the last two decades on Argentière
704 glacier, Mont Blanc area, Journal of Glaciology, 62, 805-815, 2016.
705 Vincent, C., Gilbert, A., Walpersdorf, A., Gimbert, F., Gagliardini, O., Jourdain, B., Roldan Blasco, J. P., Laarman, O., Piard,
706 L., and Six, D.: Evidence of seasonal uplift in the Argentière glacier (Mont Blanc area, France), Journal of Geophysical
707 Research: Earth Surface, 127, e2021JF006454, 2022.
708 Willis, I. C.: Intra-annual variations in glacier motion: a review, Progress in Physical Geography, 19, 61-106, 1995.
709 Zekollari, H., Huss, M., and Farinotti, D.: Modelling the future evolution of glaciers in the European Alps under the EURO-
710 CORDEX RCM ensemble, The Cryosphere, 13, 1125-1146, 2019.
711 Zemp, M., Hoelzle, M., and Haeberli, W.: Six decades of glacier mass-balance observations: a review of the worldwide
712 monitoring network, Annals of Glaciology, 50, 101-111, 2009.
713 Zemp, M., Nussbaumer, S. U., Gärtner-Roer, I., Bannwart, J., Paul, F., and Hoelzle, M.: Global Glacier Change Bulletin Nr. 4
714 (2018-2019), WGMS, 4, 2021.
715 Zemp, M., Huss, M., Eckert, N., Thibert, E., Paul, F., Nussbaumer, S. U., and Gärtner-Roer, I.: Brief communication: Ad hoc
716 estimation of glacier contributions to sea-level rise from the latest glaciological observations, The Cryosphere, 14, 1043-1050,
717 2020.

718

719

Morphodynamics of the Mont Blanc glaciers and their recent evolution

Fabrizio Troilo[1,4], Niccolò Dematteis[3], Francesco Zucca[4], Martin Funk[2], Daniele Giordan[3].

[1]Fondazione Montagna sicura, Glaciers, snow and avalanche research area, Courmayeur, 11013, Italy.
[2]ETH-VAW, Versuchsanstalt für Wasserbau, Hydrologie und Glaziologie, Zurich, CH-8092, Switzerland.
[3]Research Institute for Geo-Hydrological Protection IRPI, Italian National Research Council, Turin, 10135, Italy.
[4]University of Pavia, Department of Earth and Environmental Sciences, Pavia, 27100, Italy.

Correspondence to: Niccolò Dematteis (niccolo.dematteis@irpi.cnr.it); Fabrizio Troilo (ftroilo@fondms.org).

1 Supplementary material

1.1 Single glaciers description

In this supplementary section we give a brief geographical and geomorphological description for every glacier on which the velocity time series analysis of our study was performed. The 30 glaciers are described in order of their ID number of the study that follows increasing Randolph Glacier Inventory numbering.

ID:1 A Neuve N Glacier: this (RGI60-11.02859) is a small (Area= 0.269km2) glacier located in the Swiss part of the Mont Blanc massif. It is the northernmost of different small glaciers formed by the retreat and fragmentation of the once unique A Neuve Glacier. Its aspect is mostly south-east and its accumulation area is overlooked by Grand-Luy Peak (3508m) by less than 100 vertical meters of cliffs. It drains in the Swiss Val Ferret in the Canton of Wallis.

ID:2 A Neuve Central Glacier: this (RGI60-11.02864) is a medium-sized (Area: 0.889km2) glacier located in the Swiss part of the Mont Blanc massif. The analysed part of the A Neuve Glacier is the central section, one which is nowadays distinct from the northern (RGI60-11.02859) and southern parts (RGI60-11.02884); its aspect is mostly east and its accumulation area is overlooked by Tour Noir (3836m) from which the glacier originates with rock walls as high as 800m. It drains in the Swiss Val Ferret in the Canton of Wallis.

ID:3 Pré de Bard Glacier: this (RGI60-11.02916) is a medium-sized (Area: 3.011km2) glacier located in the Italian part of the Mont Blanc massif. Its aspect is mostly south-east and its accumulation area is overlooked by rock faces from Mont Dolent (3823m), reaching a vertical drop as high as 600m. It drains in Val Ferret, in the Aosta valley region.

ID:4 Greuvettaz E Glacier: this (RGI60-11.02978) is a small (Area: 0.196km2) glacier located in the Italian part of the Mont Blanc massif. Its aspect is mostly south-east and its accumulation area is overlooked by rock faces from Mont Greuvettaz (3684m), reaching a vertical drop as high as 400m. It drains in the Val Ferret, in the Aosta valley region.

ID:5 Greuvettaz W Glacier: this (RGI60-11.02981) is a small (Area: 0.169km2) glacier located in the Italian part of the Mont Blanc massif. Its aspect is mostly south-east and its accumulation area is overlooked by rock faces from Mont Greuvettaz (3684m), reaching a vertical drop as high as 400m. It drains in the Val Ferret, in the Aosta valley region.

ID:6 Planpincieux Glacier: this (RGI60-11.02991) is a medium-sized (Area: 1.013km2) glacier located in the Italian part of the Mont Blanc massif. Its aspect is mostly south and its accumulation area is overlooked by rock faces from Grandes Jorasses (4208m), reaching a vertical drop as high as 700m. It drains in Val Ferret, in the Aosta valley region.

ID:7 Grandes Jorasses Glacier: this (part of RGI60-11.02991) is a small (Area: 0.482km2) glacier located in the Italian part of the Mont Blanc massif. It is mapped as a single glacier together with Planpincieux glacier in the Randolph Glacier inventory but it is classified as a single glacial complex in the Italian glacier inventory (Smiraglia, 2015). Its aspect is mostly south-east and its accumulation area is overlooked by Grandes Jorasses (4208m) from which the glacier originates with almost no cirque. It drains in Val Ferret, in the Aosta valley region.

ID:8 Pra-Sec Glacier: this (RGI60-11.02996) is a small (Area: 0.119km2) glacier located in the Italian part of the Mont Blanc massif. Its aspect is mostly south-east and its accumulation area is overlooked by rock faces from Grandes Jorasses (4208m), reaching a vertical drop as high as 1000m. It drains in Val Ferret, in the Aosta valley region.

ID:9 Rochefort Glacier: this (RGI60-11.03000) is a small (Area: 0.558km2) glacier located in the Italian part of the Mont Blanc massif. Its aspect is mostly south and its accumulation area is overlooked by rock faces from Dent du Géant (4014m), reaching a vertical drop as high as 900m. It drains in Val Ferret, in the Aosta valley region.

ID:10 Brenva Glacier: this (RGI60-11.03001) is a large (Area: 6.579km2) glacier located in the Italian part of the Mont Blanc massif. Despite a unique glacial complex reaching as low as 1400m, as mapped in the Randolph glacier inventory, since 2005 it has separated into a lower stagnant tongue and a higher part. Its aspect is mostly south-east and its accumulation area is overlooked by the Mont Blanc summit (4809m). Huge cirque head rockwalls dominate the accumulation areas towards Mont Maudit (4465m) on the eastern part and towards Aiguille Blanche de Peuterey (4112m) on the western side. It drains in Val Veny, in the Aosta valley region.

ID:11 Thoula Glacier: this (RGI60-11.03002) is a small (Area: 0.580km2) glacier located in the Italian part of the Mont Blanc massif. Its aspect is mostly south-east and its accumulation area is overlooked by rock faces from Aiguille d'Entrèves (3596m), reaching a vertical drop as high as 400m. It drains in Val Ferret, in the Aosta valley region.

ID:12 Mont Blanc Glacier: this (part of RGI60-11.03005 - Miage Glacier complex) is a medium-sized (Area: 0.764km2) glacier located in the Italian part of the Mont Blanc massif. As mapped in the Randolph glacier inventory and other glacier inventories, it is a tributary of the large Miage Glacier complex. Even though it is part of the same glacier for inventory purposes, it has both a particular distinct behaviour in terms of cinematics and it has its own topographical designation in cartographies from all of the three bordering nations. Therefore, manual digitalisation of the glacier area was carried out based on Sentinel-2 Satellite Imagery. Its aspect is mostly south-east and its accumulation area is overlooked by the Mont Blanc summit (4809m). Huge cirque head rock walls dominate the accumulation areas towards Mont Maudit (4465m) on the eastern part and towards Aiguille Blanche de Peuterey (4112m) on the western side. It drains in Val Veny, in the Aosta valley region.

ID:13 Dome Glacier: this (part of RGI60-11.03005 - Miage Glacier complex) is a medium-sized (Area: 1.973km2) glacier located in the Italian part of the Mont Blanc massif. As for the Mont Blanc Glacier, as a tributary of the large Miage Glacier complex, it has been remapped in order to obtain morphometrical information of the single glacial body. Its aspect is mostly south-west and its accumulation area is overlooked by the Dome du Gouter summit (4304m) in the western part and by the Mont Blanc summit (4809m) in the eastern part. It drains in Val Veny, in the Aosta valley region.

ID:14 Bionassay Glacier (Italian – it has an homonymous in France): this (part of RGI60-11.03005 - Miage Glacier complex) is a medium-sized (Area: 1.354km2) glacier located in the Italian part of the Mont Blanc massif. The Mont Blanc and Dome Glaciers, as a tributary of the large Miage Glacier complex, was remapped in order to obtain morphometrical information of the single glacial body. Its aspect is mostly south-west and its accumulation area is overlooked by Dome du Gouter summit (4304m). It drains in Val Veny, in the Aosta valley region.

ID:15 Tré-la-Tête N Glacier (Italian – it has a homonymous in France): this (part of RGI60-11.03005 - Miage Glacier complex) is a medium-sized (Area: 0.312km2) glacier is located in the Italian part of the Mont Blanc massif. The Mont Blanc, Bionassay and Dome Glaciers, as a tributary of the large Miage Glacier complex, was remapped in order to obtain

morphometrical information of the single glacial body. Its aspect is mostly north-east and its accumulation area is overlooked by Aiguille de Tré-la-Tête (3920m). It drains in Val Veny, in the Aosta Valley region.

ID:16 Freney Glacier: this (RGI60-11.03013) is a medium-sized (Area: 1,017km2) glacier located in the Italian part of the Mont Blanc massif. Its aspect is mostly south-east and its accumulation area is overlooked by the Mont Blanc summit (4809m). Huge cirque head rockwalls dominate the accumulation areas. It drains in Val Veny, in the Aosta valley region.

ID:17 Brouillard Glacier: this (RGI60-11.03014) is a medium-sized (Area: 1.166km2) glacier located in the Italian part of the Mont Blanc massif. Its aspect is mostly south and its accumulation area is overlooked by the Mont Blanc summit (4809m). Huge cirque head rockwalls dominate the accumulation areas. It drains in Val Veny, in the Aosta valley region.

ID:18 Lex Blanche Glacier: this (RGI60-11.03020) is a medium-sized (Area: 2.640km2) glacier located in the Italian part of the Mont Blanc massif. Its aspect is mostly south-east and its accumulation area is overlooked by Aiguilles de Tré-la-Tête (3923m). Cirque head rockwalls dominate the accumulation areas by as much as 600-700m. It drains in Val Veny, in the Aosta valley region.

ID:19 Petit Mont Blanc Glacier: this (Part of RGI60-11.03020 – Lex Blanche Glacier) is a small (Area: 0.556km2) glacier located in the Italian part of the Mont Blanc massif. It is mapped in the RGI as a unique glacier complex together with the Lex Blanche Glacier (RGI60-11.03020). Its aspect is mostly south and its accumulation area originates at Aiguille de Tré-la-Tête (3920m). It drains in Val Veny, in the Aosta valley region.

ID:20 Estelette Glacier: this (RGI60-11.03022) is a small (Area: 0.291km2) glacier located in the Italian part of the Mont Blanc massif. Its aspect is mostly south-east and its accumulation area is overlooked by Aiguille des Glaciers (3815m). Cirque head rockwalls dominate the accumulation areas by as much as 600m. It drains in Val Veny, in the Aosta valley region.

ID:21 Pierre Joseph Glacier: this (RGI60-11.03258) is a small (Area: 0.275km2) glacier located in the French part of the Mont Blanc massif. Its aspect is mostly south-west and it originates from Aiguille de Talèfre (3730m) with rockwalls as high as 400m. It drains in the Isère valley, in the Haute Savoie Département.

ID:22 Nant Blanc Glacier: this (RGI60-11.03263) is a small (Area: 0.363km2) glacier located in the French part of the Mont Blanc massif. Its aspect is mostly west and it is overlooked by Aiguille Verte (4122m) with up to 800m of cirque headwalls. It drains in the Isère valley, in the Haute Savoie Département.

ID:23 Charpoua Glacier: this (RGI60-11.03284) is a small (Area: 0.405km2) glacier located in the French part of the Mont Blanc massif. Its aspect is mostly south-west and its accumulation area is overlooked by high rock faces from Aiguille Verte (4122m), reaching a vertical drop as high as 700m. It drains in the Vallée de l'Arve, in the Haute Savoie Département.

ID:24 Aiguille des Glaciers Glacier: this (RGI60-11.03339) is a small (Area: 1.091km2) glacier located in the French part of the Mont Blanc massif. Its aspect is mostly south and it originates straight from the very top of Aiguille des Glaciers (3815m). It drains in the Isère valley, in the Haute Savoie Département.

ID:25 Talèfre Glacier N: this (RGI60-11.03466) is a medium-sized (Area: 2.037km2) glacier located in the French part of the Mont Blanc massif. We concentrated the study on the westernmost part of the glacier that we mapped accordingly, as it is now almost totally disconnected from the rest of the Talèfre Glacier. It originates from the foot of Aiguille Verte (4122m) with up to 600m of cirque headwalls. It drains in the Vallée de l'Arve, in the Haute Savoie Département.

ID:26 Argentière Glacier: this (RGI60-11.03638) is a large (Area: 13.109km2) glacier located in the French part of the Mont Blanc massif. It originates from the ridges in between Aiguille de Triolet (3870m) and Mont Dolent (3823m). It drains in the Vallée de l'Arve, in the Haute Savoie Département.

ID:27 Mer de Glace Glacier: this (RGI60-11.03646) is a large (Area: 23.556km2) glacier located in the French part of the Mont Blanc massif. It originates from a large accumulation area comprised in between Col du Midi (3522m), Mont Blanc du Tacul (4248m) and Dent du Géant (4014m). It drains in the Vallée de l'Arve, in the Haute Savoie Département.

ID:28 Bossons Glacier: this (RGI60-11.03646) is a large (Area: 11.319km2) glacier located in the French part of the Mont Blanc massif. It originates straight from the very top of the Mont Blanc summit (4809m). It drains in the Vallée de l'Arve, in the Haute Savoie Département.

ID:29 Taconnaz Glacier: this (RGI60-11.03647) is a medium-sized (Area: 4,898km2) glacier located in the French part of the Mont Blanc massif. Its aspect is mostly north and it originates straight from the very top of Dome du Gouter (4304m). It drains in the Vallée de l'Arve, in the Haute Savoie Département.

ID: 30 Bionassay Glacier (FR): this (RGI60-11.03648) is a small (Area: 4.774km2) glacier located in the French part of the Mont Blanc massif. Its aspect is mostly north-east and, like the Taconnaz Glacier, it originates straight from the very top of Dome du Gouter (4304m). It drains in the Vallée de l'Arve, in the Haute Savoie Département.

1.2 Mean average velocity map of Mont Blanc 2016-2022 with velocity mapping of ice-free terrain.

In order to give a representation for the reader about data quality outside glaciated terrain, we hereby show in Figure S1 a map with Mean average velocity map of Mont Blanc 2016-2022 with velocity mapping of ice-free terrain.

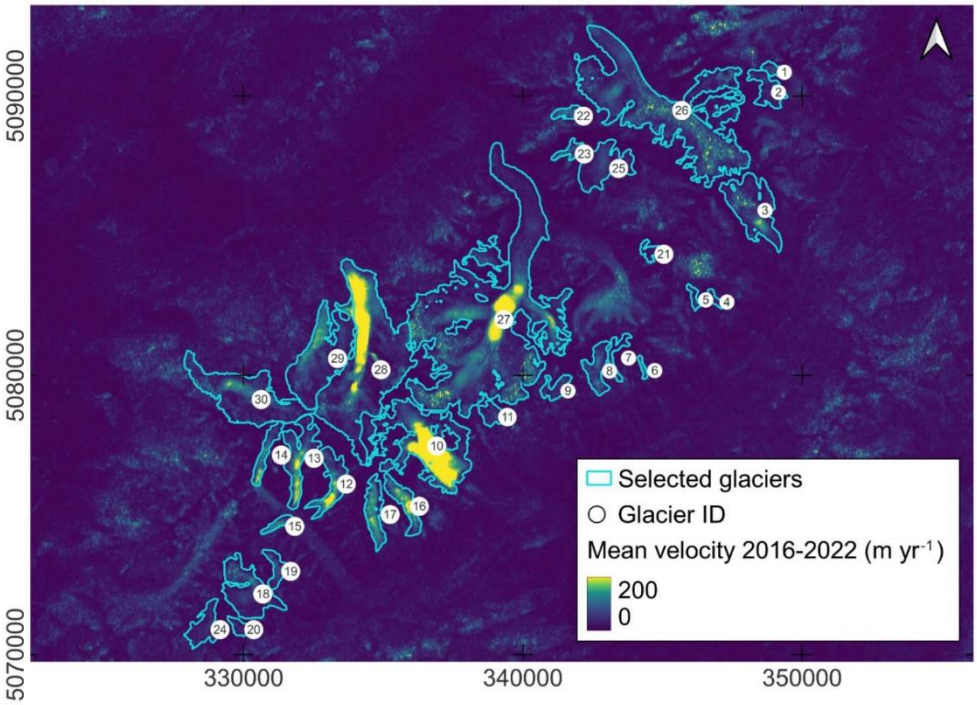

Figure S1. Surface glacier velocity map averaged in the 2016-2022 period. Selected glaciers for specific analyses are outlined in cyan.

1.3 Glacier normalised features

In Figure S2, the normalised features of the 30 selected glaciers of the study considered in the PCA analysis are represented.

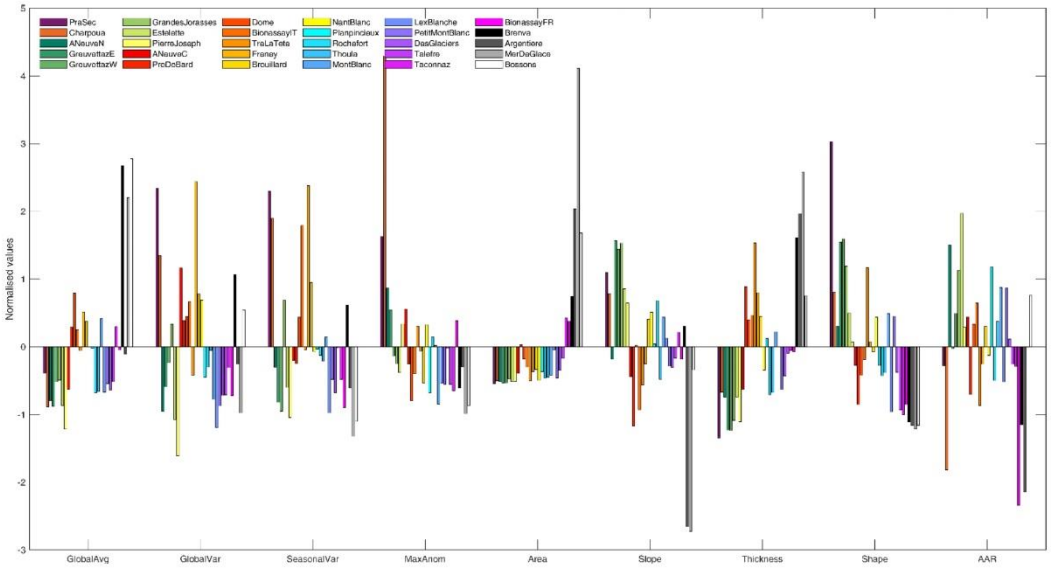

Figure S2. Glacier normalised features considered in the PCA.

1.4 Meteorological conditions

To estimate the meteorological conditions during the period of study, we analysed the data of ERA5-Land monthly averaged data of temperature and precipitation. We calculated the mean temperature and precipitation and the robust linear trends over the periods 2016-2019 and 2020-2022, considering the annual data (i.e., using all the months), the winter data (i.e., months from November to April) and summer months (i.e., from June to September). We averaged the data over the area 45.71°N–46.01°N and 6.60°E–7.10°E. We observed that, on an annual base, the temperature was +0.4°C higher in the second period, when the difference was more marked during winter (+0.6°C), but show a decrease in summer (–0.2°C). Concerning the precipitation, in the second period there was a decrease of 10% (-0.4 mm day^{-1}) on an annual base, which was mostly due by the winters 2018 and 2022, when the precipitation was respectively much higher and lower that the average, while the summer precipitation in 2020–2022 was +5% compared to 2016–2019 (Table S1). Considering the trends, in the first period both temperature and precipitation did not show much variation. In the second period, winter precipitation and temperature remained constant, while we observed similar temperature increase and precipitation decrease on an annual and summer basis (Figure S3).

TableS1. Mean values of monthly temperature (T) and daily precipitation (P) calculated over the periods between 2016–2019 and 2020–2022 considering the whole year, winter (from November to April) and summer (from June to July) months.

Period	Annual mean T [°C]	Winter mean T [°C]	Summer mean T [°C]	Annual mean P [mm/day]	Winter mean P [mm/day]	Summer mean P [mm/day]
2016-2019	2.2	-4.4	11.1	4.4	5.0	3.6
2020-2022	2.6	-3.8	10.9	4.0	4.0	3.8

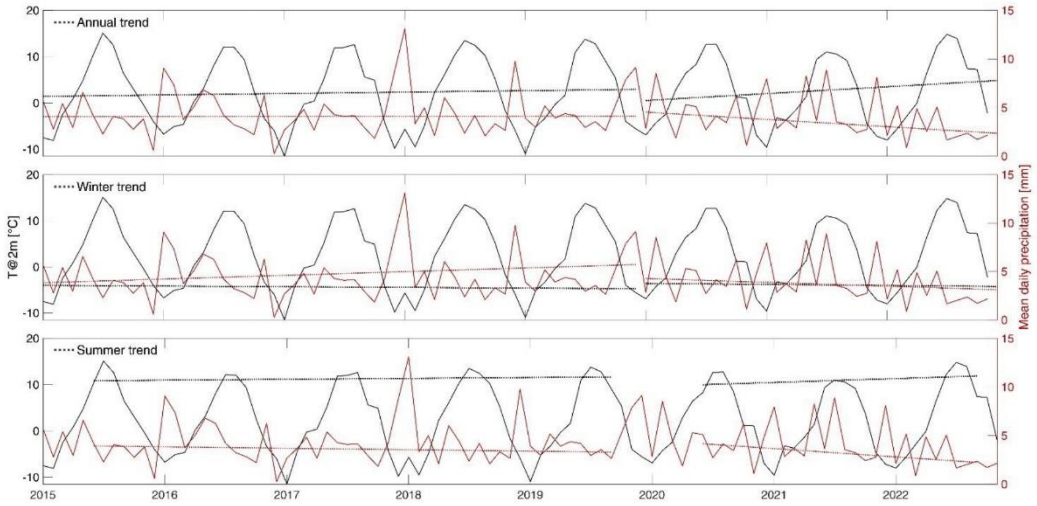

Figure S3. Mean monthly temperature (solid black line) and daily precipitation (solid red line). From the top to the bottom, the dashed lines represent the robust linear trends calculated over the periods 2016-2019 and 2020-2022 using the whole year, winter and summer months.

Evidences of bedrock forcing on glacier morphodynamics: a case study in the Italian Alps

Short summary

The publication of the research paper 'Evidences of bedrock forcing on glacier morphodynamics: a case study in Italian Alps' (Dematteis et al., 2022), highlights the integration that has been performed between Ground Penetrating Radar data and high-resolution surface elevation data at Planpincieux Glacier in order to demonstrate quantitative evidence of the influence of bedrock geometry on glacier surface morphology. The recurrence of the seasonal evolution of surface morphology is analysed as well as its application to glacial risk monitoring.

Main findings

The main findings of this publication are:

• The realisation of a GPR glacier thickness model on a steep temperate glacier.

• A multi-temporal analysis of a multi-year high resolution digital elevation and orthomosaics dataset.

• A spatial analysis of surface glacial morphological features.

• The demonstration of bedrock influence on surface glacier morphology and its implications to glacial risk monitoring and assessment.

Contributions of the PhD candidate

Conceptualisation of the research activity with the co-authors. Organisation of field surveys. Field data validation and post-processing of GPR data. Acquisition and processing of aerial photogrammetric surveys. Analysis and interpretation of the data. Contribution in the preparation and writing of the manuscript and the figures with the co-authors.

Data availability

The data are available from the authors, upon request.

Journal

Frontiers in Earth Science is an open-access journal that aims to bring together and publish on a single platform, rapidly growing and continuously expanding domains in Earth Science, involving the lithosphere (including the geosciences spectrum), the hydrosphere (including marine geosciences and hydrology, complementing the existing Frontiers journal on Marine Science) and the atmosphere (including meteorology and climatology). Impact factor 2022: 2.9

frontiers | Frontiers in Earth Science

ORIGINAL RESEARCH
published: 26 May 2022
doi: 10.3389/feart.2022.793546

Evidences of Bedrock Forcing on Glacier Morphodynamics: A Case Study in Italian Alps

Niccolò Dematteis[1], *Daniele Giordan*[1]*, *Paolo Perret*[2], *Melchior Grab*[3], *Hansruedi Maurer*[3] *and Fabrizio Troilo*[2]

[1]Research Institute for Geo-Hydrological Protection, Italian National Research Council, Turin, Italy, [2]Fondazione Montagna Sicura, Courmayeur, Italy, [3]Department of Earth Sciences, ETH Zurich, Zurich, Switzerland

In mountain glaciers, the influence of bedrock geometry on glacier surface morphology is often assumed; quantitative evidence, however, is rare. In our research, we measured the ice thickness of the Planpincieux Glacier (North-west Italy) and detected the bedrock topography using ground-penetrating radar. Additionally, we investigated the glacier surface morphology using structure from motion and the glacier kinematics using digital image correlation of terrestrial images. A digital terrain analysis showed evidence of recurrent crevasses whose position corresponded to bedrock steps. On average, since 2014, their positions varied between 6 and 14 m and were 40 ± 8 m downstream of the bedrock steps. Bedrock and glacier topography presented out-of-phase correlated undulations that approximately fit a sinusoidal function of different amplitude. Moreover, we show the morphological evolution of an unstable sector whose thickness at the end of the ablation seasons has remained approximately constant since 2014. Contrarily, the ice melting during the 2020 ablation season caused a volume loss of >30%. Since, in general, the damages provoked by a potential ice avalanche depend primarily on the involved volume, this finding demonstrates that frequent morphology monitoring is essential for correct glacial hazard assessment.

Keywords: structure from motion, ground-penetrating radar, glacier morphology, glacial hazards, image correlation, Planpincieux Glacier, ice avalanches, digital terrain analysis

OPEN ACCESS

Edited by:
Ning Huang,
Lanzhou University, China

Reviewed by:
Feiteng Wang,
Cold and Arid Regions Environmental and Engineering Research Institute (CAS), China
Kristaps Lamsters,
University of Latvia, Latvia

***Correspondence:**
Daniele Giordan
daniele.giordan@irpi.cnr.it

Specialty section:
This article was submitted to Cryospheric Sciences, a section of the journal Frontiers in Earth Science

Received: *12 October 2021*
Accepted: *11 May 2022*
Published: *26 May 2022*

Citation:
Dematteis N, Giordan D, Perret P, Grab M, Maurer H and Troilo F (2022) Evidences of Bedrock Forcing on Glacier Morphodynamics: A Case Study in Italian Alps. Front. Earth Sci. 10:793546. doi: 10.3389/feart.2022.793546

1 INTRODUCTION

Mountain glaciers are rapidly shrinking worldwide due to global warming and, in the European Alps, 90% of the glaciated areas are forecast to disappear by 2100 (Huss and Hock, 2015; Zekollari et al., 2019). In particular, small glaciers are clear geo indicators of climate change, as they are more affected by short-term meteorological variations (Huss and Fischer, 2016). They represent relevant components of the local cryosphere and their melting contributes to sea-level rise (Meier et al., 2007; Zemp et al., 2015). Besides the environmental aspect, glaciers impact anthropogenic activities in terms of local economy (Beniston, 2012), water supply (Grunewald and Scheithauer, 2010; Beniston, 2012) and tourism (Fischer et al., 2011). In addition, in specific areas, glacial hazards represent a potential threat to the population (Huggel et al., 2004), and they must be carefully assessed.

Risk assessment is defined as the combination of occurrence probability and potential damage of a given event (Huggel et al., 2004). Concerning glacial hazards, and in particular ice avalanches, the occurrence probability can be either numerically modelled (Iken, 1977; Faillettaz et al., 2011b) or

statistically estimated based on monitoring data (Faillettaz et al., 2011a, 2016; Margreth et al., 2017). In both cases, glacier surface kinematics is crucial information, which can be linked to the magnitude of the failure event (Iken, 1977; Giordan et al., 2020). On the other hand, the potential impact of an ice avalanche depends primarily on the involved volume of the collapsed ice (Margreth et al., 2011; Schweizer and Margreth, 2020). Therefore, precise estimates of unstable sector extension and thickness are of paramount importance for a correct evaluation of the level of risk.

Considering the usual remoteness of glaciers, surveying their surface kinematics can be challenging from a logistic point of view. *In situ* access is often impossible for the high risk of ice and rock falls (Dematteis et al., 2021). In alpine regions, applications based on *in situ* sensors (e.g., reflective prisms, GNSS receivers) exist (Huss et al., 2007; Sugiyama et al., 2007; Dematteis et al., 2021), but proximal remote sensing techniques are more commonly adopted, such as digital image correlation (DIC) (Evans, 2000; Ahn and Box, 2010; Messerli and Grinsted, 2015; Schwalbe and Maas, 2017).

On the other hand, estimating potentially unstable sector extension requires precise knowledge of the glacier morphology. The occurrence of surface discontinuities (e.g., transversal crevasses) or the presence of specific geometries (e.g., hanging glaciers) (Pralong and Funk, 2006) are potential destabilizing elements. However, the morphology of dangerous glaciers often evolves rapidly, as they feature high dynamics. In these cases, updated knowledge of the glacier morphology is essential. This datum can be achieved through the production of digital elevation models (DEMs) using structure from motion (SfM) conducted using drones (Ryan et al., 2015; Fugazza et al., 2018), helicopter (Girod et al., 2017), or ground-based manual acquisitions (Piermattei et al., 2015; Piermattei et al., 2016; Fugazza et al., 2018). Furthermore, SfM provides orthoimages too, which help data interpretation.

While there are various solutions for monitoring glacier surface morphodynamics, acquiring glacier thickness is more complicated. Accurate ice thickness information is crucial for managing glacial hazards, as avalanche run-out simulations rely on knowing the ice volume involved (Margreth et al., 2011). Ground-penetrating radar (GPR) and Radio Echo Sounding (RES) are common methods for measuring ice thickness (Plewes and Hubbard, 2001). On mountain glaciers, such surveys are challenging due to the scattering of the electromagnetic waves caused by debris, crevasses and reflections by mountain side walls (Dowdeswell et al., 1984; Forte et al., 2019) and increased signal attenuation caused by liquid water presence in temperate ice (Watts and England, 1976). Moreover, individual glacier sectors can be too dangerous for ground-based surveying. In these complex sectors, airborne techniques are the only possible solution (Urbini et al., 2017). Helicopter-borne GPR and RES surveys were successfully conducted in the last decades in the European Alps (Urbini et al., 2017) and in Patagonia (Blindow et al., 2012).

Besides the ice thickness, GPR and RES also provide bedrock topography description, which influences glacier hydrology (Grabiec et al., 2012). Furthermore, bedrock topography is a necessary constraint for developing numerical glacier-flow and rheological models (Faillettaz et al., 2012; Zorzut et al., 2020). It is well known that bedrock geometry determines glacier surface morphology (Paterson, 1994). Glacier surface and bedrock slope are related, even though their steepness can differ by several degrees (Grabiec et al., 2012); bedrock depressions usually yield bowl-shaped glaciers (Urbini et al., 2017); while crevasses often occur in correspondence with bedrock discontinuities, like drumlins (Lamsters et al., 2016) or bedrock steps (Jiskoot et al., 2017), because they induce strong strain rates (Vaughan, 1993). In polar regions, bedrock-glacier morphology relationship has been observed (Beitzel, 1970; Budd and Carter, 1971; Grabiec et al., 2012; Lamsters et al., 2016) and modelled (Budd, 1970; Jiskoot et al., 2017) due to easier GPR/RES surveying. On the contrary, quantitative evidence of bedrock-glacier morphology relationship in mountain glaciers is rarer (Urbini et al., 2017), even though it is often assumed to be known.

In this paper, we show evidence of the direct influence of bedrock geometry on glacier surface morphodynamics at the Planpincieux Glacier (North-west Italy). In particular, we focused on the Montitaz Lobe because its potential collapse would seriously threaten the Planpincieux village at the bottom of the Ferret Valley (Schweizer and Margreth, 2020). We conducted a GPR survey to assess bedrock topography and ice thickness along linear transects. Using SfM, we produced dense temporal series of DEMs and orthoimages since 2014, allowing us to evaluate the evolution of glacier morphology. Finally, we measured the glacier kinematics using DIC applied to daily oblique images. The contribution of our research is twofold: first, we illustrate how the bedrock topography exerts a strong forcing on glacier morphology, which in turn affects the glacier kinematics. Consequently, the bedrock geometry appears as a primary cause of glacier instabilities. Second, we show that frequent morphodynamics monitoring is crucial for assessing and managing glacial hazards.

2 STUDY AREA

The Planpincieux Glacier (6.97°E, 45.85°N; WGI # IT4L01517018) is a temperate alpine glacier with an area of about 1 km^2 located on the Italian side of the Grandes Jorasses (**Figure 1**). The Planpincieux Glacier faces towards Ferret Valley, located in the Courmayeur municipality. It ranges between 2,680 and 3,680 m a.s.l, with an average southeast aspect. Two small cirques form the accumulation area. They merge in a bowl-shaped central plateau at 2,900 m a.s.l, the snow line position lies at this altitude. The ablation area is composed of two lobes of a similar extent (approximately 0.1 km^2): the Margueraz Lobe is relatively gentle and presents large splaying crevasses. The Montitaz Lobe is a steep (>30°) icefall with transverse crevasses and seracs. Usually, the snow cover at the glacier snout remains up to late June/late July, depending on the year. The Montitaz terminus is 20–30 m-high and hangs over a bedrock step that causes frequent calving (Giordan et al., 2020). Thickness estimations performed with the GlabTop model (Linsbauer et al., 2012) provided an average thickness

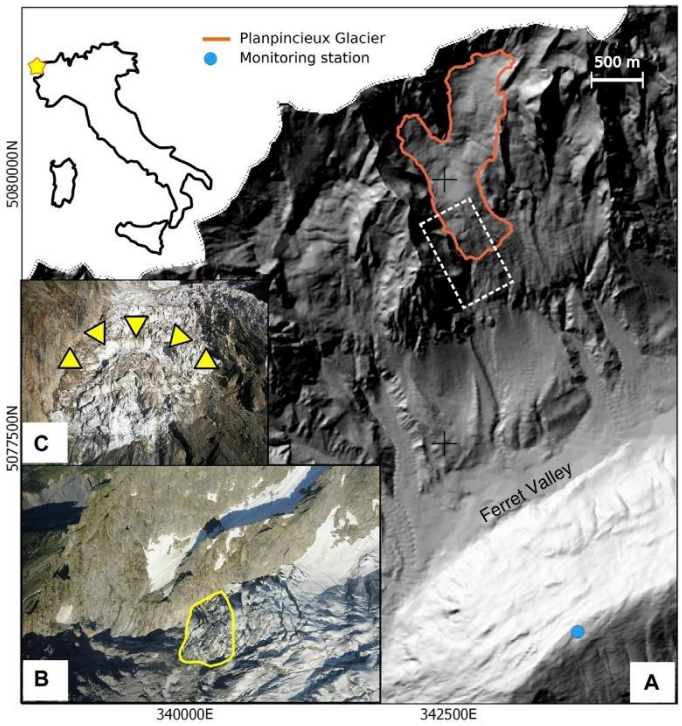

FIGURE 1 | (A) Overview of the study area, located in North-west Italy. The Planpincieux Glacier outlines are of 2019. The dashed white rectangle denotes approximately the portion shown in panel b. **(B)** Aerial view of the Montitaz Lobe in July 2020. The unstable portion is delimited in yellow. **(C)** Frontal view of the Montitaz Lobe's terminus in October 2019. Yellow triangles indicate the wide transversal crevasse above the unstable portion.

of the plateau and ablation area of 35.1 ± 18.2 m and 19.4 ± 13.8 m, respectively (Morra Di Cella, 2019).

No mass balance measurements of the Planpincieux Glacier are available. However, mass balance data are available for the nearby Toula and Petit Grapillon glaciers, located 4 and 9 km away, respectively, which have similar aspects and elevations to the Planpincieux Glacier. The mass balance of both glaciers was positive in 2012/2013 and 2013/2014 (+0.2 to +0.5 m water equivalent) and negative in the subsequent years up to 2020 (Giordan et al., 2020).

2.1 Past Planpincieux Glacier Instabilities

In the past century, break-offs and floods from the Montitaz Lobe occurred and, on a few occasions, the bridge of the Montitaz Torrent was damaged (Giordan et al., 2020). In such cases, the involved ice volume was unknown. In late August 2017, a 60′000 m^3 ice chunk detached from the Montitaz Lobe, and the ice avalanche stopped 800 m upstream of the bridge of the Montitaz Torrent. In the summers of 2019 and 2020, a wide transversal crevasse isolated two portions of the Montitaz Lobe from the main glacier body (**Figures 1B,C**), which began to accelerate rapidly (Sevestre, 2020). Estimated volumes were 250′000 and 500′000 m^3, respectively, based on 2012-dated GPR measurements and experts' image analysis. However, with the available information, the degree of uncertainty of the volume estimation was high (Giordan et al., 2020). Considering past events and their effects on the valley bottom, ice avalanche run-out simulations were conducted in 2013 and 2020 by the SLF of Davos with different hypothetical volumes involved. These simulations showed that volumes greater than 250′000 m^3 would reach the underlying Planpincieux hamlet, potentially damaging buildings and the valley's access road (Schweizer and Margreth, 2020).

3 DATASET AND METHODS

In this study, we adopted various apparatuses and approaches to investigate glacier morphodynamics and its evolution in the period 2014-2020. We analyzed 7 years of surface kinematics, repeated orthoimages and DEMs and updated glacier thickness measurements. Digital terrain analysis allowed the identification of crevasses and terminus positions throughout the years. GPR

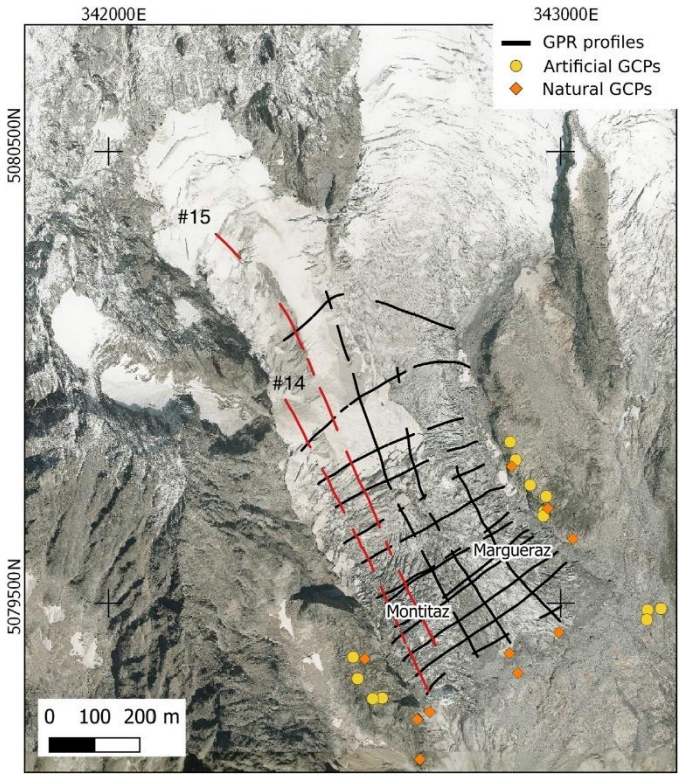

FIGURE 2 | GPR profiles acquired on 7 July 2020 at the Planpincieux glacier (black lines). The two westernmost longitudinal profiles (in red in the colored version) are n. 14 and 15. The colored dots indicate the ground control points (GCPs).

data provided ice thickness and bedrock topography along linear transects.

3.1 GPR Surveying

Usually, helicopter-borne GPR presents technical problems due to the need to acquire the position of antennas and the lack of direct contact between antennas and glacier, causing power losses due to reflection at the ice surface. In theory, it is ideal to fly with the antennas as close as possible to the glacier surface to avoid spreading losses (Forte et al., 2019). In practice, however, the distance to the ground varies within short distances along the flight trajectory, typically by around ±20 m (Grab et al., 2021). For security reasons, thus, it is advisable to aim for a target height of around 30 m.

On 7 July 2020, we conducted a helicopter-borne GPR survey of the Planpincieux Glacier with the dual-polarization Airborne Ice Radar from ETH Zürich (AIR-ETH) (Langhammer et al., 2019). This platform is equipped with two orthogonal pairs of 25 MHz antennas in broadside configuration and the SPIDAR multi channel recording unit from Sensors and Software. The two antenna pairs alternatingly recorded eight traces per second each. The positioning of the platform was conducted with three differential GNSS antennas, in order to deduce not only the position but also the pitch, roll and yaw angles. With a laser altimeter, the distance to the ground was measured to provide this information for navigation purposes and as input for the data processing. Navigation, recording, and processing of GNSS and laser altimeter data were conducted by GEOSATSA, a Swiss-based surveying company. In total, we acquired 13 cross profiles and five longitudinal profiles with a total length of about 12 km. The parts of the profile layout for which bedrock reflections have been detected are displayed in **Figure 2**. Compared to a GPR survey conducted in 2012, this layout is denser and more regular, especially at the terminus of the Montitaz Lobe.

In an initial step, the GPR traces were georeferenced. The GPR data were then processed with the software toolbox GPRglaz (Grab et al., 2018). The AIR-ETH system offers recording with two orthogonal (dual-polarization) pairs of 25 MHz dipole antennas. Therefore, GPR data from two channels, one parallel and one perpendicular to the flight direction, were available for

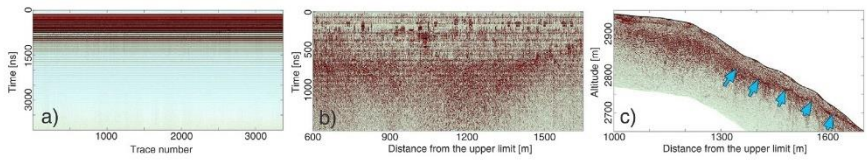

FIGURE 3 | Effects of some processing steps shown on a portion of profile n. 14. **(A)** Raw data; **(B)** after trace binning; **(C)** after Kirchhoff migration. The blue arrows in the bottom panel indicate reflections from the bedrock.

data processing. The processing procedure included the following processing steps:

- signal dewowing using PulsEKKO software;
- time-zero correction based on the arrival time of the direct wave;
- amplitude interpolation and ringing removal as detailed in Grab et al. (2018);
- picking of surface reflection using laser altimeter or manually picking, depending on the data quality;
- band-pass filtering between 10 and 75 MHz;
- trace binning to obtain a regular sampling of 0.5 m;
- image focusing (migration) using a half-space model with air and ice velocities of 0.3 m ns^{-1} (Reynolds, 1997) and 0.168 m ns^{-1} (Glen and Paren, 1975), respectively;
- manual identification of bedrock reflections.

Glacier ice at the Planpincieux Glacier altitudes is typically temperate in the European Alps. In particular, in the Mont Blanc region, Suter and Hoelzle (2002) observed the presence of cold firn at elevations higher than 3,500 m a.s.l. A propagation velocity of 0.168 m ns^{-1} was measured in the temperate Rhone Glacier (European Alps) (Church et al., 2020), adopting the common midpoint (CMP) method. Accordingly, we used this value to process the GPR data.

The effects of selected processing steps are documented in **Figure 3** using portions of profile n. 14 (location displayed in red in **Figure 2**). Since data quality is dependent on antenna orientation in combination with glacier bed topography, the identification of bedrock reflections (blue arrows in **Figure 3C**) was performed on the image from the antenna pair that provided better data quality.

As the last step, the ice thicknesses, measured along the profiles, were interpolated using the Matlab built-in thin-plate smoothing spline (TPSS) (Duchon, 1977). From geomorphological analysis, it was evident that the ice thickness at the margins assumed non-zero values, because vertical bedrock outcrops bounded the glacier, but a precise value was unknown. Therefore, manually-imposed thickness boundary constraints on the lateral margins would have suffered subjective uncertainty. Furthermore, most parts of the terminus presented vertical 10–30 m-high ice walls. To solve this issue, we adopted the following method. First, we randomly selected 1,500 bedrock and glacier surface elevation points from the GPR data and 500 elevation points outside the glacier from a DEM. Secondly, we interpolated with TPSS bedrock and surface points along with DEM points. Thereby, we obtained two surfaces that were interpolated using nodes located at the same positions; one representing the bedrock topography, the other representing the glacier surface in continuity with the bedrock outside the glacier. Therefore, the values of both surfaces in the bedrock area were the same, while their difference in the glacier area corresponded to the ice thickness. Since potential errors at the boundaries due to complex geometries were almost the same, because they were produced by identical interpolation, they should approximately compensate.

3.1.1 Ice Thickness Uncertainty

The ice thickness uncertainty is composed of two independent contributions. First, the uncertainty of the GPR measurement and, second, the uncertainty pertaining to the spatial interpolation. The first contribution is easier to evaluate and can be derived theoretically. The uncertainty of the glacier bedrock topography and the corresponding ice thickness is due to a combination of uncertainties in GPR wave velocity and the detection of bedrock reflections in the profile images.

The GPR wave velocity in temperate ice has been estimated to be 0.168 m ns^{-1} (Glen and Paren, 1975) and we used uncertainty of $\sigma_v = \pm 0.005$ m ns^{-1}. This is slightly smaller than the uncertainty of ± 0.008 m ns^{-1} assumed by Lapazaran et al. (2016), as they applied it to polythermal ice. This uncertainty could be further reduced by measuring the propagation velocity on-site by conducting CMP measurements (Bradford and Harper, 2005) or by analyzing the shape of diffraction hyperbolas in the GPR data (Karušs et al., 2022). This was not possible in our case, because CMP measurements have to be conducted on the ground, whereas no clean diffraction hyperbolas were present in our data.

The uncertainty in detecting the bedrock reflection comprises a limited vertical resolution of half a wavelength (Lapazaran et al., 2016), σ_r, and an estimated uncertainty of 15% of the ice thickness (Lapazaran et al., 2016) because we neglected the third dimension during image focusing by 2D migration, σ_m. Furthermore, an uncertainty of $\sigma_p = \pm 5$ m was assumed for manually picking bedrock reflection. Combining these uncertainty contributions by the root-square-sum, presuming them to be independent (Lapazaran et al., 2016), leads to uncertainty

$$\sigma_{gpr} = \sqrt{\sigma_v^2 + \sigma_r^2 + \sigma_m^2 + \sigma_p^2} \quad (1)$$

TABLE 1 | DEMs and orthoimages used in this study.

Date of acquisition	Data product	Technique	Resolution	Error ellipsoid (xy/Z)	# Images	# GCPs	# tie points
9 June 2014	Orthoimage	Phot. camera	0.08 m px^{-1}				
	DEM	LiDAR	0.5 m px^{-1}				
26 August 2015	Orthoimage	Phot. camera	0.2 m px^{-1}				
22 September 2017	Orthoimage	SfM	0.18 m px^{-1}	0.19/0.24 m	11	9	10′708
	DEM		0.18 m px^{-1}				
20 October 2018	Orthoimage	SfM	0.18 m px^{-1}	0.37/0.05 m	32	8	25′872
	DEM		0.37 m px^{-1}				
1 October 2019	Orthoimage	SfM	0.09 m px^{-1}	0.36/0.28 m	112	6	36′500
	DEM		0.34 m px^{-1}				
20 July 2020	Orthoimage	SfM	0.12 m px^{-1}	0.07/0.05 m	120	13	35′728
	DEM		0.46 m px^{-1}				
8 September 2020	Orthoimage	SfM	0.08 m px^{-1}	0.06/0.04 m	210	13	79′537
	DEM		0.15 m px^{-1}				

The second source of error is more difficult to quantify and can yield larger effects on the estimation of ice thickness. The internal glacier structure of the glacier, including crevasses, as well as the bedrock topography, can cause unpredictable errors. We estimated the interpolation uncertainty with cross-validation (Cressie, 1992): we compared the subset of GPR data not adopted to interpolate with the corresponding values obtained from interpolation. We assumed the standard deviation of the difference as the interpolation uncertainty, σ_i. Therefore, the global thickness uncertainty is the root square sum of five independent contributions: 1) manual picking (±5 m), 2) half wavelength (±3.4 m) (from Lapazaran et al., 2016), 3) ±15% thickness (general uncertainty from Laparazan et al., 2016), 4) ± 3% thickness (signal velocity) and 5) ±2.8 m (interpolation).

Additionally, we analyzed whether σ_i is related to the thickness or the distance of the nearest point adopted for the interpolation, as done by Farinotti et al. (2014).

3.2 DEMs and Orthoimages

Since 2014, a dense series of DEMs and orthoimages of the Planpincieux Glacier has been acquired.

- On 9 June 2014, we conducted a helicopter-borne survey that provided a high-resolution DEM, which we resampled at 0.5 m px^{-1}, using a LiDAR (RIEGL LSM-Q680i) and an orthoimage with a ground sampling distance (GSD) of 0.08 m px^{-1}, acquired with a medium-size photogrammetric Hasselblad H3DIIi camera (Giordan et al., 2020).
- On 26 August 2015, the Valle d'Aosta Region provided a 0.2 m px^{-1} orthoimage acquired during a photogrammetric survey of the whole region. This datum has not yet been validated by the Valle d'Aosta Region.
- On 22 September 2017, 20 October 2018, 1 October 2019, 20 July and 8 September 2020, we conducted helicopter-borne digital photogrammetry measurements using a Nikon 700D camera with a fixed 24-mm lens focal length, which yielded high-resolution DEMs and orthoimages. In 2019 and 2020, we acquired 45°-oblique orthomosaics along seven parallel stripes at a flying height of 250–300 m. The shooting interval was 1 s, and the image overlapping was 40%–60% (between stripes) and 80%–90% (along stripes). The 2017 and 2018 flights were not planned for photogrammetric surveys.

All the above-mentioned data concern the Montitaz and Margueraz lobes, except for the 2015 orthoimage, which covers the entire glacier. **Table 1** reports the list of DEMs and orthoimages adopted in the present study.

In July 2020, alpine guides installed a network of 13 artificial GCPs homogeneously distributed around the glacier (**Figure 2**), whose positions were measured using real-time kinematic (RTK) positioning. We used the updated GCP network to process 2020 and older datasets using SfM (Mertes et al., 2017; Lewińska et al., 2021) by Agisoft PhotoScan software. Using the 2020 orthoimage as a reference, we identified additional natural GCPs that could be recognized in previous orthoimages (**Figure 2**).

We analyzed the historical sequence of DEMs and orthoimages to assess 1) the morphological evolution of the Montitaz Lobe and 2) the position of fractures of the Montitaz Lobe. To the former aim, we calculated the area and volume of the frontal sector using all the available DEMs (**Table 1**).

To analyze the fractures' location, we first identified the position of the major recurrent transversal crevasses of the Montitaz Lobe in the period 2014-2020. To this aim, we visually analyzed orthoimages, shaded reliefs and slope gradient maps produced with the available DEMs. We observed that these crevasses appeared every year in approximately the same position. To quantify the spatial variability of every crevasse across the years, we adopted the following approach: we examined the various positions of a specific crevasse every year, which formed a spatial cluster. Subsequently, we considered five well-distributed transects that intercept such a cluster; thereby, we obtained five groups (one group for every transect) of intercept points (one point for every considered year). Finally, we calculated the planimetric distance of every intercept point with respect to the group centroid and assumed the median deviation among all the planimetric distances as the spatial variability of the crevasse's position.

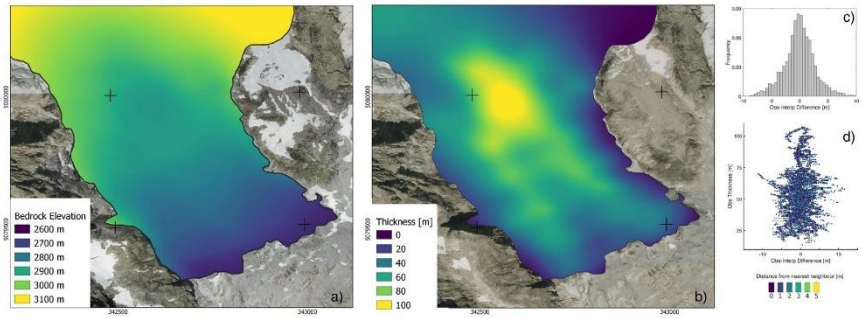

FIGURE 4 | (A,B) Bedrock elevation and glacier thickness, respectively, obtained from the interpolation of the GPR profiles acquired on 7 July 2020. **(C)** Frequency distribution of the difference between GPR thickness measurement and interpolated values. **(D)** Measured and interpolated thickness difference vs. measured thickness, the color denotes the distance from the nearest interpolating point.

3.3 Relationship Between Bedrock Geometry and Glacier Surface Morphology

We compared the crevasses' positions with the bedrock topography to evaluate the relationship between bedrock and glacier morphology. To this end, we considered the GPR profiles n. 14 and 15, which lie longitudinally onto the Montitaz Lobe (**Figure 2**). We analyzed the bedrock profile obtained with the GPR and the corresponding glacier surface profiles across the years obtained with the available DEMs. Since the elevation profiles present a general parabolic shape, to maintain only the surface-undulation-related information, we subtracted the quadratic fit of every elevation profile; then, we interpolated the undulations with a sine function.

3.4 Daily Glacier Surface Kinematics Based on Digital Image Correlation

Since August 2013, two permanent monoscopic time-lapse cameras (TLCs) have continuously monitored the surface kinematics of the Planpincieux Glacier (Dematteis et al., 2021), acquiring hourly images. They are equipped with lenses of different focal lengths to observe the glacier with diverse detail. One TLC (297 mm lens focal length) targets the Montitaz Lobe, with a GSD of approximately 0.05 m px^{-1}, while the second TLC (120 mm lens focal length) observes all the ablation area (GSD ~0.15 m px^{-1}) and part of the upper cirques (GSD ~0.20 m px^{-1}).

We analyzed the daily temporal sequence of terrestrial oblique images adopting the DIC technique, which has been used in various glaciological studies since 2000 (Evans, 2000; Ahn and Box, 2010; Messerli and Grinsted, 2015; Schwalbe and Maas, 2017). In principle, DIC is applied to a couple of registered images acquired at different times; a patch of the master image is searched for in the slave image, calculating a similarity index in every position within an interrogation area (Dematteis and Giordan, 2021). The position where the maximum similarity is found corresponds to the displacement of the patch. DIC's outcomes are spatially distributed planar vectors lying on the image plane. We adopted the Local Adaptive Multiscale image Matching Algorithm (Dematteis et al., 2022) for the DIC processing.

4 RESULTS

4.1 Glacier Ice Thickness and Bedrock Topography

Interpolated bedrock elevation and ice thickness distribution are displayed in **Figures 4A,B**. Thickness varies between 10 and 100 m over the entire glacier, and between 20 and 60 m in the Montitaz Lobe. The difference between interpolated thickness values with the GPR measurements not used in the interpolation process is shown in **Figure 4C**, it does not appear to be correlated with the thickness value and the distance to the nearest interpolating point neither (**Figure 4D**). On average, the interpolation mean difference compared with GPR measurements is < 0.1 m, while the standard deviation is σ_i = 2.8 m. Considering also the uncertainty pertaining to the GPR measurement, the estimated total error of the glacier thickness increases with depth, ranging from ±6.6 m to ±10.3 m for thicknesses of 10 and 50 m, respectively.

4.2 Crevasse Identification and Morphology Evolution of the Unstable Sector

In the considered period, we identified three main crevasses in the Montitaz Lobe that open at approximately the same location every year, while they completely close during the winter by snow filling and the motion of the upper part of the glacier. The fractures delimit distinct morphological sectors (from the terminus A-D). The planimetric deviation of the different positions throughout the years was 13.7, 5.9, and 8.7 m, respectively, for the fractures between sectors AB, BC and CD (**Figure 5**).

During the warm season, the Montitaz Lobe terminus presents high strain rates and the development of transversal crevasses that

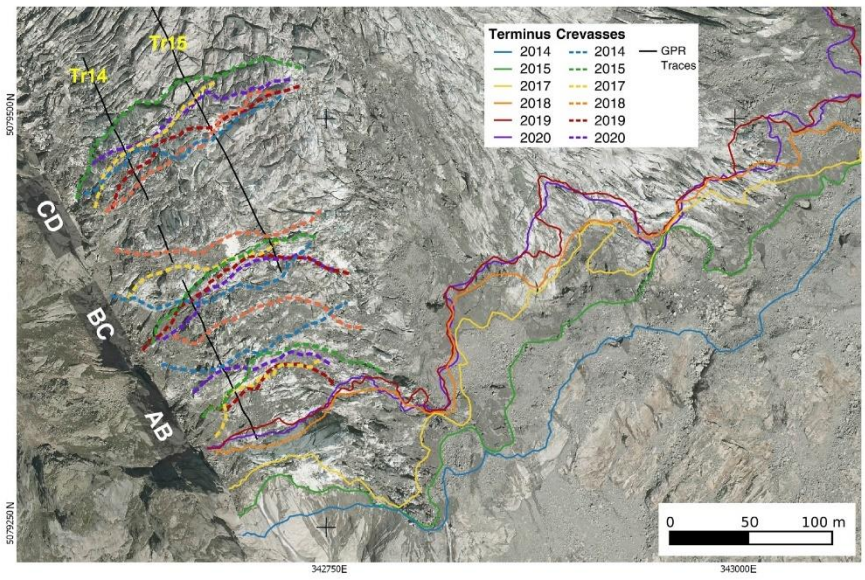

FIGURE 5 | Positions of the major crevasses and termini since 2014 are indicated by dashed and solid colored lines, respectively. The solid black line refers to GPR profiles n. 14 and 15. The grey boxes showed the locations of the sectors' limits.

TABLE 2 | Morphological evolution of the unstable sector of the Montitaz lobe (n.a. = not available).

Dates	Mean thickness	Planimetric area	Volume [× 10^3]
9 June 2014	30.8 ± 8.7 m	23′375 m^2	832 ± 234 m^3
26 August 2015	n.a	22′770 m^2	n.a
22 September 2017	23.1 ± 7.7 m	20′950 m^2	559 ± 185 m^3
20 October 2018	25.6 ± 8.2 m	18′900 m^2	559 ± 178 m^3
1 October 2019	24.1 ± 7.9 m	12′325 m^2	343 ± 112 m^3
20 July 2020	28. 3 ± 8.3 m	14′025 m^2	458 ± 135 m^3
8 September 2020	22.7 ± 7.6 m	12′125 m^2	318 ± 107 m^3

could potentially lead to the detachment of a large ice chunk (**Figures 1B,C**). Such a crevasse corresponds to the BC limit. Usually, an intense calving activity causes the disaggregation of this sector into relatively small fragments (Giordan et al., 2020). In **Table 2** and **Figure 6**, we present the size evolution of this unstable glacier sector. The areal extension was obtained by manual delineation on the orthoimages, while the volume was calculated using the available DEMs.

4.3 Bedrock Topography Relation With Glacier Surface Morphology

We compared the glacier surface and bedrock topography along GPR profiles n. 14 and n. 15 (**Figure 7**). A series of knee-shaped bedrock discontinuities are evident. On average, the bedrock slope of profiles n. 14 and n. 15 is 25° and 20°, respectively, and it increases by approximately 20° in correspondence to the bedrock knees. Note that the position of the major fractures corresponds well with that of the bedrock knees. Such spatial correspondence is also highlighted by the analysis presented in **Figure 8**. There, we show the detrended profiles of bedrock and glacier surface. A series of approximately regular undulations is evident. The glacier surface undulations along profile n. 14 have an amplitude between 7 and 10 m on average (**Figures 8A–F**), while along profile n. 15, the amplitude is approximately 5 m (**Figures 8G–L**). Conversely, bedrock undulations are lower, with an amplitude of 4 and 2 m (profiles n. 14 and 15, respectively). The period of the undulations is approximately 95 m and is constant for all the profiles except for the bedrock undulations of profile n. 15, where the period is 60 m. Compared with the bedrock, the glacier profiles along profile n. 14 are out of phase by 145° ± 30° (mean ± standard deviation), which corresponds to 40 ± 8 m, except in 2018, which is exactly in phase. Concerning profile n. 15, profiles 2017, 2018, 2019, and 2020 are approximately in phase. On average, the cross-correlation coefficient between bedrock and surface undulations is 0.52 ± 0.04 and 0.46 ± 0.12 for profiles n. 14 and 15, respectively.

4.4 Surface Glacier Kinematics

DIC outcomes provided the ice flow vectors on the image plane. Since 2014, the results show that the Montitaz and Margueraz lobes are substantially inactive in the cold season, while they reactivate during the warm season reaching maximum daily

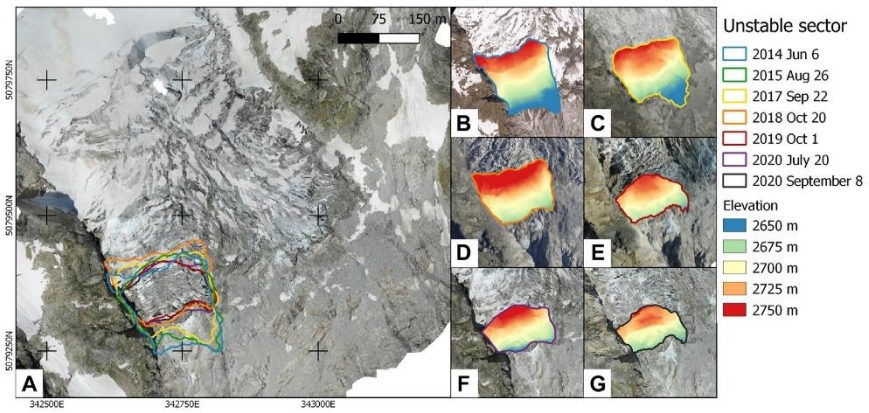

FIGURE 6 | (A) Limits of the unstable portion of the Montitaz Lobe in the years 2014–2020. Background, orthophotos of 20 July 2020. **(B–G)** Surface elevation of the unstable sector obtained with every available DEM. The orthoimages of each panel have been acquired in the same date of the corresponding DEM.

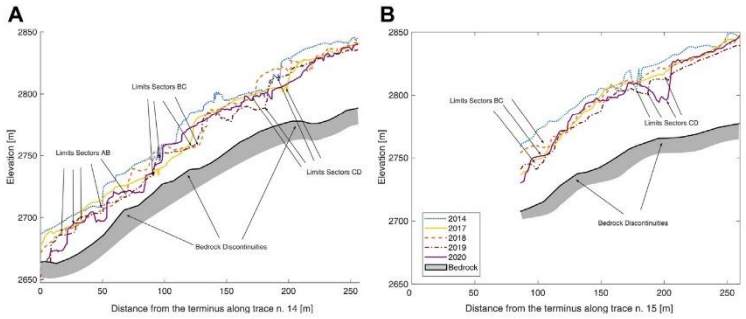

FIGURE 7 | Correspondence between bedrock discontinuities and glacier surface recurrent fractures between 2014 and 2020. The longitudinal sections are taken in correspondence of GPR profiles n. 14 **(A)** and 15 **(B)**.

displacement in August. The Montitaz Lobe moves faster, with maximum values in the frontal sector up to more than 2 m day^{-1}, while the maximum Margueraz flow is approximately 0.5 m day^{-1}. Such measurements have centimeter uncertainty (Dematteis et al., 2018). The kinematic surface pattern of the Montitaz Lobe presents four distinct kinematic domains–A, B, C and D–from the bottom to the top of the Lobe (**Figure 9A**), which correspond to the morphological sectors bounded by the crevasses shown in **Figure 5**. The motion rates increase toward the terminus, and, in the frontal domain (i.e., the A domain), the surface velocity is related to the occurrence of break-offs (Giordan et al., 2020). Between 2014 and 2018, the domains became distinguishable approximately from July. Contrarily, in 2019 and 2020, the A and B sectors accelerated with identical velocity until the beginning of September (**Figure 9B**) and there was a severe risk of an avalanche event (Magra, 2019; BBC, 2020).

5 DISCUSSION

5.1 Glacier Thickness Evolution

The measured ice thickness partially agrees with that inferred by visual investigation and monoscopic photogrammetry in the past years (Giordan et al., 2020). The GPR results also provided the representation of the bedrock topography, which can be used as a benchmark to estimate past ice thicknesses by calculating the difference with older DEMs.

We observed a general decreasing volume trend of the most unstable portion of the Montitaz Lobe, mostly due to the terminus retreat. The volumes in 2017 and 2018 were approximately 500′000 m^3, which agreed with the values estimated by Giordan et al. (2020) and Schweizer and Margreth (2020), while the 2019 and 2020 volumes corresponded well with those estimated during the emergencies of these years (Sevestre, 2020). On the other

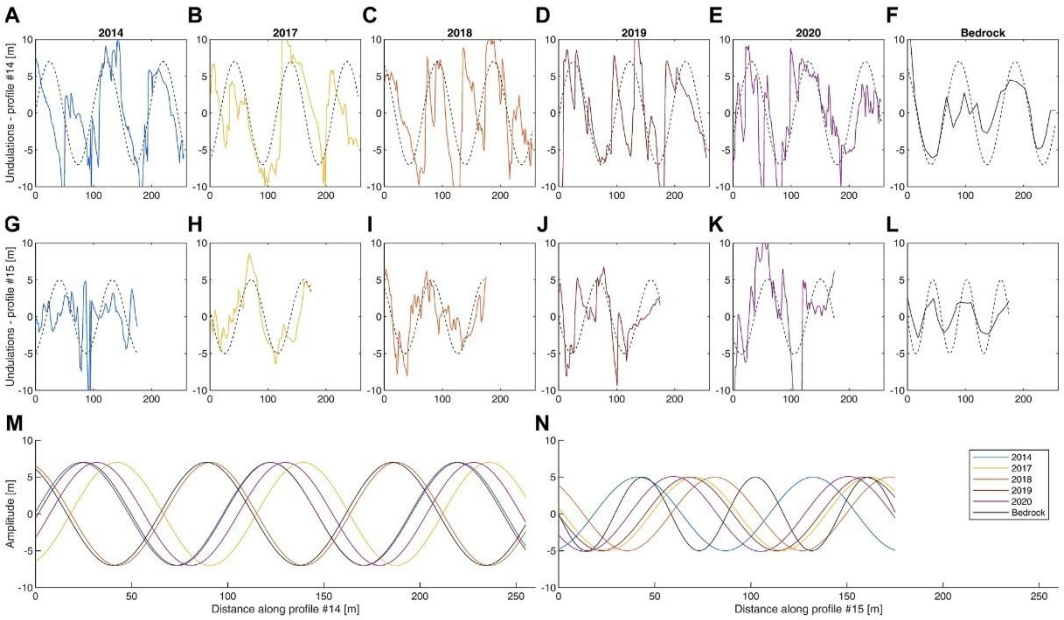

FIGURE 8 | Bedrock and glacier surface undulations obtained by subtracting a quadratic fit from the elevation profiles. **(A–E)** and **(G–K)** Surface undulations along profiles n. 14 and 15, respectively, in 2014, 2017, 2018, 2019 and 2020; **(F–L)** bedrock undulations along profiles n. 14 and 15. The dashed black line is the interpolating sine function. **(M,N)** Interpolating sin function of every undulation curve for profiles n. 14 and 15, respectively.

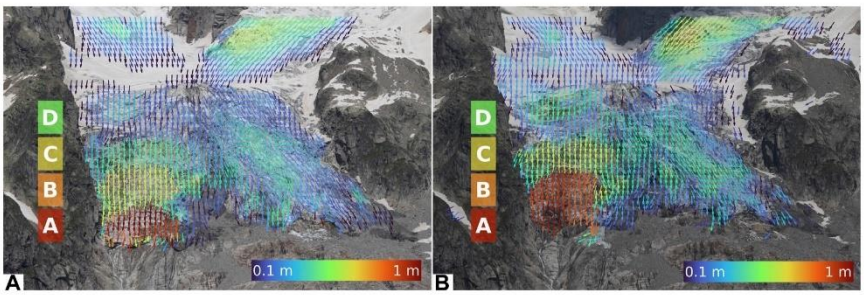

FIGURE 9 | (A) Daily surface displacement between 7 and 14 August 2016. The map evidences the presence of four distinct kinematic domains in the Montitaz Lobe, with displacement rates increasing toward the terminus. **(B)** Daily surface displacement between 29 and 1 August 2020. The kinematic domains "A" and "B" are merged and move with similar velocity.

hand, we did not observe evident ice thinning of this portion, observing thickness values between 22.7 ± 7.6 m and 25.6 ± 8.2 m in September and October. However, statistically significative thickness variation assessment requires longer periods to determine potential mass variation (Wang et al., 2014). Contrarily, we registered a significant seasonal change, probably due to seasonal snow melting mainly: the thickness variation between 20 July and 8 September 2020 was approximately 6 m (**Figures 6F,G**), which is greater than the interannual thickness change, and corresponds to a volume decrease >30%.

This finding has a relevant impact on glacial hazard assessment and management, as it shows that the potentially unstable mass can significantly vary during the season; therefore,

repeated DEM acquisitions during a single season are required to evaluate volume changes correctly. Ice thickness in 2014 (30.8 m) was acquired in June and was comparable with that measured on 20 July 2020 (28.3 m). Assuming a thinning of 6 m between July and September 2014 (i.e., which is the same thinning observed between 20 July and 8 September 2020), the volume of the unstable portion would be approximately 650′000 m^3, which agrees with the volumes observed in 2017 and 2018 (**Table 2**).

5.2 Relationship Between Bedrock Topography and Glacier Morphodynamics

We observed a limited spatial variability of the crevasses' locations during the considered period. The recurrent positions indicate a strong influence of bedrock topography on glacier surface morphology, which is appreciable by comparing the longitudinal glacier and bedrock sections along GPR profiles.

Additionally, we observed that bedrock and glacier undulations follow approximately a sinusoidal behavior, with similar amplitude and period in both profiles n. 14 and 15. Even though this is valid in general, in a few cases, the shape of the undulations does not appear as a regular sinusoid (e.g., **Figures 8C–G**). Along profile n. 14, on average, glacier undulations are out of phase by 145° with respect to the bedrock, except in 2018. This means that the ice is thinner where the bedrock is steeper and the crevasses are downstream of the bedrock knees (Paterson, 1994). Similar behavior was modelled (Budd, 1970) and observed (Beitzel, 1970; Budd and Carter, 1971) in Antarctica. There, surface undulations were caused by bedrock undulations with periods three to five times the ice thickness; accordingly, in the Montitaz Lobe, ice thickness and undulation periods are approximately 35 and 95 m, respectively, along profile n. 14 (**Figure 8M**). On the other hand, we did not observe a similar behavior along profile n. 15. The amplitude of the bedrock fluctuations (~2 m) is likely too small compared with the ice thickness (~50 m). Interestingly, the surface undulations' period is the same as that observed along profile n. 14. Contrary to the findings of Remy and Tabacco (2000), the amplitude of the surface undulations is larger than that of bedrock. This means that the effects of bedrock discontinuities are amplified on the glacier surface morphology, in particular on the development of crevasses.

The surface displacement pattern evidences the presence of various kinematic domains whose limits correspond with the morphological sectors delimited by the transversal fractures. This observation demonstrates the strong bedrock influence on glacier morphodynamics. This finding will help in the analysis of glacial risk assessment to evaluate potentially unstable sector extension, especially in contexts where bedrock topography is unknown, but surface displacement is available.

6 CONCLUSION

In this work, we adopted GPR measurements, aerial and terrestrial digital images, which provided bedrock topography and ice thickness, DEM (using SfM processing) and ice flow rates (using DIC processing), respectively, in the mountain Planpincieux Glacier (North-west Italy). We measured the maximum glacier thickness of 100 m in the central plateau and 60 m in the Montitaz Lobe. Our research directly shows the strong relationship between bedrock geometry and glacier surface morphodynamics. In particular, we illustrate that a series of bedrock steps causes the development of large crevasses, whose recurrent position is approximately 40 m downstream of the bedrock steps' positions.

Additionally, we present the morphological evolution of a large unstable sector on the Montitaz Lobe, which has not significantly thinned across the considered period. However, due to terminus retreat, this sector approximately halved its volume. Conversely, we registered substantial thinning during the 2020 warm season, which caused a volume loss of ~30% between 20 July and 8 September 2020.

Further GPR campaigns can be adopted to validate 2020 results and increase its spatial resolution; in particular, more detailed bedrock discontinuities and information about the potential presence of water at the bedrock-ice interface are two presently missing important factors, which will provide further support for glacial risk assessment. The bedrock topography provided by the GPR can be used as a benchmark to obtain future and past volumes of specific sectors.

DATA AVAILABILITY STATEMENT

The raw data supporting the conclusions of this article will be made available by the authors, without undue reservation.

AUTHOR CONTRIBUTIONS

Conceptualization, ND and DG; methodology, MG; formal analysis, ND, FT, and MG; investigation ND, FT, and DG; data curation, FT and PP; writing—original draft preparation, ND, FT and MG; writing—review and editing, DG and HM; supervision, DG and HM. All authors have read and agreed to the published version of the manuscript.

REFERENCES

Ahn, Y., and Box, J. E. (2010). Glacier Velocities from Time-Lapse Photos: Technique Development and First Results from the Extreme Ice Survey (EIS) in Greenland. *J. Glaciol.* 56, 723–734. doi:10.3189/002214310793146313

Bbc, T. (2020). *Mont Blanc: Glacier Collapse Risk Forces Italy Alps Evacuation*. BBC News. Available at: https://www.bbc.com/news/world-europe-53692476.

Beitzel, J. E. (1970). The Relationship of Ice Thicknesses and Surface Slopes in Dronning Maud Land. *IAHS* 86, 191–203.

Beniston, M. (2012). Impacts of Climatic Change on Water and Associated Economic Activities in the Swiss Alps. *J. Hydrology* 412-413, 291–296. doi:10.1016/j.jhydrol.2010.06.046

Blindow, N., Salat, C., and Casassa, G. (2012). "Airborne GPR Sounding of Deep Temperate Glaciers-Examples from the Northern Patagonian Icefield," in 2012 14th International Conference on Ground Penetrating Radar, GPR, Shanghai, China, June 4–8, 2012, 664–669. doi:10.1109/icgpr.2012.6254945

Bradford, J. H., and Harper, J. T. (2005). Wave Field Migration as a Tool for Estimating Spatially Continuous Radar Velocity and Water Content in Glaciers. *Geophys. Res. Lett.* 32, 1–4. doi:10.1029/2004GL021770

Budd, W. F., and Carter, D. B. (1971). An Analysis of the Relation between the Surface and Bedrock Profiles of Ice Caps. *J. Glaciol.* 10, 197–209. doi:10.3189/s0022143000013174

Budd, W. F. (1970). Ice Flow over Bedrock Perturbations. *J. Glaciol.* 9, 29–48. doi:10.3189/s0022143000026770

Church, G., Grab, M., Schmelzbach, C., Bauder, A., and Maurer, H. (2020). Monitoring the Seasonal Changes of an Englacial Conduit Network Using Repeated Ground-Penetrating Radar Measurements. *Cryosphere* 14, 3269–3286. doi:10.5194/tc-14-3269-2020

Cormack, R. M., and Cressie, N. (1992). *Statistics for Spatial Data*. New York: Wiley, 1300. doi:10.2307/2532724

Dematteis, N., and Giordan, D. (2021). Comparison of Digital Image Correlation Methods and the Impact of Noise in Geoscience Applications. *Remote Sens.* 13, 327. doi:10.3390/rs13020327

Dematteis, N., Giordan, D., Crippa, B., and Monserrat, O. (2022). Fast Local Adaptive Multiscale Image Matching Algorithm for Remote Sensing Image Correlation. *Comput. Geosciences* 159, 104988. doi:10.1016/J.CAGEO.2021.104988

Dematteis, N., Giordan, D., Troilo, F., Wrzesniak, A., and Godone, D. (2021). Ten-Year Monitoring of the Grandes Jorasses Glaciers Kinematics. Limits, Potentialities, and Possible Applications of Different Monitoring Systems. *Remote Sens.* 13, 3005. doi:10.3390/rs13153005

Dematteis, N., Giordan, D., Zucca, F., Luzi, G., and Allasia, P. (2018). 4D Surface Kinematics Monitoring through Terrestrial Radar Interferometry and Image Cross-Correlation Coupling. *ISPRS J. Photogrammetry Remote Sens.* 142, 38–50. doi:10.1016/j.isprsjprs.2018.05.017

Dowdeswell, J. A., Drewry, D. J., Liestøl, O., and Orheim, O. (1984). Radio Echo-Sounding of Spitsbergen Glaciers: Problems in the Interpretation of Layer and Bottom Returns. *J. Glaciol.* 30, 16–21. doi:10.3189/s0022143000008431

Duchon, J. (1977). "Splines Minimizing Rotation-Invariant Semi-norms in Sobolev Spaces," in *Constructive Theory of Functions of Several Variables* (Berlin: Springer), 85–100. doi:10.1007/bfb0086566

Evans, A. N. (2000). Glacier Surface Motion Computation from Digital Image Sequences. *IEEE Trans. Geosci. Remote Sens.* 38, 1064–1072. doi:10.1109/36.841985

Faillettaz, J., Funk, M., and Sornette, D. (2011a). Icequakes Coupled with Surface Displacements for Predicting Glacier Break-Off. *J. Glaciol.* 57, 453–460. doi:10.3189/002214311796905668

Faillettaz, J., Funk, M., and Sornette, D. (2012). Instabilities on Alpine Temperate Glaciers: New Insights Arising from the Numerical Modelling of Allalingletscher (Valais, Switzerland). *Nat. Hazards Earth Syst. Sci.* 12, 2977–2991. doi:10.5194/nhess-12-2977-2012

Faillettaz, J., Funk, M., and Vagliasindi, M. (2016). Time Forecast of a Break-Off Event from a Hanging Glacier. *Cryosphere* 10, 1191–1200. doi:10.5194/tc-10-1191-2016

Faillettaz, J., Sornette, D., and Funk, M. (2011b). Numerical Modeling of a Gravity-Driven Instability of a Cold Hanging Glacier: Reanalysis of the 1895 Break-Off of Altelsgletscher, Switzerland. *J. Glaciol.* 57, 817–831. doi:10.3189/002214311798043852

Farinotti, D., King, E. C., Albrecht, A., Huss, M., and Gudmundsson, G. H. (2014). The Bedrock Topography of Starbuck Glacier, Antarctic Peninsula, as Determined by Radio-Echo Soundings and Flow Modeling. *Ann. Glaciol.* 55, 22–28. doi:10.3189/2014AoG67A025

Fischer, A., Olefs, M., and Abermann, J. (2011). Glaciers, Snow and Ski Tourism in Austria's Changing Climate. *Ann. Glaciol.* 52, 89–96. doi:10.3189/172756411797252338

Forte, E., Bondini, M. B., Bortoletto, A., Dossi, M., and Colucci, R. R. (2019). Pros and Cons in Helicopter-Borne GPR Data Acquisition on Rugged Mountainous Areas: Critical Analysis and Practical Guidelines. *Pure Appl. Geophys.* 176, 4533–4554. doi:10.1007/s00024-019-02196-2

Fugazza, D., Scaioni, M., Corti, M., D'Agata, C., Azzoni, R. S., Cernuschi, M., et al. (2018). Combination of UAV and Terrestrial Photogrammetry to Assess Rapid Glacier Evolution and Map Glacier Hazards. *Nat. Hazards Earth Syst. Sci.* 18, 1055–1071. doi:10.5194/nhess-18-1055-2018

Giordan, D., Dematteis, N., Allasia, P., and Motta, E. (2020). Classification and Kinematics of the Planpincieux Glacier Break-Offs Using Photographic Time-Lapse Analysis. *J. Glaciol.* 66, 188–202. doi:10.1017/jog.2019.99

Girod, L., Nuth, C., Kääb, A., Etzelmüller, B., and Kohler, J. (2017). Terrain Changes from Images Acquired on Opportunistic Flights by SfM Photogrammetry. *Cryosphere* 11, 827–840. doi:10.5194/tc-11-827-2017

Glen, J. W., and Paren, J. G. (1975). The Electrical Properties of Snow and Ice. *J. Glaciol.* 15, 15–38. doi:10.3189/s0022143000034249

Grab, M., Bauder, A., Ammann, F., Langhammer, L., Hellmann, S., Church, G. J., et al. (2018). "Ice volume estimates of Swiss glaciers using helicopter-borne GPR - An example from the Glacier de la Plaine Morte," in 2018 17th International Conference on Ground Penetrating Radar, GPR, Rapperswil, Switzerland, June 18–21, 2018. doi:10.1109/ICGPR.2018.8441613

Grab, M., Mattea, E., Bauder, A., Huss, M., Rabenstein, L., Hodel, E., et al. (2021). Ice Thickness Distribution of All Swiss Glaciers Based on Extended Ground-Penetrating Radar Data and Glaciological Modeling. *J. Glaciol.* 67, 1074–1092. doi:10.1017/jog.2021.55

Grabiec, M., Jania, J., Puczko, D., Kolondra, L., and Budzik, T. (2012). Surface and Bed Morphology of Hansbreen, a Tidewater Glacier in Spitsbergen. *Pol. Polar Res.* 33, 111–138. doi:10.2478/v10183-012-0010-7

Grunewald, K., and Scheithauer, J. (2010). Europe's Southernmost Glaciers: Response and Adaptation to Climate Change. *J. Glaciol.* 56, 129–142. doi:10.3189/002214310791190947

Huggel, C., Haeberli, W., Kääb, A., Bieri, D., and Richardson, S. (2004). An Assessment Procedure for Glacial Hazards in the Swiss Alps. *Can. Geotech. J.* 41, 1068–1083. doi:10.1139/T04-053

Huss, M., Bauder, A., Werder, M., Funk, M., and Hock, R. (2007). Glacier-dammed Lake Outburst Events of Gornersee, Switzerland. *J. Glaciol.* 53, 189–200. doi:10.3189/172756507782202784

Huss, M., and Fischer, M. (2016). Sensitivity of Very Small Glaciers in the Swiss Alps to Future Climate Change. *Front. Earth Sci.* 4, 34. doi:10.3389/feart.2016.00034

Huss, M., and Hock, R. (2015). A New Model for Global Glacier Change and Sea-Level Rise. *Front. Earth Sci.* 3, 54. doi:10.3389/feart.2015.00054

Iken, A. (1977). Movement of a Large Ice Mass before Breaking off. *J. Glaciol.* 19, 595–605. doi:10.3189/s0022143000215505

Jiskoot, H., Fox, T. A., and Van Wychen, W. (2017). Flow and Structure in a Dendritic Glacier with Bedrock Steps. *J. Glaciol.* 63, 912–928. doi:10.1017/jog.2017.58

Karušs, J., Lamsters, K., Ješkins, J., Sobota, I., and Džeriņš, P. (2022). UAV and GPR Data Integration in Glacier Geometry Reconstruction: A Case Study from Irenebreen, Svalbard. *Remote Sens.* 14, 456. doi:10.3390/rs14030456

Lamsters, K., Karušs, J., Rečs, A., and Bērziņš, D. (2016). Detailed Subglacial Topography and Drumlins at the Marginal Zone of Múlajökull Outlet Glacier, Central Iceland: Evidence from Low Frequency GPR Data. *Polar Sci.* 10, 470–475. doi:10.1016/j.polar.2016.05.003

Langhammer, L., Rabenstein, L., Schmid, L., Bauder, A., Grab, M., Schaer, P., et al. (2019). Glacier Bed Surveying with Helicopter-Borne Dual-Polarization Ground-Penetrating Radar. *J. Glaciol.* 65, 123–135. doi:10.1017/jog.2018.99

Lapazaran, J. J., Otero, J., Martín-español, A., and Navarro, F. J. (2016). On the Errors Involved in Ice-Thickness Estimates I: Ground-Penetrating Radar Measurement Errors. *J. Glaciol.* 62, 1008–1020. doi:10.1017/jog.2016.93

Lewińska, P., Głowacki, O., Moskalik, M., and Smith, W. A. P. (2021). Evaluation of Structure-From-Motion for Analysis of Small-Scale Glacier Dynamics. *Measurement* 168, 108327. doi:10.1016/j.measurement.2020.108327

Linsbauer, A., Paul, F., and Haeberli, W. (2012). Modeling Glacier Thickness Distribution and Bed Topography over Entire Mountain Ranges with Glabtop: Application of a Fast and Robust Approach. *J. Geophys. Res.* 117. doi:10.1029/2011JF002313

Magra, I. (2019). *Giant Glacier on Mont Blanc Is in Danger of Collapse, Experts Warn*. New York Times. Available at: https://www.nytimes.com/2019/09/25/world/europe/glacier-italy-climate-change.html.

Margreth, S., Faillettaz, J., Funk, M., Vagliasindi, M., Diotri, F., and Broccolato, M. (2011). Safety Concept for Hazards Caused by Ice Avalanches from the Whymper Hanging Glacier in the Mont Blanc Massif. *Cold Regions Sci. Technol.* 69, 194–201. doi:10.1016/j.coldregions.2011.03.006

Margreth, S., Funk, M., Tobler, D., Dalban, P., Meier, L., and Lauper, J. (2017). Analysis of the Hazard Caused by Ice Avalanches from the Hanging Glacier on the Eiger West Face. *Cold Regions Sci. Technol.* 144, 63–72. doi:10.1016/j.coldregions.2017.05.012

Meier, M. F., Dyurgerov, M. B., Rick, U. K., O'Neel, S., Pfeffer, W. T., Anderson, R. S., et al. (2007). Glaciers Dominate Eustatic Sea-Level Rise in the 21st Century. *Science* 317, 1064–1067. doi:10.1126/science.1143906

Mertes, J. R., Gulley, J. D., Benn, D. I., Thompson, S. S., and Nicholson, L. I. (2017). Using Structure-From-Motion to Create Glacier DEMs and Orthoimagery from Historical Terrestrial and Oblique Aerial Imagery. *Earth Surf. Process. Landforms* 42, 2350–2364. doi:10.1002/esp.4188

Messerli, A., and Grinsted, A. (2015). Image Georectification and Feature Tracking Toolbox: ImGRAFT. *Geosci. Instrum. Method. Data Syst.* 4, 23–34. doi:10.5194/gi-4-23-2015

Morra Di Cella, U. (2019). *Nota tecnica su applicazione modello di spessore dei ghiacciai per la stima dei volumi glaciali sulla base dei dati topografici e di catasto*. Aosta.

Paterson, W. S. B. (1994). *The Physics of Glaciers*. 3rd ed. Oxford: Butterworth-Heinemann.

Piermattei, L., Carturan, L., De Blasi, F., Tarolli, P., Dalla Fontana, G., Vettore, A., et al. (2016). Suitability of Ground-Based SfM-MVS for Monitoring Glacial and Periglacial Processes. *Earth Surf. Dynam.* 4, 425–443. doi:10.5194/esurf-4-425-2016

Piermattei, L., Carturan, L., and Guarnieri, A. (2015). Use of Terrestrial Photogrammetry Based on Structure-From-Motion for Mass Balance Estimation of a Small Glacier in the Italian Alps. *Earth Surf. Process. Landforms* 40, 1791–1802. doi:10.1002/esp.3756

Plewes, L. A., and Hubbard, B. (2001). A Review of the Use of Radio-Echo Sounding in Glaciology. *Prog. Phys. Geogr. Earth Environ.* 25, 203–236. doi:10.1177/030913330102500203

Pralong, A., and Funk, M. (2006). On the Instability of Avalanching Glaciers. *J. Glaciol.* 52, 31–48. doi:10.3189/172756506781828980

Rémy, F., and Tabacco, I. E. (2000). Bedrock Features and Ice Flow Near the EPICA Ice Core Site (Dome C, Antarctica). *Geophys. Res. Lett.* 27, 405–408. doi:10.1029/1999GL006067

Reynolds, J. M. (1997). *An Introduction to Applied and Environmental Geophysics*. Chichester: JW & Sons Interiors. doi:10.1071/pvv2011n155other

Ryan, J. C., Hubbard, A. L., Box, J. E., Todd, J., Christoffersen, P., Carr, J. R., et al. (2015). UAV Photogrammetry and Structure from Motion to Assess Calving Dynamics at Store Glacier, a Large Outlet Draining the Greenland Ice Sheet. *Cryosphere* 9, 1–11. doi:10.5194/tc-9-1-2015

Schwalbe, E., and Maas, H.-G. (2017). The Determination of High-Resolution Spatio-Temporal Glacier Motion Fields from Time-Lapse Sequences. *Earth Surf. Dynam.* 5, 861–879. doi:10.5194/esurf-5-861-2017

Schweizer, J., and Margreth, S. (2020). *Evaluation of Hazard Caused by Ice Avalanches from the Planpincieux Glacier, Val Ferret, Courmayeur, Italy Update 2020: Part 1 Summer Scenarios*. Davos, Switzerland.

Sevestre, H. (2020). Extreme Summer Impacts Ice Shelves and Glaciers. World Meteorol. Organ. Available at: https://public.wmo.int/en/media/news/extreme-summer-impacts-ice-shelves-and-glaciers (Accessed October 1, 2020).

Sugiyama, S., Bauder, A., Weiss, P., and Funk, M. (2007). Reversal of Ice Motion during the Outburst of a Glacier-Dammed Lake on Gornergletscher, Switzerland. *J. Glaciol.* 53, 172–180. doi:10.3189/172756507782202847

Suter, S., and Hoelzle, M. (2002). Cold Firn in the Mont Blanc and Monte Rosa Areas, European Alps: Spatial Distribution and Statistical Models. *Ann. Glaciol.* 35, 9–18. doi:10.3189/172756402781817059

Urbini, S., Zirizzotti, A., Baskaradas, J., Tabacco, I., Cafarella, L., Senese, A., et al. (2017). Airborne Radio Echo Sounding (RES) Measures on Alpine Glaciers to Evaluate Ice Thickness and Bedrock Geometry: Preliminary Results from Pilot Tests Performed in the Ortles Cevedale Group (Italian Alps). *Ann. Geophys.* 60. doi:10.4401/ag-7122

Vaughan, D. G. (1993). Relating the Occurrence of Crevasses to Surface Strain Rates. *J. Glaciol.* 39, 255–266. doi:10.1017/S0022143000015926

Wang, P., Li, Z., Li, H., Wang, W., and Yao, H. (2014). Comparison of Glaciological and Geodetic Mass Balance at Urumqi Glacier No. 1, Tian Shan, Central Asia. *Glob. Planet. Change* 114, 14–22. doi:10.1016/j.gloplacha.2014.01.001

Watts, R. D., and England, A. W. (1976). Radio-echo Sounding of Temperate Glaciers: Ice Properties and Sounder Design Criteria. *J. Glaciol.* 17, 39–48. doi:10.3189/s0022143000030707

Zekollari, H., Huss, M., and Farinotti, D. (2019). Modelling the Future Evolution of Glaciers in the European Alps under the EURO-CORDEX RCM Ensemble. *Cryosphere* 13, 1125–1146. doi:10.5194/tc-13-1125-2019

Zemp, M., Frey, H., Gärtner-Roer, I., Nussbaumer, S. U., Hoelzle, M., Paul, F., et al. (2015). Historically Unprecedented Global Glacier Decline in the Early 21st Century. *J. Glaciol.* 61, 745–762. doi:10.3189/2015JoG15J017

Zorzut, V., Ruiz, L., Rivera, A., Pitte, P., Villalba, R., and Medrzycka, D. (2020). Slope Estimation Influences on Ice Thickness Inversion Models: A Case Study for Monte Tronador Glaciers, North Patagonian Andes. *J. Glaciol.* 66, 996–1005. doi:10.1017/jog.2020.64

Conflict of Interest: The authors declare that the research was conducted in the absence of any commercial or financial relationships that could be construed as a potential conflict of interest.

Periglacial cascading process in an Alpine environment: an example of an ice avalanche-induced debris flow in Val Ferret (Courmayeur, Italy).

Short summary

In the research paper 'Periglacial cascading process in an Alpine environment: an example of an ice avalanche-induced debris flow in Val Ferret (Courmayeur, Italy)', we demonstrate how a close-range monitoring system for glacial risk monitoring, coupled and integrated with specific remotely sensed data, could be used for the analysis and understanding of complex phenomena of mass movement in an Alpine environment. The paper shows:

Main findings

The main findings of this publication are:

• An analysis of the possible chain of events and inputs that triggered the debris flow analysed in the case study.

• The realisation of an accurate digital elevation model from high-resolution stereo imagery.

• The validation of satellite elevation data with Ground Control Points.

• The demonstration of chain events by the integration of field evidence and monitoring data.

• The demonstration of the vulnerability of recently deglaciated alpine slopes to the triggering of potentially destructive chain processes.

Contributions of the PhD candidate

Conceptualisation of the research and planning of research activities. Performance of field surveys. Processing of aerial photogrammetric surveys. Stereo satellite image processing and data validation. Analysis of the data from the monitoring systems. Data integration. Writing of the manuscript and figure preparation with the co-authors.

Data availability

The data are available from the authors, upon request.

Journal

Geografia Fisica e Dinamica Quaternaria is a six-monthly journal published by the COMITATO GLACIOLOGICO ITALIANO. Founded in 1978, it is the continuation of the 'Bollettino del Comitato Glaciologico Italiano'. It publishes original papers, brief communications, news and book reviews of Physical Geography, Glaciology, Geomorphology and Quaternary Geology. The journal furthermore publishes the annual reports on Italian glaciers, the official transactions of the Comitato Glaciologico Italiano and the Newsletters of the International Association of Geomorphologist. Impact Factor 2020: 1.5; 5 years Impact factor: 1.659

Geogr. Fis. Dinam. Quat.
45 (2022). 97-110, 11 figg., 3 tabb.

DOI 10.4461/ GFDQ.2022.45.8

FABRIZIO TROILO [1,4*], LUCA MONDARDINI [1], PAOLO PERRET [1], VALERIO SEGOR [2], DANIELE GIORDAN [3], NICCOLÒ DEMATTEIS [3] & FRANCESCO ZUCCA [4]

PERIGLACIAL CASCADING PROCESS IN AN ALPINE ENVIRONMENT: AN EXAMPLE OF AN ICE AVALANCHE-INDUCED DEBRIS FLOW IN FERRET VALLEY (COURMAYEUR, ITALY)

ABSTRACT: TROILO F., MONDARDINI L., PERRET P., SEGOR V., GIORDAN D., DEMATTEIS N. & ZUCCA F., *Periglacial cascading process in an alpine environment: an example of an ice avalanche-induced debris flow in Ferret Valley (Courmayeur, Italy).* (IT ISSN 0391-9838, 2022).

On 23 June, 2022, a debris flow occurred in the Montitaz Stream (Mont Blanc area), which flows off the Planpincieux Glacier snout. It destroyed the bridge that links the hamlets of Planpincieux and Rochefort. Using a multi-source dataset from UAV, satellite and terrestrial sensors belonging to the Planpincieux Glacier monitoring network, we reconstructed the series of events that led to the debris flow. We found evidence that this resulted from a cascading process which started with an ice avalanche of 4200 m^3 falling over a reformed glacieret that lies 500 m downstream from the glacier front. Subsequently, the deposited ice avalanche formed an unstable ice dam along the Montitaz Stream riverbed, causing a mixed accumulation of water and ice debris. Finally, the dam collapsed, originating a debris flow consisting of ice, water and debris from the glacial fan. DEM differencing showed that approximately 14,000 m^3 of material were mobilised overall.

KEY WORDS: Cascading process, Ice avalanche, Debris flow, Glacier monitoring, Remote sensing.

RIASSUNTO: TROILO F., MONDARDINI L., PERRET P., SEGOR V., GIORDAN D., DEMATTEIS N. & ZUCCA F., *Sequenza di processi periglaciali in ambiente alpino: un esempio di debris flow indotto da valanga di ghiaccio nella Val Ferret (Courmayeur, Italia).* (IT ISSN 0391-9838, 2022).

Il 23 giugno 2022, una colata detritica ha interessato l'alveo del Torrente Montitaz (Massiccio del Monte Bianco), il quale ha origine dalla fronte del Ghiacciaio di Planpincieux, distruggendo il ponte che collega il Villaggio di Planpincieux con il Villaggio di Rochefort. Grazie all'utilizzo di una serie di dati telerilevati da piattaforme satellitari, da sistemi UAV e da sensori terrestri appartenenti alla rete di monitoraggio del Ghiacciaio di Planpincieux, abbiamo potuto ricostruire una serie di eventi e di caratteristiche interconnesse fra loro, ricostruendo la sequenza di eventi che ha generato la colata detritica. In questo modo abbiamo scoperto che la colata detritica rappresenta la parte finale di una serie di processi a cascata innescati da un crollo di ghiaccio di circa 4200 m^3, la conseguente valanga di ghiaccio che ha raggiunto il sottostante ghiacionevato del Montitaz (a circa 500 m di dislivello a valle della fronte del ghiacciaio di Planpincieux), sovrascorrendolo e formando un deposito di detriti di ghiaccio nell'alveo del Torrente Montitaz, formando una diga effimera e conseguentemente uno sbarramento al deflusso che ha causato un accumulo di acqua e ghiaccio. Il collasso dello sbarramento effimero ha poi originato la colata detritica, prendendo in carico detrito dal conoide glaciale. L'analisi multi temporale dei dati topografici ha dimostrato infine che circa 14 000 m^3 di materiali sono stati mobilizzati durante l'evento.

TERMINI CHIAVE: Processi a cascata, Valanga di ghiaccio, Colata di detrito, Monitoraggio di ghiacciai, Telerilevamento.

INTRODUCTION

Glacier-related hazards are a major issue for mountain communities, moreover exacerbated in the context of climate change. Rapidly evolving glaciers (Zemp & *alii*, 2021) can lead to the formation of unstable glacial lakes or snouts that can evolve in dangerous processes like Glacial Lake

[1] *Fondazione Montagna Sicura, Glaciers snow and avalanche research area, Courmayeur, Italy.*
[2] *Regione Autonoma Valle d'Aosta, Mountain basins geo-hydrological department, Aosta, Italy.*
[3] *Research Institute for Geo-Hydrological Protection IRPI, Italian National Research Council, Torino, Italy*
[4] *University of Pavia, Department of Earth and Environmental Sciences, Pavia, Italy.*
** Corresponding author: F. Troilo (ftroilo@fondms.org)*

The authors would like to thank all the staff of the Fondazione Montagna sicura which supports the research activities of the research team, and the administration of the Autonomous Region of Aosta Valley for its continuous support to the Fondazione Montagna sicura especially in regards to the Coordinator of the reference department Ing. Raffaele Rocco and the General Secretary of Fondazione Montagna sicura Dr. Jean-Pierre Fosson. We would like to thank Dr. Ethienne Berthier from CNRS - LEGOS (Laboratoire d'Etudes en Géophysique et Óceanographie Spatiales) for supporting us with useful informations and test datasets in the prospective phase of the acquisition and processing of satellite stereo imagery. The authors would like to thank Prof. Martin Funk for supporting with great passion and dedication the research and monitoring activities in the field of glacial risk as a member of the scientific comeetee of the Fondazione Montagna sicura. The acquisition of the Pleiades Stereo image pair taken on the 4 September, 2020 was founded by the project Interreg Alcotra 2014-2020 (IT-FR) "RESERVAQUA" co-financed cross boarded project.

Outburst Floods (GLOF) (Carrivick & Tweed, 2016; Emmer, 2017; Harrison & *alii*, 2018; Schneider & *alii*, 2014) and ice avalanches (Pralong & Funk, 2006). Furthermore, gravitational processes involving solid or liquid phases or a combination of those (Cicoira & *alii*, 2022) can have longer runouts than single-phase processes (Mergili & *alii*, 2020). Therefore, they can easily reach the bottom of slopes and be potentially dangerous for alpine settlements, infrastructures and people (Carrivick & Tweed, 2016; Huggel & *alii*, 2013; Kääb & *alii*, 2005). Complex phenomena involving different phases and interactions, known as cascading processes (Emmer & *alii*, 2022; Mazzorana & *alii*, 2019), pose a challenge in understanding mountain processes and individuation of early warning and monitoring solutions of such potentially destructive hazards. Examples of such processes have been recently documented at Piz Cengalo in Switzerland (Mergili & *alii*, 2020) and in the Chamoli region in Uttarakhand district in India (Pandey & *alii*, 2022), where highly destructive impacts on the anthropised valley floors were noticed. Cascading events are often very dangerous because the processes that compose these events can evolve or occur in different conditions compared to the ones that are typical for single processes (Cicoira & *alii*, 2022). The case under consideration is a typical example in which a debris flow occurred in a period not characterised by heavy rainfalls, involving thus the possibility that a more complex process had triggered the event.

In this paper, we describe a cascading process occurred on 23 June, 2022 in Ferret Valley, Italy. The process started as an ice avalanche from the unstable glacier front (Cuffey & Paterson, 2010) of the Planpincieux Glacier (Dematteis & *alii*, 2021). The ice deposited in the lower Montitaz stream and partially blocked its flow. The unstable dam of ice deposits collapsed, causing a dam brake outburst flood. A mixture of ice, water and debris reached the road crossing the stream and destroyed the bridge isolating the village of Rochefort in the Courmayeur municipality. We reconstructed the dynamics of the cascading process using high-rate terrestrial systems, UAVs, and different spaceborne sensors such as Airbus Pleiades stereo imagery and Sentinel-2 and Planetscope multispectral data.

STUDY AREA

This study analyses the cascading process which occurred on 23 June, 2022 in the Montitaz Stream (UTM-WGS84 coord: E: 343014,74; N: 5077657,13; elev: 1700 m) – Ferret Valley, Courmayeur Municipality, Italy – along the road that links the hamlets of Planpincieux and Rochefort (fig. 1).

The Montitaz Stream is a small tributary of the Dora di Ferret River and originates from the right lobe (i.e., Montitaz Lobe) of the Planpincieux Glacier, at ~2650 m. It's fed by the glacier melting in the warm season, while in the cold season, its flow almost dries up. The course of the Montitaz is composed of three sections: i) above the altitude of 2100 m, the stream flows directly on a 37° steep exposed bedrock and the thalweg is narrow (20-50 m). ii) Between 2100-1800 m, the Montitaz flows across a 21° steep glacial fan, composed of easily mobilized debris. ii) Below 1800 m, the slope is gentler and the stream morphology becomes of *rapid* type (sensu Halwas and Church (2002); the road between the villages of Planpincieux and Rochefort is situated at the beginning of this last section.

The Planpincieux Glacier (RGI60-11.02991) is a medium size (area: 1.013 km^2) glacier located in the Italian part of the Mont Blanc massif. The elevation ranges between 2650 m and 3680 m, its aspect is mostly south-east and the accumulation area is overlooked by rock faces from the Grandes Jorasses (4208 m). Smaller ice avalanches of a few thousand cubic meters are frequent during the warm season (Giordan & *alii*, 2020). Since 2013, the Planpincieux Glacier has been monitored by the Autonomous Region of Aosta Valley, the Fondazione Montagna Sicura and the Research Institute for Geo-hydrological Protection for the risk of collapse of a major part of the Montitaz Lobe (Dematteis & *alii*, 2021).

A lower glacial body – hereafter called Montitaz Glacieret – fed by the accumulation of ice avalanche deposits from the upper front of the Montitaz Lobe disappeared in 2015 and reformed in 2019 due to the increased ice fall activity. The glacieret lies at 2000-2100 m at the top of the glacial fan (i.e., at the beginning of the second sector formerly described of the Montitaz Stream). Its extension can vary in one single season, mainly during the melt season, as well as between different years as a balance of ice fall activity and the ablation during the warm season (fig. 2).

DATASETS AND MATERIALS

In this study, we adopted a multi-source dataset that includes the equipment belonging to the monitoring network of the unstable Planpincieux Glacier front and other data explicitly acquired to investigate the cascading process. The list of the adopted dataset is shown in tab. 1.

The monitoring network comprises a Doppler radar, which is dedicated to the detection of ice avalanches coming from the Montitaz Lobe. The Doppler radar is linked to traffic lights on the main road to stop traffic in case of event detection (Meier & *alii*, 2016).

An AXIS Q6315-LE PTZ dome camera is scheduled to acquire hourly images. In case of an event, the Doppler radar triggers a burst of one image per second.

A Ku-band ground-based synthetic aperture radar (GB-SAR) monitors the Montitaz Lobe 24/7. Terrestrial radar interferometry (TRI) (Caduff & *alii*, 2015; Monserrat & *alii*, 2014) provides displacement values every four minutes. Alarms are sent in case of strong accelerations of the glacial mass that could be forerunners of a major destabilisation and a subsequent large ice avalanche.

Two 18 MP DSLR time-lapse cameras (TLCs) acquire hourly images and provide displacement data of the Planpincieux Glacier at a daily frequency (Dematteis & *alii*, 2021) using digital image correlation technique (DIC) (Evans, 2000; Schwalbe & Maas, 2017). Moreover, the images are used to detect glacier morphological variations and -estimate released volumes of ice break-offs (Giordan & *alii*, 2020).

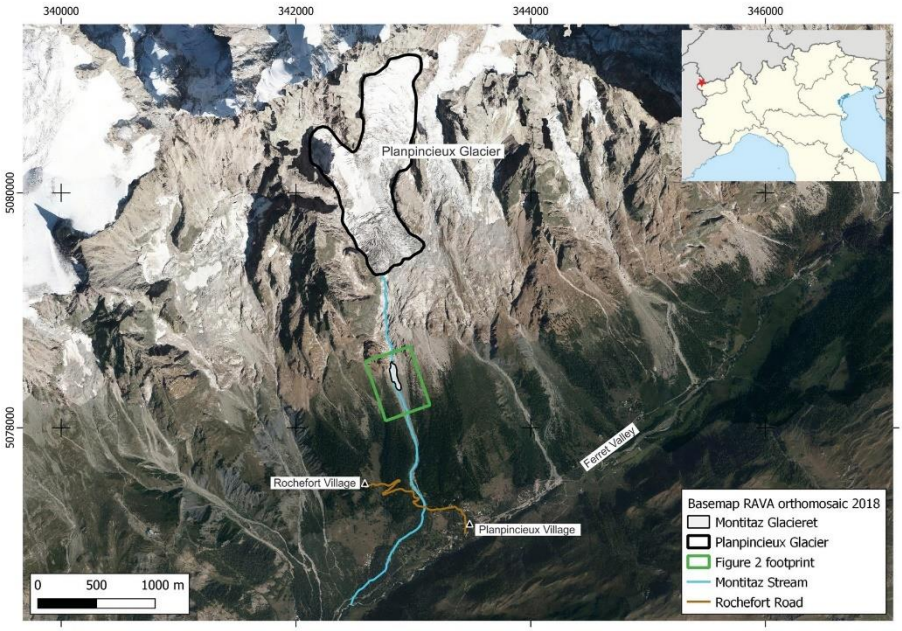

FIG. 1 - Location map of the study area. Detail of the Ferret Valley, the Planpincieux Glacier, the Montitaz Stream and the adjacent villages of Planpincieux and Rochefort. The Rochefort Road is highlighted: its crossing of the Montitaz Stream correspond to the area interested by the major impact of the debris flow studied in this paper.

FIG. 2 - View of the ice avalanche detached from the Planpincieux Glacier front and accumulated in the Montitaz Stream, between 1900 m and 2000 m a.s.l., at the base of the rocky slope downvalley the Planpincieux Glacier front. Note that the stream disappears and flows under the Montitaz Glacieret and re-emerge at the lower end of the glacieret. The photo was acquired in the morning after the debris flow event. Note the marks of flooding outside the stream (dark gray).

Doppler radar, AXIS camera and GBSAR are installed in the Planpincieux hamlet, while the TLCs are on the top of Mont de La Saxe, on the valley side opposite the Planpincieux Glacier. Furthermore, a webcam close to the bridge of the Planpincieux-Rochefort road acquires live video for surveillance.

In addition, we used available historical orthoimages and digital elevation models (DEMs) and an orthoimage and DEM acquired 5 days after the debris flow occurrence. These new acquisitions were conducted using an Autel Evo 2 Enterprise quadcopter equipped with a 20Mp digital camera (sensor width of 1"). 316 images were acquired during the survey with a resolution of 5472x3648 pixels and the geocoding was conducted in RTK mode, using 6 ground control points (GCPs) as support and a virtual base station of the SPIN GNSS (www.spingnss.it). The nearest station of the network is the "RUMI" station located at 21 km of distance and equipped with a LEIAR25.R4 LEIT antenna and a LEICA GR25 (GPS+-GLO+GAL) receiver. Errors were estimated on 3 checkpoints of the photogrammetric model. A DEM of the higher area was also used to map the extent of an ice avalanche that occurred on 10 November, 2021. The DEM was built via Structure from Motion (SfM) from the image dataset acquired with a Mavic 2 Pro UAV, equipped with a Hasselblad digital camera shooting 20 MP images. The survey was performed without GCPs, but a DEM coregistration on the UAV-acquired DEM dating from 28 June, 2022, used as a reference, was carried out to obtain higher geocoding precision. The DEM had an original resolution of 0.13 m which was resampled to 2 m to match the Pleiades DEM resolution (see below). All co-registration procedures done in the present study have been performed with the implementation of the algorithm outlined by Nuth and Kaab (2011); for that purpose, we used python code freely avalaible at https://github.com/dshean/demcoreg#demcoreg. We opted for UAV survey on UAV RTK survey DEM coregistration and Stereo satellite on Aerial Lidar DEM for coherence in spatial resolution of the products. UAV RTK survey DEM and Aerial Lidar DEM showed very small altitudinal differences on stable terrain and thus did not need to undergo further coregistration.

A 3D georeferenced point cloud of the glacial front of the Planpincieux Glacier was used to estimate the release volume of the ice avalanche of 23 June, 2022. The acquisition of the digital images was performed with a digital camera (Nikon D850, dataset of 88 images of 8256x5504 pixel resolution) shotted onboard a helicopter on the day after the event in the frame of the regular surveys in the monitoring plan of glacial risk coming from the Planpincieux Glacier front. The georeferencing of the survey was made using 13 GCPs around the glacier snout (Dematteis & *alii*, 2021). Moreover, it was also possible to acquire pictures of the lower area of the Montitaz Stream with the same camera as above, such as the image in fig. 2. Pre-event DEM was built using AIRBUS Pleiades 0.5 m-resolution Stereo pair (Berthier & *alii*, 2014) dating from 04 September, 2020. The satellite stereo imagery produced a 2 m resolution DEM over the study area.

A GNSS field survey was carried out and 6 GCPs were measured on stable ground, to assess the accuracy of the elevation information coming from different datasets. The control points were distributed in the central part of the surveyed area. In contrast, the higher area could not be surveyed at the time of the event, as the road to access the upper area remained closed for a month after the destruction of the bridge. The GNSS survey was performed with a Geomax Zenith 25 Pro receiver adopting RTK corrections via a virtual reference station of the SPIN GNSS as for the drone images georeferencing. While in the UAV data processing, all 6 GCPs could be used (3 entered as control points and 3 as checkpoints), for the processing of the satellite images, only 3 GCPs could be used because of poor visibility of some of those in the native 0.5 m resolution imagery; those 3 GCPs were used as checkpoints.

We collected meteorological data from three automatic weather stations (AWSs) managed by the regional "Centro Funzionale" of the Aosta Valley Region (www.cf.regione.vda.it). The AWSs are located close to the area of study – Ferrachet (@5.5 km, E 346984 m, N 5081340 m, alt. 2290 m), La Saxe (@2 km, E 343313 m, N 5075894 m, alt. 2110 m) and Dolonne (@5 km, E 342036 m, N 5073422 m, alt. 1200 m) – and acquire hourly precipitation data.

Finally, we adopted freely avalaible ESA (European Space Agency) Sentinel-2 (T32TLR_20220623T103031, resolution 10 m) and commercial Planet Labs Inc. Planetscope (20220623_100014_41_2483_3B_AnalyticMS_SR_8b_harmonized, resolution 3 m) multispectral images. Such images were acquired the same day of the cascading process at h12:00 local time for the Planetscope imagery and h12:38 local time for the Sentinel-2 imagery (tab. 1).

METHODS

To reconstruct the complex dynamics of the cascading process, we operated a series of tasks using the available multi source data: i) we determined the general state of the system (glacier, glacieret and stream) before the event using historical orthoimages and DEMs acquired by UAV, satellite stereo imagery, oblique images acquired by the AXIS camera, and Normalised Difference Water Index (NDWI) (McFeeters, 1996) derived by Sentinel-2 and Planetscope multispectral images; ii) we analysed the meteorological conditions (cumulated precipitation and intensity) before and during the event; iii) we determined the precise timing of the debris flow occurrence using the survey webcam of the Planpincieux-Rochefort bridge; iv) we evaluated the state of activity of the glacier using displacement data from TRI and DIC, and we analysed time-lapse and AXIS images and doppler data to identify possible ice avalanches or GLOF; finally, v) we mapped the area involved in the debris flow and measured its volume using orthoimages and DEM differencing. The abovementioned steps of the workflow are summarized in fig. 3. The aerophotogrammetrical UAV survey of 28 June, 2022 and all other photogrammetrical surveys cited in the paper (i.e., ice avalanche deposit on 10 November, 2021; Planpincieux Glacier front on 24 June, 2022), were processed using SfM from Agisoft Metashape

TABLE 1 - Available monitoring systems, products and their use.

Monitoring system	Products	Application
Sentinel-2 satellite	Orthoimage NDWI	Site state before the event
Pleiades satellite	Stereo imagery Orthorectified image DEM	Site state before the event
Planetscope	Orthoimage NDWI	Site state before the event
UAV	Orthoimage DEM	Site state before and after the event Debris flow mapping Debris flow volume estimation
Aerial Lidar	DEM	DEM coregistration, Satellite image orthorectification Satellite image orthorectification
Aerial photogrammetry RTK GNSS	Orthoimage Ground control points	DEM error quantification
AXIS camera*	Hourly photographs	Site state before and after the event
Bridge survey webcam*	Live video	Timing of the event
AWS	Semi-hourly rainfall data	Environmental conditions
Doppler radar*	Ice avalanche detection	
GB-SAR*	Near-real time glacier displacement	State of glacier activity
TLCs*	Daily glacier displacement Hourly photographs	State of glacier activity Ice avalanche / GLOF occurrence

* These apparatuses belong to the monitoring network of the Planpincieux Glacier.

(Jebur & *alii*, 2018) software. The survey conducted on 28 June, 2022 was processed with 3 checkpoints for model error estimation and 3 control points for the model construction. A georeferenced dense cloud of 127 million points was produced; using this pointcoud, a 0.13 m/pixel ground resolution DEM and an orthomosaic with 0.065 m/pixel ground resolution were extracted.

In tab. 2, the coordinates of the reference points used in this study are reported, together with calculated errors on checkpoints both on the UAV and on the Pleiades DEMs, and finally, the difference between the two DEMs is also calculated on 3 checkpoints.

The AIRBUS Pleiades Stereo pair was processed using the Orthoengine tool of PCI GEOMATICA commercial software. We processed without GCPs, using orbital parameters only, with a second step of coregistration on stable areas, following procedures highlighted by (Nuth & Kääb, 2011), together with the regional 2 m DEM acquired by Aerial Lidar in 2008. An orthorectified image was also produced starting from one of the native stereo Pleiades images with the same software as above using the Aerial Lidar regional elevation data of 2008 and classic aerophotogrammetrical regional survey data of 2005 for the positioning of control points.

RESULTS

System conditions before the event

Fig. 4 shows the NDWI on 23 June, 2022 at h 10:30, which is higher along the thalweg of the Montitaz Stream above 2100 m, thus indicating a high probability of the presence of water, and below 2000 m, where the stream runs off the glacieret (reference fig. 2 and fig. 3). In correspondence with the Montitaz Glacieret, the NDWI shows a sharp decrease, thereby marking that water flowed underneath the ice deposit. The NDWI value is relatively small, but the relevance of the data consists more on the NDWI gradient along the profiles and the e spatial coherence in the gradients along the transect. It should also be considered that such a small stream cannot build up a strong signal with the ground resolution of the available sensors (10 m and 3 m).

The high temperatures of the period when the debris flow occurred caused significant ice melting. Even though we did not have available water discharge measurements, direct visual observations showed an abundant flow in the Montitaz Stream (fig. 4).

Meteorological conditions

Fig. 4 shows hourly precipitation data collected by the Ferrachet, Dolonne and La Saxe AWSs. The maximum total precipitation registered in the 24 hours before the debris flow was 6.5 mm, and approximately 90% of the cumulated precipitation fell between h 14:00 and h 15:00. Moreover, no rainstorms were registered in the study area on the day of the event (fig. 5).

Determination of the timing

We determined the precise debris flow timing from the video of the survey webcam installed close to the bridge of the Montitaz Stream. The impact of the debris flow on the bridge occurred at h 20:45 (fig. 6A2). During the event, the bridge was severely damaged (fig. 6A3-4).

TABLE 2 - Coordinates of reference points and calculated point coordinates for error estimation of the UAV and Pleiades DEMs as well as the differences between the two DEMs.

Ground Control Points			
GCP ID	Easting (m)	Northing (m)	Altitude (m)
102	342887.051	5076953.603	1592.725
104	342902.415	5076949.896	1591.316
106	342889.792	5076981.772	1595.100
108	342878.555	5077040.699	1600.800
109	343110.180	5077322.196	1674.938
111	343108.689	5077335.473	1678.649
Pleiades Stereo DEM errors			
Point ID	Easting errors (m)	Northing errors (m)	Altitude errors (m)
102	-0.198	-0.388	-0.282
106	0.458	-0.207	-0.062
108	-1.061	-0.710	-0.547
RMSE	0.677	0.482	0.357
UAV DEM errors			
Point ID	Easting errors (m)	Northing errors (m)	Altitude errors (m)
104	0.085	0.228	0.151
106	0.181	0.054	-0.010
109	-0.237	-0.342	0.169
RMSE	0.179	0.239	0.131
UAV 2m resampled DEM vs 2m Pleiades DEM Altitudinal differences			
Point ID	UAV altitude (m)	Pleiades altitude (m)	
102	1592.514	1593.007	0.493
106	1594.888	1595.162	0.274
108	1601.432	1601.444	0.012
RMSE			0.325

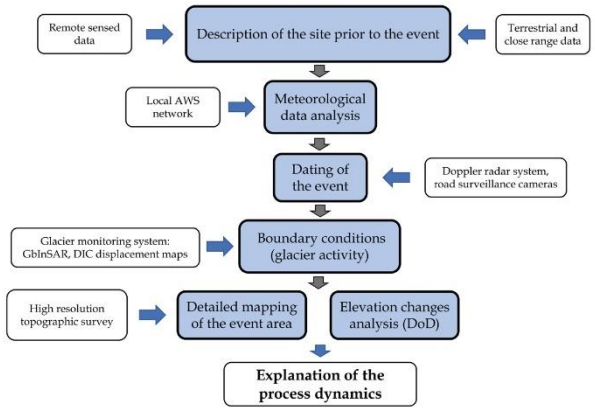

FIG. 3 - Workflow summarizing the methodology applied in this study for the reconstruction of the dynamics that caused the Montitaz Stream debris flow on 23 June, 2022.

State of the Planpincieux Glacier activity

The motion of an ice chunk at the glacier front markedly increased in the 3 days before the event. The GBSAR system detected an acceleration of the glacial front on 23 June, 2022, which culminated at around h 20:00, followed by a decrease in velocity, which is typical of a process of destabilisation, acceleration of the ice mass and subsequent collapse that generates an ice avalanche (Giordan & *alii*, 2020). Analogously, the acceleration was registered by the DIC results of the TLC, where the unstable portion was evident.

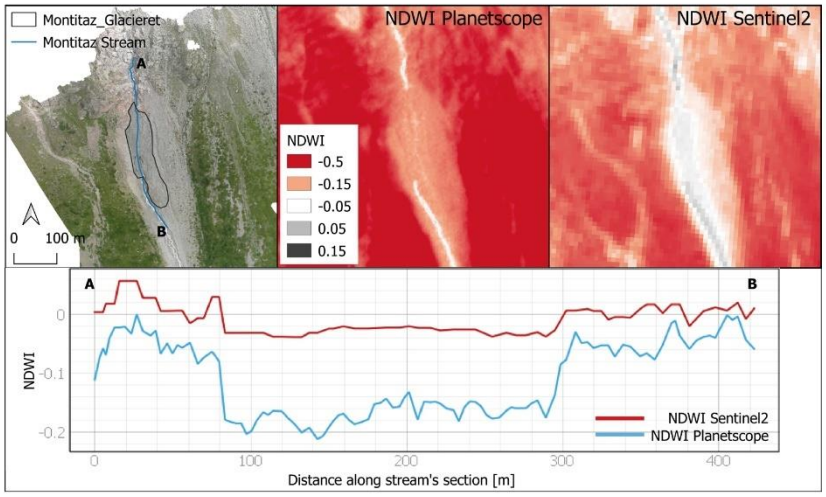

FIG. 4 - NDWI index maps obtained from Sentinel-2 and Planetscope imagery taken on the 23 June, 2022 (h 12:38 and h 12:00 local time, respectively). Water flowing into the Montitaz Stream is highlighted by higher NDWI values along the thalweg, while lower values characterise the area of the Montitaz Glacieret where the water disappears, flowing underneath the glacieret. ©Planet Labs PBC, CC BY-NC-SA 2.0.

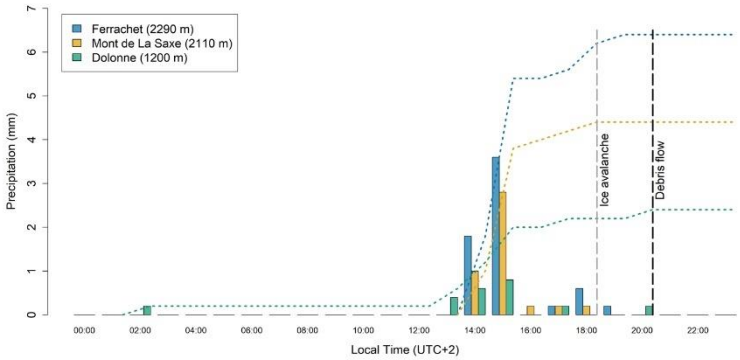

FIG. 5 - Pluviometric data from the Ferrachet, Dolonne and La Saxe AWS located in the Ferret Valley. Histogram refers to hourly precipitation, dashed blue yellow and green lines indicate cumulated precipitation of the single AWS. Vertical dashed grey and black lines indicate the timing of the ice avalanche and debris flow events.

Additionally, comparing the hourly time-lapse images, we identified an ice break-off that occurred between h 18:00 and h 19:00 (fig. 7A). The volume of 4500 ± 1500 m^3 involved in the ice fall has been performed by photogrammetric measures on the digital imagery from the TLC of the Planpincieux Glacier monitoring system (Giordan & *alii*, 2016). Due to the relatively high uncertainty of this methodology, a measurement of the ice fall scar has been made on data from the aerophotogrammetrical survey of the glacial front performed on the morning after the ice fall event. The ice fall scar could be easily located and confirmed by the confrontation of high-resolution time-lapse cameras before and after the event. The scar had a mean depth of 7 m, a width of 36.8 m and a mean ice thickness of 16.3 m, yielding a volume of 4200 m^3. With the positioning of natural reference points (homologous points on exposed bedrock found on TLC images and UAV images) for volume calculation in the order of ±20 cm on a very fine resolution (average point spacing 5 cm) georeferenced 3D point cloud, and the uncertainty of the exact geometry of the collapsed glacial front (we estimated its geometry by interpolation of the intact glacial front to the left and right of the ice fall scar) we estimate accuracy in the order of ±500 m^3. This confirmed good performance of the first estimation method, probably helped by the simple geometry of the ice chunk and the very well-defined ice fall scar. We took the volume estimation on the 3D model as a reference.

The downslope ice deposit was visible on an image acquired at h19:00 by the AXIS camera and it accumulated a few tens of meters below the Montitaz Glacieret. Such images do not show evidence of a large accumulation of ice debris, but rather show a mixture of thin accumulation of small ice debris and flowing/erosional features on the glacieret surface (fig. 7B). Therefore, there is evidence that an ice avalanche impacted the glacieret and deposited in the Montitaz Stream approximately two hours before the debris flow reached the bridge downstream. Since the volume of the break-off was relatively small, the Doppler radar did not detect the avalanche; consequently, the AXIS camera did not acquire a concurrent high-rate image burst (fig. 7).

FIG. 6 - Sequence of images of the Rochefort bridge that crosses the Montitaz Stream. A1 to A4 are images of the camera surveying the bridge when the debris flow impacted the bridge h 20:47-h 20:55. B1 and B2 are images of the camera surveying the Montitaz Stream just above the bridge at h 20:00 before and at h 08:00 the morning after the event. A significant deposition of debris is evident.

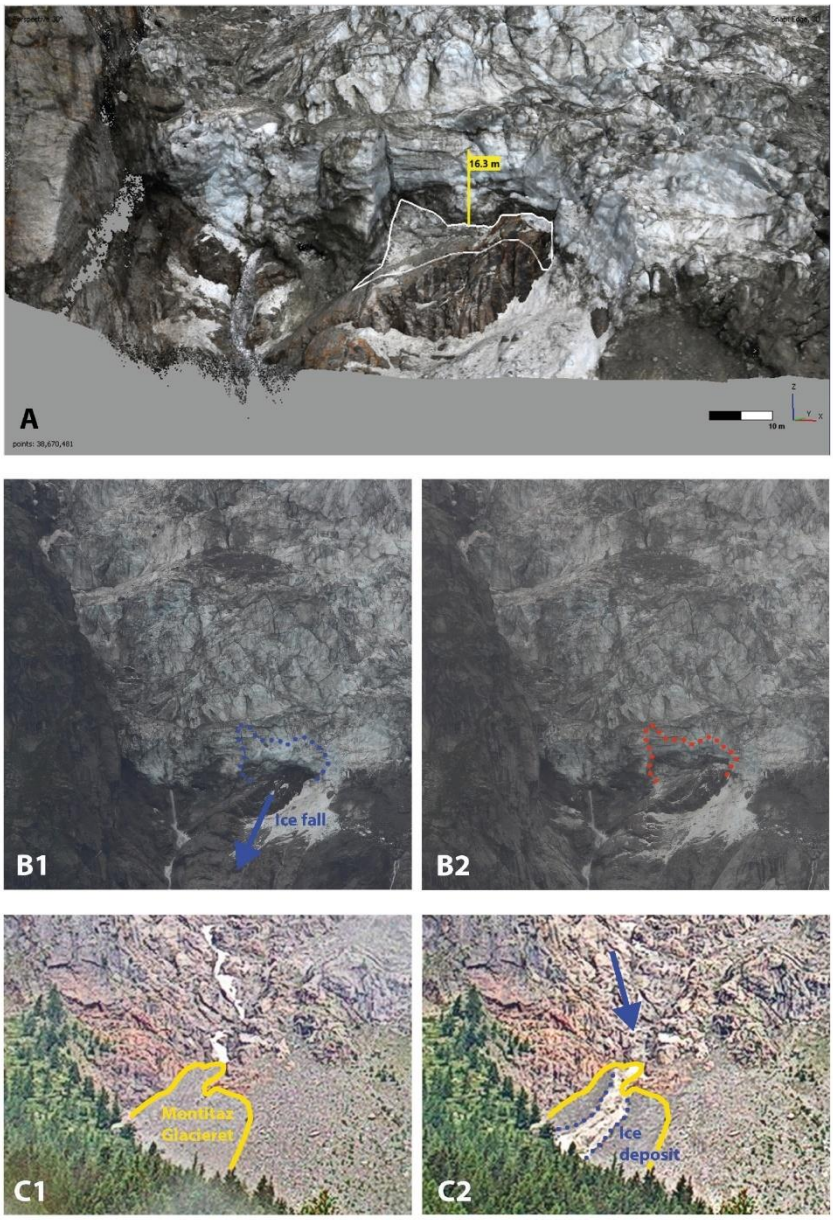

FIG. 7 - A) Individuation of the basal surface of the ice detachment on the georeferenced 3D point cloud of the Planpincieux glacier obtained by SfM processing and collapsed ice thickness measure. B1 and B2) Evidence of an ice fall from the front of Planpincieux Glacier on digital high-resolution time-lapse imagery from the 23 June, 2022 at h 18:00 and h 19:00. The collapsed volume was estimated to 4200 m^3 ± 500m^3. C1 and C2) AXIS camera images of the Montitaz Glacieret at C1 h 18:00 and C2 h 19:00. In C2, the ice deposit of the avalanche that had overflown the Montitaz Glacieret is highlighted.

Debris flow mapping and volume

The day after the event, a helicopter flight was carried out. Fig. 8 shows details that allow one to individuate the starting point of the debris flow. Fresh erosional features start to be present from 1940 m altitude on the right bank of the stream and from 1925 m on the left bank of the stream. An elongated patch of ice debris is located on top of the left margin of the stream at the same location of the first appearance of fresh erosional marks and reaching its maximum point of reach at around 1900 m. Such lateral elongated ice debris patches have already been observed on ice avalanche deposits coming from the Planpincieux Glacier and stopping in the Montitaz Stream (Mergili & *alii*, 2020).

Based on the abovementioned observations, we locate the probable deposition area of the ice avalanche that partially blocked the stream, causing the start of the mass movement, at an altitude between 1950 m and 1900 m (fig. 9).

The probability that the ice avalanche deposited in this area is also confirmed by past documented events having similar starting volumes and that have frequently had points of reach in the same area, such as the ice avalanche event of 10 November, 2021 depicted in fig. 8, which had an estimated release volume of 4900 ± 1600 m^3.

Five days after the event, a UAV survey was conducted to map the deposit and estimate the volume of the mobilised debris (fig. 10). Using a Dem of Difference (DoD) based on the confrontation of the 4 September, 2020 Pleiades DEM and the DEM acquired by UAV on 28 June, 2022, we were able to analyse the elevation changes that occurred following the event of 23 June, 2022 (tab. 3). We interpreted the elevation losses along the higher part of the stream as related to erosional processes linked to the event under analysis. Lower down the stream towards the Rochefort bridge crossing, we have instead interpreted the elevation gains as depositional features from the abovementioned event. In the accumulation area, elevation changes were matched by changes in the distribution and texture of the debris along the stream. Lateral elongated depositional features were present upstream, and a lower main body was identified just against the bridge. This main accumulation body is visible in the surveillance camera imagesin fig. 7B. The results of the DoD showed maximum thicknesses of the debris flow accumulation in this area as high as 6 m. In this way, it was possible to calculate eroded and deposited volumes that, with the introduction of the fallen ice mass that was remobilised and entrained in the gravitational process, reach similar values in the balance between eroded and accumulated volumes (fig. 10).

TABLE 3 - Description of the involved volumes in the gravitational process. A summary of estimated eroded volumes and deposited volumes of material linked to the event of 23 June, 2022. Negative volumes represent the missing volumes in the higher section of the stream comprised of the negative areas of the DoD available from pre and post event conditions that we interpret as eroded debris, and the ice volume that fell from the glacier front on 23 June, 2022 that was taken in the debris flow process and subsequently disappeared from the higher area of the Montitaz stream. Positive volumes are represented by areas of positive values in the pre and post event DoD in the lower section of the Montitaz stream.

Area type	Volume (m^3)	Accuracy (m^3)
Erosional (debris)	-4597	±1986
Erosional (Ice)	-4200	±500
Accumulation Ice+Debris	+13,533	±1530

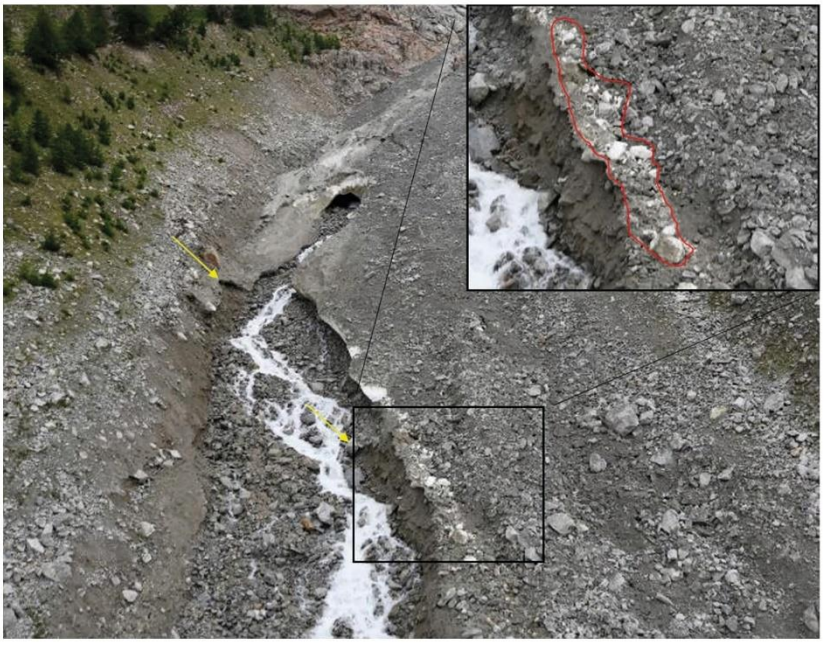

FIG. 8 - The starting points of the freshly activated erosional processes are visible on pictures from the helicopter survey carried out the morning after the debris flow event (i.e., 24 June, 2022, highlighted with yellow arrows). The ice avalanche deposit has almost completely been washed out or eroded, but a small elongated patch of ice debris is still in place on the left bank of the stream (upper right inset, red outline). The distance between the higher erosional feature and the ice debris patch is approximately 60 m.

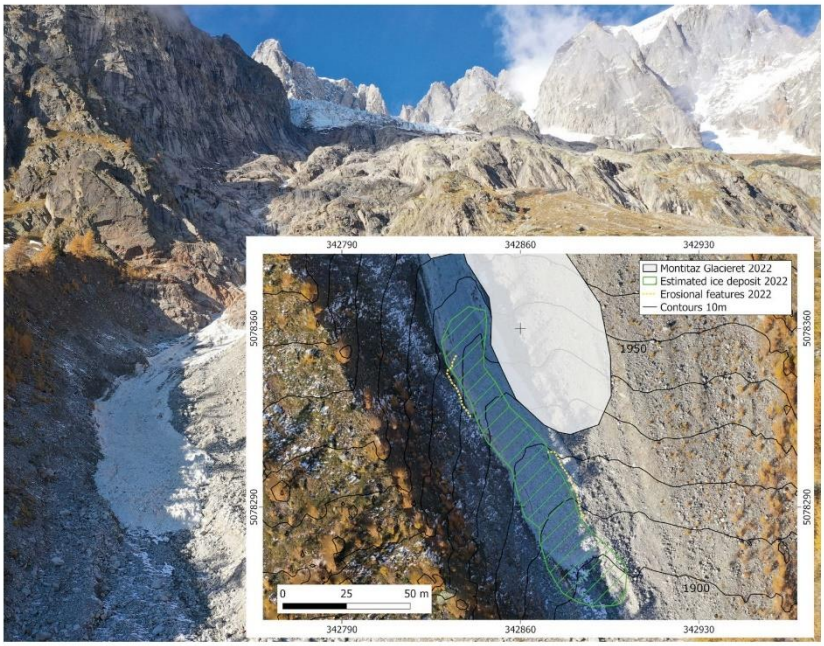

FIG. 9 - Oblique image (main panel) and orthoimage (inset) of the ice avalanche of 10th November, 2021. The estimated ice avalanche deposition of the event of 23 June, 2022 is overlayed in green for comparison. The location of the erosional features originated by the 23 June, 2022 event is highlighted in yellow.

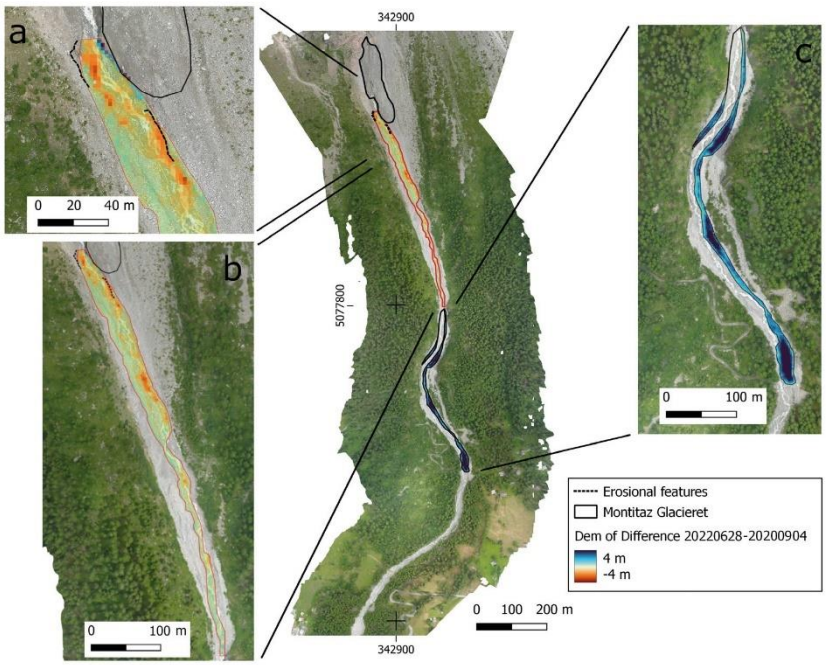

FIG. 10 - Map of the cascading process. The colours indicate the DEM differencing before and after the debris flow (04 September, 2020 – 28 June, 2022). Background: orthoimage of 28 June, 2022. Details of: a) the starting area which caused the remobilisation of the ice debris, b) the erosional area and c) the depositional area along the Montitaz Stream.

DISCUSSION

In this paper, we present a cascade process: a debris flow in the Montitaz Stream that was so intense as to be able to destroy the Rochefort bridge occurred without significant rainfall. In glacial streams, the occurrence of debris flows can be linked to a GLOF or other events that can trigger these potentially destructive phenomena (Allen & *alii*, 2022). The study of the activation of this event can be beneficial for better comprehension of the sequence of events that concurred with its arising. The presence of the Planpincieux Glacier monitoring network, one of the most complex installed in Italy and in the Alps, allowed us to collect a significant dataset by different instruments.

The multi-source dataset has been fundamental to reconstruct the state of the involved elements: Planpincieux glacier, glacieret and Montitaz stream – before the cascading process as follows:

- a large deposit of ice – the Montitaz Glacieret – is present at the top of the glacial fan, fed by the intense calving activity of the Planpincieux glacier in 2022;
- the presence of the glacieret facilitates longer runouts of relatively small ice avalanches due to the reduced friction of the ice;
- the water discharge that alimented the Montitaz Stream from the Planpincieux glacier is abundant due to the high temperatures of the warm season.

The early activation of the ice avalanching processes at Planpincieux Glacier, although still not completely understood, could be linked to high temperatures in the spring period. This would enhance snow melt and cause an increase in basal water pressure at the ice-bedrock interface that decreases basal friction and determines strong accelerations and fracturations in the ice mass. These conditions are prone to the formation of large ice avalanches detaching from the glacial front.

The sequence of events that have been documented on the day of the event is:

i) a limited rainfall event (~6.5 mm) happened in the previous 24 hours and was mostly concentrated between h 14:00 and h 15:00;
ii) an ice avalanche (~4200 m^3) broke off from the Planpincieux Glacier between h 18:00 and h 19:00, impacted on the Montitaz Glacieret and moved further downstream it;
iii) a debris flow damaged the bridge on the Montitaz Stream at h 20:47;

Therefore, the probable dynamics of the cascading process is the following: the ice avalanche deposit formed an unstable ice dam just downstream from the glacieret. The input provided by the Montitaz Stream caused water accumulation above the dam for approximately one to two hours. Subsequently, the dam collapsed. Then, water, ice debris and morainic material were released abruptly, triggering a debris flow. Flowing downstream, the debris flow entrained more debris from the glacial fan and reached the Planpincieux-Rochefort road, damaging the bridge and filling the riverbed with up to 6 m of debris deposit (fig. 11).

We obtained this reconstruction of the occurred events after considering all possible solutions. Alternative causes that might have generated the debris flow are: i) liquid precipitation alone, without the involvement of any glacial component; ii) a GLOF starting from the Planpincieux Glacier; iii) a partial collapse of the Montitaz Glacieret.

The first case is highly improbable because the cumulated precipitation and intensity were very limited and concentrated several hours before the debris flow, as shown in fig 5. The distribution of precipitations excluded a direct impact in the debris flow trigger.

The second case – a GLOF from the main glacier – is also unlikely, because similar phenomena have already been observed in the Planpincieux Glacier, and they leave typical cavities that are easily recognisable on high-resolution time-lapse photography (Giordan & *alii*, 2020). But, in this case, nothing similar was noticed nor registered by the doppler radar and the AXIS camera.

Finally, we also excluded the hypothesis of a partial collapse of the Montitaz Glacieret for two reasons: 1) we did not notice morphological variations of the glacieret terminus on the images of the AXIS camera after the event; and 2) the starting point of the debris flow corresponded exactly with the terminal part of the glacieret, as delineated on the NDWI maps less than 10 hours before the debris flow. Therefore, there was no evidence of a collapse of a substantial portion of the glacieret.

Based on our estimations of the mobilised volumes of material involved in the event of 23 June, 2022, an imbalance in the eroded vs deposited material can be noted. The main cause of the difference probably relies in the fact that the most recent DEM available for representing the pre-event status, although relatively recent, dates back to September 2020, almost two years before the event. Even if two years seems a long timespan for such a stream to preserve its morphology, this was the most recent data available to analyse the phenomena. This implies that we are missing any depositional or erosional event or process that could have happened from September 2020 to June 2022 (Roelofs & *alii*, 2022; Walter & *alii*, 2022). Therefore, we believe that depositional processes in the upper part of the stream played a significant role in the surplus of the depositional part in our calculations. The reason resides mostly in the fact that the debris fan of the Montitaz Stream is very active, both for snow avalanche activity during the winter and ice avalanche activity during the summer. UAV surveys of the area frequently showed macroscopic presence of rock debris in the ice avalanches deposits. This is normal because of the cirque morphology of the Planpincieux Glacier, surrounded by massive rock walls that are affected by frequent rock falls (some larger rock avalanches have also been documented on the glacier surface by the monitoring network in the past). The cumulated ice avalanche volume that falls from the Planpincieux Glacier front onto the Montitaz debris fan during an entire season can reach hundreds of thousands of cubic meters easily (in 2020, a total of 350,000 m^3 was estimated). Estimating a rough debris content of 0.5% in volume of the glacier ice (Hunter & *alii*, 1996; Miles & *alii*, 2021), the order of magnitude of the subsequent deposition from an entire season of ice avalanche activity falls in the range of the missing eroded volume that we noticed in our estimations.

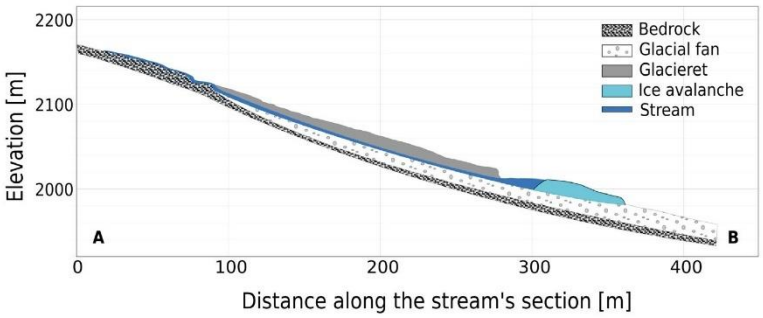

FIG. 11 - Conceptual model of the event triggering mechanism. The thickness of the glacieret and the ice avalanche are magnified for better reading.

Ice avalanches from the glacier front of the Planpincieux Glacier are frequent in summer, but the accumulations of ice avalanche debris seldom generate hydraulic problems on the Montitaz stream; in this frame, it would be possible to think that some particular conditions could have contributed to the triggering of the described event.

In the last decade, every year has shown a period of stronger ice fall activity in the summer season. Still, some years have shown larger cumulated ice avalanche accumulation, like 2020, with an estimated total of 350,000 m^3. In the years that showed less ice fall activity, like 2014, we estimated a cumulated ice avalanche accumulation of around 100,000 m^3. During the whole season of strong glacial activity, most ice volume falls in smaller events, typically falling in volume of 100-500 m^3. Ice avalanche that fall between 2000-10,000 m^3 normally range from 1 to 5 events per years. Ice fall volumes above 25,000 m^3 have been documented only once in the last 10 years.

In the mid of summer, shorter runouts of ice avalanches are noticed at Planpincieux Glacier. The total disappearance of snow patches from the gully where the ice avalanches flow and smaller extents of the Montitaz Glacieret that are normally observed, are the probable cause of such observations. The consequence is that larger release volumes of ice are needed in mid-summer conditions to reach the Montitaz Glacieret and the Montitaz Stream. Release volumes of 2000-3000 m^3 have been documented to have stopped along the bedrock gully above the Montitaz Glacieret.

In the frame of these observations, we can assess that even though ice avalanches phenomena from the Planpincieux Glacier front are recurrent, the conditions that a large enough ice avalanche is released (order of magnitude of more than 3000-4000 m^3), the Montitaz Stream is not covered by snow avalanche deposits and it has a certain amount of water flowing along its riverbed, are seldom met.

It should also be noted that a certain volume range could be more prone to generate instability and consequent debris flows: a few hundred of cubic meters of ice would not be enough to start a debris flow, but on the other hand a large accumulation of tens of thousands of cubic meters would be difficult to be saturated with water and become unstable.

Even though such a complex event was impossible to be predicted before its happening, and a certain degree of randomness in such events should be accepted, the aim of the study is to better understand hydro-geological risk of mountain environment in the present climate change scenarios; glacial and periglacial areas should be carefully taken into account as potential sources for gravitational phenomena involving ice, snow, debris and/or water by administrations, policy makers and mountain communities.

CONCLUSIONS

This study shows that detailed field surveys and the acquisition of remotely sensed data are needed to correctly describe phenomena originating in complex environments such as high alpine terrain. The availability of a complex monitoring system allowed us to collect a very detailed dataset that supported the reconstruction of an elaborate sequence of events that concur to activating a debris flow without significant rainfalls. The possible activation of a GLOF pushed us to study this event to detect all the possible evidence of this phenomenon. The analysis did not support this possibility but suggested a more complex and unusual sequence of events. The presence of a glacieret modified the behaviour of the ice avalanche and extended its runout. This combination augmented the capacity of water retention and increased the water volume at the moment of the dam break that triggered the debris flow.

The reconstruction of the series of events that led to the formation of this destructive debris flow was possible thanks to the existence of a permanent monitoring network that implements high-rate monitoring systems. A series of further analyses was carried out in this study, but we underline that without the basic inputs from the monitoring network, the reconstruction of the phenomena as a GLOF would have been very likely.

This reconstruction can be useful for the future because some events could be classified as not dangerous if considered independently. Still, when considering the possibility of cascading events, a likelihood of reaching zones at risk could arise. Therefore, knowledge about these processes should increase, and field data should be collected to correctly feed models for the simulation of such phenomena and a possible application of those in the forecast of impacts. Risk management plans should include an evaluation of the possibility of the development of chain processes originating from a single gravitational mass movement.

REFERENCES

Allen S., Frey H., Haeberli W., Hugge C., Chiarle M. & Geertsema M. (2022) - *Assessment principles for glacier and permafrost hazards in mountain regions.* In: Oxford Research Encyclopedia of Natural Hazard Science, Oxford University Press, USA. doi: 10.1093/acrefore/9780199389407.013.356

Berthier E., Vincent C., Magnússon E., Gunnlaugsson Á.Þ., Pitte P., Le Meur E., Masiokas M., Ruiz L., Pálsson F., Belart J.M.C. & Wagnon P. (2014) - *Glacier topography and elevation changes derived from Pléiades sub-meter stereo images.* The Cryosphere, 8 (6), 2275-2291.

Caduff R., Schlunegger F., Kos A. & Wiesmann A. (2015) - *A review of terrestrial radar interferometry for measuring surface change in the geosciences.* Earth Surface Processes and Landforms, 40 (2), 208-228.

Carrivick J.L. & Tweed F.S. (2016) - *A global assessment of the societal impacts of glacier outburst floods.* Global and Planetary Change, 144, 1-16.

Cicoira A., Blatny L., Li X., Trottet B. & Gaume J. (2022) - *Towards a predictive multi-phase model for alpine mass movements and process cascades.* Engineering Geology, 310, 106866.

Cuffey K.M. & Paterson W.S.B. (2010) - *The Physics of Glaciers.* Academic Press, Oxford, 704 pp.

Dematteis N., Giordan D., Troilo F., Wrzesniak A. & Godone D. (2021) - *Ten-year monitoring of the Grandes Jorasses Glaciers kinematics. Limits, potentialities, and possible applications of different monitoring systems.* Remote Sensing, 13 (15), 3005.

Emmer A. (2017) - *Glacier retreat and glacial lake outburst floods (GLOFs).* In: Oxford Research Encyclopedia of Natural Hazard Science, Oxford University Press, USA. doi: 10.1093/acrefore/9780199389407.013.275

Emmer A., Allen S.K., Carey M., Frey H., Huggel C., Korup O., Mergili M., Sattar A., Veh G. & Chen T.Y. (2022) - *Progress and challenges in glacial lake outburst flood research (2017-2021): A research community perspective.* Natural Hazards and Earth System Sciences, 22 (9), 3041-3061.

Evans A.N. (2000) - *Glacier surface motion computation from digital image sequences.* IEEE Transactions on Geoscience and Remote Sensing, 38 (2), 1064-1072.

Giordan D., Allasia P., Dematteis N., Dell'Anes, F., Vagliasindi M. & Motta E. (2016) - *A low-cost optical remote sensing application for glacier deformation monitoring in an alpine environment.* Sensors, 16 (10), 1750.

Giordan D., Dematteis N., Allasia P. & Motta E. (2020) - *Classification and kinematics of the Planpincieux Glacier break-offs using photographic time-lapse analysis.* Journal of Glaciology, 66 (256), 188-202.

Halwas K.L. & Church M. (2002) - *Channel units in small, high gradient streams on Vancouver Island, British Columbia.* Geomorphology, 43 (3-4), 243-256.

Harrison S., Kargel J.S., Huggel C., Reynolds J., Shugar D.H., Betts R.A., Emmer A., Glasser N., Haritashya U.K., Klimeš J., Reinhardt L., Schaub Y., Wiltshire A., Regmi D. & Vilímek V. (2018) - *Climate change and the global pattern of moraine-dammed glacial lake outburst floods.* The Cryosphere, 12 (4), 1195-1209. doi: 10.5194/tc-12-1195-2018

Huggel C., Giráldez C., Haeberli W., Schneider D., Frey H., Schaub Y., Cochachin A., Portocarrero C., García J. & Guillén Ludeña S. (2013) - *Climatic extreme events combine with impacts of gradual climate change: recent evidence from the Andes and the Alps.* EGU General Assembly Conference Abstracts.

Hunter L.E., Powell R.D. & Lawson D.E. (1996) - *Flux of debris transported by ice at three Alaskan tidewater glaciers.* Journal of Glaciology, 42 (140), 123-135.

Jebur A., Abed F. & Mohammed M. (2018) - *Assessing the performance of commercial Agisoft PhotoScan software to deliver reliable data for accurate 3D modelling.* MATEC Web of Conferences,

Kääb A., Reynolds J.M. & Haeberli W. (2005) - *Glacier and permafrost hazards in high mountains.* In: Huber U.M., Bugmann H.K.M. & Reasoner M.A. (Eds.), Global change and mountain regions: An overview of current knowledge, 225-234. Springer, Dordrecht, xxx pp.

Mazzorana B., Picco L., Rainato R., Iroumé A., Ruiz-Villanueva V., Rojas C., Valdebenito G., Iribarren-Anacona P. & Melnick D. (2019) - *Cascading processes in a changing environment: Disturbances on fluvial ecosystems in Chile and implications for hazard and risk management.* Science of the Total Environment, 655, 1089-1103.

McFeeters S.K. (1996) - *The use of the Normalized Difference Water Index (NDWI) in the delineation of open water features.* International Journal of Remote Sensing, 17 (7), 1425-1432.

Meier L., Jacquemart M., Blattmann B. & Arnold B. (2016) - *Real-time avalanche detection with long-range, wide-angle radars for road safety in Zermatt, Switzerland.* Proceedings of the International Snow Science Workshop, Breckenridge, Colorado, 304-308.

Mergili M., Jaboyedoff M., Pullarello J. & Pudasaini S.P. (2020) - *Back calculation of the 2017 Piz Cengalo–Bondo landslide cascade with r.avaflow: What we can do and what we can learn.* Natural Hazards and Earth System Sciences, 20 (2), 505-520.

Miles K.E., Hubbard B., Miles E.S., Quincey D.J., Rowan A.V., Kirkbride M. & Hornsey J. (2021) - *Continuous borehole optical televiewing reveals variable englacial debris concentrations at Khumbu Glacier, Nepal.* Communications Earth & Environment, 2 (1), 12.

Monserrat O., Crosetto M. & Luzi G. (2014) - *A review of ground-based SAR interferometry for deformation measurement.* ISPRS Journal of Photogrammetry and Remote Sensing, 93, 40-48.

Nuth C. & Kääb A. (2011) - *Co-registration and bias corrections of satellite elevation data sets for quantifying glacier thickness change.* The Cryosphere, 5 (1), 271-290.

Pandey V.K., Kumar R., Singh R., Kumar R., Rai S.C., Singh R.P., Tripathi A.K., Soni V.K., Ali S.N. & Tamang D. (2022) - *Catastrophic ice-debris flow in the Rishiganga River, Chamoli, Uttarakhand (India).* Geomatics, Natural Hazards and Risk, 13 (1), 289-309.

Pralong A. & Funk M. (2006) - *On the instability of avalanching glaciers.* Journal of Glaciology, 52 (176), 31-48.

Roelofs L., Colucci P. & de Haas T. (2022) - *How debris-flow composition affects bed erosion quantity and mechanisms: An experimental assessment.* Earth Surface Processes and Landforms, 47 (8), 2151-2169.

Schneider D., Huggel C., Cochachin A., Guillén S. & García J. (2014) - *Mapping hazards from glacier lake outburst floods based on modelling of process cascades at Lake 513, Carhuaz, Peru.* Advances in Geosciences, 35, 145-155.

Schwalbe E. & Maas H.G. (2017) - *The determination of high-resolution spatio-temporal glacier motion fields from time-lapse sequences.* Earth Surface Dynamics, 5 (4), 861-879.

Walter F., Hodel E., Mannerfelt E.S., Cook K., Dietze M., Estermann L., Wenner M., Farinotti D., Fengler M. & Hammerschmidt L. (2022) - *Brief communication: An autonomous UAV for catchment-wide monitoring of a debris flow torrent.* Natural Hazards and Earth System Sciences, 22 (12), 4011-4018.

Zemp M., Nussbaumer S.U., Gärtner-Roer I., Bannwart J., Paul F. & Hoelzle M. (Eds.) (2021) - *Global Glacier Change Bulletin*, 4 (2018-2019) - World Glacier Monitoring Service, Zurich, Switzerland, 278 pp.

(Ms. received 26 March 2023, accepted 23 June 2023)

Assessing the rock failure return period on an unstable Alpine rock wall based on volume-frequency relationships: the Brenva Spur (3916m asl, Aosta Valley, Italy).

Short summary

In the research paper 'Assessing the rock failure return period on an unstable Alpine rock wall based on volume-frequency relationships: the Brenva Spur (3916m asl, Aosta Valley, Italy)' (Fei et al., 2023), monitoring by means of a yearly aerophotogrammetric survey on an unstable high alpine rock wall is described. The obtained data are analysed for a possible assessment of unstable rock volumes and for a prospective frequency relationship analysis. Failure scenarios are produced in order to improve the risk assessment of potential rock-ice avalanche phenomena.

Main findings

The main findings of this publication are:

- The realisation of a series of multi-temporal aerophotogrammetric surveys in a very high alpine environment.
- The processing and integrated analysis of the obtained point clouds.
- The analysis of point clouds in order to obtain a structural analysis of the Brenva Rock Spur.
- The calculation of yearly rockfall volumes.
- The definition of a volume-frequency relationship of rock failures.

Contributions of the PhD candidate

Conceptualisation of the research and planning of research activities. Performance of field surveys. Processing of aerial photogrammetric surveys. Writing of the manuscript and figure preparation with the co-authors.

Data availability

The data are available from the authors, upon request.

Journal

Engineering Geology is an international interdisciplinary journal bridging the fields of the earth sciences and engineering, particularly geological and geotechnical engineering. The focus of the journal is on geological or engineering studies that are of interest to engineering geologists, whether their initial training is in geology or civil/mining engineering. The studies published in this journal show relevance to engineering, environmental concerns, and safety. Impact Factor 2022: 7.4

Engineering Geology 323 (2023) 107239

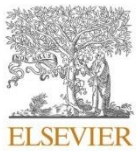

Contents lists available at ScienceDirect

Engineering Geology

journal homepage: www.elsevier.com/locate/enggeo

Assessing the rock failure return period on an unstable Alpine rock wall based on volume-frequency relationships: The Brenva Spur (3916 m a.s.l., Aosta Valley, Italy)

Li Fei [a,*], Michel Jaboyedoff [a], Antoine Guerin [a,b], François Noël [a,c], Davide Bertolo [d], Marc-Henri Derron [a], Patrick Thuegaz [d], Fabrizio Troilo [e,f], Ludovic Ravanel [g]

[a] Risk Analysis Group, Institute of Earth Sciences, University of Lausanne, CH 1015 Lausanne, Switzerland
[b] Norbert SA, Engineering Geology and Hydrogeology, CH-1920 Martigny, Switzerland
[c] Geohazard and Earth Observation, Geological Survey of Norway (NGU), NO 7491 Trondheim, Norway
[d] Struttura Attività Geologiche, Regione Autonoma Valle d'Aosta, 11020 Quart, Italy
[e] Fondazione Montagna Sicura, 11013 Courmayeur (Valle d'Aosta), Italy
[f] Department of Earth and Environmental Sciences, University of Pavia, 27100 Pavia, Italy
[g] EDYTEM, Université Savoie Mont-Blanc, 73370 Le Bourget du Lac, France

ARTICLE INFO

Keywords:
Rockfall
Photogrammetry
SLBL
Failure scenario
Return period

ABSTRACT

Defining the relationship between volume and return period is critical when estimating the risk of rockfalls and/or rock avalanche, especially during continued global warming at high altitudes that threatens rock wall stability. Characterizing the volume-frequency relationship based on historical datasets is, however, limited by observation and quantification biases, which have not received enough attention. Here, to monitor recent activities for the Brenva Spur (Mont-Blanc massif, Italy) that is also a rock avalanche scar and estimate the return period of future rock failures based on the volume-frequency relationship (and the corresponding uncertainty), a structure-from-motion photogrammetric survey was conducted from 2017 to 2021. 39 rockfall sources with volumes ranging from 11 to 13,250 m^3 were identified within the scar. The total failure volume is 22,438 m^3, with an associated erosion rate of 15.5 mm/year, indicating very active morphodynamics possibly linked to the permafrost evolution in the spur. The volumes were characterized by a negative power-law that fits significant two events in 2016 (3.4×10^4 m^3) and one in 1997 (2.0×10^6 m^3) remarkably well, and the randomness of the fit was evaluated by a Monte Carlo approach. 7 potential failure scenarios ranging from 3.1×10^4 m^3 (S_1) to 4.8×10^6 m^3 (S_7) were defined according to a structural analysis and the sloping local base level concept. Their extrapolated return periods derived by the power-law fit indicate a longer return period for the maximum failure scenario than for the smaller scenarios. S_1 has a 50% chance of occurring every 3 years, while S_7 has a 50% chance of occurring every 31 years. Though the median return period of S_7 is 31 years, the 95% and 68.2% confidence intervals range from 8 to 399 years and 14 to 93 years, respectively, which reflects a high level of uncertainty but is realistic when considering global warming, progressive rock failure, etc. In addition to characterizing recent rock failure activities in high mountains, this study offers a preliminary examination of the return periods of some extreme scenarios and provides primary data for risk management in mountainous areas that are very sensitive to global warming.

1. Introduction

Rockfalls and rock avalanches are pervasive hazards in Alpine areas and can cause severe damage to infrastructure, such as ski-lifts, transportation corridors and construction located in the propagation path of such processes (Duvillard et al., 2019). Since the late 1990s, many events have been reported in Alpine regions around the world (Coe et al., 2018; Cox and Allen, 2009; Evans and Clague, 1994; Huggel, 2009; Noetzli et al., 2003; Ravanel et al., 2017; Ravanel and Deline, 2010; Sepúlveda et al., 2021). Among several preliminary and

* Corresponding author.
E-mail address: li.fei@unil.ch (L. Fei).

https://doi.org/10.1016/j.enggeo.2023.107239
Received 12 December 2022; Received in revised form 25 May 2023; Accepted 3 July 2023
Available online 4 July 2023

predisposing factors, the warming/degradation of permafrost is increasingly emphasized and is assumed to play a fundamental role in rock slope failures (Draebing et al., 2017; Gruber and Haeberli, 2007; Legay et al., 2021), this is especially the case during continued global warming, as has been demonstrated for example during the high temperature summers of 2003 (Gruber et al., 2004) and 2015 (Ravanel et al., 2017). Thus, with continuous climate warming driving extensive permafrost degradation, associated geologic hazards are likely to increase in Alpine regions. Although larger rock-avalanches are less frequent than rockfalls, larger events have a more significant impact on the evolution of Alpine terrain and pose a more significant threat to humans and infrastructures when they occur. Therefore, hazard analysis of rockfall/rock avalanche activity is very important not only for predictive purposes but also for conservation and mitigation efforts (Bründl et al., 2009).

Magnitude-frequency relationships are the foundation of probabilistic hazard analysis, especially concerning hazard risk estimation (De Biagi et al., 2017). The hazards (rockfalls/landslides) occurring could be derived by magnitude-frequency relationships based on the empirical data. Different data sources have been used to establish these relationships for cases with various geometries and scales. These include mapping large rockslides of different ages through satellite imagery, aerial photographs, and field surveys conducted at a specific time (Coe et al., 2018; Viani et al., 2020), considering triggering events like rainstorms or earthquakes (Malamud et al., 2004). Continuous inventories obtained by terrestrial laser scanning (TLS) (Guerin et al., 2020; Ravanel et al., 2017) and unmanned aerial vehicles (UAV) photogrammetry (Westoby et al., 2012) monitoring with different temporal interval have also been used. Ravanel and Deline (2013) implemented an observation system in the Alpine mountains specifically designed to record instances of rock failure. The magnitude-frequency relations of landslides (Brunetti et al., 2009; Dussauge et al., 2002, 2003; Malamud et al., 2004; Stark and Hovius, 2001) (related to surface area or volume) or rockfalls (Guzzetti et al., 2003; Hantz et al., 2003; Hungr et al., 1999; Larsen et al., 2010; Santana et al., 2012) (related to volume) is found often sufficiently depicted by power-law distribution over a limited range, which means that smaller landslides occur more frequently than larger ones. This distribution can be influenced by various factors, including geological context, triggering events such as rainfall or earthquakes, and local environmental conditions, resulting in a various scaling parameter (b) of fitted power laws between 0.4 and 0.9 for rock slope instability (Corominas et al., 2018). The magnitude (volume)-frequency relationship was found to be similar for different types of rock failure (Corominas et al., 2018; Dussauge et al., 2002; Guzzetti et al., 2003; Hungr et al., 1999), which indicates the potential of using the same power law observed for smaller events to extrapolate return periods for potentially larger events if the provided small events record is complete. The uncertainty and range of validity of such extrapolation are questioned and high probably affected by the largest magnitude of historical landslides that is uncommon or often missing (i.e., rockfalls and rock avalanches) (Budetta et al., 2016; Copons and Vilaplana, 2008; Graber and Santi, 2022; Guzzetti et al., 2004). Nevertheless, it is inevitable that rock failure predictions based on power-law distribution are subject to substantial uncertainties. This is especially the case for epistemic uncertainties that mainly arise due to limited knowledge (i.e., the statistical uncertainty due to the small datasets) (Straub and Schubert, 2008; Ravanel et al., 2017). Bootstrap analysis (De Biagi et al., 2017) and Monte Carlo simulations (Jaboyedoff et al., 2021; Strunden et al., 2015) are usually used to evaluate the uncertainty of magnitude-frequency relationship fittings. These fast and straightforward approaches obtain the confidence bounds of the fitted distributions to evaluate the associated uncertainties. A significant population of samples could improve a robust fit.

In the context of quantitative risk assessment of rock slope instability, a comprehensive understanding of the various potential failure scenarios (referring to reasonably expected potential slope failure sources and corresponding volumes) and their corresponding frequencies or return periods (referring to the recurrence interval at which a particular event is expected to occur) assumes critical significance in the effective prediction and protection against hazards (De Biagi et al., 2017; Fell et al., 2008; Ho, 2004). Unfortunately, the research concerning the relationship between these aspects based on the power law fitting within the domain of risk assessment of rock failure is still significantly lacking. The primary factors contributing to this deficiency are the perceived low probability associated with such scenarios and the lack of standardized definitions or assessment procedures (Corominas et al., 2005, 2018). Nonetheless, it is imperative to duly consider these potential failures, irrespective of their non-occurrence in the past. This becomes especially crucial in light of the consequence of permafrost warming induced by global climate change. More than that, there have been few studies that assess the risk (i.e., the return period of the potential large failure scenarios) posed by large historical rock avalanche scar located in the high mountainous regions where the instability of rock slope is often underestimated and poorly recorded due to inaccessibility and observation difficulties (Ravanel and Deline, 2010). A more accurate and comprehensive knowledge regarding the volume-frequency relationships of potential Alpine rock failure hazards is needed, especially under the continued climate warming (Stephan Gruber and Haeberli, 2007; Hartmeyer et al., 2020b).

Herein, the southeastern flank of the Brenva Spur (3916 m a.s.l.; Mont-Blanc massif, Aosta Valley, Italy) was investigated and studied, mainly because it corresponds to the source of the 1997 rock avalanche (2×10^6 m^3) that caused two deaths and led to the destruction of a large forest area (Deline, 2001; Giani et al., 2001). The rock avalanche scar was reactivated in September 2016 with a total failure volume (two events) of approximately 3.4×10^4 m^3, which indicated an increasing instability of the scar. This paper presents the recent rock failure activity detected within the Brenva rock avalanche scar since July 2017 by employing a structure from motion (SfM) photogrammetric survey. Coupled with a detailed structural analysis of the rock mass, the sloping local base level (SLBL) algorithm is then used to define the potential future rock instabilities of the rock avalanche scar. Finally, 7 possible failure scenarios and their assessed return period are discussed based on the power-law fit considering the uncertainties (quantified by Monte Carlo simulations) associated with the distribution of the eroded volumes (including the one in 1997 and two in 2016) and the volumes that could collapse in the future.

2. Study site and geologic setting

The Brenva rock avalanche scar, mainly formed by the large rock avalanche of 1997, is located at the southeastern flank of the Brenva Spur (3916 m a.s.l.; Deline, 2001). The scar is approximately 250 m wide and 300 m high (Deline, 2009) (Fig. 1d). The Brenva Spur belongs to the upper part of the Brenva glacial basin (Mont-Blanc massif, Aosta Valley, Italy) (Fig. 1b), which is a slope glacier that now only covers 4.4 km^2 (7.3 in the late 1990s according to Giani et al., 2001), with a maximum length of 3.6 km, and a maximum width of 1.4 km. Before the recent disconnection of its front, the terminus of the Brenva glacier reached 1415 m a.s.l., which was the lowest glacier altitude in the Italian Alps. It is now at 2400 m a.s.l. Brenva Spur is permafrost-affected as suggested by permafrost statistical distribution models at the scale of the Alps (Boeckli et al., 2012) as well as at the scale of the Mont-Blanc massif (Magnin et al., 2015). The presence of cold hanging glaciers and ice aprons near the spur and on its northern slope also attest to this presence (Ravanel et al., 2023).

From a large scale geological point of view, granite intrusions in the gneissic basement, which occurred approximately 300 My ago (Guermani and Pennacchioni, 1998), formed the Mont-Blanc massif (mainly a granitic batholith) during the Hercynian orogeny. These two intrusion units meet at the summit of Mont Blanc (Ravanel et al., 2010). Coarse grained granites characterize the central part of the Mont-Blanc massif, while medium grain granites are distributed along its edges.

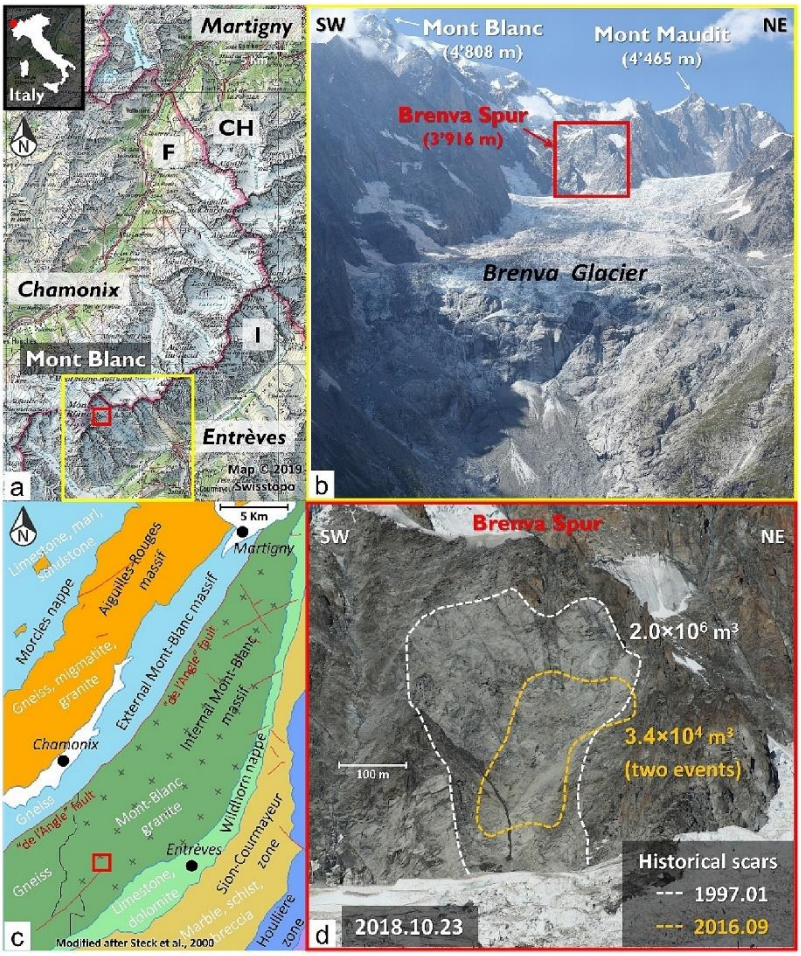

Fig. 1. Location and geological setting of the study area. (a) Location of the Brenva glacier basin (yellow frame) within the Mont-Blanc massif; (b) overview of the Brenva glacier basin, the red frame indicates the location of the Brenva rock avalanche scar (ph.: Joëlle Hélène Vicari, 2 September 2021); (c) simplified geotectonic map of the Mont-Blanc massif (modified after Steck et al., 2001); (d) detail view of the Brenva rock avalanche scar showing the external boundaries of the 1997 rock avalanche (white dotted line) and two large rockfall events in 2016 (orange dotted line). Elevations are in m a.s.l. (For interpretation of the references to colour in this figure legend, the reader is referred to the web version of this article.)

Additionally, the southern region is primarily made up of fine-grained granite (Guermani and Pennacchioni, 1998). More specifically, the southeastern slopes of the Mont-Blanc massif are composed of rocks originating from the Helvetic basement (Fig. 1c). These consists primarily of granites with medium or coarse biotite, sometimes porphyritic, leucocratic veins, and subvertical magmatic foliation and show weak, low grade alpine metamorphism (Steck et al., 2001).

Slopes of the Italian side around the Mont Blanc summit, including the Brenva Spur, are very steep and composed mainly of granites and massive crystalline schists. Cataclastic and mylonitic zones, with a NE–SW strike, dip steeply to the northwest and alternate with these granites. A complex system of joints and faults breaks up the slopes (Bertini et al., 1985) and form a rock mass with multiple planes and fractures consisting of highly variable directions and densities. However, the shear zones of the 1997 rock avalanche are clearly visible in the source area (Barla et al., 2000). In this Italian region, highly fractured rock masses, steep slopes, and glacier retreat have resulted in frequent rock slope failures over the centuries (Deline et al., 2015). During the 20th century, the Brenva glacial basin saw two large rock avalanches. As a result of retrogressive failures originating from the same source, five large rock masses (Deline, 2009; Deline et al., 2015) fell from the east face of the Grand Pilier d'Angle between 14 and 19 November 1920. The total volume of the failed rock ranges between 2.4 and 3.6 $\times$ 10^6 m^3. On 18 January 1997, 2 $\times$ 10^6 m^3 of rock detached from the Brenva Spur. In the frontal part of the avalanche, two skiers were killed at Plan Pontquet near Entrèves (1306 m a.s.l.), and the shock wave destroyed a significant portion of the forest located on the other side of the slope (Deline, 2009; Fort et al., 2009; Giani et al., 2001). The 1997 Brenva rock avalanche scar was reactivated on 22 and 30 September 2016 with two large rockslide events estimated at (1.2 $\pm$ 0.3) $\times$ 10^4 and (1.5 $\pm$ 0.4) $\times$ 10^4 m^3, respectively. The maximum total volume of the two events was estimated to be about 3.4 $\times$ 10^4 m^3 (Fig. 1).

3. Materials and methods

3.1. Data acquisition

Following the reactivation of the Brenva rock avalanche scar in September 2016, SfM surveying was implemented to characterize the subsequent rock slope failure activity. Five helicopter flights performed between July 2017 and September 2021 enabled the manual acquisition of five series of high-resolution photographs of the scar using single-lens

reflex cameras. Further details of the surveys are shown in Table 1. Of the cameras used, only the Canon 7D Mark II had an integrated GPS system. However, this feature was not utilized during the data collection process. Additionally, none of the cameras were connected to any external GPS devices during the survey. Overlap between photographs varies from 60 to 80%. Due to the difficulties of access to the Brenva Spur, no ground control points (GCPs) were set during these surveys that would have been used for the generation of SfM models.

3.2. Data processing

3.2.1. 3D points cloud model generation

All the photographs were processed with Agisoft Metashape Professional (version 1.6.2) (AMP) software (Agisoft, 2020), a dedicated photogrammetric program that uses SfM-MVS (Multi View Stereo) algorithms to generate high resolution 3D models. The main workflow followed to generate 3D point clouds by AMP includes photo pre-inspection and importation, high accuracy photo alignment, and the generation of high-quality dense point clouds (Cook and Dietze, 2019). Due to the differences in camera resolution, the number of photos and the shooting distances, the density of the final SfM point clouds over the interesting part on the Brenva rock avalanche scar is variable. As a result, the surveys conducted in July 2017, August 2017, October 2018, September 2020, and September 2021 had average point cloud densities of 83 pts./m^2 (0.11 m point-to-point spacing), 42 pts./m^2 (0.15 m point-to-point spacing), 14 pts./m^2 (0.27 m point-to-point spacing), 84 pts./m^2 (0.11 m point-to-point spacing), and 24 pts./m^2 (0.20 m point-to-point spacing), respectively.

3.2.2. Georeferencing and registration of 3D model

These five sets of SfM points clouds were exported to CloudCompare (version 2.12. alpha) (CloudCompare, 2021) to perform further alignment and comparisons. The 3D point cloud (1 m resolution) extracted from the 2008 Digital Terrain Model (DTM) of the *Valle d'Aosta Autonomous Region* was used as the reference for the geolocation of the 3D point clouds obtained by the SfM photogrammetry surveys. Initially, rough alignment was carried out by picking at least three feature-based point pairs from the entire 3D point cloud. Then, an iterative closest point (ICP) algorithm (Besl and McKay, 1992) was applied to improve the coarse alignment by minimizing the root mean square error (RMSE) between the 3D point clouds and meshes (Abellán et al., 2010). Next, two manually selected areas were considered as stable, and the ICP was applied. The transformation matrix obtained by this process was applied to the remaining portions of the datasets that were considered as unstable. The 3D mesh was generated using the Poisson Surface Reconstruction algorithm (Kazhdan and Hoppe, 2013) and was completed in 3DReshaper software (Hexagon-Technodigit, 2016) and CloudCompare. It is worth noting that to address the absence of GCPs, the points cloud was divided into several smaller parts that were aligned independently by the ICP algorithm one by one.

3.2.3. Change detection and noise filtering

The cloud-to-mesh nearest orthogonal distance (C2M distance) (Kiryati and Székely, 1993) was computed to detect surface change between two models. As a result, each point on the 3D model was assigned a scalar value corresponding to the C2M distance. Surface changes with positive and negative values are caused by an accumulation (e.g., debris, snow) or a loss (e.g., rockfall, snow melting), respectively. A visual inspection of the RGB images helps identify artefacts (shown as positive changes) along the model's edges. The raw C2M distance was denoised using a noise filter (Abellán et al., 2009) based on the nearest neighbour averaging algorithm to remove spatial noise caused by doming and spike phenomena that arise in the process of photographic 3D modelling (Guerin et al., 2017). The value from 100 neighbours was chosen for the denoising process for all the datasets in our study. Then, change detection thresholds were set to twice the standard deviations of the C2M distance for the parts supposed to be stable (Abellán et al., 2009), resulting in detection thresholds of 0.28, 0.48, 0.50, and 0.50 m for the 4 successive comparisons, respectively.

3.2.4. Rockfall clustering and volume calculation

All points whose calculated C2M distance was below the threshold of detection were removed from the point cloud. The change plots and RGB photos were inspected to identify points related to rockfalls (Tonini and Abellan, 2014). Subsequently, the clusters of points associated with rockfalls were manually delineated and segmented. The rockfall volume calculation was performed using the 3D alpha-shape method following the guidelines suggested by Guerin et al. (2017) and Van Veen et al. (2017).

An example of the change calculation and rockfall sources detection method applied to the comparison between July 2017 and October 2018 that follow the above processes (Fig. 2) is shown in Fig. 3.

3.3. Structural analysis

Using georeferenced 3D point cloud data obtained with SfM photogrammetry and Coltop3D software (Jaboyedoff et al., 2007), we created a 3D shaded, coloured relief map that reveals topographic orientation (slope aspect and slope angle). This approach enabled us to conduct topographic structural analysis, which is crucial for studying rock mass slopes at high elevations. These areas are often remote and inaccessible, making conventional field investigations challenging. By employing this method, we detected discontinuities responsible for rock slope instabilities. On the Brenva rock avalanche scar (Fig. 4), we identified a total of seven main joint sets (rock face (RF) and J1 to J6). To gain a better understanding of how discontinuities contribute to progressive slope failure, it is essential to determine the families of discontinuities involved in past events. To achieve this, we exported the point cloud of each discontinuity family from Coltop3D and imported them into CloudCompare. Subsequently, we linked the point clouds independently with the locations of rockfall sources on the 3D model (Matasci et al., 2018). Through this method, we could determine the number of rockfalls each joint set was involved in.

3.4. Defining the rock instability scenarios

3.4.1. Instability scenarios based on the structural analysis

In the context of steep rock slopes, the significance of main discontinuities in determining potential instability is widely acknowledged (Stead and Wolter, 2015; Wyllie and Mah, 2004). These discontinuities,

Table 1
Key features of the five helicopter-based SfM photogrammetry surveys.

	Survey 1	Survey 2	Survey 3	Survey 4	Survey 5
Date of acquisition	4th July 2017	25th August 2017	23rd October 2018	18th September 2020	2nd September 2021
Camera model	Nikon D810	Nikon D700	Canon EOS 7D Mark II	Canon EOS 7D Mark II	Sony ILCE 7 M2
Image resolution (pixels)	7360 × 4912	4256 × 2832	5472 × 3648	5472 × 3648	6000 × 4000
Focal length (mm)	50	24	24	100	35
Number of processed images	600	62	162	367	126
Average size of images (MB)	15	9.8	7.7	9.3	6.3

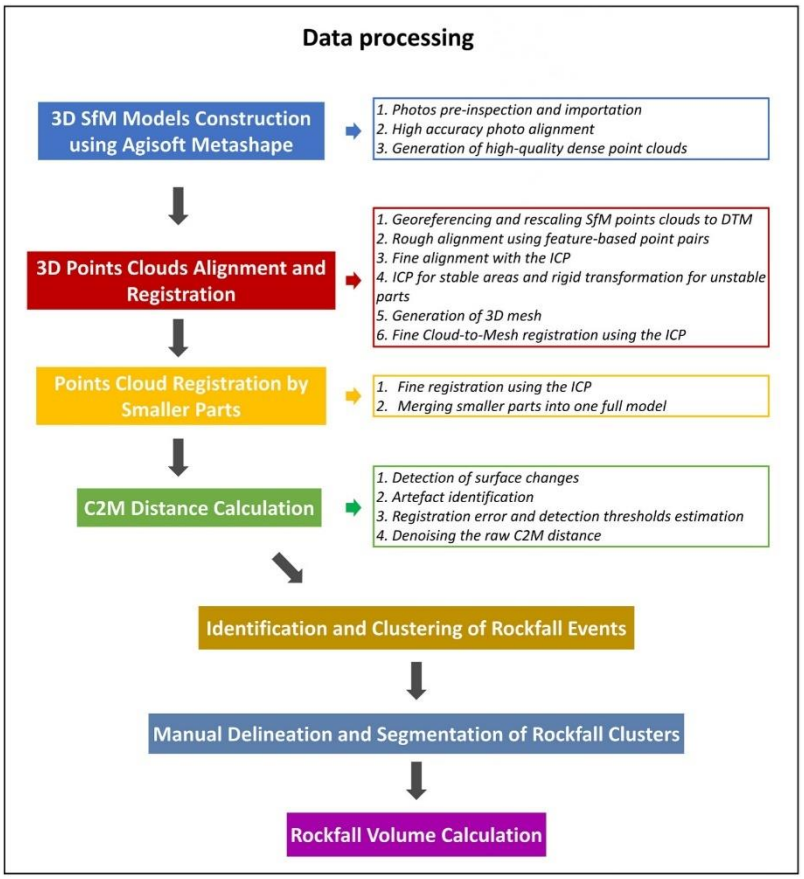

Fig. 2. Flowchart of the 3D points cloud processing for the rockfall detection and volume estimation.

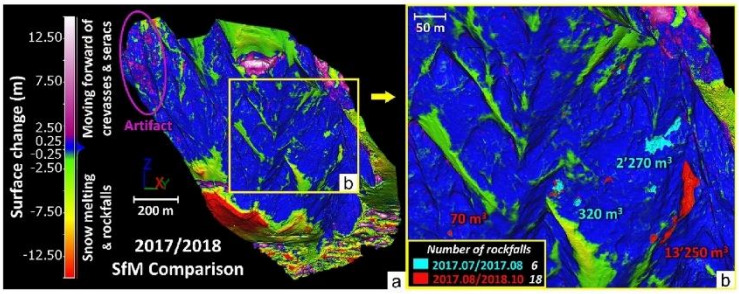

Fig. 3. Results of the change detection between July 2017 and October 2018. (a) Filtered point-to-mesh differences between the 2017 point cloud and the 2018 reference mesh. Positive surface changes correspond to debris and snow accumulation. Negative surface changes indicate rockfalls and snow melting. (b) Detail of the surface change and the locations of the rockfall sources (indicated in light blue and red) in Panel a. (For interpretation of the references to colour in this figure legend, the reader is referred to the web version of this article.)

which are visible at rock outcrops, can be examined by analyzing their intersecting characteristics, thereby identifying critical rock mass structures (Jaboyedoff et al., 2020). By integrating a 3D points cloud with a visual inspection of the RGB image of the scar, it becomes possible to assess the extent of potential instability scenarios, referred to as the "failure volume". This assessment mainly involves fitting planes on the exposed portions of relevant unfavourable discontinuities and analyzing the interrelationship, which aims to delineate the large kinematically unstable rock mass, between the extrapolated planes of various exposed joints. The following procedure outlines the detailed methodology employed for defining instability scenarios based on the 3D point cloud data.

1. Define at least three unfavourable discontinuities, permitting the large kinematically mobilization, based on the major historical slope

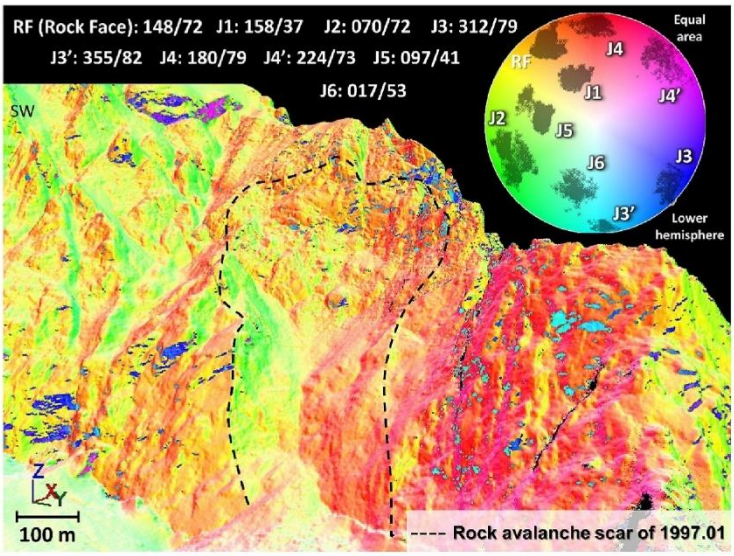

Fig. 4. Results of the structural analysis performed on the 2018 SfM 3D point cloud. Seven main joint sets were detected within the Brenva rock avalanche scar (spatial orientation of dip direction/dip angle is indicated by degrees). The stereographic projection displays the poles of each joint set (Schmidt stereoplot, equal area, lower hemisphere).

failure features and the spatial distribution characteristics of the main discontinuities identified in Section 3.3.

2. Extrapolate each discontinuity and fit unconstrained planes to intersect each other and delineate the contour of the instability in CloudCompare.
3. Separate out and calculate the volume delineated by the slope surface and the fitted planes.

3.4.2. Instability scenarios based on the SLBL method

The SLBL method was developed from the concept of base level in geomorphology (Jaboyedoff et al., 2019, 2020). It refers to a lower limit of the erosion process and is represented by a surface that is defined based on the altitude of streams. The SLBL method applies a similar principle to calculate the surface elevation above which the rock mass is considered susceptible to erosion. This calculation provides a potential 3D failure surface for determining the volume of instability of slopes when applied to a gridded DEM. Before calculating the failure surface, the instability's limits or perimeter must be defined using geomorphic features such as streams or morphological instability features. For example, the base of the unstable mass could be identified as either the bottom of the valley or a change in the slope angle, while the top could be defined as tension cracks or any trace of main discontinuities. The lateral boundaries could be determined by the extent of the upper geomorphic feature. Subsequently, the failure surface can be obtained using the following iterative routine (Jaboyedoff et al., 2020):

1. At each iteration *t* (Fig. 5), for each grid node of the DEM, the SLBL method is calculating an "average" altitude $z_{temp}(t)_{i,j}$ of all the four direct neighbouring altitudes of the previous iteration $z_n(t-1)_{i,j}$, minus a positive, constant *C*(tolerance), *i,j* represents the number of the node, i.e., for example:

$$z_{temp}(t)_{i,j} = \frac{\left(z_n(t-1)_{i,j+1} + z_n(t-1)_{i,j-1} + z_n(t-1)_{i+1,j} + z_n(t-1)_{i-1,j}\right)}{4} - C \quad (1)$$

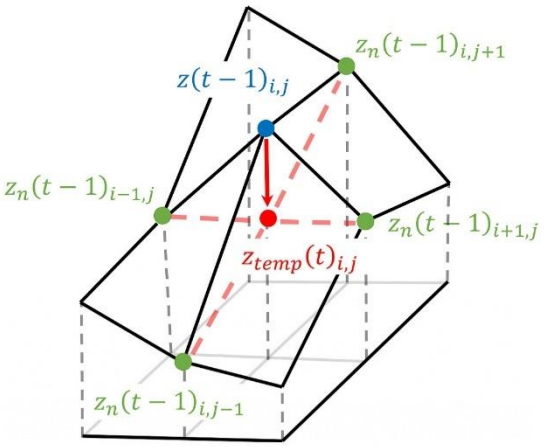

Fig. 5. Illustration of the SLBL iteration process (modified after Jaboyedoff et al. (2009)).

2. This process can be performed by either a simple average of a given number of neighbours or by fitting a surface. The result is a new grid which is compared to the previous one, and if $z_{temp}(t)_{ij} < z(t-1)_{i,j}$, then $z(t)_{ij} = z_{temp}(t)_{i,j}$; otherwise, the value is unchanged. An additional condition can be added by limiting the $z(t)_{i,j}$ value changes by another DEM or by assuming a limiting slope angle.
3. This calculation is performed iteratively and repeated until all the differences over the grid are smaller than a given threshold.

After the sliding surface is generated in 3D, the sliding volume is determined by comparing it with the original DEM.

3.5. Power-law and statistical analysis

It is possible to deduce the power laws that link the magnitude of a particular natural event to its frequency based on statistical analysis. For future events, these mathematical relationships can be employed to predict their type, extent, return time, and magnitude. Dussauge et al. (2003), Hungr et al. (1999), and Williams et al. (2018) found that rockfall volume and cumulative rockfall frequency have a demonstrated relationship, which can be visualized by using a complementary cumulative distribution function (CCDF) that is commonly adopted, as it avoids the ambiguities caused by the subjective selection of the bin size within the probability density function (PDF) method (Bennett et al., 2012; Strunden et al., 2015). The relationship is described by a power-law as follows (Hantz et al., 2003; Hungr et al., 1999):

$$N(V) = a\,V^{-b} \tag{2}$$

where N is the cumulative number of rockfalls larger than or equal to the volume V (in m^3) per unit of time, with a and b representing the preliminary factor and power-law exponent, respectively. Rockfall activity is directly connected to parameter a, which represents rockfall frequency, and the slope of the power-law is related to the b component. Specifically, a higher value of a means that more frequent rock failures occur, and a higher value of b indicates that the proportion of smaller rockfall volumes is more significant than that of larger rockfall volumes. The value of b can be estimated either by a least squares linear regression or the maximum likelihood estimation (MLE) approach proposed by Aki (1965):

$$b = 1/ln(10)(\langle logV > - logV_0) \tag{3}$$

Where $ln(10)$ is a constant, $< logV >$ is the average value of $logV$, and V_0 is the minimum volume considered (cut off volume) for the fitting, above which the power-law relationship is robust (Dussauge et al., 2002).

Assuming that the rockfall volumes follow a power-law frequency distribution, and because of the limitation of the short span of monitoring in natural environments, which would lead to epistemic uncertainties in the statistical model and prevent an exact prediction of the return period for a particular volume for a rock failure event (Straub and Schubert, 2008), we used Monte Carlo simulations to estimate the confidence intervals (uncertainties) of the return period of the potential rock failure scenarios. The simulation principle is done by simply inverting a certain sets of the power-law generating volumes, rather than removing a certain amount of sample from the large database and repeating the simulations, as suggested by Strunden et al. (2015):

$$V = \left(\frac{F_{min} + rand \times (F_{max} - F_{min})}{a}\right)^{\frac{-1}{b}} \tag{4}$$

where *rand* is a random number between 0 and 1, constant a and b hold same meaning as described in Eq. (2), and F_{min} is the minimum frequency corresponding to the approximate time separating the 1997 event from subsequent events. F_{max} is the maximum frequency corresponding to the high rockfall frequency between 2017 and 2021 in this case. In this approach, 1×10^5 datasets of rockfall inventories were simulated. It's important to emphasize again that the validity of this proposed statistical approach depends on the assumption that the rock failure volume distribution follows a power law.

4. Result

4.1. Rockfall occurrence and involved structures

Comparisons between 3D SfM point clouds allowed to identify the volumes of rock that fell from the scar, except for areas obscured by snow. As a result, the volume of the rockfall source inventory for the entire Brenva rock avalanche scar between 2017 and 2021 was established. The results showed 39 rockfall source areas, with volumes ranging from 11 to 13,250 m^3: 6 rockfalls occurred between July and August 2017, 18 between August 2017 and October 2018, 11 between October 2018 and September 2020, and 4 between September 2020 and September 2021 (Fig. 6). The total accumulated volume of rockfalls between 1997 and 2021 is approximately 2.05×10^6 m^3. In average, 9.75 events occurred per year (5600 m^3) during the period 2017–2021. Both the average volume (or corresponding area) and number of events each year on the Brenva rock avalanche scar has decreased in recent years (Table 2). However, the frequency of events before 2017 could be higher even though only two significant events in 2016 were listed. The rock face erosion rate was calculated by dividing the related failure volume by the scar area (3.74×10^6 m^2). Table 2 reveals that the erosion rate of the rock wall was significantly higher at 44 mm/year during the period of 2017 to 2018 compared to the subsequent period of 2018 to 2021 (1.3 mm/year). The average erosion rate from 2017 to 2021 was 15.5 ± 2.3 mm/year. Additionally, a noticeable trend can be observed in the average depth of rockfall scars, which has progressively decreased from 1.8 m in 2017 to 0.6 m in 2021. Similarly, the average maximum scar depth has decreased from 3.7 m to 1.7 m. The largest rock failure was approximately 1.3×10^4 m^3 (Fig. 6). It occurred, between 2017 and 2018; the corresponding scar was first observed on the 02 September 2018. It is the only event that exceeded the magnitude of 1.0×10^4 m^3 during our investigation, resulting in a high erosion rate. This event was triggered on the steep ridge of the scar, where a subvertical rock face was formed by the 1997 rock avalanche and remained exposed to gravitational readjustment for 21 years. Such a large event detached from the scar is less frequent than small boulder falls. Specifically, we only documented two instances of large event in 2016 and one in 2018.

The rockfalls detected during the investigation were not clustered in specific areas, but smaller rockfalls occurred more easily in the highly fractured zone (Fig. 7) of the scar where restricted movements are expected to partly affect the upper smaller instability scenarios. Unfortunately, we could not trace the distribution of rockfall deposits, as it's challenging to determine the exact location where the rockfall has settled based on annual remote sensing surveys, especially considering the impact of melting glaciers and snow at the base. The statistical results (Fig. 8) show that the families of discontinuities RF, J1, J2, J4, and J5 are most often involved in these 39 events. Generally, the developed and persistent J1 discontinuity served as the basal plane of sliding in most detected rockfall cases. J2, J4 and J5 formed the lateral release face that constrained the volumes. The traces of the same joint sets as RF (indicated by the long purple dotted line in Fig. 7) are still extensively exposed in parallel at the top of the Brenva rock avalanche scar. The highly persistent discontinuity, RF, played a significant role as the large back release surface in the 1997 rock avalanche. Considering the importance of RF in historical large events and recent 39 boulder falls, we need to fully consider the role played by the RF discontinuity in defining potentially reasonable large rockfall scenarios in the future, which is described in Section 4.2.

4.2. Potential slope failure volumes

The primary progression of rock failure occurs at the intersections of major joints (Stead and Wolter, 2015). We adopted an assessment approach that incorporates both the analysis of exposed discontinuities and the SLBL concept outlined in Section 3.4 to evaluate potential failure volume scenarios. This approach led to the identification of seven rock failure scenarios, labeled as S_1 to S_7, based on their volume magnitude from smallest to largest. Among these scenarios, three were identified through geo-structural analysis, while four were derived from the SLBL concept. In the subsequent sections, we will provide a comprehensive

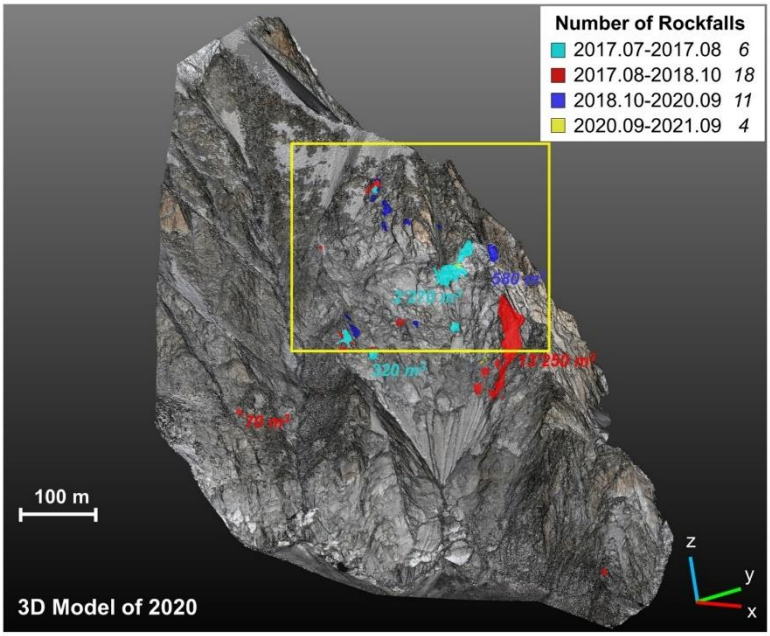

Fig. 6. Rock failure activity highlighted for the Brenva rock avalanche scar by employing SfM monitoring from July 2017 to September 2021. 39 rockfall sources were detected during this period. The zone demarcated by the yellow rectangle corresponds to the background photo shown in Fig. 7. (For interpretation of the references to colour in this figure legend, the reader is referred to the web version of this article.)

Table 2
Characteristics of the rockfalls between 2017 and 2021 in the Brenva Spur.

Periods	Rockfalls number	Total failure volume (m^3)	Total failure scar area (m^2)	Average scar depth (m)	Average maximum scar depth (m)	Erosion rate (mm/year)
07/2017 to 10/2018	24	20,576 ± 2563	6180 ± 214	1.8 ± 0.7	3.7 ± 0.6	44 ± 5.5
10/2018 to 09/2020	11	1740 ± 612	1225 ± 54	1.2 ± 0.5	2.5 ± 0.2	2.3 ± 0.8
09/2020 to 09/2021	4	121 ± 95	190 ± 34	0.6 ± 0.3	1.7 ± 0.2	0.33 ± 0.2

overview of the results obtained from both methods.

4.2.1. Scenarios defined by structural analysis

It is worth noting that there are some assumptions in the procedure described in Section 3.4.1, such as that the scenarios defined here are supposed to represent one single detachment each and that the main joints have enough persistence under the rock mass to intersect each other. The mentioned assumptions are applicable when considering the specific case of the large rock avalanche event in 1997 that is constrained by the top tension crack developed from high persistent RF under the force of gravity, lateral limit J6, and basal plane stepped J1. Following the above approach and assumptions, we characterized three largest potential rock failures of the Brenva Spur resting on the unfavourable basal plane J1. The geometric characteristics and the volumes of three scenarios (S_3, S_5, and S_7) identified by such geo-structural constraints are shown in Fig. 9. The largest rock mass failure scenario (S_7) has a calculated volume of 4.8×10^6 m^3. This volume was delimited by J1 (basal sliding plane), J6 (lateral limit plane), and RF (upper limit plane), which could be an extreme and potential continuation scenario of 1997 rock avalanche. S_7 shows a wedge sliding failure mode plotted by Dips (Rocscience, 2022) (Fig. 10). S_3 is bounded by J1 (basal sliding plane), J4 (lateral limit), and J6 (lateral limit). S_5 are bounded by J1 (basal sliding plane), J2 (lateral limit), and J5 (bottom limit). S_3 and S_5 exhibit similar kinematically unstable characteristics as S_7 and could be potential sub-level continuations of the 1997 event.

4.2.2. Scenarios defined by SLBL method

As mentioned in Section 3.4.2, before using the SLBL method, the limits of the potentially unstable rock mass should be defined. In this study, the structural and morphological characteristics of the Brenva spur are considered in defining the perimeter of potential instability, for instance, particular attention is given to notable features like the distinct RF trace adjacent to the scarp of the 1997 scar and the niche present on the summit. Four scenarios (S_1, S_2, S_4, and S_6) were defined based on the trace of joint set RF as the upper limit and the traces of joint sets J2, J4, and J6 as the lateral boundaries. The lower limit, referencing the base, corresponds to the slope angle break below the main scarp. Scenario S_1, with a calculated volume of 3.1×10^4 m^3, primarily encompasses the niche located at the top. S_2 and S_4 have a larger coverage area, extending southwest from S_1. S_6 expands northeastward, reaching the edge of the scar, building upon the foundation established by S_4. The failure volume and thickness, computed using the SLBL criteria, are illustrated in

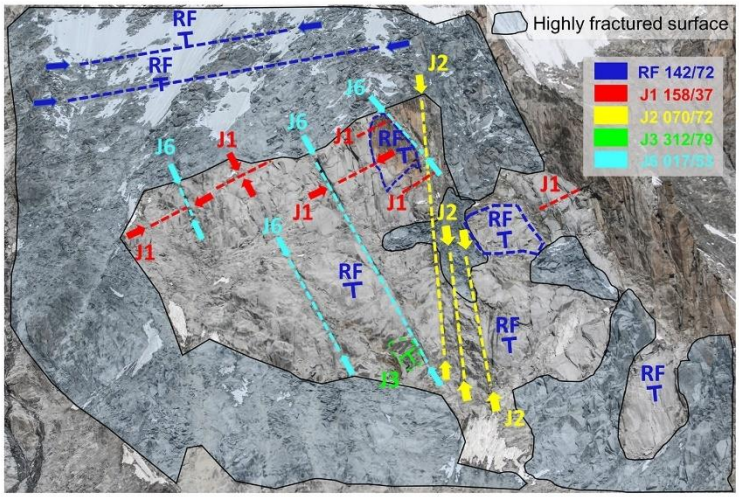

Fig. 7. Highly fractured scar surface located at the top of the Brenva rock avalanche scar (the background photo refers to the yellow rectangular area shown in Fig. 6). The main discontinuities, RF, JI, J2, and J6, were located on the scar and intersected with each other. Most of the small boulders fell from the highly fractured zone delineated by the closed black polyline. (For interpretation of the references to colour in this figure legend, the reader is referred to the web version of this article.)

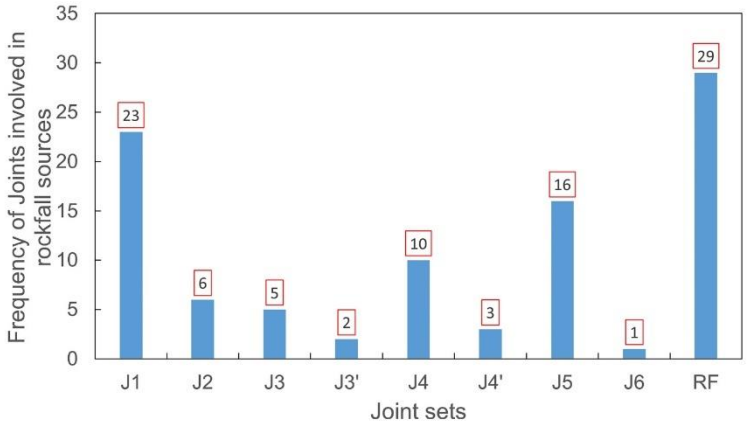

Fig. 8. Statistical distribution of the discontinuities involved in the 39 detected rockfall sources. The number in the red frame indicates the number of rockfalls related to the corresponding joint. RF (rock face), J1, J5, and J4 are the joint sets most involved in a rockfall in sequence. (For interpretation of the references to colour in this figure legend, the reader is referred to the web version of this article.)

Fig. 11.

We conducted a comparison between volumes computed using the SLBL method and those estimated from the structure-based analysis conducted in the previous step. The results indicate that the volumes of scenarios S_1, S_2, and S_3 were of similar magnitude, ranging from 3.1×10^4 m^3 to 8.0×10^4 m^3. In contrast, scenarios S_5 (reconstructed using structural analysis) as well as S_4 and S_6 (reconstructed using the SLBL method) exhibited higher magnitudes, ranging from 1.3×10^5 m^3 to 8.0×10^5 m^3. Comparing S_1 and S_2 with S_3, and S_4 with S_5, and S_6 with S_7 reveals that the volumes obtained using the structural analysis consistently exceed those obtained using the SLBL method. This can be attributed to the fact that the structural analysis-based approach does not account for interruptions caused by minor discontinuities (composite structures) or the presence of rock bridges, resulting in a simplified sliding surface and larger volume estimates. Conversely, the SLBL method creates a potential failure surface by interpolating the instability limit without considering identified structures such as J1 (bottom plane), which is assumed persistent and acts as the basal sliding plane in most instability scenarios defined by the structural approach.

4.3. Volume-Frequency (V-F) relationship

The method described in Section 3.5 has been used to estimate the volume-frequency (V-F) relationship for rockfalls and rock avalanches that is distributed according to a power law. Not all small events were observed and listed during the period before 2017, which may be conservative and give rock failure a calculated return period differing from its actual occurrence but agreeing with the power law. The relationship

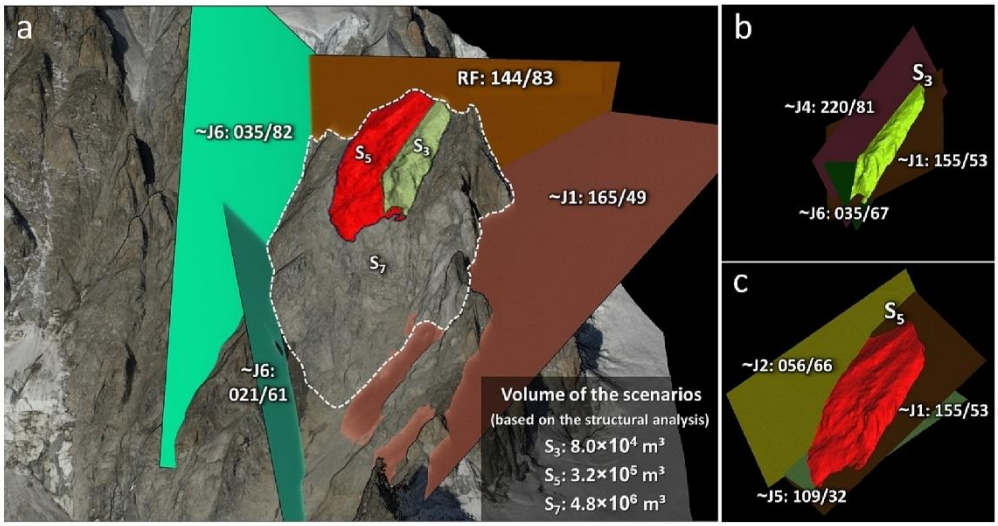

Fig. 9. (a) Representation of three (S_3, S_5, and S_7) of the seven defined large scenarios. S_7 controlled by discontinuity planes J1, J6, and rock face (RF), which were identified on the Brenva rock avalanche scar by the SfM model and RGB photos. (b) Plot of S_3 controlled by J1, J4, and J6. (c) Plot of S_5 controlled by J1, J2, and J5.

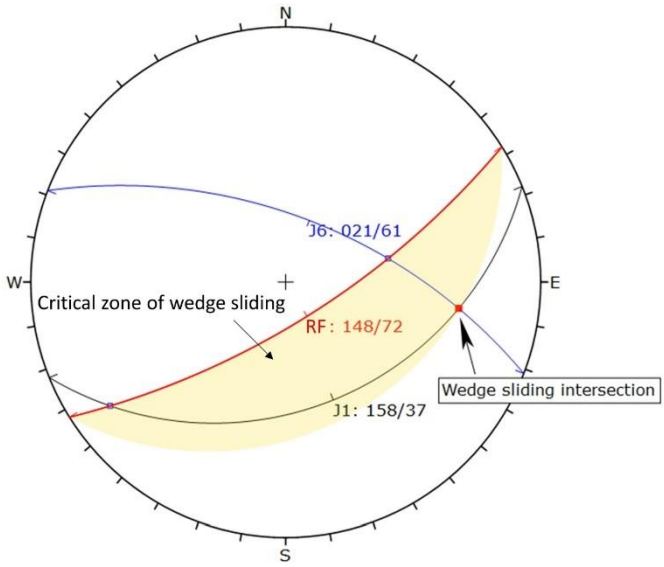

Kinematic Analysis	Wedge Sliding		
Slope Dip	72		
Slope Dip Direction	148		
Friction Angle	30°		
	Critical	Total	%
Wedge Sliding	1	3	33.33%

	Color	Dip	Dip Direction	Label
User Planes				
1		72	148	RF: 148/72
2		37	158	J1: 158/37
3		61	21	J6: 021/61

Plot Mode	Pole Vectors
Vector Count	0 (0 Entries)
Intersection Mode	User Planes
Intersections Count	3
Hemisphere	Lower
Projection	Equal Angle

Fig. 10. Kinematic analysis for the main joint sets involved in the defined extreme scenario S_7 using structural analysis. The black circular arc indicates J1, the red circular arc indicates the rock face (RF), and the blue circular arc indicates J6. The red solid rectangle indicates the intersection of J1 and J6, which is in the light orange zone (referred to as the critical zone of wedge sliding). (For interpretation of the references to colour in this figure legend, the reader is referred to the web version of this article.)

differs if we consider only the events from 2017 to 2021 or if we include two large events from 2016 and one from 1997 (Fig. 12). The corresponding power law fittings are as follows: $N(V) = 48.65\ V^{-0.58}$ and $N(V) = 33.78\ V^{-0.47}$ obtained using least square linear regression (LR). In this case, the minimum, or cut off, volume (V_0) of the power law fitting is set as 11.35 m^3. No apparent truncation or rollover and tail are observed from the distributions. The value of the latter power-law fitting exponent b is equal to 0.47 and 0.43 ± 0.14, which was estimated using LR and MLE within the CCDF approach, respectively. Both values are in the range of an average value of 0.5 ± 0.2 for subvertical rock slopes and close to the value from Dussauge et al. (2002, 2003) and Hungr et al. (1999). The MLE yields a lower exponent than the LR, which indicates that larger volumes dominate the tail of the power law decay produced by MLE, or that a particular large rock failure has a shorter return period

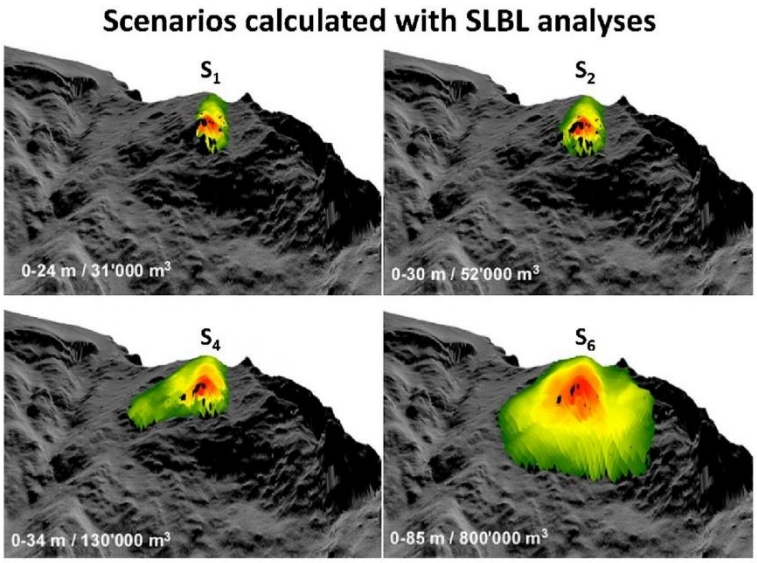

Fig. 11. Four (S_1, S_2, S_4 and S_6) of seven large potential failure volumes identified by the SLBL concept shown with the DEM shading of the Brenva rock avalanche scar.

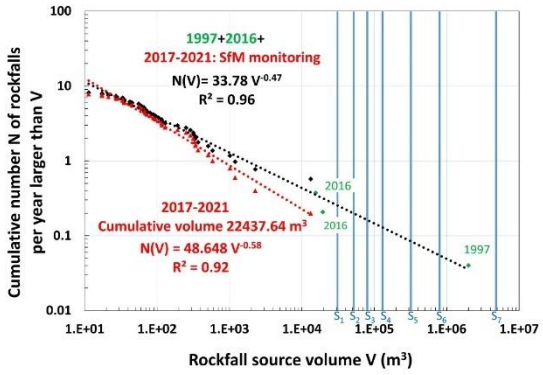

Fig. 12. Rockfall source volume-frequency relationship for the Brenva rock avalanche scar between 1997, 2016 and 2017–2021. Red and black data points are from SfM monitoring (2017–2021), and green data points are the 1997 and 2016 historical events. The black dashed line indicates the power law fitting for the 42 rock failures using least square regression, while the red dashed line indicates that for 39 rockfalls from 2017 to 2021. S_1 to S_7 represent seven potential rock failure scenarios defined by the combination of structural analysis and SLBL, as discussed in Section 4.2. (For interpretation of the references to colour in this figure legend, the reader is referred to the web version of this article.)

and a higher frequency by MLE, which is not supported by historical inventory.

Graber and Santi (2022) concluded that the maximum rock failure volume recorded by the historical inventory poses a more significant influence on the value of scaling exponent *b* than the minimum volume. They accomplished this by regressing these two types of volumes and by applying the scaling exponent *b* derived from published references. Undersampling large rock failure events in the fitting power-law tail profoundly affects the capacity to determine the frequency of future larger magnitude events. This also implies that the maximum rock failure magnitude in the inventory would be beneficial to constrain the unrealistic extrapolation and to obtain the accurate frequency or return period of larger failure events. These very large events are generally missing in studies on recent dynamics such as Ravanel et al. (2017). Therefore, we use the power-law fitting $N(V) = 33.78\ V^{-0.47}$ that included three large historical events as the basis for the following return period analysis and interpretation. Based on this fitting, we can preliminarily assume that an event greater than or equal to 1×10^5 m^3 could occur every 6.6 years, while events greater than or equal to 1×10^6 m^3 could occur every 20 years. Additionally, rockfalls with volumes greater than or equal to the maximum scenario (4.8×10^6 m^3) would occur approximately every 41 years, though this is not observed. The frequency of events with volumes between 1×10^5 m^3 and 8×10^5 m^3 would occur every 11 years, which is close to the observed event frequency but still high for the present situation. At last, if we extrapolate the return period of the 1997 event (25 years ago) using the $N(V) = 48.65\ V^{-0.58}$ (2017 to 2021), it yields a value of 93 years that does not align with reality. This discrepancy indicates the impact of large events on the constraints of the power law distribution (referring to the *b*).

5. Interpretation and discussion

5.1. Rock failure feature and rock wall erosion

The power law distribution observed in the study fits well and does not exhibit clear truncation (Fig. 12). The absence of truncation is likely attributed to the limited observations of small events before 2017 that are yet very numerous in the Mont-Blanc massif (Ravanel and Deline, 2010, 2013). Slope failures can be divided into two types of processes based on the power-law distribution. 1) One kind of failure is the small magnitude, but very frequent, boulder falls and/or rockfalls from a highly fractured zone of granite. The stronger fitting distribution usually appears among the volumes of these types of failures. 2) Another type of failure consists of larger rock failure event that occurs with much less frequency along the intersections of the established discontinuities (Bennett et al., 2012; Katz and Aharonov, 2006). The larger the involved

rock failure volume is, the longer it takes to develop the conditions that make it prone to collapse (Abele, 1994; Bolla and Paronuzzi, 2020) also in permafrost-affected areas (Gruber and Haeberli, 2007; Hartmeyer et al., 2020a; Messenzehl and Dikau, 2017). The upper and gentler slope (48°) of the Brenva scar, characterized by highly fractured granite and exposed isolated blocks, experiences a higher frequency of small boulder detachments, with 22 rockfalls smaller than 100 m^3 recorded. Notably, the prominent discontinuities, such as J2, J6, and RF, as well as the north-eastern subvertical ridge (Fig. 7), greatly control the stability of the rock wall. Along these discontinuities and ridge, four rockfalls exceeding 1000 m^3 in size have been identified, comprising 80% of the total volume. The occurrence of these rockfalls (locate at the tail of the power law distribution) has directly contributed to the pronounced erosion rates evident on the rock wall.

During the five-year monitoring period, the average erosion rate of the rock wall was 15.5 mm/year. Specifically, between 2017 and 2018, the erosion rate reached 44 mm/year. The recent erosion rate from 2020 to 2021 has decreased significantly to 0.33 mm/year. When compared to other rock walls, this average erosion rate is much lower than the erosion rate observed at Drus (French side of Mont Blanc massif), which was 121.3 mm/year from 2005 to 2011 (Guerin et al., 2020). On the other hand, it is higher than the erosion rate at Gemsstock (2961 m a.s.l., Swiss Alps) (6.5 mm/year between 2006 and 2010) and at Tour Ronde (3792 m a.s.l., French Alps) (8.4 mm/year between 2005 and 2006) (data extracted from Hartmeyer et al. (2020a)). Furthermore, compared to the erosion rate of 10.32 mm/year on the Kitzsteinhorn (3060 m, a.s.l., Austrian Alps) north face in a cirque environment (recently deglaciated area) during 2011–2017 (Hartmeyer et al., 2020b), the erosion rate at our monitored rock wall is higher. However, it is important to note that the highest retreat rates in the proximal areas (closer to the glacier surface) of the Kitzsteinhorn (north face) reached 57.32 mm/year, surpassing the rate observed for Brenva between 2017 and 2018. From a long-term perspective, it is worth noting that erosional processes exhibit high discontinuity and temporal variability. Typically, the mean rock wall retreat rates (long term) for the reported cirques in high altitudes are below 1.0 mm/year (Hartmeyer et al., 2020b). Based on the remarkably high erosion rates described before in the high Alps since 2005, all the findings consistently indicate enhanced rock wall retreat during deglaciation, despite the inherent challenge of comparing geomorphic evidence across significantly different spatiotemporal scales.

5.2. Driving factors of rock failure

Due to the slope aspect and high elevation, the small rock detachments in the fractured zone on the Brenva scar are driven primarily by the initial condition of the slope, such as a well-developed fracture network coupled with mechanical weathering (probably driven by the thermally induced stress from cooling-heating cycles (Guerin et al., 2019)), frost weathering (caused by freeze–thaw cycles (Viani et al., 2020)), the seepage of rainwater and melting snow that induces hydraulic pressures in fractures (Krautblatter et al., 2013) (a snow source and water run-off can be seen on the upper slope and the left gully in the summer, as shown in Fig. 7), and cryogenic processes within the active layer of the permafrost (subsurface layer that thaws seasonally) (Legay et al., 2021).

However, outside of fundamental factors such as topography and structural features, the effects of climate change on the Brenva rock avalanche scar are also worth considering. Some recent large rockfalls in Mont-Blanc massif and the enhanced rockfall activities during the heat waves of 2003 and 2015 showed the impact that the permafrost degradation and glacier retreat caused by global warming has on rock instability (Deline, 2001; Ravanel et al., 2010, 2017; Viani et al., 2020). Gradually, permafrost thaw associated with unexpected heat waves over the past few decades/years might have contributed to the rock collapses in 2016 and 2018 since rock failure caused by such climate warming effects could occur rapidly or with a delay of only months or years (i.e., a direct response) (Gruber et al., 2004) by the deepening of the active layer and/or by the warming of the permafrost at depth. These parameters are measured since 2010 in 10-m-deep boreholes at the Aiguille du Midi (3842 m a.s.l.; (Magnin et al., 2015)), on the French side of the Mont-Blanc massif, 4.7 km north of the Brenva Spur. The southern borehole is located at 3753 m a.s.l. on a slope that is geologically and topographically very similar to the Brenva spur. In this south face, the average depth of the active layer for the years 2010, 2011, 2014 and 2015 (no data for 2012 and 2013) was 5.5 m with a maximum of 5.9 m for 2011. For 2016, 2017 and 2018, the depth of the active layer was quite homogeneous and much more important with an average of 6.9 m, i.e., 1.4 m more than for the previous years, indicating an accelerated degradation of the permafrost in those years. At a depth of 10 m, the mean annual rock temperature rose by >0.5 °C between 2010 and 2018, from −1.6 to −1.1 °C, again indicating a significant warming that might have contributed to the triggering of the main events of 2016 and 2018 at the Brenva Spur, which also can be strengthen by the rockfall scar depth decreasing from 3.7 m (2017–2018) to 1.7 m (2020-2021).

To other elements support the role of the permafrost degradation in the triggering: ice was observed at the scar after the event (see e.g. Cremonese et al., 2011), and the timing of the event (end of September) corresponding roughly to the period during which the depth of the active layer is maximum at the Aiguille du Midi. In addition, it can be assumed that the ridge that collapsed in 2018 seemingly experienced a faster and deeper thaw than other areas on the scar due to its sharp topography (Noetzli et al., 2003), especially after experiencing two summer heatwaves in 2003 and 2015 in the Mont-Blanc massif. Despite the lack of direct evidence for individual cases of rock slope instability and the lack of timing information on rockfalls, along with temperature and rainfall data, the impact of warming permafrost on rock failure cannot be ruled out for the Brenva rock avalanche scar. In such a remote environment it is almost impossible to have a permanent survey of the topography like the study by Williams et al. (2018). As the temperature rises rapidly in higher mountains (Gobiet et al., 2014), the magnitude and frequency of rock failure would exhibit uncertainty and likely occur at rates beyond the historical range in the future. Overall, the knowledge gained from rockfall activities in high mountains caused by permafrost degradation confirms the necessity of conducting continuously updated risk assessments for potential extreme rock instability scenarios on the 1997 Brenva rock avalanche scar.

5.3. Extrapolated return period of potential scenarios and uncertainty

Return period estimation is important in rockfall hazard assessment because it provides valuable information about the frequency at which rockfall events of a certain magnitude are expected to occur in a given area. It helps in understanding the long-term behavior and likelihood of future rockfall events, which is crucial for effective rockfall or rock avalanche hazard mitigation and management. We use the power law distribution calculated in the Section 4.3 (see the slanted red solid line in Fig. 13a) to extrapolate the return period of those defined 7 scenarios and use the Monte Carlo simulation to estimate the corresponding statistical uncertainties. Applying Eq. (4) for the 1.0×10^5 simulations of the distribution and assuming values for the minimum frequency, $F_{min} = 1/(25 years)$, and maximum frequency, $F_{max} = 39/(5 years) = 7.8$ events per year, it emerges that events of $>1.0 \times 10^4$ m^3 (served as the reference scenario S_0) have an approximately 50% chance of occurring every 2.1 years (simulated median power law fitting is indicated by bold slanted black solid line in Fig. 13a. However, during the 5 years of observation, the rock failure events seem to have exceeded this volume (S_0) only once. This event has a volume of 1.3×10^4 m^3, it can be assumed that at least one event was larger than 1.0×10^4 m^3 in five years. Based on above observation and assumption, we can evaluate the power-law fitting of these data. Using the observed frequency of approximately 0.2 events per year to exceed 1.0×10^4 m^3, we

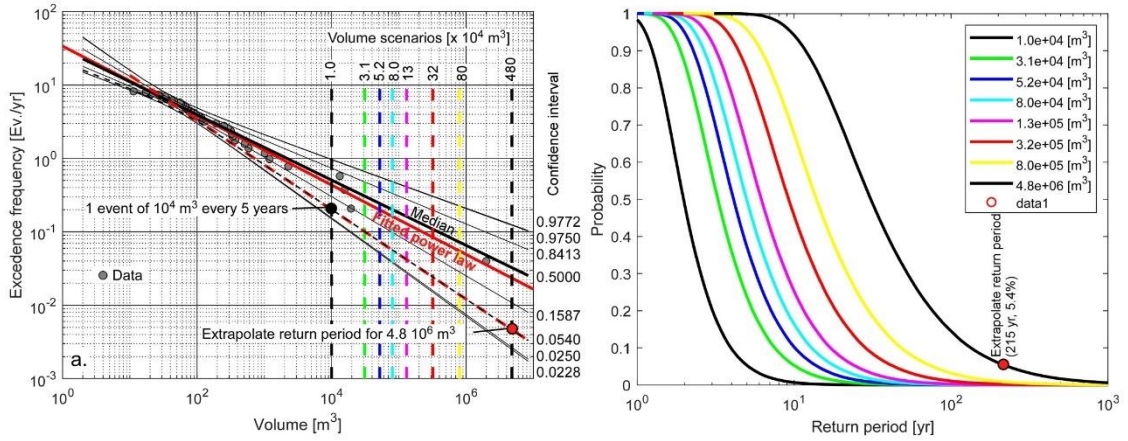

Fig. 13. (a) Bounds of different confidence intervals of the power-law based on Monte Carlo simulations. The dashed line indicates one of the most plausible hypotheses for the power-law. (b) Exceeding probability associated with the return period for each scenario. The black dots indicate the return period used to estimate the apparent return period based on recent past large events.

extrapolated a power-law (see the slanted red dotted line in Fig. 13a) using a second point defined by the average of $\pm\ \sigma$ (in the log) of the zone with the minimum confidence interval. This leads to an estimated return period of 215 years for the extreme event (scenario S_7) with a probability of 5.4%. The relationship between probability and return period for each scenario (Fig. 13b) indicates that smaller events have a shorter return period compared to larger events, assuming an equal probability of occurrence. In addition, as the magnitude of the scenarios decreased, the exceeding probability reduced while maintaining the same return period.

Upon analyzing the confidence intervals of the power law distribution obtained through Monte Carlo simulation, we observed that for S_7, the 95% confidence interval ranged from 8 to 399 years (a width of 391 years). Furthermore, the interval of one standard deviations for S_7 spanned from 14 to 93 years (a width of 79 years). The corresponding results for other scenarios are presented in Table 3. It is evident that an increase in failure volume corresponds to a wider 68% and 95% confidence interval, indicating greater variability in return period values. Thus, the uncertainty is substantial, especially for the extreme large scenarios.

The comparison between the calculated power law fitting in Section 4.3 and the simulated median power law fitting $N(V) = 30.77\ V^{-0.45}$, as depicted in Fig. 13a, clearly indicates a close resemblance. Utilizing this simulated median fitting, we estimated the median return periods for various volume scenarios, as illustrated in Fig. 14, which reveals that the median return period increases by 4 years per million cubic meters when the volume exceeds 10^6 m^3. The 10^4 m^3 (10^5 m^3) failure will occur every 2 years (5.5 years). It will take 15 years for a failure volume of 10^6 m^3 to occur. In the case of S_7, the median return period, which amounts to 31 years, surpasses the duration of our inventory (25 years) by 6 years. However, it is worth noting that this additional time span is not extensive when considering the rare rock avalanche magnitude. It is important to acknowledge that our data is based on annual observations of rockfall source monitoring. Consequently, the slope of the power-law distribution may be steeper due to the possibility of multiple events occurring within a single year, as observed by Williams et al. (2018), which would result in a longer return period for those defined failure scenarios. Nevertheless, whether the large volumes were released in a single event or multiple events still remains uncertain. This ambiguity is partly accounted for within the interval of the simulated power law fitting using the Monte Carlo approach.

While caution should be exercised when extrapolating extreme volume beyond the considered volume range (De Biagi et al., 2017), it is important to highlight that all scenarios in this study, except S_7, remain below the largest recorded event in history occurred in 1997. These estimated return periods considering uncertainties for the six scenarios associated with the Brenva spur offer valuable references for risk assessment of rockfall/rock avalanche hazards. Anyway, improving the quality of the volume-frequency law and reducing statistical errors in the procedure can be achieved by maintaining detailed and extensive event records, along with conducting comprehensive surveys and proper definition of potential failure volumes as we did in this study.

Table 3
Return period and the probability of exceeding that period for the reference scenario (S_0:1.0 × 10^4 m^3) and seven defined scenarios.

Scenario	Volume [m^3]	Return periods with different exceeding probabilities (years)						
		2.3%	*2.5%*	*15.9%*	*50.0%*	*84.1%*	*97.5%*	*97.7%*
S_0	1.00E+04	7	7	3	2	1	1	1
S_1	3.10E+04	14	14	6	3	2	2	2
S_2	5.20E+04	20	19	8	4	3	2	2
S_3	8.00E+04	27	25	10	5	3	2	2
S_4	1.30E+05	37	35	13	6	4	3	2
S_5	3.20E+05	66	63	22	9	5	3	3
S_6	8.00E+05	122	115	35	14	7	5	4
S_7	4.80E+06	399	375	93	31	14	8	8

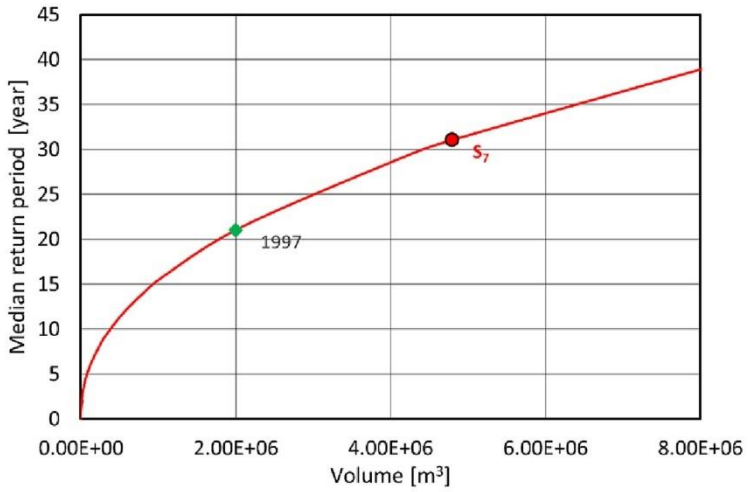

Fig. 14. Evolution of the median return period as a function of the rockfall volumes. The red dot indicates the median return period for S_7 with a volume of 4.8×10^6 m^3. The extrapolated median return period of 1997 rock avalanche is around 21 years indicated by the green solid diamond frame. (For interpretation of the references to colour in this figure legend, the reader is referred to the web version of this article.)

5.4. Issues in an overturned climatic context

Considering all of these findings and the ongoing global warming, it is highly probable that cryospheric conditions will undergo rapid changes. The current climate warming is expected to alter the occurrence of rockfalls in glacial environments over several decades following glacier downwasting (Hartmeyer et al., 2020b). Therefore, it is suggested that historical rockfall patterns in rock walls impacted by glacier retreat and permafrost degradation can only serve as reliable indicators for future events if the power law distribution is updated by the latest rock failure event accordingly. Thus, the uncertainties put forwards in our study could be real and cannot be further constrained. However, the observation made on the Drus tends to prove that rockfall activity can follow cycles after a major event (Guerin et al., 2020). For the Drus in 2005 (0.3×10^4 m^3; Guerin et al., 2020) and the Brenva Spur in 1997, a rock avalanche exposed a new rock wall which, exposed to air temperatures and solar radiation, must have developed a new active layer which, in addition to mechanical readjustments linked to the main event, can trigger rockfalls. In both cases, the decay phase of disruptive activity observed today could be followed by a new phase of instability as presently suggested by the increased rockfall activities like during the very hot summer of 2022 when 282 rockfall events ($V > 100$ m^3) have been documented in the central part of the Mont-Blanc massif by a network of observers (Ravanel and Deline, 2013), a record since it became operational in 2007 (the previous record was for 2019 with 222 events).

Moreover, the observed decrease in rockfall activity does not mean that the entire rock avalanche scar is more stable and will be less active in the long term. The scar can be reactivated and produce a larger event (Guerin et al., 2020) as seen recently at Piz Cengalo (3678 m a.s.l.; Swiss Alps): on the 23 August 2017, around 3×10^6 m^3 of granitoid rock broke off from the eastern face (Mergili et al., 2020) already affected by a rock avalanche of 1.5×10^6 m^3 on the 27 December 2011 (Walter et al., 2020). Indeed, climate change could have a significant impact on the failure probabilities of the different scenarios. On the other hand, it is also difficult to quantify the effect of the presence of highly fractured zones (characterized by a small spacing of many families of fractures) on the gradual dismantling of the rock mass in small volumes.

6. Conclusions

Through five SfM photogrammetry surveys conducted in the Brenva rock avalanche scar (Aosta Valley, Italy), we identified 39 rockfall occurrences ranging from 11 to 13,250 m^3 between July 2017 and September 2021. This resulted in a high rock wall retreat rate of 15.5 ± 2.3 mm/year, possibly attributed to permafrost degradation. Monitoring data indicated a decrease in rockfall activity, with erosion rates reducing from 44 ± 5.5 mm/year to 0.33 ± 0.2 mm/year. Nevertheless, cyclical patterns in rockfall activity were observed, as exemplified by the potential activation or acceleration during heat waves in 2022 within the Mont Blanc massif.

Applying a power law-based volume-frequency relationship, we estimated the return period and corresponding uncertainties for seven potential instability volume scenarios derived from the integration of the SLBL concept and geo-structural analysis. The median return period for rock failures with volumes of 1.0×10^4 m^3 was estimated to be 2 years, indicating relatively frequent occurrences. However, the high confidence intervals for return periods in various scenarios introduce significant uncertainty, potentially extending the estimated return period to several decades, unless global warming initiates a new cycle of larger failures.

Considering the observed activity of small rockfalls, it is probable that the extreme scenario S_7 (4.8×10^6 m^3) will collapse into multiple fragments due to fracking, with similar implications for other defined scenarios. Permafrost thaw and glacier retreat driven by global warming could result in shorter return periods. Nonetheless, any signs of increased activities such as boulder falls and small rockfalls should be promptly recognized as potential signals of future major rock avalanches. Regular and direct observations utilizing SfM photogrammetry or terrestrial laser scanning are essential for monitoring the evolution of the Brenva rock avalanche scar. These observations will contribute to updating the power-law fitting of rockfall sources and rockslides, thereby improving the prediction of rock slope instability scenarios regarding the return period.

CRediT authorship contribution statement

Li Fei: Data curation, Investigation, Methodology, Writing – original

draft, Writing – review & editing. **Michel Jaboyedoff:** Conceptualization, Project administration, Supervision, Validation, Writing – review & editing. **Antoine Guerin:** Investigation, Methodology, Supervision. **François Noël:** Investigation. **Davide Bertolo:** Investigation, Project administration, Resources. **Marc-Henri Derron:** Methodology, Supervision. **Patrick Thuegaz:** Investigation. **Fabrizio Troilo:** Investigation. **Ludovic Ravanel:** Supervision, Validation, Writing – review & editing.

Declaration of Competing Interest

The authors declare that they have no known competing financial interests or personal relationships that could have appeared to influence the work reported in this paper.

Data availability

Data will be made available on request.

References

Abele, G., 1994. Large rockslides: their causes and movement on internal sliding planes. Mt. Res. Dev. 14, 315–320. https://doi.org/10.2307/3673727.

Abellán, A., Jaboyedoff, M., Oppikofer, T., Vilaplana, J.M., 2009. Detection of millimetric deformation using a terrestrial laser scanner: experiment and application to a rockfall event. Nat. Hazards Earth Syst. Sci. https://doi.org/10.5194/nhess-9-365-2009.

Abellán, A., Calvet, J., Vilaplana, J.M., Blanchard, J., 2010. Detection and spatial prediction of rockfalls by means of terrestrial laser scanner monitoring. Geomorphology 119, 162–171. https://doi.org/10.1016/j.geomorph.2010.03.016.

Agisoft, 2020. AgiSoft Metashape Professional (Version 1.6.2 Bulid 10247) (Software). Retrieved from. http://www.agisoft.com/downloads/installer/.

Aki, K., 1965. Maximum likelihood estimate of b in the formula logN= a-bM and its confidence limits. Bull. Earthq. Res. Inst., Univ. Tokyo 43, 237–239.

Barla, G., Dutto, F., Mortara, G., 2000. Brenva glacier rock avalanche of 18 January 1997 on the Mount Blanc range, Northwest Italy. Landslide News 13, 2–5.

Bennett, G.L., Molnar, P., Eisenbeiss, H., Mcardell, B.W., 2012. Erosional power in the Swiss Alps: characterization of slope failure in the Illgraben. Earth Surf. Process. Landf. 37, 1627–1640. https://doi.org/10.1002/esp.3263.

Bertini, G., Marcucci, M., Nevini, R., Passerini, P., Sguazzoni, G., 1985. Patterns of faulting in the Mont Blanc granite. Tectonophysics 111, 65–106.

Besl, P.J., McKay, N.D., 1992. A Method for Registration of 3-D Shapes. In: IEEE Transactions on Pattern Analysis and Machine Intelligence. International Society for Optics and Photonics, pp. 239–256. https://doi.org/10.1109/34.121791.

Boeckli, L., Brenning, A., Gruber, S., Noetzli, J., 2012. Permafrost distribution in the European Alps: calculation and evaluation of an index map and summary statistics. Cryosphere 6, 807–820.

Bolla, A., Paronuzzi, P., 2020. Geomechanical Field Survey to Identify an Unstable Rock Slope: the Passo della Morte Case History (NE Italy). Rock Mech. Rock. Eng. 53, 1521–1544. https://doi.org/10.1007/s00603-019-01963-w.

Bründl, M., Romang, H.E., Bischof, N., Rheinberger, C.M., 2009. The risk concept and its application in natural hazard risk management in Switzerland. Nat. Hazards Earth Syst. Sci. 9, 801–813. https://doi.org/10.5194/nhess-9-801-2009.

Brunetti, M.T., Guzzetti, F., Rossi, M., 2009. Probability distributions of landslide volumes. Nonlinear Process. Geophys. 16, 179–188. https://doi.org/10.5194/npg-16-179-2009.

Budetta, P., De Luca, C., Nappi, M., 2016. Quantitative rockfall risk assessment for an important road by means of the rockfall risk management (RO.MA.) method. Bull. Eng. Geol. Environ. 75, 1377–1397. https://doi.org/10.1007/s10064-015-0798-6.

CloudCompare, 2021. CloudCompare (Version 2.12.alpha) [GPL Software]. Retrieved from. http://www.cloudcompare.org/.

Coe, J.A., Bessette-Kirton, E.K., Geertsema, M., 2018. Increasing rock-avalanche size and mobility in Glacier Bay National Park and Preserve, Alaska detected from 1984 to 2016 Landsat imagery. Landslides 15, 393–407. https://doi.org/10.1007/s10346-017-0879-7.

Cook, K.L., Dietze, M., 2019. Short Communication: a simple workflow for robust low-cost UAV-derived change detection without ground control points. Earth Surf. Dyn. 7, 1009–1017. https://doi.org/10.5194/esurf-7-1009-2019.

Copons, R., Vilaplana, J.M., 2008. Rockfall susceptibility zoning at a large scale: from geomorphological inventory to preliminary land use planning. Eng. Geol. 102, 142–151. https://doi.org/10.1016/j.enggeo.2008.03.020.

Corominas, J., Copons, R., Moya, J., Vilaplana, J.M., Altimir, J., Amigó, J., 2005. Quantitative assessment of the residual risk in a rockfall protected area. Landslides 2, 343–357. https://doi.org/10.1007/s10346-005-0022-z.

Corominas, J., Mavrouli, O., Ruiz Carulla, R., 2018. Magnitude and frequency relations: are there geological constraints to the rockfall size? Landslides 15, 829–845. https://doi.org/10.1007/s10346-017-0910-z.

Cox, S.C., Allen, S.K., 2009. Vampire rock avalanches of January 2008 and 2003, Southern Alps, New Zealand. Landslides 6, 161–166. https://doi.org/10.1007/s10346-009-0149-4.

Cremonese, E., Gruber, S., Phillips, M., Pogliotti, P., Böckli, L., Noetzli, J., Suter, C., Bodin, X., Crepaz, A., Kellerer-Pirklbauer, A., 2011. Brief Communication:" an inventory of permafrost evidence for the European Alps". Cryosphere 5, 651–657.

De Biagi, V., Lia Napoli, M., Barbero, M., Peila, D., 2017. Estimation of the return period of rockfall blocks according to their size. Nat. Hazards Earth Syst. Sci. 17, 103–113. https://doi.org/10.5194/nhess-17-103-2017.

Deline, P., 2001. Recent Brenva rock avalanches (Valley of Aosta): new chapter in an old story? Geogr. Ann. Ser. A Phys. Geogr. 55–63.

Deline, P., 2009. Interactions between rock avalanches and glaciers in the Mont Blanc massif during the late Holocene. Quat. Sci. Rev. 28, 1070–1083. https://doi.org/10.1016/j.quascirev.2008.09.025.

Deline, P., Akçar, N., Ivy-Ochs, S., Kubik, P.W., 2015. Repeated Holocene rock avalanches onto the Brenva Glacier, Mont Blanc massif, Italy: a chronology. Quat. Sci. Rev. 126, 186–200. https://doi.org/10.1016/j.quascirev.2015.09.004.

Draebing, D., Krautblatter, M., Hoffmann, T., 2017. Thermo-cryogenic controls of fracture kinematics in permafrost rockwalls. Geophys. Res. Lett. 44, 3535–3544.

Dussauge, C., Helmstetter, A., Grasso, J.R., Hantz, D., Desvarreux, P., Jeannin, M., Giraud, A., 2002. Probabilistic approach to rock fall hazard assessment: potential of historical data analysis. Nat. Hazards Earth Syst. Sci. 2, 15–26. https://doi.org/10.5194/nhess-2-15-2002.

Dussauge, C., Grasso, J.-R., Helmstetter, A., 2003. Statistical analysis of rockfall volume distributions: implications for rockfall dynamics. J. Geophys. Res. Solid Earth 108. https://doi.org/10.1029/2001JB000650.

Duvillard, P.-A., Ravanel, L., Marcer, M., Schoeneich, P., 2019. Recent evolution of damage to infrastructure on permafrost in the French Alps. Reg. Environ. Chang. 19, 1281–1293. https://doi.org/10.1007/s10113-019-01465-z.

Evans, S.G., Clague, J.J., 1994. Recent climatic change and catastrophic geomorphic processes in mountain environments. Geomorphology 10, 107–128. https://doi.org/10.1016/0169-555X(94)90011-6.

Fell, R., Corominas, J., Bonnard, C., Cascini, L., Leroi, E., Savage, W.Z., 2008. Guidelines for landslide susceptibility, hazard and risk zoning for land-use planning. Eng. Geol. 102, 99–111. https://doi.org/10.1016/j.enggeo.2008.03.014.

Fort, M., Cossart, E., Deline, P., Dzikowski, M., Nicoud, G., Ravanel, L., Schoeneich, P., Wassmer, P., 2009. Geomorphic impacts of large and rapid mass movements: A review. In: Geomorphologie: Relief, Processus, Environnement. Groupe français de géomorphologie. https://doi.org/10.4000/geomorphologie.7495.

Giani, G.P., Silvano, S., Zanon, G., 2001. Avalanche of 18 January 1997 on Brenva glacier, Mont Blanc group, Western Italian Alps: an unusual process of formation. Ann. Glaciol. 32, 333–338. https://doi.org/10.3189/172756401781819157.

Gobiet, A., Kotlarski, S., Beniston, M., Heinrich, G., Rajczak, J., Stoffel, M., 2014. 21st century climate change in the European Alps—a review. Sci. Total Environ. 493, 1138–1151. https://doi.org/10.1016/j.scitotenv.2013.07.050.

Graber, A., Santi, P., 2022. Power law models for rockfall frequency-magnitude distributions: review and identification of factors that influence the scaling exponent. Geomorphology 418, 108463. https://doi.org/10.1016/j.geomorph.2022.108463.

Gruber, S., Haeberli, W., 2007. Permafrost in steep bedrock slopes and its temperature-related destabilization following climate change. J. Geophys. Res. Earth Surf. 112 https://doi.org/10.1029/2006JF000547.

Gruber, S., Hoelzle, M., Haeberli, W., 2004. Permafrost thaw and destabilization of Alpine rock walls in the hot summer of 2003. Geophys. Res. Lett. 31 https://doi.org/10.1029/2004GL020051.

Guerin, A., Abellán, A., Matasci, B., Jaboyedoff, M., Derron, M.-H., Ravanel, L., 2017. Brief communication: 3-D reconstruction of a collapsed rock pillar from Web-retrieved images and terrestrial lidar data – the 2005 event of the west face of the Drus (Mont Blanc massif). Nat. Hazards Earth Syst. Sci. 17, 1207–1220. https://doi.org/10.5194/nhess-17-1207-2017.

Guerin, A., Jaboyedoff, M., Collins, B.D., Derron, M.-H., Stock, G.M., Matasci, B., Boesiger, M., Lefeuvre, C., Podladchikov, Y.Y., 2019. Detection of rock bridges by infrared thermal imaging and modeling. Sci. Rep. 9, 13138. https://doi.org/10.1038/s41598-019-49336-1.

Guerin, A., Ravanel, L., Matasci, B., Jaboyedoff, M., Deline, P., 2020. The three-stage rock failure dynamics of the Drus (Mont Blanc massif, France) since the June 2005 large event. Sci. Rep. 10, 1–20. https://doi.org/10.1038/s41598-020-74162-1.

Guermani, A., Pennacchioni, G., 1998. Brittle precursors of plastic deformation in a granite: an example from the Mont Blanc massif (Helvetic, western Alps). J. Struct. Geol. 20, 135–148. https://doi.org/10.1016/S0191-8141(97)00080-1.

Guzzetti, F., Reichenbach, P., Wieczorek, G.F., 2003. Rockfall hazard and risk assessment in the Yosemite Valley, California, USA. Nat. Hazards Earth Syst. Sci. 3, 491–503. https://doi.org/10.5194/nhess-3-491-2003.

Guzzetti, F., Reichenbach, P., Ghigi, S., 2004. Rockfall hazard and risk assessment along a transportation corridor in the Nera Valley, Central Italy. Environ. Manag. 34, 191–208. https://doi.org/10.1007/s00267-003-0021-6.

Hantz, D., Vengeon, J.M., Dussauge-Peisser, C., 2003. An historical, geomechanical and probabilistic approach to rock-fall hazard assessment. Nat. Hazards Earth Syst. Sci. 3, 693–701. https://doi.org/10.5194/nhess-3-693-2003.

Hartmeyer, I., Delleske, R., Keuschnig, M., Krautblatter, M., Lang, A., Christoph Otto, J., Schrott, L., 2020a. Current glacier recession causes significant rockfall increase: the immediate paraglacial response of deglaciating cirque walls. Earth Surf. Dyn. 8, 729–751. https://doi.org/10.5194/esurf-8-729-2020.

Hartmeyer, I., Keuschnig, M., Delleske, R., Krautblatter, M., Lang, A., Schrott, L., Prasicek, G., Otto, J.C., 2020b. A 6-year lidar survey reveals enhanced rockwall retreat and modified rockfall magnitudes/frequencies in deglaciating cirques. Earth Surf. Dyn. 8, 753–768. https://doi.org/10.5194/esurf-8-753-2020.

Hexagon-Technodigit, 2016. 3DReshaper: The 3D Scanner Software (version 11.0.7.23169). Technodigit part of Hexagon.

Ho, K., 2004. Recent advances in geotechnology for slope stabilization and landslide mitigation – Perspective from Hong Kong. In: Landslides: Evaluation and Stabilization/Glissement de Terrain: Evaluation et Stabilisation, Set of 2 Volumes, pp. 1507–1560. https://doi.org/10.1201/b16816-216.

Huggel, C., 2009. Recent extreme slope failures in glacial environments: effects of thermal perturbation. Quat. Sci. Rev. 28, 1119–1130. https://doi.org/10.1016/j.quascirev.2008.06.007.

Hungr, O., Evans, S.G., Hazzard, J., 1999. Magnitude and frequency of rock falls and rock slides along the main transportation corridors of southwestern British Columbia. Can. Geotech. J. 36, 224–238. https://doi.org/10.1139/t98-106.

Jaboyedoff, M., Metzger, R., Oppikofer, T., Couture, R., Derron, M.H., Locat, J., Turmel, D., 2007. New insight techniques to analyze rock-slope relief using DEM and 3D-imaging cloud points: COLTOP-3D software. In: Proceedings of the 1st Canada-US Rock Mechanics Symposium - Rock Mechanics Meeting Society's Challenges and Demands. OnePetro, pp. 61–68.

Jaboyedoff, M., Couture, R., Locat, P., 2009. Structural analysis of Turtle Mountain (Alberta) using digital elevation model: toward a progressive failure. Geomorphology 103, 5–16. https://doi.org/10.1016/j.geomorph.2008.04.012.

Jaboyedoff, M., Chigira, M., Arai, N., Derron, M.H., Rudaz, B., Tsou, C.Y., 2019. Testing a failure surface prediction and deposit reconstruction method for a landslide cluster that occurred during Typhoon Talas (Japan). Earth Surf. Dyn. 7, 439–458. https://doi.org/10.5194/esurf-7-439-2019.

Jaboyedoff, M., Carrea, D., Derron, M. H., Oppikofer, T., Penna, I.M., Rudaz, B., 2020. A review of methods used to estimate initial landslide failure surface depths and volumes. Eng. Geol. 267, 105478.

Jaboyedoff, M., Choanji, T., Derron, M.H., Fei, L., Gutierrez, A., Loiotine, L., Noel, F., Sun, C., Wyser, E., Wolff, C., 2021. Introducing uncertainty in risk calculation along roads using a simple stochastic approach. Geosciences (Switzerland) 11, 143. https://doi.org/10.3390/geosciences11030143.

Katz, O., Aharonov, E., 2006. Landslides in vibrating sand box: what controls types of slope failure and frequency magnitude relations? Earth Planet. Sci. Lett. 247, 280–294. https://doi.org/10.1016/j.epsl.2006.05.009.

Kazhdan, M., Hoppe, H., 2013. Screened poisson surface reconstruction. In: ACM Transactions on Graphics. https://doi.org/10.1145/2487228.2487237.

Kiryati, N., Székely, G., 1993. Estimating shortest paths and minimal distances on digitized three-dimensional surfaces. Pattern Recogn. 26, 1623–1637. https://doi.org/10.1016/0031-3203(93)90018-R.

Krautblatter, M., Funk, D., Günzel, F.K., 2013. Why permafrost rocks become unstable: a rock–ice-mechanical model in time and space. Earth Surf. Process. Landf. 38, 876–887.

Larsen, I.J., Montgomery, D.R., Korup, O., 2010. Landslide erosion controlled by hillslope material. Nat. Geosci. 3, 247–251. https://doi.org/10.1038/ngeo776.

Legay, A., Magnin, F., Ravanel, L., 2021. Rock temperature prior to failure: Analysis of 209 rockfall events in the Mont Blanc massif (Western European Alps). Permafr. Periglac. Process. 32, 520–536.

Magnin, F., Brenning, A., Bodin, X., Deline, P., Ravanel, L., 2015. Statistical modelling of rock wall permafrost distribution: application to the Mont Blanc massif. Géomorphol. Relief Process. Environ. 20.

Malamud, B.D., Turcotte, D.L., Guzzetti, F., Reichenbach, P., 2004. Landslide inventories and their statistical properties. Earth Surf. Process. Landf. 29, 687–711. https://doi.org/10.1002/esp.1064.

Matasci, B., Stock, G.M., Jaboyedoff, M., Carrea, D., Collins, B.D., Guérin, A., Matasci, G., Ravanel, L., 2018. Assessing rockfall susceptibility in steep and overhanging slopes using three-dimensional analysis of failure mechanisms. Landslides 15, 859–878. https://doi.org/10.1007/s10346-017-0911-y.

Mergili, M., Jaboyedoff, M., Pullarello, J., Pudasaini, S.P., 2020. Back calculation of the 2017 Piz Cengalo–Bondo landslide cascade with r. avaflow: what we can do and what we can learn. Nat. Hazards Earth Syst. Sci. 20, 505–520.

Messenzehl, K., Dikau, R., 2017. Structural and thermal controls of rockfall frequency and magnitude within rockwall–talus systems (Swiss Alps). Earth Surf. Process. Landf. 42, 1963–1981. https://doi.org/10.1002/esp.4155.

Noetzli, J., Hoelzle, M., Haeberli, W., 2003. Mountain permafrost and recent Alpine rock-fall events: A GIS-based approach to determine critical factors. In: Permafrost. Swets & Zeitlinger Lisse Zürich, pp. 827–832.

Ravanel, L., Deline, P., 2010. Climate influence on rockfalls in high-Alpine steep rockwalls: The north side of the Aiguilles de Chamonix (Mont Blanc massif) since the end of the 'Little Ice Age.'. Holocene 21, 357–365. https://doi.org/10.1177/0959683610374887.

Ravanel, L., Deline, P., 2013. A network of observers in the Mont Blanc massif to study rockfalls in high alpine rockwalls. Geogr. Fis. Din. Quat. 36, 151–158.

Ravanel, L., Allignol, F., Deline, P., Gruber, S., Ravello, M., 2010. Rock falls in the Mont Blanc Massif in 2007 and 2008. Landslides 7, 493–501. https://doi.org/10.1007/s10346-010-0206-z.

Ravanel, L., Magnin, F., Deline, P., 2017. Impacts of the 2003 and 2015 summer heatwaves on permafrost-affected rock-walls in the Mont Blanc massif. Sci. Total Environ. 609, 132–143. https://doi.org/10.1016/j.scitotenv.2017.07.055.

Ravanel, L., Guillet, G., Kaushik, S., Preunkert, S., Malet, E., Magnin, F., Trouvé, E., Montagnat, M., Yan, Y., Deline, P., 2023. Ice aprons on steep high-alpine slopes: insights from the Mont-Blanc massif, Western Alps. J. Glaciol. 1–17.

Rocscience, 2022. Dips. Retrieved from. https://www.rocscience.com/software/dips.

Santana, D., Corominas, J., Mavrouli, O., Garcia-Sellés, D., 2012. Magnitude-frequency relation for rockfall scars using a Terrestrial Laser Scanner. Eng. Geol. 144–145, 50–64. https://doi.org/10.1016/j.enggeo.2012.07.001.

Sepúlveda, S.A., Alfaro, A., Lara, M., Carrasco, J., Olea-Encina, P., Rebolledo, S., Garcés, M., 2021. An active large rock slide in the Andean paraglacial environment: the Yerba Loca landslide, Central Chile. Landslides 18, 697–705. https://doi.org/10.1007/s10346-020-01564-7.

Stark, C.P., Hovius, N., 2001. The characterization of landslide size distributions. Geophys. Res. Lett. 28, 1091–1094. https://doi.org/10.1029/2000GL008527.

Stead, D., Wolter, A., 2015. A critical review of rock slope failure mechanisms: the importance of structural geology. J. Struct. Geol. https://doi.org/10.1016/j.jsg.2015.02.002.

Steck, A., Epard, J. L., Esher, A., Gouffon, Y., Masson, H., 2001. Carte tectonique des Alpes de Suisse occidentale et des régions avoisinantes 1:100000. Office féd. Eaux Geologie (Berne) Carte géol, 73 p.

Straub, D., Schubert, M., 2008. Modeling and managing uncertainties in rock-fall hazards. Georisk 2, 1–15. https://doi.org/10.1080/17499510701835696.

Strunden, J., Ehlers, T.A., Brehm, D., Nettesheim, M., 2015. Spatial and temporal variations in rockfall determined from TLS measurements in a deglaciated valley, Switzerland. J. Geophys. Res. Earth Surf. 120, 1251–1273. https://doi.org/10.1002/2014JF003274.

Tonini, M., Abellan, A., 2014. Rockfall detection from terrestrial lidar point clouds: a clustering approach using R. J. Spat. Inform. Sci. 8, 95–110. https://doi.org/10.5311/JOSIS.2014.8.123.

Van Veen, M., Hutchinson, D.J., Kromer, R., Lato, M., Edwards, T., 2017. Effects of sampling interval on the frequency - magnitude relationship of rockfalls detected from terrestrial laser scanning using semi-automated methods. Landslides 14, 1579–1592. https://doi.org/10.1007/s10346-017-0801-3.

Viani, C., Chiarle, M., Paranunzio, R., Merlone, A., Musacchio, C., Coppa, G., Nigrelli, G., 2020. An integrated approach to investigate climate-driven rockfall occurrence in high alpine slopes: the Bessanese glacial basin, Western Italian Alps. J. Mt. Sci. 17, 2591–2610. https://doi.org/10.1007/s11629-020-6216-y.

Walter, F., Amann, F., Kos, A., Kenner, R., Phillips, M., de Preux, A., Huss, M., Tognacca, C., Clinton, J., Diehl, T., Bonanomi, Y., 2020. Direct observations of a three million cubic meter rock-slope collapse with almost immediate initiation of ensuing debris flows. Geomorphology 351, 106933. https://doi.org/10.1016/j.geomorph.2019.106933.

Westoby, M.J., Brasington, J., Glasser, N.F., Hambrey, M.J., Reynolds, J.M., 2012. "Structure-from-Motion" photogrammetry: a low-cost, effective tool for geoscience applications. Geomorphology 179, 300–314. https://doi.org/10.1016/j.geomorph.2012.08.021.

Williams, J.G., Rosser, N.J., Hardy, R.J., Brain, M.J., Afana, A.A., 2018. Optimising 4-D surface change detection: an approach for capturing rockfall magnitude-frequency. Earth Surf. Dyn. 6, 101–119. https://doi.org/10.5194/esurf-6-101-2018.

Wyllie, D.C., Mah, C., 2004. Rock Slope Engineering. CRC Press.

Recent evolution of high alpine areas: multi-sensor optical satellite imagery analysis in the Monte Rosa Massif, Western Alps

Short summary

In recent years, mountaineers and researchers have observed a concerning degradation of high-altitude glacierised areas, marked by permafrost thawing, increased rockfall incidents, and the expansion of exposed rock formations. Pilot studies, while valuable, have underscored the need for comprehensive data across various regions. Our study, conducted between 2017 and 2022, utilised remote sensing data for rock body mapping. Comparing Sentinel-2 (10m resolution) and Pléiades (0.5 m resolution) imagery, we found a notable increase in high-altitude rock outcrops. Pléiades data revealed a 10% expansion, highlighting the efficacy of medium-resolution multispectral imagery in illustrating rapid glacial area reduction. While large glacier accumulations remained stable, surrounding areas showed significant changes in the context of climate change. Expanding our research to a regional scale is essential to better understand these dynamics, especially considering the potential impact of the warm summer of 2022. Continuous monitoring is crucial to confirm long-term trends in high-altitude Alpine environments, emphasising the importance of observing and comprehending evolving mountain processes. Our work underscores the necessity of vigilance in monitoring rapidly changing trends.

Main findings

The main findings of this publication are:

- Mapping of high-altitude rock outcrops at the massif scale for four different timesteps.
- Highlighting areal variations from 1999 to 2022.
- Testing the feasibility of the analysis by means of semi-automatic classification.

Contributions of the PhD candidate

Conceptualisation of the research activity. Collection of the data. Stereo DEM production. Orthorectification of satellite imagery. Classification of multispectral imagery. Writing of the manuscript and figures elaboration.

Data availability

The data are available from the authors, upon request.

Journal

The proceedings of the conference will be published in the Euro-Mediterranean Journal for Environmental Integration. With the specific aim of promoting Euro-Mediterranean scientific partnership so as to develop and integrate environmental research and findings into the activities of related sectors in the region, a group of Euro-Mediterranean scientists have recently launched the Euro-Mediterranean Journal for Environmental Integration. This journal (published by Springer and owned by the University of Sfax, Tunisia), which started in 2016, has been now indexed in the Web of Science and Scopus. It offers a scientific platform for presenting and discussing the latest advances in research with a focus on emerging environmental issues and challenges in the region. 2022 impact factor: 2.0

Recent evolution of high Alpine areas: multi-sensor optical satellite imagery analysis in the Monte Rosa massif, Western Alps

Fabrizio Troilo[1-3], Pietro Di Sopra[1], Paolo Perret[1], Luca Mondardini[1], Niccolò Dematteis[2] and Daniele Giordan[2]

[1] Fondazione Montagna sicura (FMS), loc. Villard de La Palud 1, 11013 Courmayeur, Italy
[2] Italian National Research Council, Research Institute for Geo-Hydrological Protection (CNR-IRPI), Strada delle Cacce 73, 10135 Torino, Italy
[3] Università di Pavia, Dipartimento di Scienze della Terra e dell'Ambiente, Pavia, Italy

Abstract.
In recent years, both mountaineers and researchers have documented an increased degradation of high-altitude glacierized areas, leading to processes such as permafrost thawing, increased rockfall activity and expansion of rock outcrops. Pilot studies have been performed, but data from different massifs and regions are needed to better understand these phenomena. To study the evolution of these high-altitude areas, we mapped rock bodies using remotely sensed data. Analysis of rock outcrop areas have been performed between 2017 and 2022. Semi-automatic classification of free-access Sentinel2 (10 m resolution) images and manual digitization on commercial Pléiades (0.5 m resolution) imagery has been compared. Our study shows an increase in rock outcrop areas in high-altitude environments. Both datasets show similar results coherent with literature data. The Pleiades dataset, having higher accuracy, shows an areal expansion of rock outcrops in between 2017 and 2022 of +10% on a total analyzed area of 30 km^2, out of which 5 km^2 represent rock outcrops. The feasibility of using medium-resolution multispectral imagery to document the aforementioned geomorphological process has proven effective in showing the very fast shrinking of glacial areas during the study period. Even though the high-altitude portions of large glaciers do not show significant local mass loss in the accumulation areas, the adjacent areas showed important areal changes in the present climate change context. We conducted our study in a pilot area, where field observations indicated a probable fast evolution of degradation processes. Still, an extension to a regional scale is needed to better define those dynamics and their recent evolution. A possible exacerbation of the processes due to the warm summer of 2022, which falls within the study period, has to be considered. Furthermore, the evolution in the next decades still has to be monitored to confirm a specific trend. High mountain processes of the Alpine environment, such as the one outlined in the present study, have to be better observed and understood. Nevertheless, our work shows that rapidly evolving trends exist and should be monitored.

Keywords: Glacier, Ice, Remote sensing, Climate change, Permafrost.

Introduction

The aim of this paper is to investigate the evolution of glacier surfaces and rocks outcrops in recent years using satellite imagery in high-altitude Alpine terrain. The study is focused on the Monte Rosa massif, a high-alpine area covering approximately 150 km^2, located on the Italian-Swiss border, culminating with the Dufour peak (4.635 m a.s.l.). The area is characterized by the widespread presence of glaciers, seracs, and ice walls, also known as ice aprons (Ravanel et al., 2023). In recent decades, both mountaineers (Ravanel et al., 2023) and researchers have observed significant changes in high Alpine areas. Repeated photographs of the area of study show macroscopic changes of rock outcrops at very high altitude (Fig.1). To better understand this phenomenon, we analysed satellite imagery and historical orthophotographs of the Monte Rosa Massif.

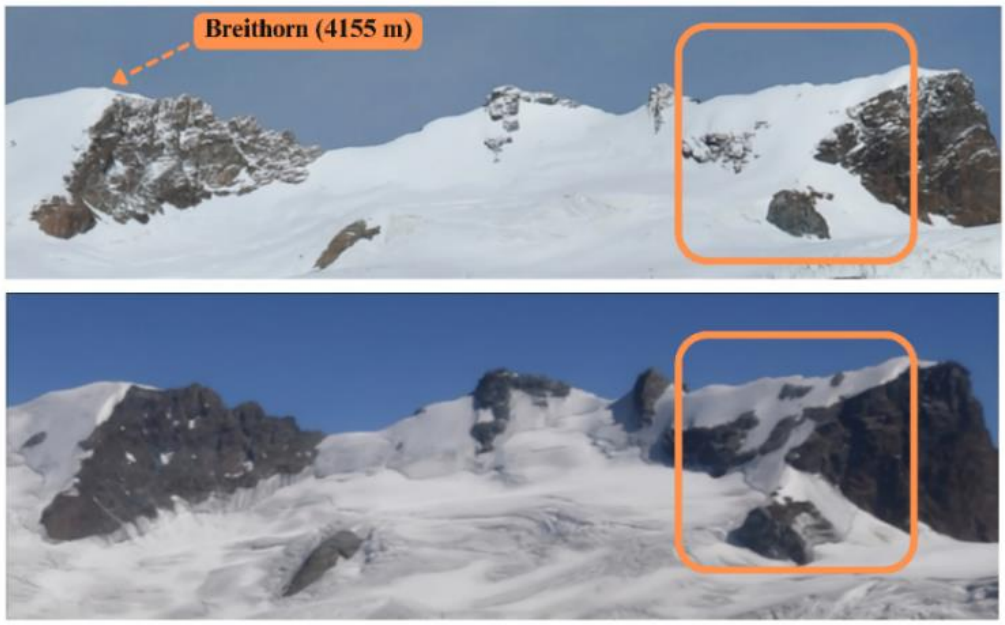

Fig. 1 The eastern ridge of the Central Breithorn peak (4155m a.s.l.) shows large changes in the areal extension of rock outcrops. Photographs from 2017 and 2022 (Fondazione Montagna Sicura archive).

Materials and Methods

A multi-temporal and multi-sensor approach was chosen for this study. We analyzed two distinct datasets: (i) AIRBUS Pléiades (0.5 m spatial resolution) optical imagery acquired on 15/08/2017 and 18/09/2022 and (ii) freely available European Space Agency Sentinel2 (10 m spatial resolution) optical imagery captured on 19/07/2017 and 15/07/2022. To focus exclusively on high-altitude areas, we defined an Area of Interest (AOI_f) using the NASA Shuttle Radar Topography Mission DEM, encompassing elevation bands above 3700 m a.s.l. For the purpose of comparing results with historical data, we also integrated aerial orthophotographs from 1999 and 2005, obtained from the Aosta Valley Autonomous Region covering Italian territory only.

The analysis of Pléiades imagery involved manual digitization performed by a trained technician using QGIS software, with a scale of 1:1000. We applied the same methodology to map rock outcrops on historical orthophotos. Sentinel2 images were processed through a semi-automatic classification on ESA SNAP software, using band combinations and ratios as outlined by Paul et al. (2016). We chose the band ratio in equation (1), with th1 and th2 as thresholds, set to 3.00 and 0.11 respectively, in accordance with literature ranges and iterative testing (Paul et al., 2015).

$$(B04/B11) > th1 \text{ AND } B02 > th2 \qquad (1)$$

To estimate the evolution of glacier surfaces, rock outcrops and ice aprons throughout the reference period, we compared the obtained polygons of high-altitude rock outcrops between 2017 and 2022, together with comparative assessment of the historical data from 1999 and 2005.

Results

In the present study, we measured the areal extension of high-altitude rock outcrops on the Monte Rosa Massif in 4 different timesteps: 1999, 2005, 2017, 2022. We conducted an analysis of the areal changes between 2017 and 2022 on the whole cloud free areas of the AOI_f (28.09 km^2). However, to ensure spatial coherence from the year 1999, we reduced the AOI_f to a subset of 17.54 km^2 (AOI_s), based on image overlap.

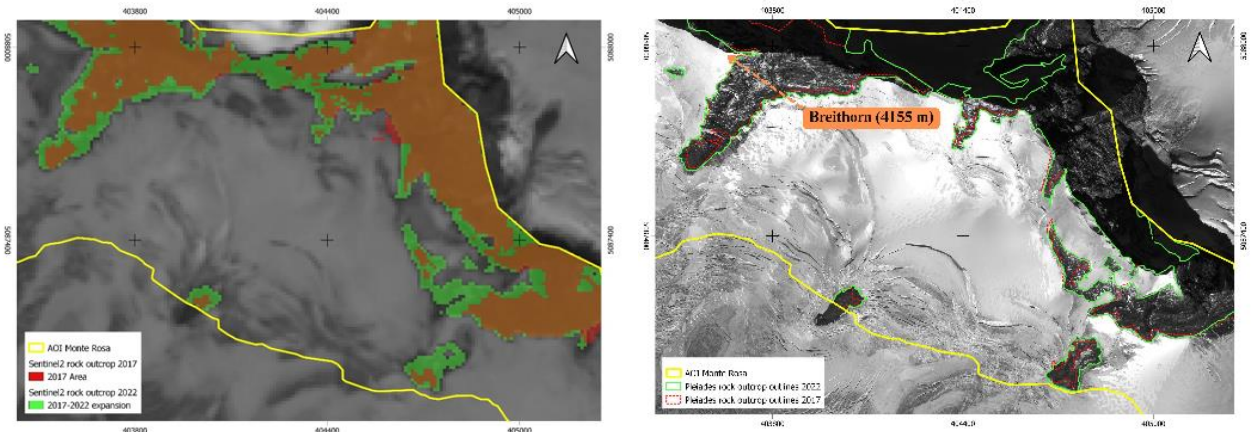

Fig. 2. Satellite imagery of the areas shown in Fig.1. The left panel shows the Semi-automatic classification of rock outcrops form Sentinel2 imagery while the right panel displays the manual classification on Pléiades imagery (2017 v. 2022).

Errors during the manual digitization can mostly arise from: (i) variations in manual picking of pixels, (ii) differences in snow cover conditions and (iii) local geometric distortions linked to the orthorectification process. Manual mapping accuracy (i and ii) was estimated in 1% of the calculated area, as the interpretation of rock outcrops was supported by high quality dataset, previous terrain knowledge and the analyst's expertise in photo interpretation (Paul et al., 2013). Differences linked to geometric distortions were estimated to account for 0.047 km² on the AOI_f (0.17 % of the total area), therefore we estimate the accuracy of the manual mapping of rock outcrops at +/-1.17% of the total mapped areas. We measured areal changes of rock outcrops in the AOI_s that can be summarized as follows:

Table 1. Temporal evolution rock outcrops extension (1999 to 2022) by manual digitization.

Year	Area (km²)	Difference from previous measure (km²)	Difference from t_0 (km²)
1999	3.440 +/- 0.040	/	/
2005	3.578 +/- 0.042	+ 0.138	+ 0.138
2017	3.533 +/- 0.041	- 0.045	+ 0.093
2022	3.884 +/- 0.045	+ 0.351	+ 0.444

On the 2017-2022 timeframe, we explored the feasibility of multispectral Sentinel2 satellite imagery semi-automatic classification, for (i) avoiding time consuming manual digitization of perimeters for future studies (ii) free availability of 3 to 5 days satellite revisit time. We therefore plotted the differences between manually digitized mapping from Pléiades imagery and the Sentinel2 semi-automatic classification mapping on the AOI_f above 3700 m (28.09 km²). We obtained the following results:

Table 2. Differences between the mapping based on Pléiades and on Sentinel2 imagery.

Year	Pléiades Area (km²)	Sentinel2 Areas (km²)	Difference Sentinel2/Pléiades (km²)
2017	5.063 +/- 0.059	4.705	- 0.358
2022	5.516 +/- 0.064	6.281	+ 0.765

Discussion

The present study demonstrates the possibility of an ongoing variation in the degradation trends of the high-altitude cryosphere, potentially leading to an increased rate of expansion of high-altitude rock outcrops. Analysis of the manual mapping on Pléaides imagery reveals a +10% increase in rock outcrops both on AOI_s and on AOI_f within 5 years (2017 to 2022), while data from 1999, 2005 and 2017 show a substantial steadiness in the areal extent of rock outcrops. The semi-automatic mapping of the 2017 Sentinel2 imagery shows an underestimation of total rock outcrop areas by 0.358 km² compared to the Pléiades manually digitized surfaces. In 2022, the same comparison shows an overestimation of 0.765 km². This considerable variability is likely to be caused by the difference in the acquisition dates. As a matter of fact, given that only two images were available from the Pléiades archive, the best image match had to be found in terms of date similarity, shadows, cloud and snow cover. Finally, the trade-off among all these parameters led to the selection of a July 2017 Sentinel2 acquisition. However, this image still had a considerable amount of seasonal snow cover onto the rock outcrops, resulting in a misclassification of rocky areas as snow/ice zones. Similar errors were detected onto the completely snow free 2022 Sentinel2 image, where misclassification of dirty/debris covered ice were mainly caused by rockfalls and ice darkening.

Conclusions

Although the present study identifies an increased rate of expansion of high-altitude rock outcrops, it is important for future observations over a longer timescale to either confirm or refute the trend highlighted in this study. The feasibility of using Sentinel2 imagery is likely acceptable for a decadal timescale comparison, especially when based on imagery acquired under very similar conditions of snow cover, rockfall activity and light. Given the current climate change scenarios characterized by unprecedented rates of warming and the potential Altitude Dependent Warming effects (Pepin et al., 2015), the identified trend should be monitored in the future. The exacerbation of the phenomenon highlighted in this work seems possible in the coming decades. The present study was partly financed by the Interreg Italia-Svizzera 2014/2020 RESERVAQUA (ID 3864298) cooperation project.

References

Paul, F., Barrand, N. E., Baumann, S., Berthier, E., Bolch, T., Casey, K., Frey, H., Joshi, S., Konovalov, V., & Le Bris, R. (2013). On the accuracy of glacier outlines derived from remote-sensing data. *Annals of Glaciology*, *54*(63), 171-182.

Paul, F., Bolch, T., Kääb, A., Nagler, T., Nuth, C., Scharrer, K., Shepherd, A., Strozzi, T., Ticconi, F., & Bhambri, R. (2015). The glaciers climate change initiative: Methods for creating

glacier area, elevation change and velocity products. *Remote Sensing of Environment*, *162*, 408-426.

Paul, F., Winsvold, S. H., Kääb, A., Nagler, T., & Schwaizer, G. (2016). Glacier remote sensing using Sentinel2. Part II: Mapping glacier extents and surface facies, and comparison to Landsat 8. *Remote Sensing*, *8*(7), 575.

Pepin, N., Bradley, R., Diaz, H., Baraer, M., Cáceres, B., Forsythe, N., Fowler, H., Greenwood, G., Hashmi, M., Liu, X., Miller, J., Ning, L., Ohmura, A., Palazzi, E., Rangwala, I., Schöner, W., Severskiy, I., Shahgedanova, M., Wang, M., & Yang, D. (2015). Elevation-dependent warming in mountain regions of the world. *Nature climate change*, *5*, 424-430. https://doi.org/10.1038/nclimate2563

Ravanel, L., Guillet, G., Kaushik, S., Preunkert, S., Malet, E., Magnin, F., Trouvé, E., Montagnat, M., Yan, Y., & Deline, P. (2023). Ice aprons on steep high-alpine slopes: insights from the Mont-Blanc massif, Western Alps. *Journal of Glaciology*, 1-17.

5. Discussion

The present PhD thesis summarises different aspects and topics related to the study of glacial hazards and subsequent risk situations that may arise in populated contexts. The work that was performed during the three-year PhD course has enjoyed great positive feedback on the glacial risk monitoring activities in the Aosta Valley Region. International collaborations have started and ideas and projects have been multiplying in the past few years. The growth of applied and research activities gave rise to the idea that this territory should be used as a 'pilot area' and an open-air laboratory in the field of glacial hazards and risk. A specific convention with the commitment of interest in the creation of an official open-air laboratory has already been signed between the Fondazione Montagna Sicura and the National Research Council (CNR). The present work has achieved some important results that open up further research topics that should be investigated in the future. Some of the topics for future research, such as those in section 4.4, already have a plan of future development and this is another remarkable achievement of the PhD project. Not only those of section 4.4 but the other specific objectives highlighted in the present PhD work should also be pursued and further developed in the future. Scientific achievements, the diffusion of new models, new software and new technological equipment that sees continuous evolution should give hope for the filling of knowledge gaps that pose many questions and potential threats in the field of glacial risk as of today.

Looking into the direction that specific topics that were developed in the present project could be focused into further future development, short individual discussions are summarised for each of the presented manuscripts in the following chapter.

5.1 Discussion of individual manuscripts

1) Ten-Year Monitoring of the Grandes Jorasses Glaciers Kinematics. Limits, Potentialities, and Possible Applications of Different Monitoring Systems

The publication of Dematteis et al. (2021) was a fundamental step in the organisation of all the work that followed in the PhD project. In fact, during this project, we faced the problem of retrieving historical data from different sources, different monitoring systems and archived by different people using different methodologies. This part of data back analysis made it possible to standardise procedures for the coding of standardised data formats, data naming and archive structures. The integration of different data was one of the great goals in this work. In the perspective of the PhD project, having a well-organised database of the different monitoring data was an important milestone for future work. I believe that the wider relevance of this work was to share with the scientific community an organised synthesis of all the monitoring data that exist to date for the Whymper Serac and Planpincieux Glacier, on which anyone interested in further research on the topic could rely as a starting database. As of today, the major open question regarding Whymper Serac monitoring concerns its evolution towards a polythermal and, eventually, temperate basal thermal regime. The start of the transition has been demonstrated by the temperature measurements performed in 2020 and 2021, and the first outputs in trends highlighted by the thermo-mechanical modelling (an ongoing project with IGE Grenoble) suggest that actual climatic trends are causing a warming of the serac and the

distribution of temperature obtained by modelling activity reflects those that have been measured. The forcing of the model towards modelled climatic conditions predicted for 2050 suggests a transition towards a state where the proportions between cold and temperate basal surfaces will see the temperate areas becoming more abundant than the cold ones. In such a state, the serac will lose its stability on such a steep slope, and its total collapse is highly likely. Predicting such destabilisation is very difficult and poses a great question for the safety of the valley and the villages endangered by a major failure of the Whymper Serac. Research efforts should be increased in order to achieve a new safety concept and plan for this risk scenario, one that will not be manageable with an acceptable degree of safety for the population with today's knowledge and monitoring systems.

Present knowledge would suggest only extreme solutions for the management of human activities in the areas potentially affected by a major collapse of the Whymper Serac: delocalisation of human activities or the artificial triggering of a total collapse of the serac. Both solutions would engender massive economic losses and no feasibility studies have been carried out to date.

On the other hand, for the monitoring of the Planpincieux Glacier, and for the monitoring of destabilising temperate glacier tongues in general, the major open research question resides in the understanding of the causes of accelerations and decelerations of the destabilising ice masses. As a generic cause of accelerations, it is generally accepted that these should be linked to variations in pressure of the basal hydrological drainage network but it is not known, as of today, how to possibly measure drivers of those pressure changes. Therefore, it is not possible to hypothesise a prediction of motion based on the measurement or modelling of the water inputs in the glacial drainage system as it is impossible, today, to monitor the state and evolution of the drainage network itself. The activity planned for 2024 on the Planpincieux Glacier in the FSC 'Val Ferret Glaciers as sentinels of climate change' project will go in the direction of gaining knowledge in the evolution of the subglacial environment and its relations to ice flow and velocity variations, but it still is far from answering the larger research question and the possibility of monitoring such dynamics. Nonetheless, it is important to stimulate research on this topic in order to gain knowledge for possible future potentials in the prediction of temperate glaciers collapses.

As a long-term perspective, on those specific sites, in 2070-2100, in line with current climatic trends, the Montitaz lobe will have probably gradually disappeared from the steep section of the slope by glacial front retreat; the Whymper Serac may no longer form. The pathway toward this state might see one or more large collapse occur along their evolution.

2) Morphodynamics of the Mont Blanc glaciers and their recent evolution

I believe the work that followed the first objective to be the largest research topic covered during the PhD activity. Once the results are finalised for publication on a peer-reviewed paper, it could possibly be the major scientific outcome of the PhD project. First of all, in this paper we managed to measure, on a monthly basis, the velocities of 30 glaciers for seven years from freely available optical satellite imagery. Therefore, a prime achievement of this study was to demonstrate that the extraction of velocity time series with remote-sensing techniques on alpine glaciers is possible using limited computing effort and both freely available data and processing software. This opens a large pathway in the monitoring of alpine glaciers by remote-sensed techniques, with certain limits that could, eventually, be overcome in the future. This work could analyse

the behaviour of the Planpincieux Glacier as a whole glacial body, not relying only on data from the small destabilising section. Therefore, it could provide some context for the data relative to the accelerations of the frontal Montitaz lobe. Moreover, we could place the Planpincieux Glacier in a larger context along with the other 29 glaciers located in the neighbouring areas in the same massif. Consequently, we proposed a classification of those glaciers and highlighted other sites where large variations of velocities exist in this region. In the future, an analysis of velocity time series from remotely sensed data may, possibly, be based on higher resolution data both in terms of spatial and temporal resolution (satellite revisit times), so that remote sensing could become a real monitoring tool to measure glacier surface velocities. In this scenario, the automated processing of data on a large number of glaciers could provide more possibilities to begin studying the forcing factors of glacier velocity variations (meteo-climatic, mass balance, thermal regime variations, sliding, deformation etc…) and this should be an important topic for future further research.

3) Evidence of bedrock forcing on glacier morphodynamics: a case study in the Italian Alps

Another important achievement in the course of the PhD project was the demonstration that the morphologic and kinematic separations that form onto the Planpincieux Glacier have a recurrency and are directly linked to changes in slope of the bedrock. This was possible thanks to the realisation of a large helicopter-borne GPR Survey. This was performed in cooperation with the ETH of Zurich and with the integration of the multitemporal high resolution topographical data that I personally collected and processed by means of drone and helicopter-borne photogrammetric flights and subsequent Structure from Motion processing. This analysis was also very relevant with regards to the possible future analysis and experiments regarding the ice-bedrock environment at Planpincieux Glacier.

Potential evolutions in geophysical methods and equipment might provide new insights in the possibility to indirectly measure and monitor water presence and activity under/inside glacial bodies. In this direction, an experimental activity of multitemporal GPR helicopter-borne acquisitions is planned for 2024. A new configuration of antennas and a GNSS system on the AIR-ETH system has been tested in 2023 for this purpose, and the experimental activity focused on finding variations in the water presence at difference times of the year in the GPR soundings has already been included and financed as part of the FSC 'Val Ferret Glaciers as sentinels of climate change' project. This is also aimed at being a first step in further research on this topic.

4) Periglacial cascading process in an Alpine environment: an example of an ice avalanche-induced debris flow in Val Ferret (Courmayeur, Italy)

The chance to have a sophisticated monitoring system provided an opportunity to document a large number of events and to carry out specific targeted surveys immediately or very soon after the events themselves. One major event, when a road at the bottom of the Val Ferret was blocked and a bridge damaged by a debris flow, fortunately with no casualties, was well mapped after its occurrence. Nonetheless, after the first field surveys, it was very evident that such a large event could not have been generated due to rainfall as there was far too little to create debris flows along the streams of the Vel Ferret. Owing to this, a specific in-depth analysis of the available data and specific processing of additional data allowed a hypothesis to be formulated on the triggering of this destructive event. This is relevant as the study highlighted

the possibility that further process chains can be activated on this site where a single type of event is monitored. This additional knowledge will, possibly, be integrated in the future in the official municipality and civil protection management procedures. Specific geomorphological analyses could be conceived in order to quantify possible cascading process triggering. However, research and development activities on this matter are much needed.

The study demonstrated that new technologies such as DEM production with the use of UAV with airborne RTK GPS modules, and the production of DEMs from stereo satellite high resolution imagery, provide new possibilities in the study of gravitational phenomena. Further evolution of those techniques will open up new possibilities in the study and back analysis of gravitational processes.

5) Assessing the rock failure return period on an unstable Alpine rock wall based on volume-frequency relationships: the Brenva Spur (3916m asl, Aosta Valley, Italy)

An additional goal achieved during this PhD project was the definition of specific updated risk scenarios for the possible failure of the Brenva Rock Spur and the subsequent genesis of an ice-rock avalanche. I actively participated in the conception of the workflow in the research group that led to the results highlighted in the publication mentioned prior. Once it was decided that helicopter photogrammetry would be the methodology used to monitor and assess both the structural analysis of the rock mass and to perform a DoD operation in order to calculate yearly rock volumes of failure, I also carried out one of the photogrammetrical surveys used in the study.

A re-analysis of the dynamic modelling of possible rock-ice avalanches should be undertaken in the future, accounting for precise failure volumes determined in this study and, possibly, for updated topography of the Brenva Glacier, large volume changes having been noted in recent years.

Large-scale dynamic modelling, with the identification of possible source areas for rock avalanches at high altitudes, could be initiated in the future. The modelling might also become a useful tool regarding the exacerbation of high-altitude large slope failures related to permafrost degradation present in current climate change scenarios.

Specific monitoring studies on rockfall activity at high altitudes should also be stimulated in the future and major improvements might also come in this field from remotely sensed data analysis.

6) Recent evolution of high alpine areas: multi-sensor optical satellite imagery analysis in the Monte Rosa Massif, Western Alps

If the Brenva rock Spur is a large rock instability at high altitude, it is not yet clear whether permafrost degradation is the main driver of the past and present rock failures at this specific site. This considered, an increase in small to medium failures of rock masses during summer

and autumn in high alpine mountain areas, has been noted and documented in very recent years both by the mountaineering community and by several studies dedicated to this subject. The other phenomenon that accompanies a high number of instabilities is a poorly documented trend in the rapid enlargement of rock outcrops at very high altitudes. Owing to this, we performed a pilot study on the Monte Rosa Massif where we determine if these sparse observations of rock outcrop enlargement have quantitative evidence, at least at a massif scale. The results of the study document preliminary evidence that a possible rupture in the trend of recent decades could be underway. Though this topic certainly requires an analysis of larger datasets on other areas and on larger timespans in order to confirm this trend, it does suggest that the very highest parts of the Alps, considered to be much more stable than the lower zones, could be on the threshold of an era of intense variations in the current climate change scenarios. This will be relevant for the study, the monitoring and the prediction of possible future large slope instabilities in high mountain rock faces that could engender larger ice-rock avalanche scenarios in the future setting of the high alpine landscapes.

5.2 Discussion of an integrated general approach in glacial risk monitoring

In the present work, we dedicated our study to a specific mountain region. Nonetheless, many processes described in this work are processes typical of mountain regions globally. It is beyond the possibilities of the present PhD project to provide a full review of glacial risk processes, their identification and their monitoring. Nonetheless, a preliminary framework to be further developed, with the aim of realising guidelines for the identification and monitoring of glacial instabilities based on the present PhD project, and especially on the work carried out with the realisation of Dematteis et al. (2021), can be outlined as a final chapter of the thesis. In fact, in the last decade, the Grandes Jorasses glaciers complex, comprising both the Whymper Serac and the Montitaz lobe of the Planpincieux Glacier, have become a real open-air laboratory for the study of glacier destabilisation and ice avalanches in particular. Thanks to this huge concentration of studies, measurements and experiments, we can consider that almost all monitoring techniques that can be applied in this field have been implemented or at least attempted, and their pros and cons highlighted. So, a preliminary, but updated review regarding the detection and the monitoring of glacial instabilities can be summarised in the following paragraphs, primarily to be further developed in future studies.

Glacial risk monitoring integrated general approach

We hereby summarise a possible general framework for the monitoring and management of glacial risks. It is synthesised in the following workflow (Figure 16) and subsequently commented on in the following paragraphs.

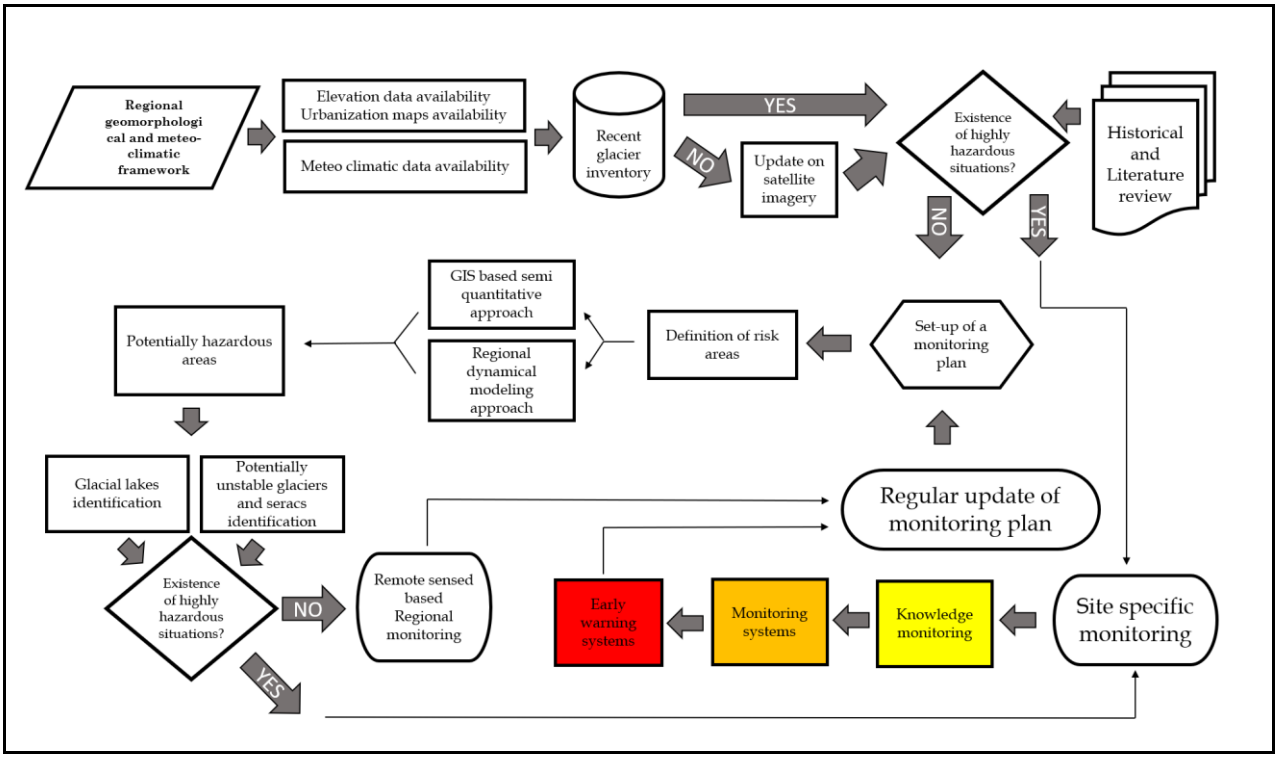

Figure 15. Workflow of a general approach to glacial risk monitoring and management.

When facing the problem of the identification of potential glacial risk situations at a regional scale, the regional geomorphological and meteo-climatic framework in which the analysis will be performed should first be assessed.

Regional geomorphological and meteo-climatic framework

Meteorological data of the area should be collected, and both the presence of Automated Weather Stations or the existence of historical time series data should be checked. Mean annual temperature at different altitudes should be determined and precipitation regimes and intensities assessed. A preliminary assessment of the altitude where glaciers could be cold, based in the region, should be made as well as the presence of continuous permafrost.

It is fundamental to retrieve whatever **altitudinal data** is available in the region. NASA's SRTM 30 metre resolution DEM is available globally, and it could be suitable in off-glacier terrain, but dated 2000, considerations should be made on the use of such data regarding glaciers. Aster DEMs also offer almost global coverage (geographic coverage of the ASTER

GDEM extends from 83° North to 83° South) at 30m ground resolution, with acquisition dates ranging from 1 March 2000 to 30 November 2013. Therefore, depending on the location of the area, this dataset could be more recent than the SRTM DEM. The production of a regional updated DEM should be considered by checking the availability of archive stereo satellite imagery or requesting specific tasking by the satellites with stereo capability. Some radar satellite data can be used to obtain updated topographic data and commercial satellite companies also offer for sale of processed DEMs from specific satellite acquisitions.

The availability of maps of the principal **urbanisation structures and infrastructures** should be checked, and if no specific product is available from governmental agencies, products such as Open Street Maps or similar can be used for this purpose. Specific digitisation can be made by the use of high-resolution satellite imagery, if needed and if available.

Location and extent of glaciers in the region of interest can be made by the use of the Randoph Glacier Inventory. This also includes the principal morphometric parameters of the glacial bodies. The year of update of glacier outlines can be variable (for example, on Mont Blanc outlines are dated 2003) but updates of the inventory are also planned and published. A local update of glacier outlines based on Optical Satellite imagery should generally be undertaken.

Historical and bibliographic background

Bibliographic research on historical events of glacier instability and/or destabilisation should be made. If possible, local authorities and/or citizens could provide insights on historical or recent hazardous events. If very evident, risk situations should be easily identified and this should immediately activate further site-specific investigations and the possible monitoring of the phenomena. A **scientific literature review** should be made specifically to understand if and what kind of glaciological research has been or is being performed in the region.

Definition of hazards

At this stage, it is possible to start **specific large-scale hazard mapping** and identify zones that could, potentially, be impacted and represent **zones at risk**. An initial **qualitative risk assessment** can be made as a matrix of distances between potentially hazardous glaciers (if there is an indication of any) or between all glaciers of the Randoph Glacier Inventory and human settlements and infrastructure. Maximum run-out distances for historical phenomena can be found in literature and may be used as a reference for extreme phenomena in order to discard very remote areas and concentrate the analysis on glacier areas that are closer to human settlements and infrastructure. A first simple approach could be based on simple buffer polygons built on the Randoph Glacier Inventory glacier outline polygons. Further refinement can be made by the use of **dynamic models for flow routing**. At the regional scale, only simple models can normally be used due to the computational effort required to analyse large regions. Arbitrary volumes of ice, when considering ice avalanches, and arbitrary water volumes, when considering GLOFs, can be used based on literature studies (Huggel et al., 2004). This workflow is based on the simplistic assumption that an ice avalanche could occur on any Randoph Glacier Inventory glacier, as could a GLOF.

This approach will overestimate the number of glaciers that could potentially be dangerous, and a subsequent further discrimination is needed after this first analysis. The eye of a trained glaciologist can quickly discern very small or very flat glacial bodies that can be discarded from the inventory of potentially hazardous glaciers for ice avalanche phenomena. A morphometric analysis of the selected glacial bodies can also provide the same results but should also be carefully reviewed by an expert as the identification of potentially hazardous sites is very relevant. **Glacier thickness global modelled databases** should be integrated at this stage in order to provide an initial estimate of possible destabilisation volumes of specific sites. If a critical setting is spotted, specific surveys for updated site-specific estimations of ice thickness should be made together with updated site-specific topographic surveys. Ice thicknesses can generally be identified by ground or heliported **GPR** soundings, while topography may be updated by drone **photogrammetry**, aerial **lidar** or **satellite stereo acquisition**, depending on the extent of the area, the required resolution and accuracy and the financial resources available.

Regarding potential GLOFs, if the hypothesis of a subglacial water accumulation could cause flooding, then all glaciers should be considered. If this option is not taken into account, then the **identification of glacial lakes** with a free surface can be performed by remote sensing techniques and semi-automatic classification algorithms. The evolution of glacial lakes can then be performed with an update using the same techniques. Lakes with potentially unstable geometries can thus be spotted. **Geomorphological analyses** by a trained eye may reveal unusual surface features on remotely sensed imagery that could be indicative of destabilisation processes such as freshly formed crevasses or large ice avalanche deposits. This could call for the further site-specific surveys and eventually monitoring. When performing geomorphological analyses, the identification of potentially hazardous glacial lakes by a trained eye **can be compared** or integrated to the semi-automatic classification proposed above. If remote sensing analyses identify specific sites with potentially hazardous glacial dynamics, specific monitoring can be undertaken.

When specific estimation of volumes is available for a certain site, **tailored run out modelling**, with the use of sophisticated modelling software, may be undertaken if needed.

Glacial hazard monitoring

If anomalous glacial dynamics are detected, a first assessment of the kinematics can be made by the use of globally averaged displacement maps (Millan et al., 2022) and a subsequent check of the actual surface displacement rates. If glaciers are large enough, automated global displacement maps can be used, otherwise site-specific processing should be made.

When dealing with serac falls or glacier collapses, almost all the monitoring possibilities in glacial environments are highlighted in Dematteis et al. (2021). Some specific cases might be suited to other techniques not highlighted in this glacial complex, for example very slow-moving ice masses could be also monitored by radar satellite interferometry, which was not suitable on the Grandes Jorasses Glacier complex. A few other techniques can be shared from experiences in the monitoring of other slope instabilities. It is possible to refer to specific landslide monitoring literature for alternative solutions, such as inclinometers or crack-meters, which could suit certain glacial settings. The monitoring of potentially unstable glacial lake dams could require a search for and adaption of different technologies. The **principal techniques used for monitoring of deformations are:** TLCs, TRI, RTS, GNSS and satellite

interferometry. Most of the pros and cons of the abovementioned techniques can be found and are carefully reviewed in Dematteis et al., 2021. The monitoring phases should be approached as a semaphoric 3-level monitoring of different intensity levels (for example, if a massive GLOF is expected very soon and just being detected, the phase switches immediately to the application of safety measures). At first, a **knowledge monitoring** phase is expected. In order to characterise phenomena and understand the dynamics and the data related to it, a first phase of data acquisition and data analysis should be performed. When the knowledge monitoring provides information and possibilities about the monitoring of the phenomena, this phase can be translated into a fully active **monitoring system.** If the monitoring systems detects potential instabilities, this could require the monitoring system to feature an **alarm monitoring phase** with the integration of specific early warning systems.

Risk management

Should an **early warning system** be needed, possible solutions can be copied from snow avalanche, debris flow or rockfall early warning monitoring systems. The main technologies used for this purpose normally are Doppler radar, seismic sensors and pendulum systems.

Few private companies specialised in this sector exist, and tailored as well as experimental solutions can be studied with highly experienced technicians.

For the monitoring of **GLOF**s, water-level sensors have been successfully tested to trigger alarms downslope if water level lowering is detected. Active intervention can also be planned with different techniques used for artificial water-level lowering such as water pumping, syphoning, or channel excavation. However, these should be carefully planned in order not to trigger unexpected lake emptying (see the case study of the Giétro GLOF (Ancey et al., 2019)).

It should be remembered that, when dealing with monitoring and early warning systems, **safety plans** to cope with emergency situations should be carefully conceived and communicated to the local populations and authorities.

Nonetheless, **communication strategies** to transmit alerts to local communities and authorities should be planned so that safety measures are understood and accepted and, therefore, can have a positive impact on people's safety.

Regular **updates** of the full monitoring plan, and the approaches used, should be regularly reviewed and updated.

6. Conclusion

In this PhD project, a wide array of themes was considered and developed, all of which had one main objective. The objective was to answer several major research questions such as: what is the current situation regarding the knowledge and monitoring of glacial related risks? What are the main gaps in knowledge of the observed processes? Which are the main research questions on this topic? The PhD project was structured around these questions and a series of specific

actions it was possible develop in the three-year course of the project were initiated. Most of the topics were directly related to the monitoring of glacial risks and, when possible, a direct relation and integration with the regional glacial risk monitoring plan managed by the Fondazione Montagna Sicura was undertaken.

Some major improvements were achieved during the course of the PhD project and, above all, a real integration of research activities and practical applications has been structured. In many fields and for many reasons, such integrations struggle to be undertaken and, in some cases, science and practice do not often meet along their evolution. As the objectives of academic institutes and private companies tend to differ, it can often be difficult to integrate the two sectors.

We believe that advancements in earth observation techniques could, in the near future, boost studies related to glacial risk processes. Nonetheless, expensive and time-consuming field experiments are still needed for a better understanding of the processes leading to glacial instabilities. A series of knowledge gaps and research questions were developed and represent the core of the present PhD project. Certainly, not all such gaps and questions could be developed but a stronger base on which to develop future research has been built in regard to what was analysed in 2019, before the start of the present project. Research on glacial related hazards is a niche research topic but efforts like the ones made for this project should be continued in order for communities to be able to adapt to future mountain environment settings around the globe.

Acknowledgements

I would like to thank Dr Jean Pierre Fosson, Dr Raffaele Rocco, Dr Valerio Segor, Dr Guido Giardini and Professor Martin Funk for their support and their will to stimulate cryospheric research activities in the Aosta Valley Region and the Mont Blanc Massif. I thank all my colleagues at the Technical and Research Area of the Fondazione Montagna Sicura as well as all the staff at the Foundation for their support. I also would like to thank Professor Christian Vincent for his advice on research activity and for providing useful additional information, especially on the French glaciers of Mont Blanc. A special acknowledgment goes to my tutors, Daniele Giordan and Francesco Zucca, as well as Niccolò Dematteis for their continuous support and passionate input into this work. Most of all, I am grateful to my family: Bianca, Ilaria, Mum and Dad for being on my side in many stressful times while balancing work and research activity into everyday life.

7. Bibliography

Ahn, Y., & Box, J. E. (2010). Glacier velocities from time-lapse photos: technique development and first results from the Extreme Ice Survey (EIS) in Greenland. Journal of Glaciology, 56(198), 723-734.

Alean, J. (1985). Ice avalanches: some empirical information about their formation and reach. Journal of Glaciology, 31(109), 324-333.

Allen, S., Frey, H., Haeberli, W., Huggel, C., Chiarle, M., & Geertsema, M. (2022). Assessment principles for glacier and permafrost hazards in mountain regions. In Oxford Research Encyclopedia of Natural Hazard Science.

Allstadt, K., Shean, D., Campbell, A., Fahnestock, M., & Malone, S. (2015). Observations of seasonal and diurnal glacier velocities at Mount Rainier, Washington, using terrestrial radar interferometry. The Cryosphere, 9(6), 2219-2235.

Altena, B., Scambos, T., Fahnestock, M., & Kääb, A. (2019). Extracting recent short-term glacier velocity evolution over southern Alaska and the Yukon from a large collection of Landsat data. The Cryosphere, 13(3), 795-814.

Ancey, C., Bardou, E., Funk, M., Huss, M., Werder, M., & Trewhela, T. (2019). Hydraulic reconstruction of the 1818 Giétro glacial lake outburst flood. Water Resources Research, 55(11), 8840-8863.

Arendt, A., Bliss, A., Bolch, T., Cogley, J., Gardner, A., Hagen, J.-O., Hock, R., Huss, M., Kaser, G., & Kienholz, C. (2017). Randolph Glacier inventory–A dataset of Global glacier outlines: Version 6.0: Technical report, Global land ice measurements from space.

Barnett, T. P., Adam, J. C., & Lettenmaier, D. P. (2005). Potential impacts of a warming climate on water availability in snow-dominated regions. Nature, 438(7066), 303-309.

Beniston, M., Farinotti, D., Stoffel, M., Andreassen, L. M., Coppola, E., Eckert, N., Fantini, A., Giacona, F., Hauck, C., & Huss, M. (2018). The European mountain cryosphere: a review of its current state, trends, and future challenges. The Cryosphere, 12(2), 759-794.

Benn, D. I., & Evans, D. J. (2014). Glaciers & glaciation. Routledge.

Berthier, E., Vadon, H., Baratoux, D., Arnaud, Y., Vincent, C., Feigl, K., Remy, F., & Legresy, B. (2005). Surface motion of mountain glaciers derived from satellite optical imagery. Remote Sensing of Environment, 95(1), 14-28.

Berthier, E., Vincent, C., Magnússon, E., Gunnlaugsson, Á., Pitte, P., Le Meur, E., Masiokas, M., Ruiz, L., Pálsson, F., & Belart, J. (2014). Glacier topography and elevation changes derived from Pléiades sub-meter stereo images. The Cryosphere, 8(6), 2275-2291.

Bindschadler, R. (1983). The importance of pressurized subglacial water in separation and sliding at the glacier bed. Journal of Glaciology, 29(101), 3-19.

Buisson, A., Dumas, C., Reynaud, L., & Valla, F. (1999). Les risques naturels d'origine glaciaire: inventaire dans les Alpes françaises et typologie. La Houille Blanche(5), 47-53.

Congedo, L. (2021). Semi-Automatic Classification Plugin: A Python tool for the download and processing of remote sensing images in QGIS. Journal of Open Source Software, 6(64), 3172.

Cuffey, K. M., & Paterson, W. S. B. (2010). The Physics of Glaciers. Academic Press.

Davaze, L., Rabatel, A., Dufour, A., Hugonnet, R., & Arnaud, Y. (2020). Region-wide annual glacier surface mass balance for the European Alps from 2000 to 2016. Frontiers in Earth Science, 8, 149.

Dehecq, A., Gourmelen, N., & Trouve, E. (2015). Deriving large-scale glacier velocities from a complete satellite archive: Application to the Pamir–Karakoram–Himalaya. Remote Sensing of Environment, 162, 55-66.

Deilami, K., & Hashim, M. (2011). Very high resolution optical satellites for DEM generation: a review. European Journal of Scientific Research, 49(4), 542-554.

Deline, P. (2002). Étude géomorphologique des interactions entre écroulements rocheux et glaciers dans la haute montagne alpine: le versant sud-est du massif du Mont-Blanc (Vallée d'Aoste, Italie) Chambéry.

Deline, P., Akçar, N., Ivy-Ochs, S., & Kubik, P. W. (2015). Repeated Holocene rock avalanches onto the Brenva Glacier, Mont Blanc massif, Italy: a chronology. Quaternary Science Reviews, 126, 186-200.

Deline, P., Bolon, P., Chiarle, M., Fioraso, G., Fosson, J. P., Gay, M., Gardent, M., Di Cella, U. M., Ott, L., & Pogliotti, P. (2010). GlaRiskAlp, a French-Italian project (2010-2013) on glacial hazards in the Western Alps in relation with the glacier retreat. 14th Alpine Glaciological Meeting,

Deline, P., Gardent, M., Magnin, F., & Ravanel, L. (2012). The morphodynamics of the Mont Blanc massif in a changing cryosphere: a comprehensive review. Geografiska Annaler: Series A, Physical Geography, 94(2), 265-283.

Deline, P., Gruber, S., Delaloye, R., Fischer, L., Geertsema, M., Giardino, M., Hasler, A., Kirkbride, M., Krautblatter, M., & Magnin, F. (2015). Ice loss and slope stability in high-mountain regions. In Snow and ice-related hazards, risks, and disasters (pp. 521-561). Elsevier.

Dematteis, N., & Giordan, D. (2021). Comparison of digital image correlation methods and the impact of noise in geoscience applications. Remote Sensing, 13(2), 327.

Dematteis, N., Giordan, D., & Allasia, P. (2019). Image classification for automated image cross-correlation applications in the geosciences. Applied Sciences, 9(11), 2357.

Dematteis, N., Giordan, D., Perret, P., Grab, M., Maurer, H., & Troilo, F. (2022). Evidences of bedrock forcing on glacier morphodynamics: a case study in Italian Alps. Frontiers in Earth Science, 10, 793546.

Dematteis, N., Giordan, D., Troilo, F., Wrzesniak, A., & Godone, D. (2021). Ten-year monitoring of the Grandes Jorasses Glaciers kinematics. Limits, potentialities, and possible applications of different monitoring systems. Remote Sensing, 13(15), 3005.

Dematteis, N., Giordan, D., Zucca, F., Luzi, G., & Allasia, P. (2018). 4D surface kinematics monitoring through terrestrial radar interferometry and image cross-correlation coupling. ISPRS Journal of Photogrammetry and Remote Sensing, 142, 38-50.

Dematteis, N., Luzi, G., Giordan, D., Zucca, F., & Allasia, P. (2017). Monitoring Alpine glacier surface deformations with GB-SAR. Remote Sensing Letters, 8(10), 947-956.

Diolaiuti, G., Bocchiola, D., Vagliasindi, M., D'agata, C., & Smiraglia, C. (2012). The 1975-2005 glacier changes in Aosta Valley (Italy) and the relations with climate evolution. Progress in Physical Geography, 36(6), 764-785.

Diolaiuti, G., Kirkbride, M., Smiraglia, C., Benn, D., D'agata, C., & Nicholson, L. (2005). Calving processes and lake evolution at Miage glacier, Mont Blanc, Italian Alps. Annals of Glaciology, 40, 207-214.

Einarsson, B., Magnússon, E., Roberts, M. J., Pálsson, F., Thorsteinsson, T., & Jóhannesson, T. (2016). A spectrum of jökulhlaup dynamics revealed by GPS measurements of glacier surface motion. Annals of Glaciology, 57(72), 47-61.

Emmer, A. (2017). Glacier retreat and glacial lake outburst floods (GLOFs). In Oxford Research Encyclopedia of Natural Hazard Science.

Emmer, A., Allen, S. K., Carey, M., Frey, H., Huggel, C., Korup, O., Mergili, M., Sattar, A., Veh, G., & Chen, T. Y. (2022). Progress and challenges in glacial lake outburst flood research (2017–2021): a research community perspective. Natural Hazards and Earth System Sciences, 22(9), 3041-3061.

Evans, A. N. (2000). Glacier surface motion computation from digital image sequences. IEEE Transactions on Geoscience and Remote Sensing, 38(2), 1064-1072.

Fahnestock, M., Scambos, T., Moon, T., Gardner, A., Haran, T., & Klinger, M. (2016). Rapid large-area mapping of ice flow using Landsat 8. Remote Sensing of Environment, 185, 84-94.

Faillettaz, J., Funk, M., & Sornette, D. (2012). Instabilities on Alpine temperate glaciers: new insights arising from the numerical modelling of Allalingletscher (Valais, Switzerland). Natural Hazards and Earth System Sciences, 12(9), 2977-2991.

Faillettaz, J., Funk, M., & Vagliasindi, M. (2016). Time forecast of a break-off event from a hanging glacier. The Cryosphere, 10(3), 1191-1200.

Faillettaz, J., Funk, M., & Vincent, C. (2015). Avalanching glacier instabilities: Review on processes and early warning perspectives. Reviews of Geophysics, 53(2), 203-224.

Faillettaz, J., Pralong, A., Funk, M., & Deichmann, N. (2008). Evidence of log-periodic oscillations and increasing icequake activity during the breaking-off of large ice masses. Journal of Glaciology, 54(187), 725-737.

Fei, L., Jaboyedoff, M., Guerin, A., Noël, F., Bertolo, D., Derron, M.-H., Thuegaz, P., Troilo, F., & Ravanel, L. (2023). Assessing the rock failure return period on an unstable Alpine rock wall based on volume-frequency relationships: The Brenva Spur (3916 m asl, Aosta Valley, Italy). Engineering Geology, 323, 107239.

Frenierre, J. L., & Mark, B. G. (2014). A review of methods for estimating the contribution of glacial meltwater to total watershed discharge. Progress in Physical Geography, 38(2), 173-200.

Friedl, P., Seehaus, T., & Braun, M. (2021). Global time series and temporal mosaics of glacier surface velocities derived from Sentinel-1 data. Earth System Science Data, 13(10), 4653-4675.

FUKUZONO, T. (1985). A method to predict the time of slope failure caused by rainfall using the inverse number of velocity of surface displacement. Landslides, 22(2), 8-13_11.

Fyffe, C. L. (2012). The hydrology of debris-covered glaciers, University of Dundee.

Gilbert, A., Leinss, S., Kargel, J., Kääb, A., Gascoin, S., Leonard, G., Berthier, E., Karki, A., & Yao, T. (2018). Mechanisms leading to the 2016 giant twin glacier collapses, Aru Range, Tibet. The Cryosphere, 12(9), 2883-2900.

Giordan, D., Adams, M. S., Aicardi, I., Alicandro, M., Allasia, P., Baldo, M., De Berardinis, P., Dominici, D., Godone, D., & Hobbs, P. (2020). The use of unmanned aerial vehicles (UAVs) for engineering geology applications. Bulletin of Engineering Geology and the Environment, 79, 3437-3481.

Giordan, D., Allasia, P., Dematteis, N., Dell'Anese, F., Vagliasindi, M., & Motta, E. (2016). A low-cost optical remote sensing application for glacier deformation monitoring in an alpine environment. Sensors, 16(10), 1750.

Giordan, D., Dematteis, N., Allasia, P., & Motta, E. (2020). Classification and kinematics of the Planpincieux Glacier break-offs using photographic time-lapse analysis. Journal of Glaciology, 66(256), 188-202.

Glen, J. (1952). Experiments on the deformation of ice. Journal of Glaciology, 2(12), 111-114.

Gottardi, F., Obled, C., Gailhard, J., & Paquet, E. (2012). Statistical reanalysis of precipitation fields based on ground network data and weather patterns: application over French mountains. Journal of hydrology, 432, 154-167.

Haeberli, W., Alean, J.-C., Müller, P., & Funk, M. (1989). Assessing risks from glacier hazards in high mountain regions: some experiences in the Swiss Alps. Annals of Glaciology, 13, 96-102.

Heid, T., & Kääb, A. (2012). Evaluation of existing image matching methods for deriving glacier surface displacements globally from optical satellite imagery. Remote Sensing of Environment, 118, 339-355.

Heid, T., & Kääb, A. (2012). Repeat optical satellite images reveal widespread and long term decrease in land-terminating glacier speeds. The Cryosphere, 6(2), 467-478.

Hock, R., Jansson, P., & Braun, L. N. (2005). Modelling the response of mountain glacier discharge to climate warming. Global change and mountain regions: an overview of current knowledge, 243-252.

Huggel, C., Haeberli, W., Kääb, A., Bieri, D., & Richardson, S. (2004). An assessment procedure for glacial hazards in the Swiss Alps. Canadian Geotechnical Journal, 41(6), 1068-1083.

Humbert, A., Greve, R., & Hutter, K. (2005). Parameter sensitivity studies for the ice flow of the Ross Ice Shelf, Antarctica. Journal of Geophysical Research: Earth Surface, 110(F4).

Jawak, S. D., Kumar, S., Luis, A. J., Bartanwala, M., Tummala, S., & Pandey, A. C. (2018). Evaluation of geospatial tools for generating accurate glacier velocity maps from optical remote sensing data. Proceedings 2018, 2, 341.

Jiskoot, H. (2011). Dynamics of glaciers. Physical Research, 92(B9), 9083-9100.

Jolliffe, I. T., & Cadima, J. (2016). Principal component analysis: a review and recent developments. Philosophical transactions of the royal society A: Mathematical, Physical and Engineering Sciences, 374(2065), 20150202.

Kääb, A., Huggel, C., Fischer, L., Guex, S., Paul, F., Roer, I., Salzmann, N., Schlaefli, S., Schmutz, K., & Schneider, D. (2005). Remote sensing of glacier-and permafrost-related hazards in high mountains: an overview. Natural Hazards and Earth System Sciences, 5(4), 527-554.

Kääb, A., Jacquemart, M., Gilbert, A., Leinss, S., Girod, L., Huggel, C., Falaschi, D., Ugalde, F., Petrakov, D., & Chernomorets, S. (2021). Sudden large-volume detachments of low-angle mountain glaciers–more frequent than thought? The Cryosphere, 15(4), 1751-1785.

Kääb, A., Winsvold, S., Altena, B., Nuth, C., Nagler, T., & Wuite, J. (2016). Glacier Remote Sensing using Sentinel-2. Part I: Radiometric and geometric performance, and application to ice velocity. Remote Sensing, 8(7).

Kamb, B. (1987). Glacier surge mechanism based on linked cavity configuration of the basal water conduit system. Journal of Geophysical Research: Solid Earth, 92(B9), 9083-9100.

Kenner, R., Phillips, M., Limpach, P., Beutel, J., & Hiller, M. (2018). Monitoring mass movements using georeferenced time-lapse photography: Ritigraben rock glacier, western Swiss Alps. Cold Regions Science and Technology, 145, 127-134.

Kingsland, K. (2020). Comparative analysis of digital photogrammetry software for cultural heritage. Digital Applications in Archaeology and Cultural Heritage, 18, e00157.

Lesca, C. (1974). Emploi de la photogrammetrie analytique pour la determination de la vitesse superficielle des glaciers et des profondeurs relatives.

Luzi, G., Dematteis, N., Zucca, F., Monserrat, O., Giordan, D., & López-Moreno, J. I. (2018). Terrestrial radar interferometry to monitor glaciers with complex atmospheric screen. IGARSS 2018-2018 IEEE International Geoscience and Remote Sensing Symposium.

Luzi, G., Pieraccini, M., Mecatti, D., Noferini, L., Macaluso, G., Tamburini, A., & Atzeni, C. (2007). Monitoring of an alpine glacier by means of ground-based SAR interferometry. IEEE Geoscience and Remote Sensing Letters, 4(3), 495-499.

Maltese, A., Pipitone, C., Dardanelli, G., Capodici, F., & Muller, J.-P. (2021). Toward a comprehensive dam monitoring: on-site and remote-retrieved forcing factors and resulting displacements (GNSS and PS–InSAR). Remote Sensing, 13(8), 1543.

Margreth, S., Faillettaz, J., Funk, M., Vagliasindi, M., Diotri, F., & Broccolato, M. (2011). Safety concept for hazards caused by ice avalanches from the Whymper hanging glacier in the Mont Blanc Massif. Cold Regions Science and Technology, 69(2-3), 194-201.

Margreth, S., & Funk, M. (1999). Hazard mapping for ice and combined snow/ice avalanches—Two case studies from the Swiss and Italian Alps. Cold Regions Science and Technology, 30(1-3), 159-173.

Margreth, S., Funk, M., Tobler, D., Dalban, P., Meier, L., & Lauper, J. (2017). Analysis of the hazard caused by ice avalanches from the hanging glacier on the Eiger west face. Cold Regions Science and Technology, 144, 63-72.

Marsy, G., Vernier, F., Trouvé, E., Bodin, X., Castaings, W., Walpersdorf, A., Malet, E., & Girard, B. (2021). Temporal consolidation strategy for ground-based image displacement time series: application to glacier monitoring. IEEE Journal of Selected Topics in Applied Earth Observations and Remote Sensing, 14, 10069-10078.

Marta, C., Viani, C., Giovanni, M., Deline, P., Andrea, T., & Guido, N. (2023). Large glacier failures in the Italian Alps over the last 90 years. Geografia Fisica e Dinamica Quaternaria, 45, 19-40.

Meier, L., Jacquemart, M., Steinacher, R., Jäger, D., & Funk, M. (2018). Monitoring of the Weissmies Glacier before the failure event of September 10, 2017 with radar interferometry and high-resolution deformation camera. Proceedings, International Snow Science Workshop, Innsbruck, Austria,

Mergili, M., Jaboyedoff, M., Pullarello, J., & Pudasaini, S. P. (2020). Back calculation of the 2017 Piz Cengalo–Bondo landslide cascade with r.avaflow: what we can do and what we can learn. Natural Hazards and Earth System Sciences, 20(2), 505-520.

Millan, R., Mouginot, J., Rabatel, A., Jeong, S., Cusicanqui, D., Derkacheva, A., & Chekki, M. (2019). Mapping surface flow velocity of glaciers at regional scale using a multiple sensors approach. Remote Sensing, 11(21), 2498.

Millan, R., Mouginot, J., Rabatel, A., & Morlighem, M. (2022). Ice velocity and thickness of the world's glaciers. Nature Geoscience, 15(2), 124-129.

Mondardini, L., Perret, P., Frasca, M., Gottardelli, S., & Troilo, F. (2021). Local variability of small Alpine glaciers: Thoula Glacier geodetic mass balance reconstruction (1991-2020) and analysis of volumetric variations. Geografia Fisica e Dinamica Quaternaria, 44(1), 29-38.

Monserrat, O., Crosetto, M., & Luzi, G. (2014). A review of ground-based SAR interferometry for deformation measurement. ISPRS Journal of Photogrammetry and Remote Sensing, 93, 40-48.

Mourey, J., & Ravanel, L. (2017). Evolution of access routes to high mountain refuges of the Mer de Glace Basin (Mont Blanc Massif, France). An example of adapting to climate change effects in the Alpine High mountains. Journal of Alpine Research | Revue de géographie alpine(105-4).

Nanni, U., Gimbert, F., Vincent, C., Gräff, D., Walter, F., Piard, L., & Moreau, L. (2020). Quantification of seasonal and diurnal dynamics of subglacial channels using seismic observations on an Alpine glacier. The Cryosphere, 14(5), 1475-1496.

Nye, J. F. (1952). The mechanics of glacier flow. Journal of Glaciology, 2(12), 82-93.

Ogier, C., Werder, M. A., Huss, M., Kull, I., Hodel, D., & Farinotti, D. (2021). Drainage of an ice-dammed lake through a supraglacial stream: hydraulics and thermodynamics. The Cryosphere, 15(11), 5133-5150.

Pandey, V. K., Kumar, R., Singh, R., Kumar, R., Rai, S. C., Singh, R. P., Tripathi, A. K., Soni, V. K., Ali, S. N., & Tamang, D. (2022). Catastrophic ice-debris flow in the Rishiganga River, Chamoli, Uttarakhand (India). Geomatics, Natural Hazards and Risk, 13(1), 289-309.

Paradis, E. (2022). Probabilistic unsupervised classification for large-scale analysis of spectral imaging data. International Journal of Applied Earth Observation and Geoinformation, 107, 102675.

Paul, F., Barrand, N. E., Baumann, S., Berthier, E., Bolch, T., Casey, K., Frey, H., Joshi, S., Konovalov, V., & Le Bris, R. (2013). On the accuracy of glacier outlines derived from remote-sensing data. Annals of Glaciology, 54(63), 171-182.

Paul, F., Bolch, T., Kääb, A., Nagler, T., Nuth, C., Scharrer, K., Shepherd, A., Strozzi, T., Ticconi, F., & Bhambri, R. (2015). The glaciers climate change initiative: methods for creating glacier area, elevation change and velocity products. Remote Sensing of Environment, 162, 408-426.

Paul, F., Piermattei, L., Treichler, D., Gilbert, L., Girod, L., Kääb, A., Libert, L., Nagler, T., Strozzi, T., & Wuite, J. (2022). Three different glacier surges at a spot: what satellites observe and what not. The Cryosphere, 16(6), 2505-2526.

Paul, F., Winsvold, S. H., Kääb, A., Nagler, T., & Schwaizer, G. (2016). Glacier remote sensing using Sentinel-2. Part II: Mapping glacier extents and surface facies, and comparison to Landsat 8. Remote Sensing, 8(7), 575.

Pelfini, M., Santilli, M., Leonelli, G., & Bozzoni, M. (2007). Investigating surface movements of debris-covered Miage glacier, Western Italian Alps, using dendroglaciological analysis. Journal of Glaciology, 53(180), 141-152.

Pepin, N., Bradley, R., Diaz, H., Baraer, M., Cáceres, B., Forsythe, N., Fowler, H., Greenwood, G., Hashmi, M., Liu, X., Miller, J., Ning, L., Ohmura, A., Palazzi, E., Rangwala, I., Schöner, W., Severskiy, I., Shahgedanova, M., Wang, M., & Yang, D. (2015). Elevation-dependent warming in mountain regions of the world. Nature climate change, 5, 424-430. https://doi.org/10.1038/nclimate2563

Pfeffer, W. T., Arendt, A. A., Bliss, A., Bolch, T., Cogley, J. G., Gardner, A. S., Hagen, J.-O., Hock, R., Kaser, G., & Kienholz, C. (2014). The Randolph Glacier Inventory: a globally complete inventory of glaciers. Journal of Glaciology, 60(221), 537-552.

Pralong, A., Birrer, C., Stahel, W. A., & Funk, M. (2005). On the predictability of ice avalanches. Nonlinear Processes in Geophysics, 12(6), 849-861.

Pralong, A., & Funk, M. (2006). On the instability of avalanching glaciers. Journal of Glaciology, 52(176), 31-48.

Rabatel, A., Ducasse, E., Millan, R., & Mouginot, J. (2023). Satellite-derived annual glacier surface flow velocity products for the European Alps, 2015–2021. Data, 8(4), 66.

Rankl, M., Kienholz, C., & Braun, M. (2014). Glacier changes in the Karakoram region mapped by multimission satellite imagery. The Cryosphere, 8(3), 977-989.

Ravanel, L. (2009). Évolution géomorphologique de la haute montagne alpine dans le contexte actuel de réchauffement climatique. In: Collection EDYTEM-Cahiers de Géographie, n° 8.

Ravanel, L., Guillet, G., Kaushik, S., Preunkert, S., Malet, E., Magnin, F., Trouvé, E., Montagnat, M., Yan, Y., & Deline, P. (2023). Ice aprons on steep high-alpine slopes: insights from the Mont-Blanc massif, Western Alps. Journal of Glaciology, 1-17.

Samsonov, S., Tiampo, K., & Cassotto, R. (2021). SAR-derived flow velocity and its link to glacier surface elevation change and mass balance. Remote Sensing of Environment, 258, 112343.

Scambos, T. A., Dutkiewicz, M. J., Wilson, J. C., & Bindschadler, R. A. (1992). Application of image cross-correlation to the measurement of glacier velocity using satellite image data. Remote Sensing of Environment, 42(3), 177-186.

Schwalbe, E., & Maas, H.-G. (2017). The determination of high-resolution spatio-temporal glacier motion fields from time-lapse sequences. Earth Surface Dynamics, 5(4), 861-879.

Shugar, D. H., Jacquemart, M., Shean, D., Bhushan, S., Upadhyay, K., Sattar, A., Schwanghart, W., McBride, S., De Vries, M. V. W., & Mergili, M. (2021). A massive rock and ice avalanche caused the 2021 disaster at Chamoli, Indian Himalaya. Science, 373(6552), 300-306.

Smiraglia, C., Azzoni, R. S., D'Agata, C., Maragno, D., Fugazza, D., & Diolaiuti, G. A. (2015). The evolution of the Italian glaciers from the previous data base to the New Italian Inventory. Preliminary considerations and results. Geografia Fisica e Dinamica Quaternaria, 38(1), 79-87.

Smiraglia, C., Diolaiuti, G., Casati, D., & Kirkbride, M. P. (2000). Recent areal and altimetric variations of Miage Glacier (Monte Bianco massif, Italian Alps). IAHS-AISH publication, 227-233.

Span, N., & Kuhn, M. (2003). Simulating annual glacier flow with a linear reservoir model. Journal of Geophysical Research: Atmospheres, 108(D10).

Stocker-Waldhuber, M., Fischer, A., Helfricht, K., & Kuhn, M. (2019). Long-term records of glacier surface velocities in the Ötztal Alps (Austria). Earth System Science Data, 11(2), 705-715.

Taylor, C., Robinson, T. R., Dunning, S., Rachel Carr, J., & Westoby, M. (2023). Glacial lake outburst floods threaten millions globally. Nature Communications, 14(1), 487.

Travelletti, J., Delacourt, C., Allemand, P., Malet, J.-P., Schmittbuhl, J., Toussaint, R., & Bastard, M. (2012). Correlation of multi-temporal ground-based optical images for landslide monitoring: application, potential and limitations. ISPRS Journal of Photogrammetry and Remote Sensing, 70, 39-55.

Van Wyk De Vries, M., & Wickert, A. D. (2021). Glacier Image Velocimetry: an open-source toolbox for easy and rapid calculation of high-resolution glacier velocity fields. The Cryosphere, 15(4), 2115-2132. https://doi.org/10.5194/tc-15-2115-2021

Vincent, C., Cusicanqui, D., Jourdain, B., Laarman, O., Six, D., Gilbert, A., Walpersdorf, A., Rabatel, A., Piard, L., & Gimbert, F. (2021). Geodetic point surface mass balances: a new approach to determine point surface mass balances on glaciers from remote sensing measurements. The Cryosphere, 15(3), 1259-1276.

Vincent, C., Gilbert, A., Jourdain, B., Piard, L., Ginot, P., Mikhalenko, V., Possenti, P., Le Meur, E., Laarman, O., & Six, D. (2020). Strong changes in englacial temperatures despite insignificant changes in ice thickness at Dôme du Goûter glacier (Mont Blanc area). The Cryosphere, 14(3), 925-934.

Vincent, C., Gilbert, A., Walpersdorf, A., Gimbert, F., Gagliardini, O., Jourdain, B., Roldan Blasco, J. P., Laarman, O., Piard, L., & Six, D. (2022). Evidence of seasonal uplift in the Argentière glacier (Mont Blanc area, France). Journal of Geophysical Research: Earth Surface, 127(7), e2021JF006454.

Vincent, C., & Moreau, L. (2016). Sliding velocity fluctuations and subglacial hydrology over the last two decades on Argentière glacier, Mont Blanc area. Journal of Glaciology, 62(235), 805-815.

Wang, W., Zhang, T., Yao, T., & An, B. (2022). Monitoring and early warning system of Cirenmaco glacial lake in the central Himalayas. International Journal of Disaster Risk Reduction, 73, 102914.

Willis, I. C. (1995). Intra-annual variations in glacier motion: a review. Progress in Physical Geography, 19(1), 61-106.

Zekollari, H., Huss, M., & Farinotti, D. (2019). Modelling the future evolution of glaciers in the European Alps under the EURO-CORDEX RCM ensemble. The Cryosphere, 13(4), 1125-1146.

Zemp, M., Hoelzle, M., & Haeberli, W. (2009). Six decades of glacier mass-balance observations: a review of the worldwide monitoring network. Annals of Glaciology, 50(50), 101-111.

Zemp, M., Huss, M., Eckert, N., Thibert, E., Paul, F., Nussbaumer, S. U., & Gärtner-Roer, I. (2020). Brief communication: Ad hoc estimation of glacier contributions to sea-level rise from the latest glaciological observations. The Cryosphere, 14(3), 1043-1050.

Zemp, M., Nussbaumer, S. U., Gärtner-Roer, I., Bannwart, J., Paul, F., & Hoelzle, M. (2021). Global Glacier Change Bulletin Nr. 4 (2018-2019). WGMS, 4.